THE UNIVERSITY OF MICHIGAN

INDUSTRY PROGRAM OF THE COLLEGE OF ENGINEERING

OPTICAL OBSERVATION BY TRANSMITTED LIGHT OF THE TETRAGONAL TO CUBIC PHASE TRANSITION IN $(Ba,Sr)TiO_3$ CERAMICS

Viola C. Sanvordenker

A dissertation submitted in partial fulfillment
of the requirements for the degree of
Doctor of Philosophy in the
University of Michigan
Department of Geology and Mineralogy
1963

January, 1964

IP-652

To my parents

who, through times of political turmoil, have

given me what they value most,

an education.

ACKNOWLEDGEMENTS

The writer wishes to express her thanks to:

Professor Reynolds M. Denning, Chairman of the Doctoral Committee, for his encouragement and counsel throughout the course of this work;

Professor Howard Diamond, for many valuable discussions, and for his assistance in the mathematical analysis of the problem;

Professors Chester B. Slawson, Paul L. Cloke, and Wilbur C. Bigelow, for their advice;

Mr. William W. Raymond, Mr. Ralph M. Olson, and Miss Constanza Roca, for their technical assistance and helpful discussions;

Dr. Keshav S. Sanvordenker, her husband, without whose patient support this investigation would not have been completed;

Miss Maryon Wells, for her help in typing and editing;

the U. S. Air Force, Rome Air Development Center, and Caswell Electronics Corporation for their financial support during the experimental stages of the work;

the Departments of Mineralogy, Chemical and Metallurgical Engineering, and Electrical Engineering for the use of their facilities;

the staff of the Industry Program of the College of Engineering, for the final preparation and reproduction of the manuscript.

TABLE OF CONTENTS

		Page
ACKNOWLEDGEMENTS		iii
LIST OF TABLES		vii
LIST OF FIGURES		viii
I	INTRODUCTION	1
II	BACKGROUND	5
	A. General Structure of Perovskite-type Ferroelectrics	5
	B. Dielectric Behavior of Single Crystal Barium Titanate and Ceramic Barium Titanate and Barium-Strontium Titanates	9
	C. Proposed Explanation of the Dielectric Field Non-Linearity in Ceramic Barium Titanate and Barium-Strontium Titanate	12
	D. Optical Investigation of $(Ba,Sr)TiO_3$ Ceramic with Variables of Temperature and Electric Field	20
III	BARIUM TITANATE AND (Ba,Sr) TITANATE MATERIALS	22
	A. Structural and Optical Data	22
	B. Domain Structure and Twinning	23
	C. Electrical Data	26
	D. Domain Motion	28
	E. Solid Solutions	29
	F. Theoretical Considerations	31
	G. Ceramic Perovskite Ferroelectrics	34
	H. Optical Observation of Ceramic Ferroelectrics	37
IV	EXPERIMENTAL PROCEDURE	38
	A. Preparation of Samples	38
	B. Measuring Equipment	40
	1. The Heating Stage	40
	2. Capacitance Measurements	43
	3. Intensity Measurements	45
V	DATA AND OBSERVATIONS	47
	A. Data	48

TABLE OF CONTENTS (CONT'D)

		Page
	1. Presentation of Data	48
	2. Analysis of Curves	62
B.	Observations	76
	1. Short Term Effects	76
	2. Long Term Effects	89
VI	CALCULATION ON THE LIGHT INTENSITIES TRANSMITTED BY (Ba,Sr) TITANATE CERAMIC THIN SECTIONS	92
A.	Fraction of Light Transmitted by a $(Ba,Sr)TiO_3$ Ceramic Thin Section, at Some Temperature T in the Ferroelectric Region	94
	1. Calculation of Θ	96
	2. Calculation of the Birefringence of the Equivalent Crystallite	98
	3. Calculation of the Relative Intensity for all Wave Lengths from 5200Å to 6200Å	100
	4. Discussion of the Calculated Relative Transmitted Intensities	101
B.	Change with Temperature in the Relative Amount of Light Transmitted by a $(Ba,Sr)TiO_3$ Thin Section	105
C.	Change with Temperature and Applied DC Field in the Relative Amount of Light Transmitted by a Barium-Strontium Titanate Thin Section	113
D.	Comparison of the Relative Theoretical and Experimental Light Transmission Curves	115
	1. Consideration of Tr, the Peak Incremental Permittivity Temperature of the ceramic at zero Field.	115
	2. Consideration of Tr*, the Peak Incremental Permittivity Temperature of a Ceramic Under the Influence of an Electric Field	121
	3. Discussion of α , the Variance Parameter of the Ceramic Distribution	122
	4. Comparison of the Experimental and Theoretical Transmitted Light Intensity Curves	126

TABLE OF CONTENTS (CONT'D)

	Page
VII CONCLUSIONS	139
APPENDIX A	145
APPENDIX B	155
APPENDIX C	163
APPENDIX D	171
BIBLIOGRAPHY	172

LIST OF TABLES

Table		Page
4.1	COMPOSITION AND DIELECTRIC DATA FOR SEVEN BARIUM-STRONTIUM TITANATE CERAMICS.....	39
5.1	INCREASE IN PERCENT LIGHT TRANSMISSION IN LARGE-GRAINED MIXED TITANATE COMPOSITIONS PRODUCED BY STRONG DC FIELDS..	70
6.1	RELATIVE LIGHT INTENSITY $\bar{R}$ (BETWEEN 5200Å AND 6200Å) TRANSMITTED BY A $(Ba,Sr)TiO_3$ CRYSTALLITE BETWEEN CROSSED POLARS.....	102
6.2	SHIFT IN THE PEAK INCREMENTAL PERMITTIVITY TEMPERATURE WITH FIELD FROM Tr TO Tr*, USED IN THE EVALUATION OF THE THEORETICAL PERCENT LIGHT TRANSMISSION CURVES.....	135
6.3	CONSTANTS USED TO EVALUATE THE THEORETICAL PERCENT LIGHT TRANSMISSION CURVES, BASED ON EQUATIONS (6.35) and (6.40).	137

LIST OF FIGURES

Figure		Page
2.1	Some Typical Ferroelectric Hysteresis Loops.....	6
2.2	Structure of Cubic Barium Titanate.....	8
2.3	ϵ_Δ TE Surface for Pure Ceramic Barium Titanate.....	11
2.4	ϵ_Δ TE Surface for a Typical $Ba_{.65}$ $Sr_{.35}$ TiO_3 Ceramic..	13
2.5	Dielectric Behavior of Single Crystal Barium Titanate, as a Function of Temperature.....	14
3.1	Variation of Birefringence and Axial Ratio of Barium Titanate with Temperature.....	24
3.2	Variation with Temperature of the Cell Edges and the Cube Root of the Cell Volume of Barium Titanate.....	24
3.3	Schematic 180° Domain Pattern in Barium Titanate.....	25
3.4	Domain Formation in Tetragonal Barium Titanate.....	27
3.5	90° and 180° Walls Near the Surface of a Barium Titanate Crystal.....	27
3.6	Nucleation of 90° Domains in an a-Crystal of Barium Titanate.....	30
3.7	Free Energy Curve of $BaTiO_3$ as a Function of Polarization According to Devonshire's Theory.....	30
4.1	Sample Configuration of a $(Ba,Sr)TiO_3$ Ceramic.....	40
4.2	Heating Stage (a) and Mounted Sample (b) Used in the Observation of a Ceramic Thin Section by Transmitted Light.....	40
4.3	Ceramic Thin Section Observed Through a Polarizing Microscope.....	42
4.4	Circuit for Capacitance Measurements.....	43
4.5	Circuit for Light Intensity Measurement by a Photocell.	46

LIST OF FIGURES (CONT'D)

Figure		Page
5.1	Incremental Permittivity vs Temperature of Ceramic Sample 1, with Voltage as a Parameter.....	49
5.2	Percent Light Transmission vs Temperature of Ceramic Sample 1, with Voltage as a Parameter.....	50
5.3	Incremental Permittivity vs Temperature of Ceramic Sample 2, with Voltage as a Parameter.....	51
5.4	Percent Light Transmission vs Temperature of Ceramic Sample 2, with Voltage as a Parameter.....	52
5.5	Incremental Permittivity vs Temperature of Ceramic Sample 3, with Voltage as a Parameter.....	53
5.6	Percent Light Transmission vs Temperature of Ceramic Sample 3, with Voltage as a Parameter.....	54
5.7	Incremental Permittivity vs Temperature of Ceramic Sample 4, with Voltage as a Parameter.....	55
5.8	Percent Light Transmission vs Temperature of Ceramic Sample 4, with Voltage as a Parameter.....	56
5.9	Incremental Permittivity vs Temperature of Ceramic Sample 5, with Voltage as a Parameter.....	57
5.10	Percent Light Transmission vs Temperature of Ceramic Sample 5, with Voltage as a Parameter.....	58
5.11	Incremental Permittivity vs Temperature of Ceramic Sample 6, with Voltage as a Parameter.....	59
5.12	Percent Light Transmission vs Temperature of Ceramic Sample 6, with Voltage as a Parameter.....	60
5.13	Percent Light Transmission vs Temperature of Ceramic Sample 7, with Voltage as a Parameter.....	61
5.14	Effect of a Strong DC Field on the Optical Anisotropy of a Ferroelectric Ceramic, Sample 3.....	72
5.15	Effect of a strong DC Field on the Optical Anisotropy of a Fine-Grained Ceramic, Sample 6.....	75

LIST OF FIGURES (CONT'D)

Figure		Page
5.16	Effect of Poling on the (101) Twinning Structure of a Ferroelectric Sample, Sample 1.....	79
5.17	Variation of Birefringence with Temperature in Tetragonal Barium Titanate and $(Ba,Sr)TiO_3$ Ceramic.....	82
5.18a	Schematic: Rotation of the Polar Axis in a Ferroelectric Domain Produced by an Applied DC Field.....	86
5.18b	Field Produced Rotation of the Polar Axes in Antiparallel Domains.....	86
5.19	Extinction of an Anisotropic Area in a Ferroelectric Grain of Sample 1, upon Applying a Strong DC Field.....	88
5.20	Poling in Sample 1.....	91
6.1	Orientation of the Privileged Directions of a Crystal in the Optical Field of a Polarizing Microscope.....	94
6.2	Relative Intensity R_1 of the Equivalent Crystallite with Respect to the Phase Difference Angle.....	97
6.3	Ellipsoid of Rotation.....	98
6.4	Spectral Sensitivity Curve of RCA Photocell 6957.....	103
6.5	Birefringence Δn of a Barium-Strontium Titanate Crystal as a Function of Angle β.....	104
6.6	Assumed Distribution of the Tetragonal to Cubic Phase Transitions of the Ceramic Grains about the Peak Incremental Permittivity Temperature Tr of the Ceramic.	107
6.7	The Error Function erf $(x) = \frac{2}{\sqrt{\pi}} e^{-x^2}$.....	107
6.8	Comparison of Theoretical and Experimental Percent Light Transmission Curves for a Ceramic Thin Section, Sample 1.....	116
6.9	Comparison of Theoretical and Experimental Percent Light Transmission Curves for a Ceramic Thin Section, Sample 2.....	117

LIST OF FIGURES (CONT'D)

Figure		Page
6.10	Comparison of Theoretical and Experimental Percent Light Transmission Curves for a Ceramic Thin Section, Sample 3	118
6.11	Comparison of Theoretical and Experimental Percent Light Transmission Curves for a Ceramic Thin Section, Sample 4	119
6.12	Polarization as a Function of Temperature, with and without a Biasing Field	122
6.13	Theoretical Incremental Permittivity vs Temperature Curves for Various Values of the Parameter α	125
6.14	Comparison of Theoretical and Normalized Experimental Incremental Permittivity vs Temperature Curves for Sample 1	127
6.15	Comparison of Theoretical and Normalized Experimental Incremental Permittivity vs Temperature Curves for Sample 2	128
6.16	Comparison of Theoretical and Normalized Experimental Incremental Permittivity vs Temperature Curves for Sample 3	129
6.17	Comparison of Theoretical and Normalized Experimental Incremental Permittivity vs Temperature Curves for Sample 4	130
6.18	Temperature Dependence of the Optical Transmission of Barium Titanate with Various Applied Fields Near 120°C.	132

I INTRODUCTION

Barium titanate has attained importance as a ferroelectric material relatively recently. Toward the end of the Second World War the industrial need for low loss materials of high dielectric constant led to the thorough investigation of titania and titanate compounds in this country.[1,2,3] It was found that titania, magnesium titanate, calcium titanate, and strontium titanate form useful capacitor dielectrics. Very high dielectric condensers were also manufactured from barium titanate, but, unlike the other dielectrics, they were surprisingly temperature and field dependent. A series of measurements showed that ferroelectricity was the cause of the dielectric anomaly. Dielectric hysteresis loops were observed on the barium titanate ceramic up to about 120°C, beyond which temperature the material acted like an ordinary dielectric.

At about the same time as the study on titania compounds was in progress in the U.S.A., Wul and Goldman[4,5] in Russia independently reported on the ferroelectric behavior of barium titanate.

The material, which in its ceramic form, is piezoelectric when poled, was soon widely used in the manufacture of electro-mechanical transducers and dielectric amplifiers. It proved to be a piezoelectric of high mechanical strength and chemical stability, and a good dielectric.

With the growth of single crystals by the Swiss group of Battner, Matthias, Merz, and Scherrer,[6] and later by Remeika[7] it was possible to conduct some basic studies on the new ferroelectric. Within a relatively short time, a wealth of optical, electrical, and mechanical data on barium titanate were gathered. Although barium titanate was not the first

ferroelectric to be discovered -- the occurence of ferroelectricity was first noticed in Rochelle Salt (sodium potassium tartrate tetrahydrate, $NaKC_4H_4O_6 \cdot 4H_2O$) in 1921[8] and subsequently in potassium dihydrogen phosphate (KH_2PO_4) in 1935[9] -- its relatively simple structure facilitated the analysis of the dielectric phenomena associated with ferroelectricity. Some of the important aspects are: 1) the large polarization in ferroelectric barium titanate, 2) the high dielectric constants at the phase transitions (barium titanate has 3 ferroelectric phases), 3) the onset of spontaneous polarization at the Curie point, 4) the changes in polarization at the lower transitions, 5) the formation of domains in the ferroelectric phases, and 6) the manner in which domain processes contribute to the changes in capacitance in barium titanate single crystals. Both phenomenological[10] and model theories[11-20] have been advanced to account for these and other aspects of ferroelectricity in barium titanate.

While much fundamental knowledge was gained from the study of single crystals of barium titanate, research on ceramic barium titanate and barium titanate-type materials proceeded in a relatively empirical manner. The industrial interest in ferroelectric ceramics had increased considerably since the discovery of titania compounds in 1945. Efforts were made to improve the dielectric and piezoelectric properties of barium titanate and barium-strontium titanate ceramics.[21-29] New ferroelectric ceramics were rapidly being discovered and various solid solutions of ferroelectric materials, some with "additives," began to appear on the market.[30-46] As a result, the manufacturer of dielectric and piezoelectric devices was able to draw from a steadily growing supply of raw materials.

An important aim in the manufacture of ceramics has been the production of materials with reproducible electrical and mechanical properties. It required rigorous standardization of every step in the manufacturing cycle. Other aspects, such as the "poling" and "aging" [47-49] processes in piezoelectric ceramics were thoroughly investigated. ("Poling" refers to the cooling of a piezoelectric material in a strong DC electric field, such that the ceramic has a net piezoelectric vector. Since a poled ceramic is, strictly speaking, not in an equilibrium state, its bulk piezoelectricity will change (lessen) with time. This is referred to as "aging").

The literature on ferroelectric ceramics, which is very extensive, can be roughly classified under:

1. new and improved ferroelectric ceramics, [21-46]
2. the problems encountered in the manufacture and processing of the ceramics, [50-55] and
3. the development of devices using these materials. [56-60]

In comparison, with the developmental work, very little has been written on the fundamental processes in feroelectric ceramics. The complexity of the ceramic structure no doubt is in some part responsible for this scarcity of basic information. One of the important properties of ceramic ferroelectrics which has had practical applications (modulating devices and amplifiers), but which has not been thoroughly understood, is the dielectric non-linearity of these materials, i.e., the ability of the capacitance to vary with strong, low frequency fields. It was generally thought that the dielectric non-linearity proceeded by a mechanism of

domain motion and domain reorientation, similar to those observed in single crystals of barium titanate.

Relatively recently a theory on the "variation of permittivity with electric field in perovskite-like ferroelectrics"[62] was published. It proposed that the non-linear dielectric effect is the result of an induced ferroelectric state in the ceramic rather than of domain motion. This view was substantiated by electrical data obtained on $(Ba,Sr)TiO_3$ ceramic materials.[62] It appeared to the present investigator that a dynamic (i.e., under conditions of varying temperatures and electric fields), optical study on $(Ba,Sr)TiO_3$ ceramics would enable the direct observation of the processes associated with the dielectric non-linearity in these materials. The present thesis describes the results of such a study, and it attempts to correlate and interpret the numerous optical observations made on thin sections of $(Ba,Sr)TiO_3$. The aim has been to obtain some understanding of the mechanism of the field non-linearity in perovskite-type titanates.

II BACKGROUND

A. General Structure of Perovskite-type Ferroelectrics

All crystalline materials fall into one of the thirty-two crystallographic symmetry classes. Of these, eleven have a center of symmetry, whereas the other twenty-one are non-centrosymmetric. Materials belonging to twenty of the non-centrosymmetric classes have been described as piezoelectric, i.e., they become electrically polarized when subjected to stress or to a temperature gradient. Of the twenty piezoelectric classes, ten are termed the polar or pyroelectric classes. The truly pyroelectric materials are spontaneously polarized in their stressed state. Their inherent polarization can be detected by heating or by cooling the substance uniformly and thereby effecting a change in the existing polarization.

Among the pyroelectric crystals there is a smaller group in which the direction of spontaneous polarization can be reversed by applying an electrical DC field opposite in sign to the polarity of the crystal. Such materials are described as ferroelectric. Their behavior is illustrated in the ferroelectric hysteresis loops in Figures 2.1a, 2.1b, and 2.1c. Hence a ferroelectric crystal can be broadly defined as having an inherent polarization along some specified crystallographic direction. In addition, the direction of polarization in the crystal can be reversed by a large, external electric field.

In the following the perovskite type ceramic ferroelectrics such as polycrystalline barium titanate and solid solutions of barium and strontium titanate are considered in some detail. The adjective "perovskite-type" has been used for many ferroelectric and antiferroelectric materials whose structure can be derived from the ideal perovskite

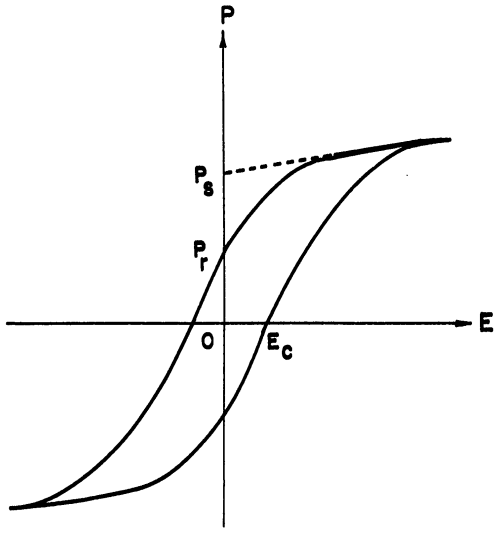


Figure 2.1a. Schematic Ferroelectric Hysteresis Loop

OP_s = spontaneous polarization
OP_r = remanent polarization
OE_c = coercive field

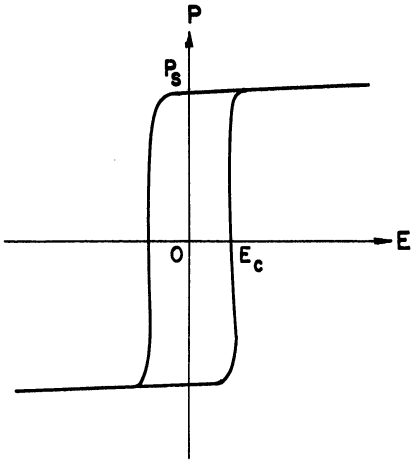


Figure 2.1b. Hysteresis Loop of a Barium Titanate Single Crystal at 60 cps (after Merz, Reference 78)

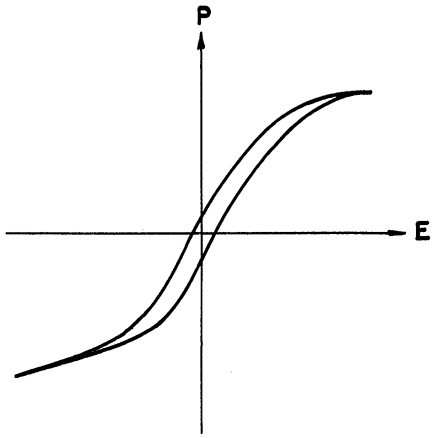


Figure 2.1c. Hysteresis Loop of a Typical Commercial Titanate Ceramic at 100 cps

Figure 2.1. Some Typical Ferroelectric Hysteresis Loops.

structure by small modifications in its atomic positions or even by omissions of atoms not essential to the perovskite framework. (The mineral perovskite, $CaTiO_3$, from which the family name was derived, is orthorhombic, and has the space group Pcmn. It is not an "ideal perovskite," but rather a distorted multiple cell perovskite, and it is not ferroelectric.)

As Megaw[63] has described in some detail, ideal perovskite-type structures are cubic and have the formula ABO_3. A is a divalent cation, B a tetravalent cation and O the oxygen ion. In addition, the A cation must be twelve-coordinated and the cation B six-coordinated. The structure can be considered as a framework of linked BO_6 octahedra with the A cation occupying the interstices between the octahedra.

Barium titanate, whose structure is shown in Figure 2.2, can be classified as an ideal cubic perovskite in its non-ferroelectric form. Its unit cell length is about 4 Å and the cell contents is one formula unit. The lower temperature forms of barium titanate, which are ferroelectric, have been classified by Megaw[63] as distorted small-cell perovskite. These forms are no longer cubic but can be derived from the cubic structure by small distortions in the atomic positions. Their cell edges, if referred to the original cubic unit cell, are still about 4 Å long and their cell contents remains one formula unit. The three crystallographic transitions of perovskite-type barium titanate are:

1. the cubic to tetragonal transition at about 120 °C,
2. the tetragonal to orthorhombic transition near 0°C, and
3. the orthorhombic to rhombohedral transition near -90°C.[63]

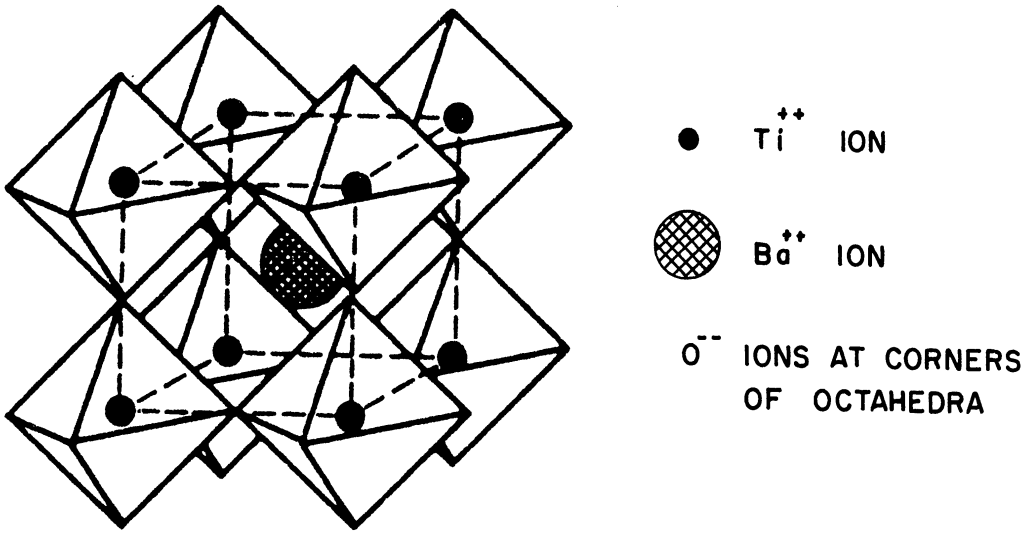


Figure 2.2. Structure of Cubic Barium Titanate.
(After Megaw, Reference 63)

Only the high temperature transition which represents the transition from the cubic, non-ferroelectric, to tetragonal, ferroelectric state is considered in the present investigation.

In solid solutions of barium and strontium titanate, the upper transition is linearly shifted to lower temperatures with increasing amounts of strontium titanate.[64,65] Dielectric measurements on solid solutions of barium titanate and strontium titanate taken at the Electromagnetics Materials Laboratory, Electrical Engineering Department, The University of Michigan, show a similar trend for the tetragonal to orthorhombic transition temperature of barium-strontium titanate materials. Similar to barium titanate, these mixed titanate ceramics (the term "mixed" will be used here for solid solutions of barium and strontium titanate) likewise occur in the ideal cubic perovskite and distorted small cell perovskite form. Due to the substitution of the smaller strontium ion in the barium titanate lattice, the average unit cell of the mixed barium strontium titanate ceramic is somewhat smaller than that of pure barium titanate.

B. Dielectric Behavior of Single Crystal Barium Titanate and Ceramic Barium Titanate and Barium-Strontium Titanates

The ferroelectric hysteresis loops shown in Figures 2.1a, 2.1b, and 2.1c are examples of the polarization versus electric field characteristics of titanate ferroelectrics. Hysteresis loops can be easily observed on a cathode ray oscilloscope by means of a Sawyer and Tower circuit.[66] Figure 2.1a shows a schematic hysteresis loop obtained by cycling a ferroelectric sample with an AC field. P_s, the spontaneous polarization, is obtained by extrapolating the slope of the saturation polarization back

to the P-axis. P_r, the remanent polarization, is that polarization which remains in the ferroelectric at zero field. E_c, the coercive field, is the field required to remove the remanent polarization. Figure 2.1b shows a square hysteresis loop taken on a "good" single crystal* of barium titanate at about room temperature.

A sudden reversal in the polarization of the crystal occurs when a sufficiently large field of opposite polarity, i.e., the coervice field, is applied to the crystal. Poorer crystals and large grained oriented polycrystalline aggregates will show more rounded loops, indicating that polarization reversal occurs over a narrow range of fields. (Materials with square hysteresis loops are applicable to memory and switching units.)

Figure 2.1c shows a hysteresis loop taken on a fine-grained commercial ceramic material. 180° polarization reversal in the domains of the ferroelectric ceramic occurs over a wide range of fields, with the slope of the curve, dP/dE, being steep near coercive fields and relatively flat at large applied fields. (The narrow loop materials are employed for modulation and as amplifiers.)

The dielectric behavior of ceramic barium titanate as a function of temperature and applied DC field is illustrated in Figure 2.3. The

* A good single crystal is mostly strain-free. It has few imperfections and can easily be poled into an area of uniform polarization by an electric field. On the other hand, "poor" crystals are usually highly twinned. They do not lend themselves to successful poling, or, to the alignment of all the twin vectors in one direction by means of an externally applied DC field.(67,68,69) Twins, or ferroelectric domains, as they are termed in the literature, tend to renucleate at imperfections as soon as the external field is removed.

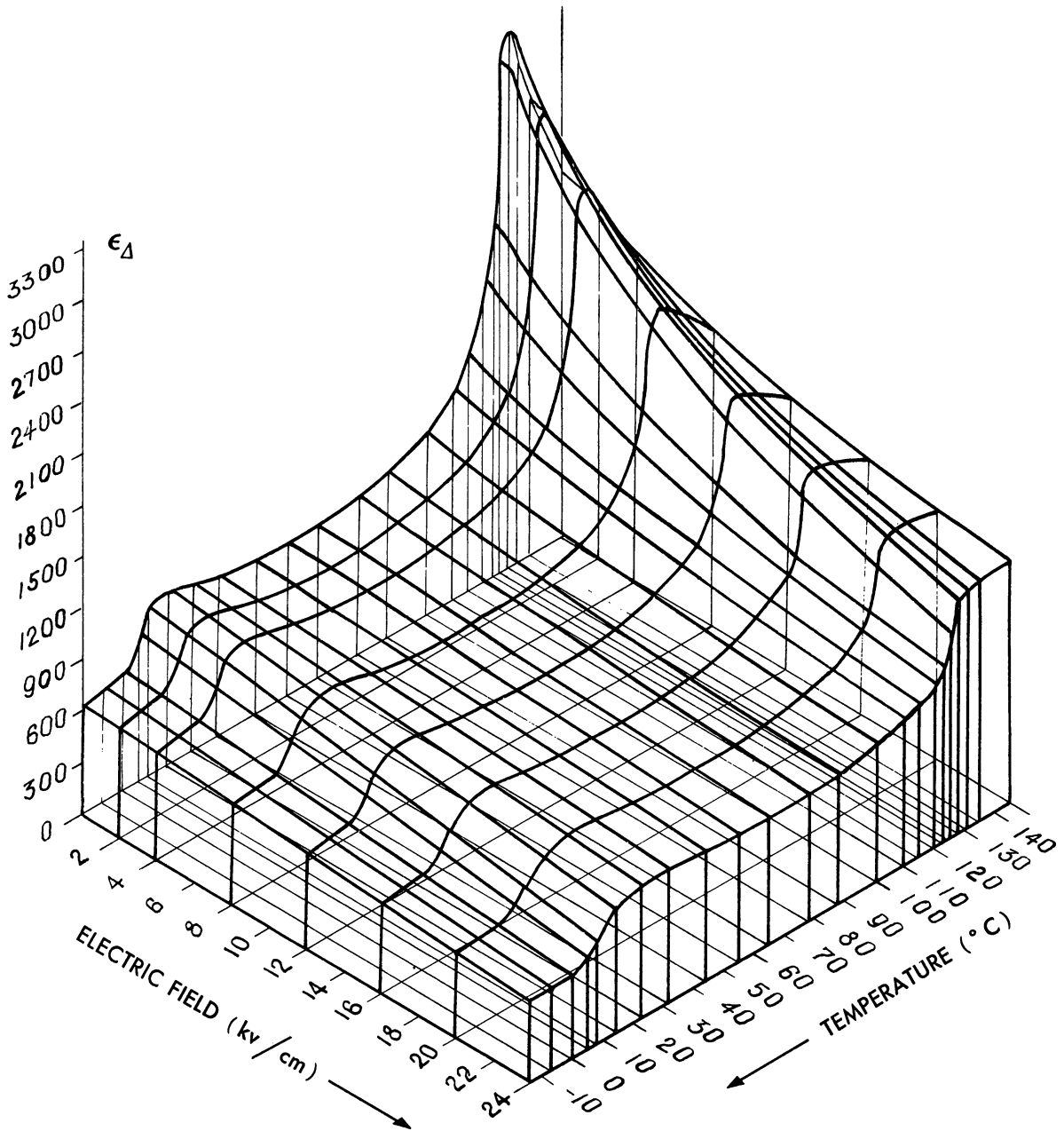


Figure 2.3. Surface for Pure Ceramic Barium Titanate.

incremental permittivity* reaches a maximum of 120°C with zero applied field. The effect of an increasing electric field on the ceramic is to steadily lower the peak incremental permittivity and to raise the temperature at which the peak permittivity is observed.

Figure 2.4 shows a surface relating incremental permittivity, applied field, and temperature for a mixed barium-strontium titanate ceramic of composition $Ba_{0.65}Sr_{0.35}TiO_3$.[62] Here the paraelectric to ferroelectric transition occurs at a lower temperature, and the incremental permittivity peak is somewhat broader than for pure barium titanate. Generally speaking, however, both DC field and temperature have a similar effect on the two ceramics.

C. Proposed Explanation of the Dielectric Field Non-Linearity in Ceramic Barium Titanate and Barium-Strontium Titanate

It has been observed[69] that whenever a DC field is applied to a multidomain single crystal, the domains tend to align themselves in the direction of the field. The incremental permittivity of such a "poled" crystal, when measured parallel to the field direction, is lower than that of the crystal before poling. This is a result of the large directional variation of the small signal permittivity (or incremental permittivity), ϵ_Δ, in barium titanate. The ϵ_Δ measured parallel to the c-axis is of the order of 200, the ϵ_Δ perpendicular to the axis is about 4000[70] (see Figure 2.5). A crystal with domains oriented in

* The incremental permittivity ϵ_Δ is the permittivity dP/dE obtained by measuring the dielectric with a very small, high frequency signal. The high frequency measuring signal is superimposed on a large, low frequency AC signal or on a large DC biasing field. The data in Figure 2.4, for example, were obtained by sweeping the ceramic from 0 to 40 kv/cm at a slow, cycling field of 0.5 cps and by measuring it with a high frequency field of 10,000 cps.

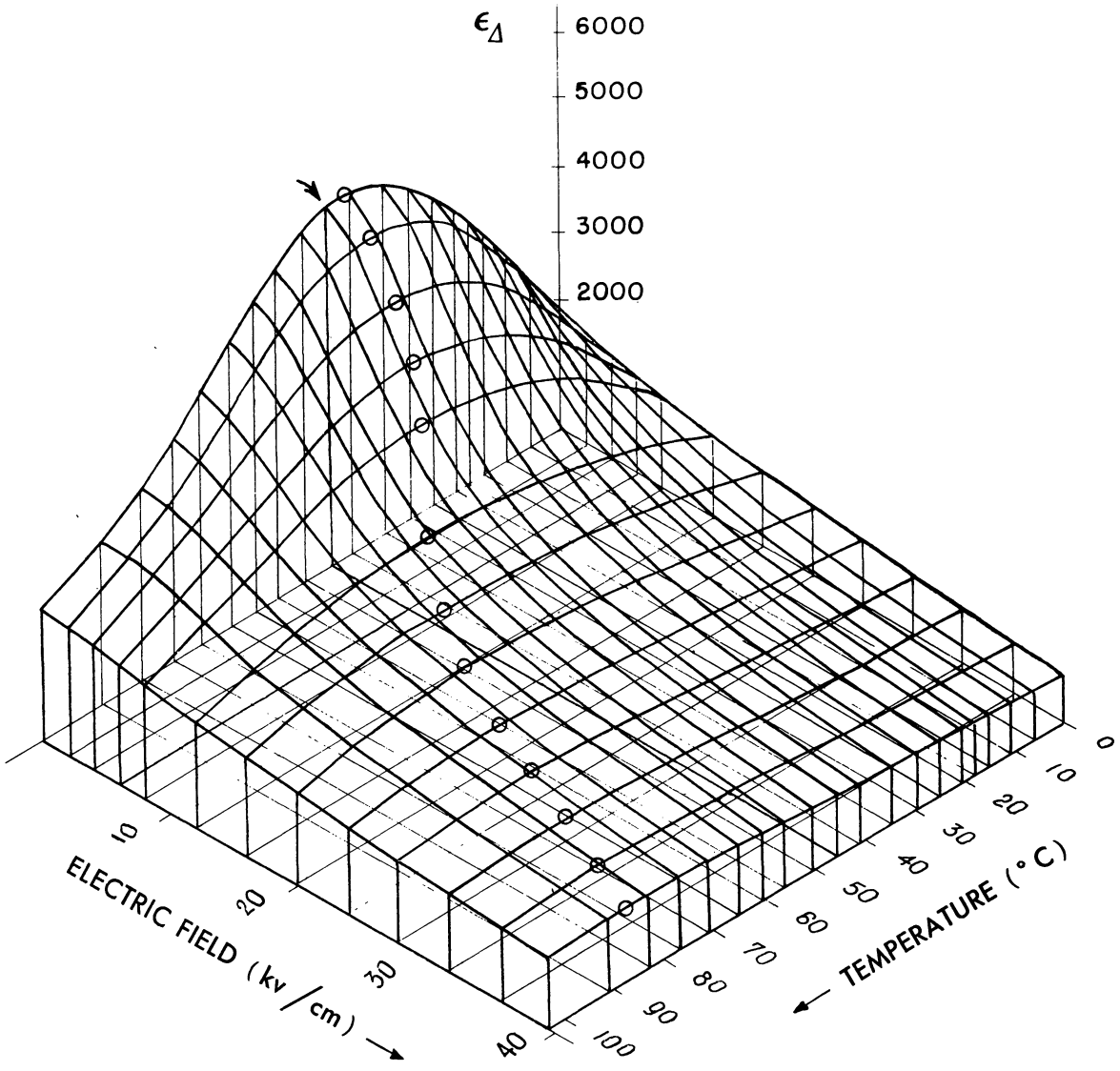


Figure 2.4. Surface for a Typical $Ba_{.65}$ $Sr_{.35}$ TiO_3 Ceramic.

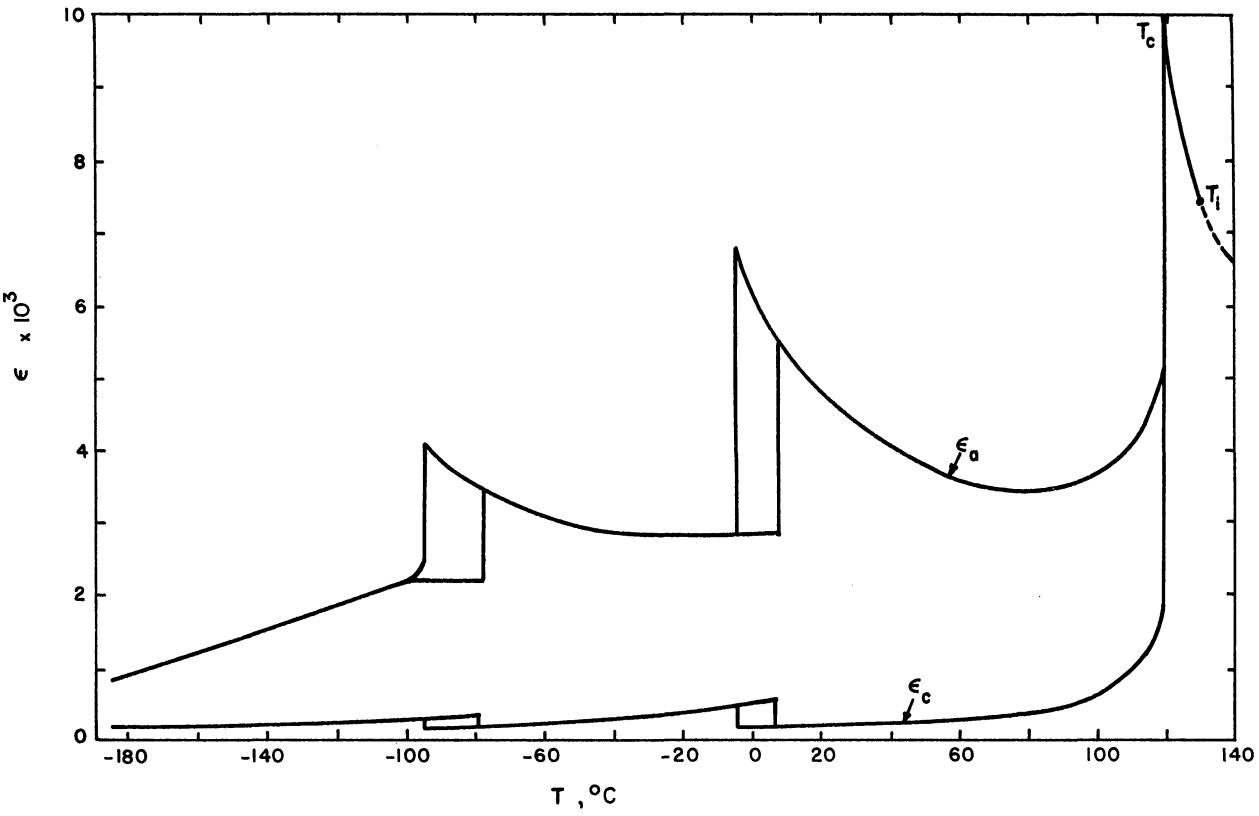


Figure 2.5. Dielectric Behavior of Single Crystal Barium Titanate, as a Function of Temperature. (After Merz, Reference 70)

different directions will have an incremental permittivity somewhere in between these values. When exposed to a DC field, the domains tend to orient themselves in the direction of the field.[68,69] This results in a lowering of the incremental permittivity of the crystal in the field direction.

It is well known that a DC biasing field also decreases the incremental permittivity of ceramic barium titanate[71] or barium-strontium titanate. Before any work had been published which attempted to explain the observed dielectric field non-linearity in the ceramic, McQuarrie[72] proposed three possible explanations for the process. He suggested that the effect might be caused:

1. by a field produced shift of 90° domain walls in the ceramic, similar to the one observed in single crystals of barium titanate,
2. by a change in the basic polarizability of the material, and
3. by the removal of 180° domain walls, assuming that they did contribute some value to the permittivity of the ceramic in the unbiased state.

If the first explanation were correct, McQuarrie reasoned, one might possibly detect a mechanical distortion in the material as a result of the field produced 90° domain movement. He ruled out the other two hypotheses as not being significant enough to account for the observed, large field-produced changes in the dielectric value of the ceramic.

As mentioned in the beginning of this section, a field produced alignment of 90° domains in the ceramic would result in a decrease in the incremental permittivity of the ceramic when measured parallel, and an increase in the incremental permittivity when measured perpendicular to the field direction. It can be experimentally shown,[73] however, that in the transition region of a ceramic, the incremental permittivity ϵ_Δ decreases with increasing DC fields, regardless of whether the sample is measured parallel or transverse to the applied field.

A theoretical model has been developed[62] which provides an explanation for the field produced dielectric non-linearity in solid solutions of barium-strontium titanate.* The model proposes that the domains in a fine-grained ferroelectric are not free to move with the applied external field, but that they are essentially "frozen in." The observed lowering of the incremental permittivity peak with field in the ferroelectric to paraelectric transition region is considered due to an induced ferroelectric state in those grains in the ceramic which are paraelectric.

It is characteristic of the ceramic perovskite ferroelectrics that their transitions to the paraelectric, isotropic state occur over a temperature range rather than at a sharply defined temperature. The reason for this lies in the distribution of Curie temperatures of the crystallites that compose the ceramic. The tetragonal to cubic transition temperature is strongly affected by stresses.[74,75] Stresses occur in the ceramic at imperfections and also result from the approximately 1% linear contraction[76,77] which occurs when the ceramic is cooled from the sintering

* See section III-G

temperature of about 1400°C to about 120°C. Furthermore, the cubic to tetragonal transition is accompanied by a 1% change in the axial ratio of the perovskite-type titanate.(76) Some of the strains are subsequently relieved by complex patterns of twinning within the individual ceramic grains.

In a mixed barium-strontium titanate ceramic, small compositional variations in the grains cause a further spread in the Curie temperatures and result in a still broader permittivity peak. Within the region of the peak incremental permittivity, both ferroelectric and paraelectric grains exist side by side, with more ferroelectric grains at the low temperature end of the transition range, and more paraelectric grains at the high temperature end.

The lowering of the incremental permittivity with induced ferroelectricity can be simply illustrated on a single crystal of barium titanate. Figure 2.5 represents the dielectric behavior of a single barium titanate crystal with respect to temperature. T_c at 120°C is the Curie temperature, Ti , an arbitrary point on the curve, is 130°C. ϵ_a and ϵ_c represent the incremental permittivities in the two axial directions of the ferroelectric grain. A crystal of barium titanate at 125°C is paraelectric (see Figure 2.5) and has an ϵ_Δ of about 8000. The formation of a ferroelectric state by applying a field can in a sense be represented by a shift of the entire curve to higher temperatures.* By applying a DC field of 7000 volts/cm to barium titanate at 125°C, the transition temperature is shifted upward by about 10°C to 130°C. (These

* Strictly speaking, a field would shift the curve to higher temperatures and also lower the overall permittivity of the biased ceramic.

figures are based on calculations by Merz. Merz reports having observed a field produced shift of the Curie temperature on single crystals of barium titanate of 1.4×10^{-3} degrees/volt cm^{-1}).[78] The field exposed crystal is therefore ferroelectric at 125°C, with an ϵ_c of about 1000 and an ϵ_a of about 4500 or less (see footnote p. 17). These values are considerably lower than the incremental permittivity of 8000 for the paraelectric crystal at 125°C and zero field.

In the following the observations made above on a single crystal of barium titanate will be applied to the case of ceramic barium titanate and mixed barium-strontium titanate compositions. The effect of a DC field on the ceramic at temperatures slightly above its peak incremental permittivity temperature is briefly outlined. Some of the assumptions on which the model of the field-produced dielectric non-linearity in perovskite-like ferroelectrics[62] is based, are thereby illustrated.

The ceramic is simply regarded as an aggregate of crystallites. At a temperature slightly above the peak incremental permittivity temperature, most of the grains in the ceramic are paraelectric. However, due to the distribution of the individual Curie temperatures of the grains over a temperature range, some grains have remained ferroelectric. At the temperature in question -- namely, at a temperature somewhat above the peak incremental permittivity temperature -- a distinction can be made between not only two, but three possible states of the ceramic crystallites.

1. There are a number of ferroelectric grains in the ceramic which are considered to be essentially clamped, and on which

the field has little effect. They contribute to the total permittivity by a constant fraction.

2. It can be shown from thermodynamic relationships developed for barium titanate[10,78,79] that a narrow temperature range beyond the Curie peak exists in which a ferroelectric state can be induced in a paraelectric single crystal, i.e., 12°C for barium-titanate. At higher temperatures, the field has a comparatively small effect on the incremental permittivity of the crystal. Hence, in the ceramic, the contribution to the total permittivity from these completely paraelectric grains will be considered another constant.

3. Finally, there remain those paraelectric grains which lie in the "inducible" range and which are sensitive to an applied field. As the field is gradually increased, the incremental permittivity of these crystallites first increases until it reaches a maximum at the induced "Curie" temperature. The phenomenon is illustrated on a single crystal of barium titanate in Figure 2.5 where the permittivity of the crystal at T_c is higher than that at T_i. With larger fields, a ferroelectric state is induced in the grains, and the incremental permittivity drops considerably (Figure 2.5).

The non-linear behavior of the ceramic can therefore be considered mainly due to this latter group of grains whose incremental permittivies vary substantially with field. This is very well shown in Figures 2.3 and 2.4, which represent the dielectric behavior of a barium titanate

and a barium-strontium titanate sample with temperature and field. It is seen that the largest changes in the incremental permittivity of the ceramic occur when an electric field is applied to the peak incremental permittivity of the ceramics. The peak marks the temperature at which a maximum number of ceramic grains change from a ferroelectric to a paraelectric state. The farther away from the peak, the more linear the ϵ_Δ vs E characteristics of the material.

D. Optical Investigation of $(Ba,Sr)TiO_3$ Ceramic with Variables of Temperature and Electric Field

The model of induced ferroelectricity proposes that the observed dielectric field non-linearity in ceramic perovskite-type ferroelectrics is not the result of domain rotation in the ferroelectric grains (the grains are considered to be essentially clamped), but the result of an induced ferroelectric state in those grains which are paraelectric in the region of the ferroelectric to paraelectric transition of the ceramic.

It was hoped that an optical study of ceramic barium-strontium titanate by transmitted light would provide a direct means of observing the effect of an electric field in the material. Such an investigation might possibly reveal whether a biased ferroelectric material differed, in some fundamental way, from a biased single crystal.

The mineralogical technique of thin sectioning was chosen to prepare several solid solutions of barium and strontium titanate for observations under the polarizing microscope. This technique, rather than the metallographic one of polishing and etching, has the advantage that it permits detection of any immediate changes which varying temperature

and/or electric fields may have on the anisotropy of the material. The ferroelectric to paraelectric transition in the perovskite titanates is closely connected with their tetragonal to cubic transition. Hence, when viewed between crossed polars, the changes in the optical anisotropy of the grains can be directly related to changes in the state and structure of the entire ceramic.

The results of the optical observation on thin sections of $(Ba,Sr)TiO_3$ are mainly discussed in Section V.

III BARIUM TITANATE AND (Ba,Sr) TITANATE MATERIALS

Various experimental and theoretical observations on barium titanate and barium-strontium titanate materials, which are not essential to the understanding of the present investigation, have been briefly treated below. The reader is referred to this section for more extensive information on several aspects discussed in the thesis.

A. Structural and Optical Data

Barium titanate can occur in five modifications, hexagonal $C6_3/mmc$,[80,81] cubic $Pm\bar{3}m$,[82] tetragonal $P4mm$,[82] orthorhombic $Bmm2$,[83,84] and rhombohedral $R\bar{3}m$.[83,84] The transitions occur at 1460°C, 120°C, 0°C, and -90°C respectively. The high temperature transition between hexagonal and cubic is slow, non-ferroelectric, and reconstructive. (The term reconstructive implies here that the transition proceeds by a break-down of the old structure and a subsequent reassembling of the crystalline network to form the second structure.) All other transitions are displacive, i.e., they involve small displacements of the atomic network.[85] The transition at 120°C occurs between a non-ferroelectric and a ferroelectric phase. The remaining two low temperature transitions take place between ferroelectric phases.

In the cubic form, barium titanate has the ideal perovskite structure. The titanium ion is situated at the center of an oxygen octahedron. Hence it is six-coordinated. The oxygen octahedra are linked together at their corners.[63] The barium ion, which is 12 coordinated, lies in the large interstices between the oxygen octahedra (Figure 2.2).

Alternately the barium ion can be visualized as being at the center of a cube, with the titanium ions at the eight corners and the oxygen ions at the midpoint of the twelve edges.

All ferroelectric transitions in barium titanate occur with only small displacements in the ionic positions. A slight stretching of one of the crystal axes of the original perovskite cube gives rise to the tetragonal modification, with the c-axis forming the polar axis ($c/a = 1.01$). An elongation along the cubic face diagonal yields an orthorhombic form, with the orthorhombic a-axis now representing the ferroelectric axis. Finally, a displacement along the cube body diagonal leads to the rhombohedral, low temperature ferroelectric modification, with [111] being the polar direction.

The refractive index of barium titanate is $n_D = 2.46$ at the Curie point. Below 120°C the birefringence of the crystal is strongly dependent on temperature (Figure 3.1)[84] and wavelength.[87] Tetragonal barium titanate is optically negative. At 110°C $\epsilon - \omega \cong (n_c - n_a) \cong -0.03$ for sodium light, and at room temperature $\epsilon - \omega = (n_c - n_a) \cong -0.055$.[88] The variation of the cell dimension with temperature is shown in Figure 3.2.[84]

B. Domain Structure and Twinning

Many studies have been made on the very colorful and intricate twinning or domain patterns in ferroelectric, tetragonal barium titanate.[67,88-96] There are essentially two types of twins, the so-called 180° domains and the 90° domains. The 180° domains represent areas of anti-parallel polarization. (Figure 3.3). The c-axis of the

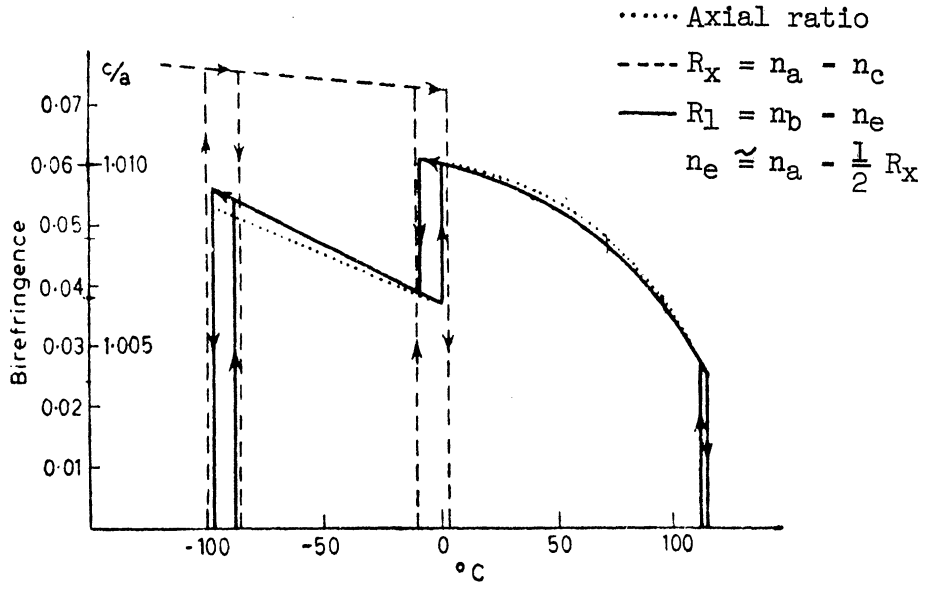


Figure 3.1. Variation of Birefringence and Axial Ratio of Barium Titanate with Temperature. (After Kay and Vousden, Reference 84)

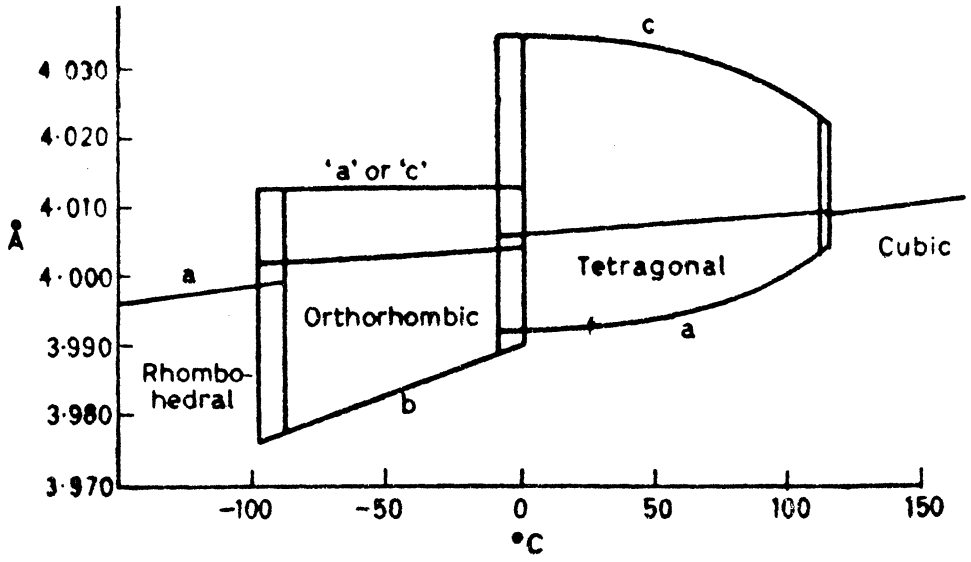


Figure 3.2. Variation with Temperature of the Cell Edges and the Cube Root of the Cell Volume of Barium Titanate. (After Kay and Vousden, Reference 84)

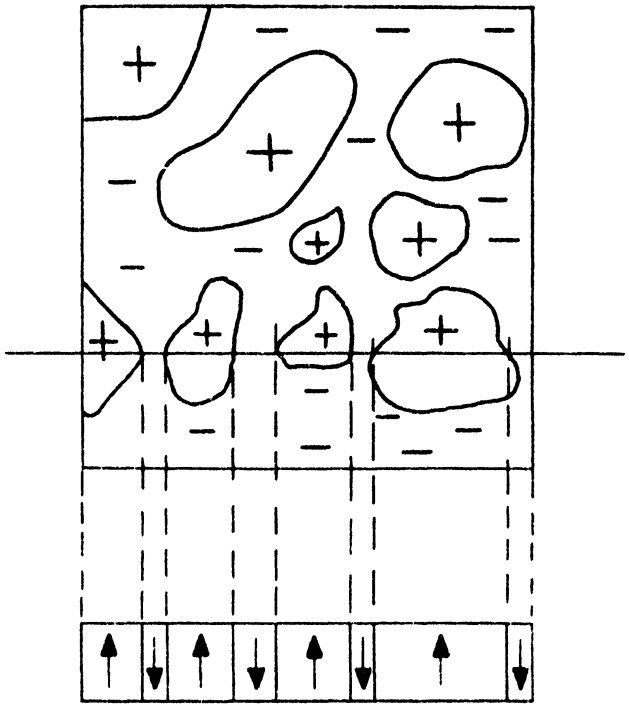


Figure 3.3. Schematic 180° Domain Pattern in Barium Titanate. (After Kaenzig, Reference 97)

twin individuals are oriented at 180° with respect to each other, with (100) forming the composition plane. In 90° domains the c-axes lie at almost 90° to each other in a head to tail arrangement, so that no surface charge is built up at the domain walls. The "90° wall" is a (101) composition plane[91] (Figure 3.4). Combination of the two types of twins occur frequently and lead to complicated domain patterns[92] (Figure 3.5). Twinning in the orthorhombic and rhombohedral structures have been reported by Kay[91] and Forsbergh.[88]

C. Electrical Data

Merz,[78] Cross,[98] and Drougard and Young[99] have reported values for the spontaneous polarization of tetragonal barium titanate, taken on almost perfect single crystals. The room temperature value is 24-26 microcoulomb/cm^2. The spontaneous polarization decreases steadily to 16-18 microcoulomb/cm^2, as the crystal is heated to the Curie temperature, where it falls off sharply. The coercive force at room temperature is about 500 volts/cm at 60 cycles/sec.[78]

The variations of the dielectric constants with temperature, measured perpendicular, ϵ_a, and parallel, ϵ_c, to the c-axis are shown in Figure 2.5. Above the 120°C transition, at which the crystal is no longer ferroelectric, the permittivity follows a Curie-Weiss law of the form

$$\epsilon = \epsilon_o + \frac{C}{T-T_o} . \qquad (3.1)$$

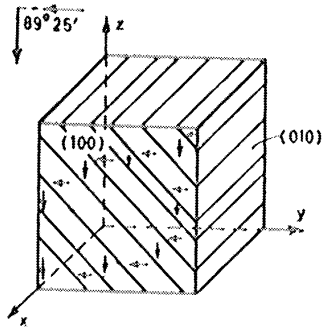


Figure 3.4. Domain Formation in Tetragonal Barium Titanate.

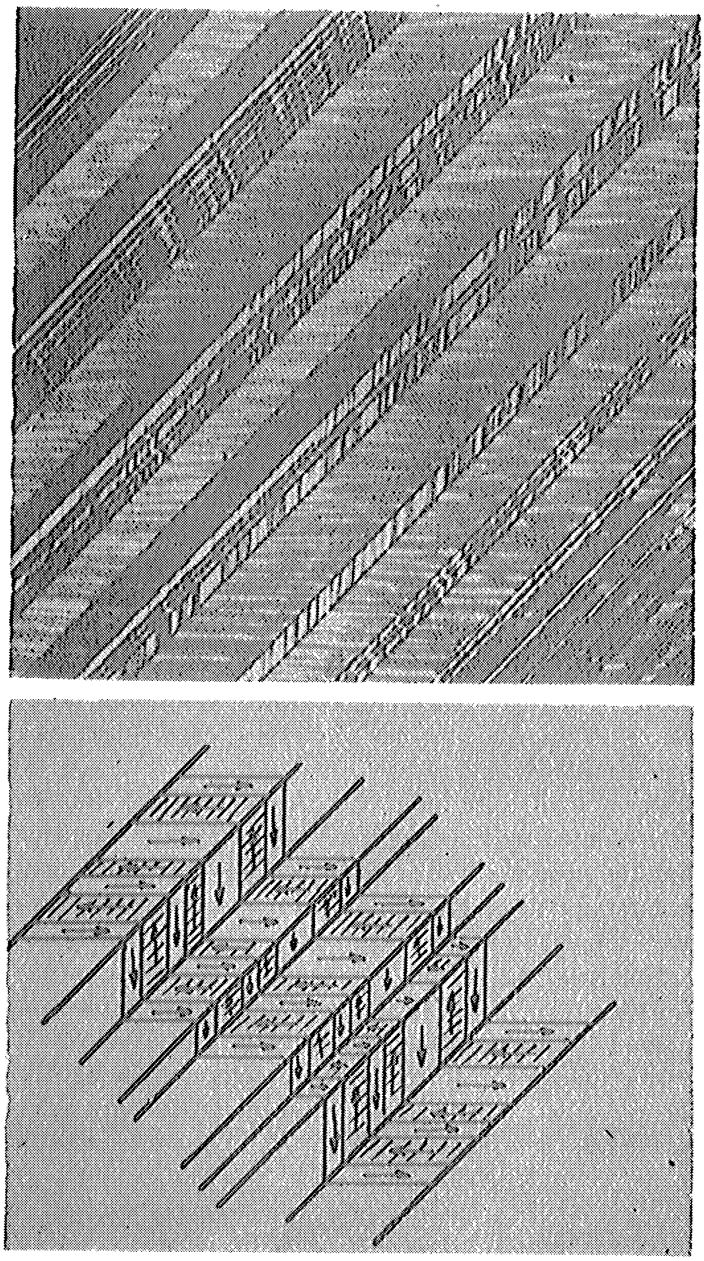


Figure 3.5. 90° and 180° Walls Near the Surface of a Barium Titanate Crystal. (After Hooton and Merz, Reference 92)

ϵ is the dielectric constant, ϵ_o the electronic contribution to the dielectric constant, C the Curie constant, T the absolute temperature, and T_o the extrapolated Curie temperature.

The Curie point in barium titanate is easily varied by internal strains, pressure, electric field, and solid solutions. Hydrostatic pressure tends to decrease the temperature of the cubic to tetragonal transition,[74] whereas pressure parallel or perpendicular to the c-axis raises the transition temperature.[75] An applied DC electric field also shifts the Curie point to higher temperatures. Merz,[78] Kaenzig and Maikoff[79] and Kawabe[100] have calculated the shift to be 1.43 x 10^{-3}°C/volt/cm, 1.2 x 10^{-3}°C/volt/cm, and 1.6 x 10^{-3}°C/volt/cm respectively.

D. Domain Motion

In their study on the dynamic behavior of domains in single crystals of barium titanate, Merz[68] and Little[69] have shown that polarization reversals proceed by the nucleation and growth of spike like domains. When an electric field of opposite polarity to the direction of the polar vector is applied along the c-axis of a single domain crystal, 180° domains nucleate at the electrodes and grow across the crystal in the form of thin wedges until the polarity of the original crystal is completely reversed. The growth is rapid and stable, the domain wall is thin (around two lattice constants in width[68]), and there is little sideward motion of the domain wall. The widening of the wedges proceeds by a series of dipole flips parallel to the polar axis.[69]

When an electric field is applied along the a-axis of a tetragonal crystal, 90° domains nucleate at one of the electrode surfaces, mostly the cathode. They subsequently propagate diagonally across the crystal. (Figure 3.6). Unless a spike of this type has traversed the entire crystal, it is usually not stable and is forced out by internal stresses when the field is removed. The stresses arise from the pseudocubic, tetragonal nature of the crystal.[69] Little has shown[69] that the direction of the polar axes in neighboring 90° domains deviate slightly from 90°. Hence the (101) composition plane cannot be strictly considered a 90° domain wall. The formation of "90° domains" is therefore accompanied by electrical-mechanical distortions in the crystal. The latter tend to revert the crystal back to its original state, once the field is removed. Existing 90° domain walls are many lattice spacings thick and sidewise motion of the walls has been observed.

When a sufficiently strong DC field is applied to a crystal having a complex pattern of both 90° and 180° domains, the domains tend to align themselves in the direction of the field. It is not possible to reverse the overall polarization of a crystal by 90° domain formation alone. The mechanism by which this switching process takes place consists of a complex sequence of interactions between domain walls, as explained in some detail by Little.[69] More recently studies on domain walls have been continued by several Japanese [101-104] and other workers.[105-107]

E. Solid Solutions

Ionic substitution in the perovskite structure of barium titanate has a considerable influence on the paraelectric to ferroelectric transition

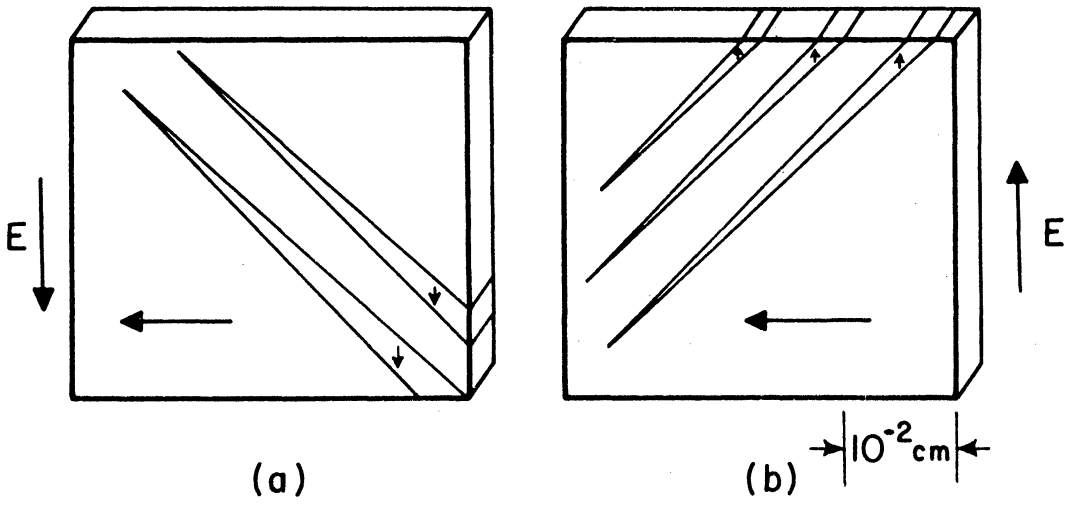


Figure 3.6. Nucleation of 90° Domains in an a-crystal of Barium Titanate. (After Little, Reference 69)

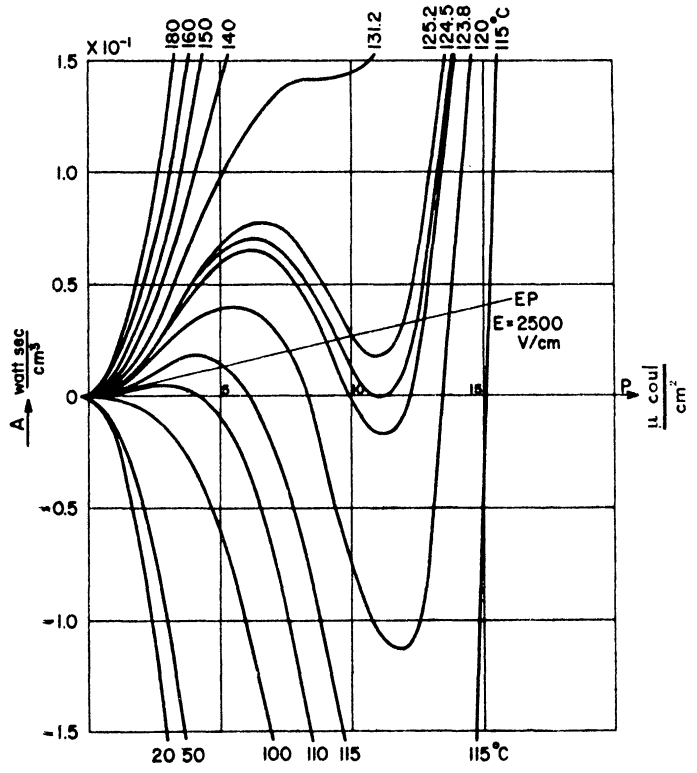


Figure 3.7. Free Energy Curve of $BaTiO_3$ as a Function of Polarization According to Devonshire's Theory. (After Kaenzig and Maikoff, Reference 79)

temperature. The direction of the shift depends on the particular ion substituted. In the solid solution of barium-strontium titanate the transition temperature decreases linearly with increasing concentration of strontium.(64) In solid solutions of barium-lead titanate, on the other hand, the Curie point increases up to 490° for 100% lead titanate.(64) Solid solutions of these and other perovskite-type ferroelectric ceramics have been found very useful in industry because they permit some control of the transition temperature as well as the dielectric values of the final product.

F. Theoretical Considerations

Several theories of ferroelectricity have been advanced to explain the wealth of information obtained from barium titanate ceramic and single crystals. Among them are the model theories of Slater,(12) Jaynes,(13) and Mason and Matthias,(11) and a phenomenological theory by Devonshire.(10) The latter has perhaps been the most successful of all. Since much of the theoretical treatment on ceramic barium-strontium titanate materials is based on Devonshire's thermodynamic description of single crystal barium titanate, some essential points of his theory are outlined below. The present description is restricted to the tetragonal and cubic phases of barium titanate.

In general, a piezoelectric solid can be described by the equation:

$$dA = EdP - \bar{X}dx - SdT \, . \qquad (3.2)$$

A is the Helmholtz free energy, E the applied electric field, P the polarization, X the stress, x the strain, S the entropy, and T the temperature of the system. Devonshire assumes that all phases of barium titanate can be considered as strained forms of the cubic structure. He then develops a free energy expression for barium titanate as a function of temperature, polarization and stress. Two cases are considered; first, the case of a free, unstrained crystal, and secondly, that of a strained crystal. For the unstrained crystal, the differential free energy at zero stress becomes

$$dA = EdP - SdT \quad . \tag{3.3}$$

The free energy of the system, which is considered to be zero for the unstressed, unpolarized crystal, can be expanded in terms of increasing powers of polarization. Odd powers in polarization are omitted in order that the free energy function remain the same for any reversal in sign of a polarization component.

$$\begin{aligned} A(P,T) = {} & \frac{a}{2}(P_x^2 + P_y^2 + P_z^2) + \frac{1}{4}b_{11}(P_x^4 + P_y^4 + P_z^4) \\ & + \frac{1}{2}b_{12}(P_y^2P_z^2 + P_z^2P_x^2 + P_x^2P_y^2) \\ & + \frac{c}{6}(P_x^6 + P_y^6 + P_z^6) \\ & + \frac{1}{2}d\,(P_y^4P_z^4 + P_z^4P_x^4 + P_x^4P_Y^4) + \cdots \quad . \end{aligned} \tag{3.4}$$

P_x, P_y, P_z are components of polarization in the x, y, and z directions. The coefficients a, b, c, d, are taken at constant stress (i.e., the crystal is free to deform). The coefficients are strictly speaking

temperature dependent. For the transition from the cubic to tetragonal phase, Equation (3.4) can be simplified to

$$A(P,T) = \frac{a}{2} P^2 + \frac{b}{4} P^4 + \frac{c}{6} P^6 + \cdots \qquad (3.5)$$

since the polarization vector in the tetragonal phase lies along the z-axis. Hence $P_x = P_y = 0$, and $P_z = P$.

At the upper transition temperature, a barium titanate crystal goes from an isotropic to a ferroelectric state, that is, it becomes spontaneously polarized. At this transition, both the cubic and tetragonal states are thermodynamically stable forms, as seen from the free energy vs polarization curves (Figure 3.7). Figure 3.7 shows two equal minima in the free energy function at 124.5°C, the transition temperature. For the unstrained, cubic crystal, the free energy, as a function of polarization, is defined as zero.

$$A = \frac{a}{2} P_s^2 + \frac{b}{4} P_s^4 + \frac{c}{6} P_s^6 = 0 \qquad (3.6)$$

P_s is the spontaneous polarization. The free energy of the tetragonal form of barium titanate at the Curie transition is also zero.

Hence

$$\frac{dA}{dP} = aP_s + bP_s^3 + cP_s^5 = 0 \qquad (3.7)$$

From (3.6) and (3.7) Devonshire obtained the relations

$$P_s^2 = -\frac{3}{4}\frac{b}{c}, \qquad (3.8)$$

and

$$a = \frac{3}{16}\frac{b^2}{c}. \qquad (3.9)$$

Having determined the experimental values for P_s and a, (from the dielectric behavior of barium titanate which follows the Curie-Weiss law above the tetragonal to cubic transition temperature), he was able to determine the coefficients b and c . He extended his theoretical analysis to the low temperature forms of barium titanate and was able to determine correctly the transition temperatures of the tetragonal to orthorhombic and orthorhombic to rhombohedral forms.

Devonshire has also discussed the case where barium titanate is measured under constant strain. He finds that the strains are proportional to the square of the polarization. Furthermore, he predicts that the ferroelectric to paraelectric transition in a clamped single crystal is of the second order rather than the first order, (i.e., the temperature dependency of the polarization is continuous at the transition temperature, whereas it shows a sharp discontinuity for the unstressed crystal).

Subsequently additional coefficients in Devonshire's equations, (e.g., coefficients b, c), were determined by other investigators. Kaenzig and Maikoff[79] published a series of free energy curves of barium titanate as a function of polarization (Figure 3.7), and Merz[78] showed curves of the variation of polarization with electric field.

G. Ceramic Perovskite Ferroelectrics

Ceramic ferroelectric materials can be crudely visualized as a tightly bonded aggregate of rather imperfect and randomly oriented single crystals. The interaction of the crystallites in the ceramic is complicated by the occurrence of stresses, internal strains, and in the case of

mixed titanate compositions, by small compositional variations among the grains. This results in a ceramic having properties which differ substantially in some respects from that of a single, unclamped crystal. For example, the transition temperature of the ceramic does not occur at a well defined temperature, but rather over a narrow temperature range because the crystallites themselves have slightly differing Curie temperatures. The value of the permittivity peak in the ceramic is not as high as it is in the single crystal.

There are other notable differences. A ferroelectric crystal of $BaTiO_3$ responds to an externally applied DC field by orienting its polar axis in the field direction.(69) This occurs within the entire ferroelectric temperature range.(69)

A ceramic barium titanate or mixed barium-strontium titanate type ceramic, however, responds to the field mainly in the region of its tetragonal to cubic transition. It is quite insensitive to the field at lower temperatures where the ceramic is actually composed of a larger number of ferroelectric grains (see Figure 2.3, 2.4). Diamond(62) has developed a theory of non-linear processes in mixed titanate ferroelectric ceramics which provides an explanation for the observed behavior in the ceramics. He demonstrates that the change in permittivity with electric field may be explained as an induced ferroelectric state in grains which are paraelectric at zero bias rather than due to domain orientation. The ferroelectric ceramic is represented as a collection of individual grains whose permittivities depend on composition, field, and temperature. The net incremental permittivity of the material

$\langle \epsilon(T,E) \rangle$ is taken as a statistical average of the permittivities $\epsilon(T, T_c^*, E)$ of the individual grains composing the ceramic. Hence

$$\langle \epsilon(T,E) \rangle = \frac{\int_0^\infty \epsilon(T, T_c^*, E)\, e^{-\left(\frac{T_c - \gamma E - T_r}{\alpha}\right)^2} dT_c^*}{\int_0^\infty e^{-\left(\frac{T_c^* - \gamma E - T_r}{\alpha}\right)^2} dT_c^*} \qquad (3.10)$$

T_r is the temperature of the peak incremental permittivity, T_c the Curie temperature of the crystal at zero field. T_c is approximately related to T_c^*, the Curie temperature of the crystal with field, by the equation $T_c = T_c^* - \gamma E$. T is the temperature, and α is the variance of the statistical distribution. α is largely determined by the history of the ceramic, i.e., how it is prepared, how well it is fired, and how complete the solid solution, etc.

Basing his assumptions on Merz's data on the dielectric behavior of barium titanate single crystals[70] (Figure 2.5), Diamond[62] has set up three conditions to describe the permittivity contributions of the ceramic crystallites to the total incremental permittivity of the ceramic in the tetragonal to cubic temperature range. They are:

$$\epsilon(T_c^*, T, E) = \begin{cases} \dfrac{4\pi C}{T - T_o} & \text{for } T > T_c^* \\ \begin{bmatrix} \epsilon_a & \text{for } \perp \text{ field} \\ \epsilon_c & \text{for } /\!/ \text{ field} \end{bmatrix} & \text{for } T_c \leq T \leq T_c^* \\ \epsilon_{av.} & \text{for } T < T_c \end{cases} \qquad (3.11)$$

Equation (3.11) states that (1) for $T > T_c^*$ the grains follow a Curie-Weiss law as for single crystals; (2) for $T_c \leq T \leq T_c^*$, the grains which were non-ferroelectric in the absence of an electric field now have a ferroelectric state induced in them in accordance with the free energy function. It is assumed that the polar axis of the induced ferroelectric state lies in the field direction; (3) for any grain in which $T < T_c$, ϵ is presumed to be $\epsilon_{av.}$, that is, all ferroelectric domains are considered to be frozen in. Evaluation of the integral leads to results which are in excellent agreement with the experimental dielectric data.

The optical examination of ceramic barium-strontium titanate ceramics discussed in the following sections represents an observational check of the non-linear processes with field in the ceramic grains at their ferroelectric to paraelectric transition.

H. Optical Observation of Ceramic Ferroelectrics

A number of investigators[108-115] have gathered much illuminating information on the twinning structure of ferroelectric titanates by employing the metallographic techniques of polishing and etching, and then by examining the surfaces with petrographic as well as electron microscopes. 90° domains have been found in abundance as well as 180° domains. By renewed polishing and etching of a sample after exposure to high DC fields, DeVries and Burke[112] were able to transform some anti-parallel 180° domains into a region of uniform polarization. They found however, that the 90° domains had only been very little affected by the field. This seems to bear out similar observations made on single crystals.

IV EXPERIMENTAL PROCEDURE

A. Preparation of Samples

Seven compositions of mixed barium-strontium titanate ceramics were chosen for optical observation and capacitance measurements. They are listed by their compositions in Table 4.1. The ferroelectrics all have peak incremental permittivities at or above room temperature, so that they can be observed at the temperature of their tetragonal to cubic transition by simply using a heating stage.

In order to prepare a sample for microscopic observation by transmitted light, a thin slab is imbedded in a thermosetting resin and then ground flat on a metallurgical wheel, using a series of graded silicon carbide papers. Subsequently the material is polished with coarse and fine diamond paste, until a minimum of pits and scratches are observed. The sample is then removed from the plastic, is cut into the desired size, and is glued to a microscope slide with the polished side down. Eastman 910[116] adhesive, a strong, colorless polymerizing cement of index $n = 1.45$, has proved to be satisfactory for this purpose. The mounted sample is then reimbedded in plastic, with the rough ceramic side exposed, and is ground and polished to 30 - 40 microns thickness. After removing the plastic, the sample is electroded along its edges (Figure 4.1) with evaporated silver or silver paint. Aluminum foil leads are attached to the electrodes, and the sample is then ready to be measured.

Unfortunately, thin sections of the dimensions described, namely approximately 1 cm x .1 cm x .004 cm (Figure 4.1a), have electrical capacitances of less than 1$\mu\mu$f. Any variation in sample capacitance with

TABLE 4.1

COMPOSITION AND DIELECTRIC DATA FOR SEVEN
BARIUM-STRONTIUM TITANATE CERAMICS

Sample	Composition, mole %	Approximate Peak,	Curie Temp., °C
1	75% $BaTiO_3$ 25% $SrTiO_3$	3100	49
2	75.0% $BaTiO_3$ 24.9% $SrTiO_3$ .1% $UO_2(NO_3)_2$	4500	51
3	73.5% $BaTiO_3$ 24.5% $SrTiO_3$ 2.0% CdO	5500	52
4	85% $BaTiO_3$ 15% $SrTiO_3$	1110	83
5	Aerovox Corp. Formula	1950	30
6	85% $BaTiO_3$ 14% $SrTiO_3$ 1% Fe_2O_3	1200	48
7	74.25% $BaTiO_3$ 24.75% $SrTiO_3$ 1.00% Nb_2O_5	(6000)*	(20)*

* Value obtained from a larger ceramic sample of the same composition. The Sample 7 used for transmitted light intensity measurements had too low a capacitance for accurate determination.

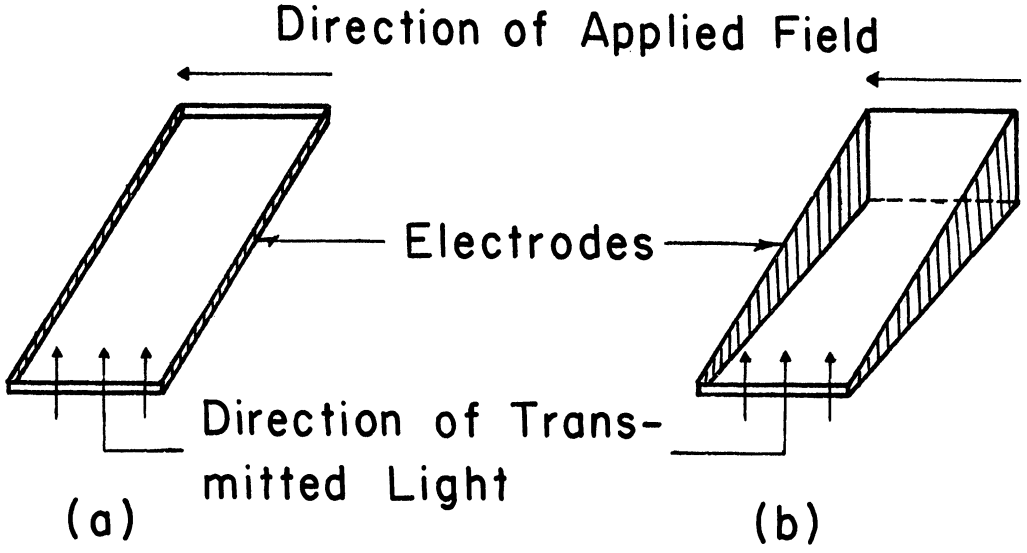


Figure 4.1. Sample Configuration of a (Ba,Sr)TiO_3 Ceramic.
(a) Uniform Thin Section
(b) Wedge

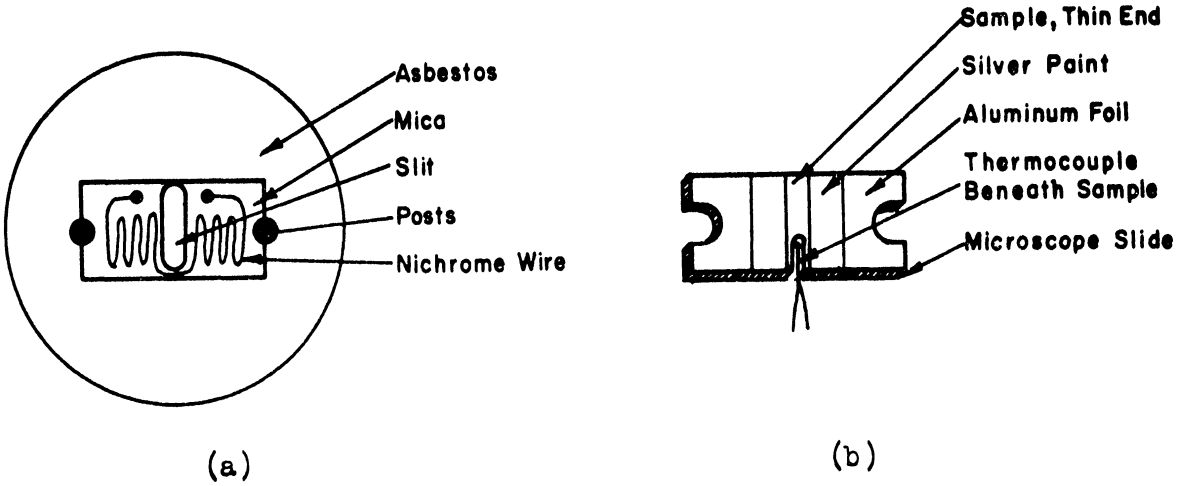


Figure 4.2. Heating Stage (a), and Mounted Sample (b), Used in the Observation of a Ceramic Thin Section by Transmitted Light.

field or temperature can only be detected with great difficulty because of stray capacitances in the circuit and surrounding media. It was therefore necessary to resort to a new, wedge-shaped geometry. The modified sample is thin enough at one end to allow observation by transmitted light, yet it has a sufficiently high total capacitance to enable accurate electrical measurement (Figure 4.1b). The wedges prepared were approximately .8 cm long, .1 cm wide and had a thickness of around .1 cm at one end and .004 cm at the other. They were mounted on a glass slide as before, provided with electrodes, and placed on a heating stage.

B. Measuring Equipment

1. The Heating Stage

A simple stage was devised to observe the ferroelectric to paraelectric transition in the samples. Nichrome wire wound around a strip of mica is attached to an asbestos disk (Figure 4.2a). A slit in the center of the disk allows passage of light to the sample which is placed over the slit (Figure 4.2b). Metal posts on the disk keep the sample in position and act as contacts for the electrical circuitry. An iron-constantan thermocouple is placed in a notch directly beneath the thick end of the sample and the temperature is obtained from the potentiometer readings of the thermocouple voltage. The heating rate of the stage during the course of an experiment is manually regulated by a variac. The entire holder is placed on the stage of a Leitz Panphot microscope (Figure 4.3).

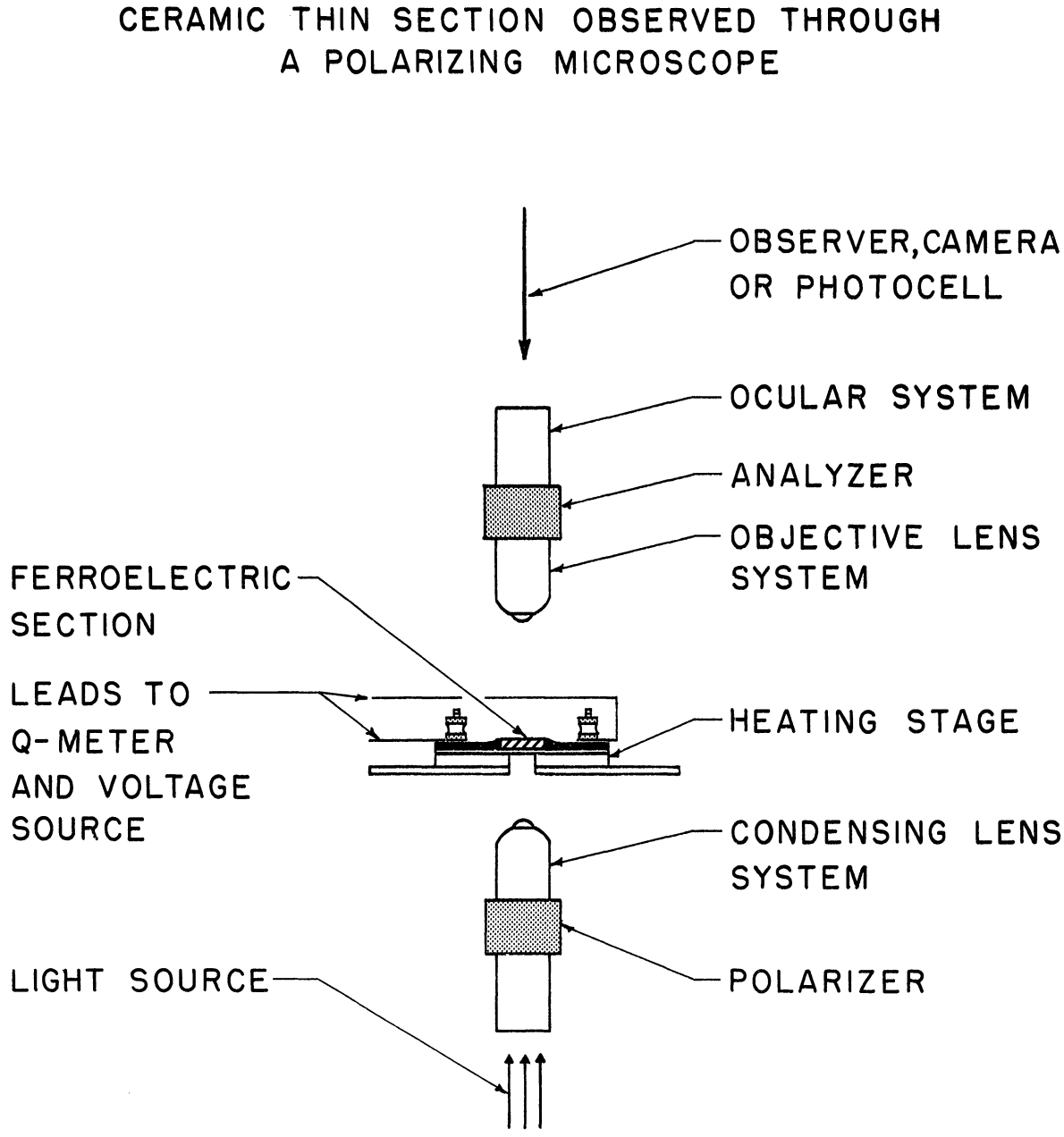


Figure 4.3. Ceramic Thin Section Observed Through a Polarizing Microscope.

2. Capacitance Measurements

Capacitance measurements were taken at 1600 KC on a Bontoon Radio Corporation Q-Meter. A 1300 volt battery box supplied the DC field applied to the ferroelectric wedge. Figure 4.4 shows a schematic of the circuit. A standard resistor, $R_{standard} \cong 10$ megohm and a standard capacitor, $C_{standard} \cong 110$ μμf are introduced as protective measures. The resistor prevents a large current flow through the sample, and the capacitor isolates the Q-meter from the large DC voltage source. The capacitance of the sample holder, C_h, is approximately 24 μμf, the capacitance of the sample, C_o, is about 15-60μμf.

The actual sample capacitance can be easily computed by determining the capacitance C_o as measured across the Q-meter terminals and the capacitance of the sample holder (microscope slide with foil leads, heating stage posts, and coax cables leading to the Q-meter, Figure 4.2 and 4.3).

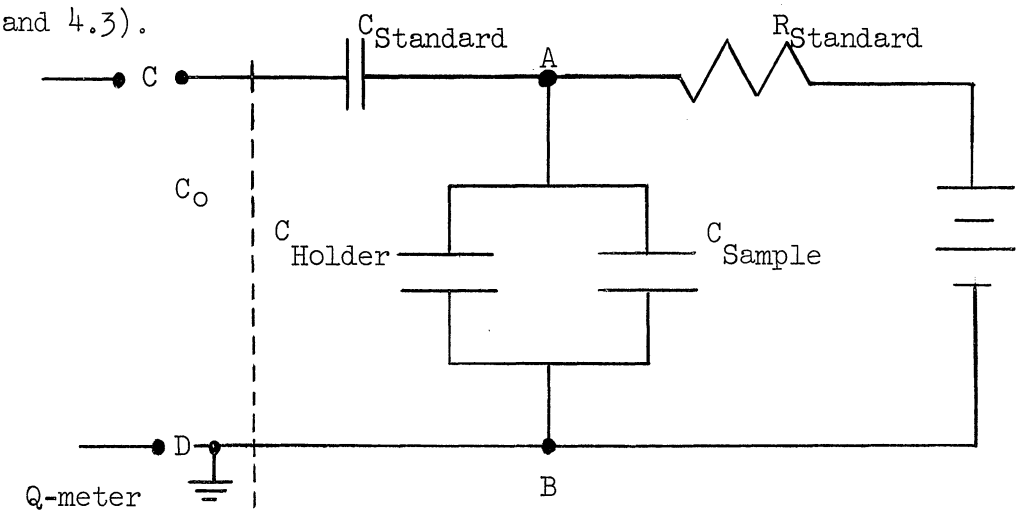


Figure 4.4. Circuit for Capacitance Measurements

Let C_o be the measured capacitance across the Q-meter terminals C-D,

let C_{ST} be the standard capacitance,

C_H the capacitance of the sample holder,

and C_S the actual capacitance of the sample.

Let the impedance across the Q-meter terminals be

$$Z_{CD} = \frac{-j}{\omega C_o} = Z_{AB} \frac{-j}{\omega C_{ST}} . \tag{4.1}$$

Then the impedance across AB (see Figure 4.4) is

$$Z_{AB} = \frac{-j}{\omega(C_H+C_S)} . \tag{4.2}$$

After combining Equations 4.1 and 4.2,

$$\frac{-j}{\omega C_o} = \frac{-j}{\omega(C_H+C_S)} \frac{-j}{\omega C_{ST}} . \tag{4.3}$$

Therefore

$$\frac{1}{C_o} = \frac{1}{C_H+C_S} + \frac{1}{C_{ST}} , \tag{4.4}$$

and

$$\frac{1}{C_o} = \frac{C_{ST} + C_H + C_S}{C_{ST}\,(C_H + C_S)} . \tag{4.5}$$

Hence the actual capacitance of the sample is given by

$$C_S = \frac{C_o\,(C_{ST} + C_H) - C_{ST}\,C_H}{C_{ST} - C_o} . \tag{4.6}$$

Prior to taking measurements, the sample is heated and cooled a number of times through its peak permittivity temperature. Capacitance measurements are then taken on the sample at zero field and three different voltages. Simultaneously, the thin end of the material is observed optically and measurements of light transmission are taken with a cadmium sulfide photocell placed directly over the microscope eyepiece (Figure 4.3).

3. Intensity Measurements

Intensity measurements of the light transmitted by a thin section between crossed polars give an indication of the integrated birefringence of the ferroelectric grains under observation. The measured intensities can be empirically correlated with the proportion of ferroelectric grains in the mixed titanate samples, as shown in Section VI.

While observing a barium strontium titanate ceramic, the following assumptions are made:

1. A total extinction of the optical field indicates a completely isotropic, paraelectric material.
2. Maximum brightness of the optical field indicates an extensively ferroelectric material in which all grains are tetragonal.
3. In the region of the peak permittivity the percent of light transmitted by the thin section can be correlated with the percentage of ferroelectric grains in the sample.

The light measurements were taken with a cadmium sulfide photocell. Microammeter readings of the light transmitted by a sample were compared with readings obtained from a calibrated Kodak density film strip. For this purpose the strip was placed in the same position as the sample.

During the measurements of both film strip and sample, the intensity of the light source was held as nearly constant as possible. The graded densities of the film yielded successive microammeter readings which were then converted to a calibration curve of percent transmission vs microamperes. (See Appendix B).

The entire light detecting device consists of the cell, a 75 volt battery, a microammeter, and several resistances (Figure 4.5). The light source of the microscope, a tungsten filament lamp, appeared to have a steady light output. As a precaution, a regulating transformer was introduced between the main line and the microscope. At times a slight drift was observed in the voltage output of the mains over a period of several hours. To correct for this change, the photocell was calibrated against the density strip before and after every run, and appropriate adjustments were made in the intensity values of the samples measured. (See Appendix B.)

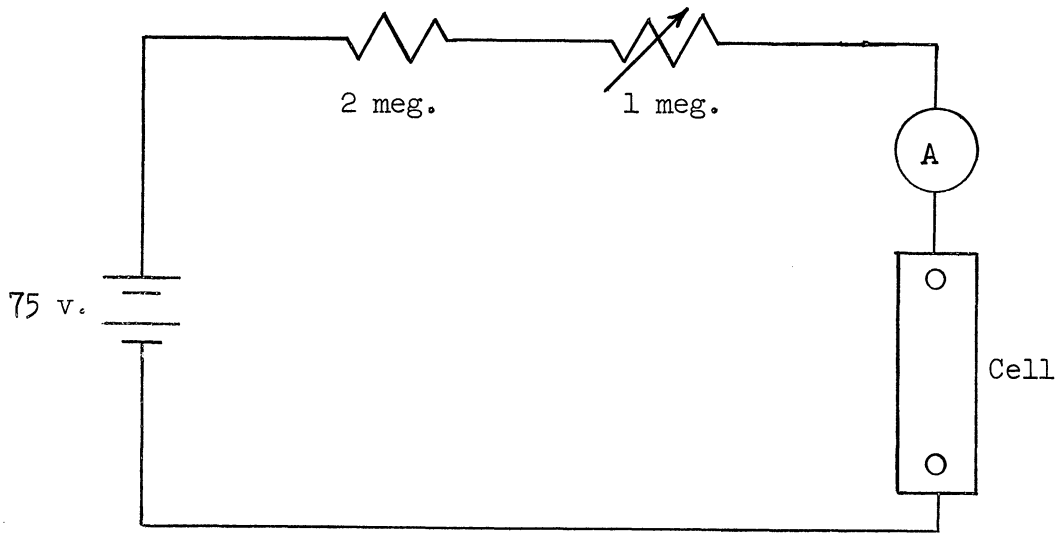


Figure 4.5. Circuit for Light Intensity Measurements by a Photocell.

V DATA AND OBSERVATIONS

The material in this section has been classified under two main headings: "Data" and "Observations."

"Data," taken on ceramic wedges of mixed barium-strontium titanate compositions, contain the results of the capacitance versus temperature and the percent light transmission versus temperature measurements, with voltage as a parameter. A distinction is made between large-grained (50 - 150μ) and fine-grained (3 - 15μ) ceramics because of some important differences in their dielectric as well as optical behavior. (None of the investigated samples consisted of grains of an intermediate size, i.e., approximately 15 - 50 μ.) The data are analyzed with respect to two proposed explanations of the field produced non-linear dielectric effect in ceramic titanate ferroelectrics. They are:

1. Nonlinearity due to the alignment of ferroelectric domains in the direction of an applied DC field, and
2. Nonlinearity due to a field induced ferroelectric effect in the peak permittivity region of the ceramic.

"Observations" include all optical phenomena that were observed in individual grains during the course of this investigation. They are confined to the thin section end of large-grained ceramic wedges where the grains are readily visible by transmitted polarized light. The fine-grained "thin sections" are almost opaque in transmitted light due to the light scattered at the many grain boundaries in the ceramic.

The changes produced in the large-grained samples with varying temperature and field have been classified as (1) short term and (2) long

term effects. They are defined in the following manner:

1. Short term effects occur instantaneously when a sample is exposed to a change in temperature or to an applied DC field. As soon as temperature and field are returned to their initial condition, the ceramic reverts to its original state.
2. Long term effects are also brought about by an applied voltage or by a temperature change, but they persist for some time after the original values of external condition have been restored.

Both effects are discussed in some detail and interpretations have been provided wherever possible.

A. Data

1. Presentation of Data

Figures 5.1 - 5.13 illustrate the data taken on ceramic wedges of barium-strontium titanate compositions. They represent the capacitance versus temperature of the samples, with a DC field as a parameter. For the sake of visual clarity, no data points have been shown on the curves. The points lie close together, especially on either side of the peak incremental permittivity temperature, where they tend to crowd the figures. The data for each sample is tabulated in Appendix A.

Furthermore, to facilitate comparison of the figures, the heating and cooling curves obtained for each set of measurements have been averaged into a single curve. This is considered permissible for the

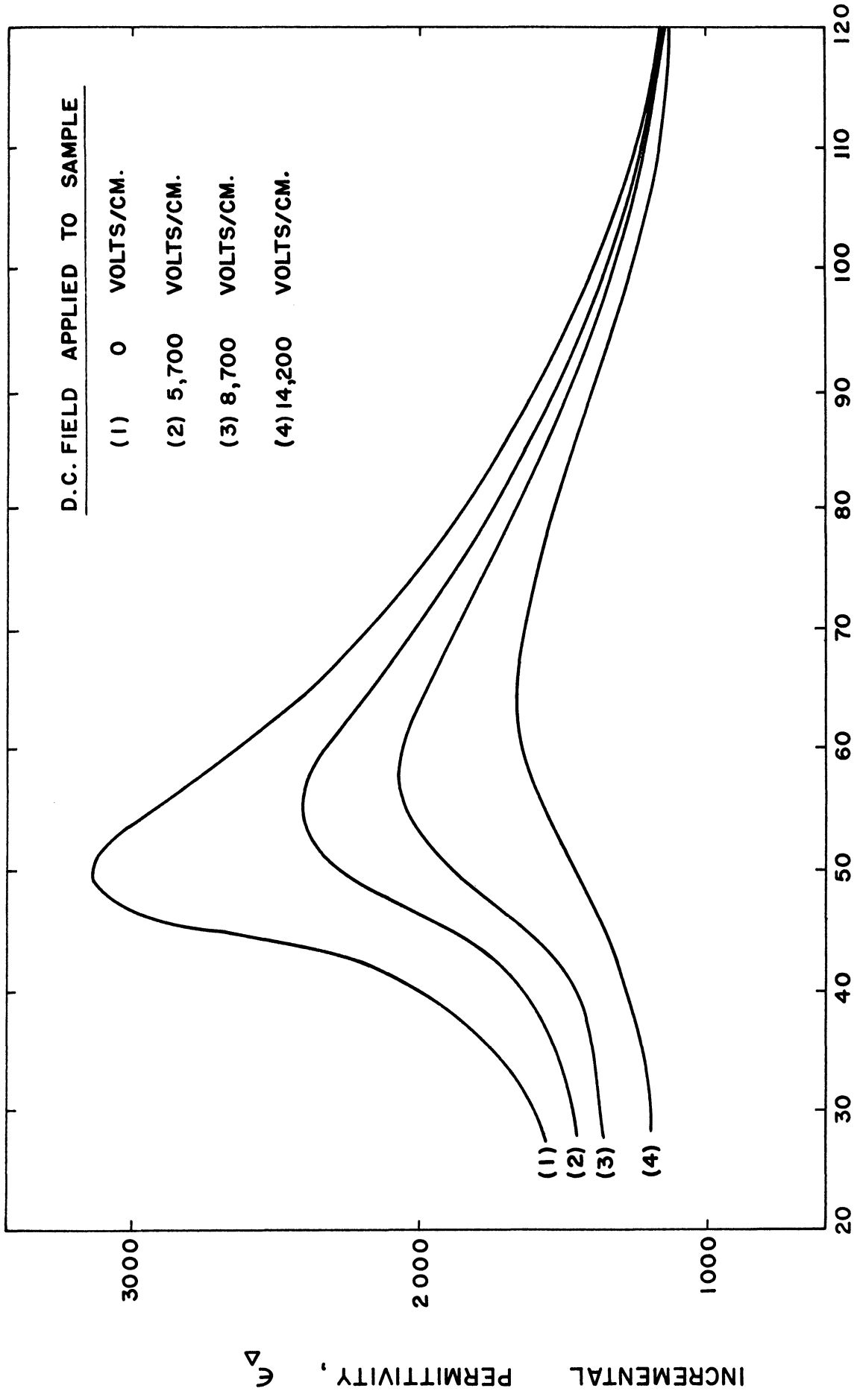


Figure 5.1. Incremental Permittivity vs. Temperature of Ceramic Sample 1, with Voltage as a Parameter.

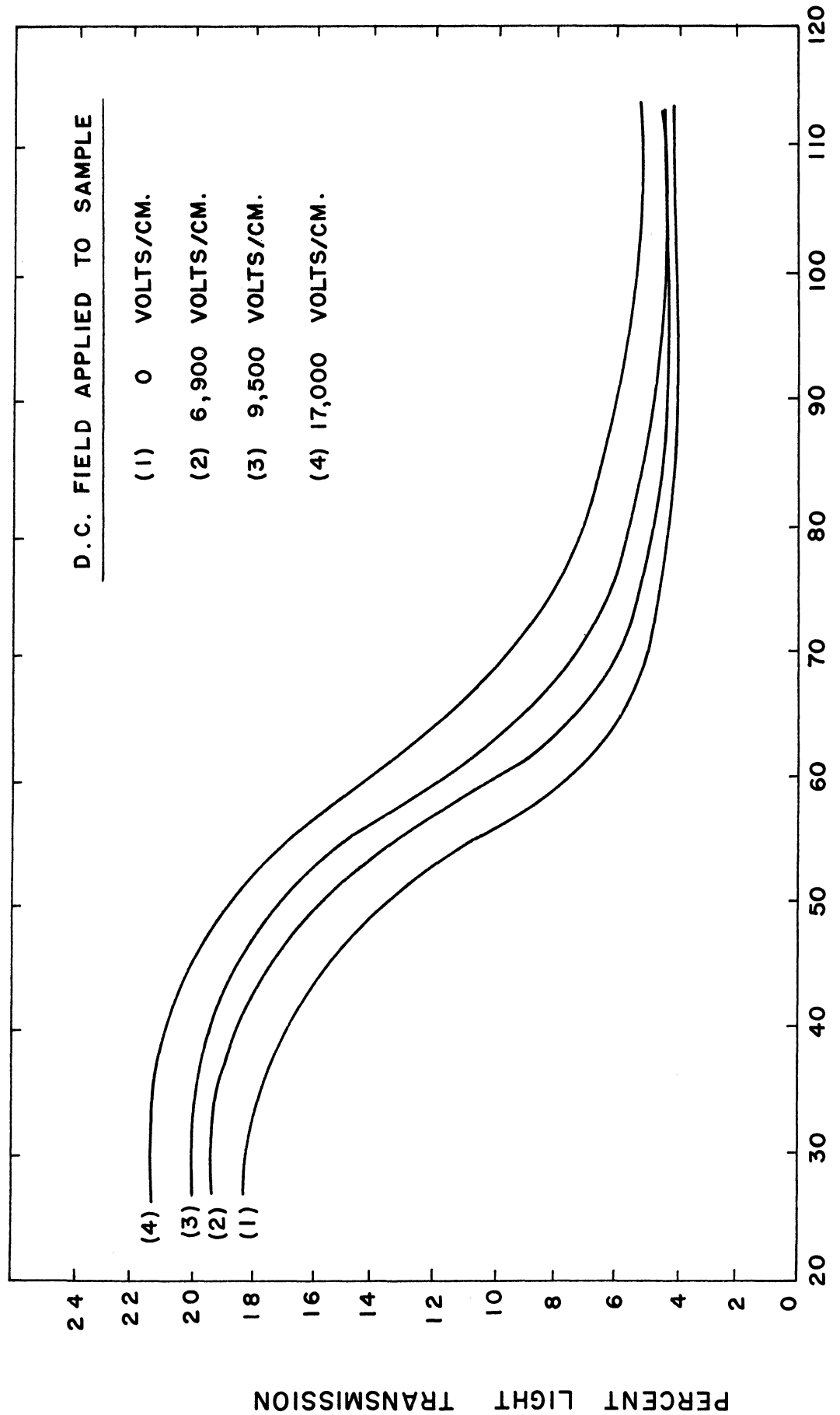


Figure 5.2. Percent Light Transmission vs. Temperature of Ceramic Sample 1, with Voltage as a Parameter.

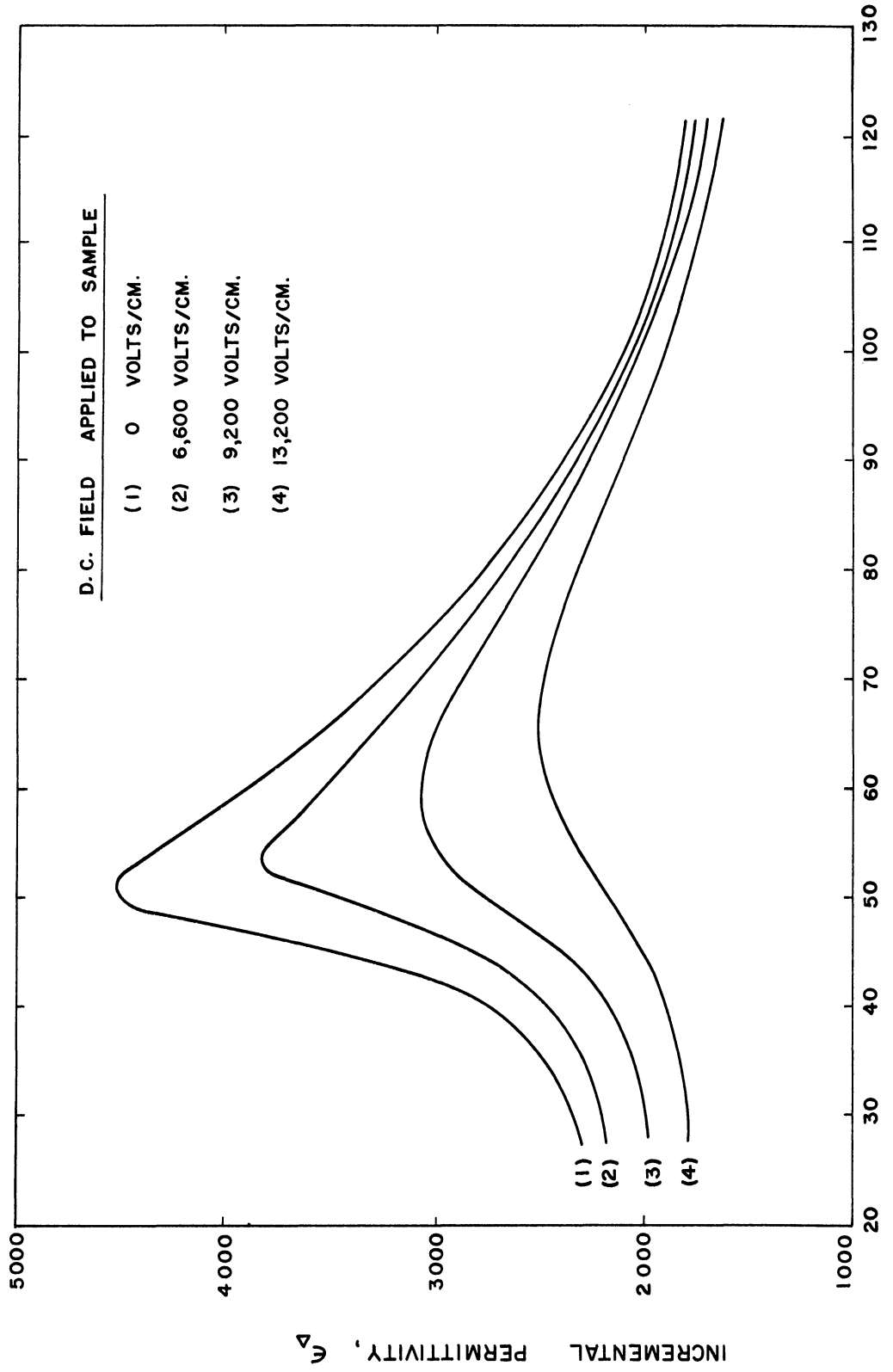


Figure 5.3. Incremental Permittivity vs. Temperature of Ceramic Sample 2, with Voltage as a Parameter.

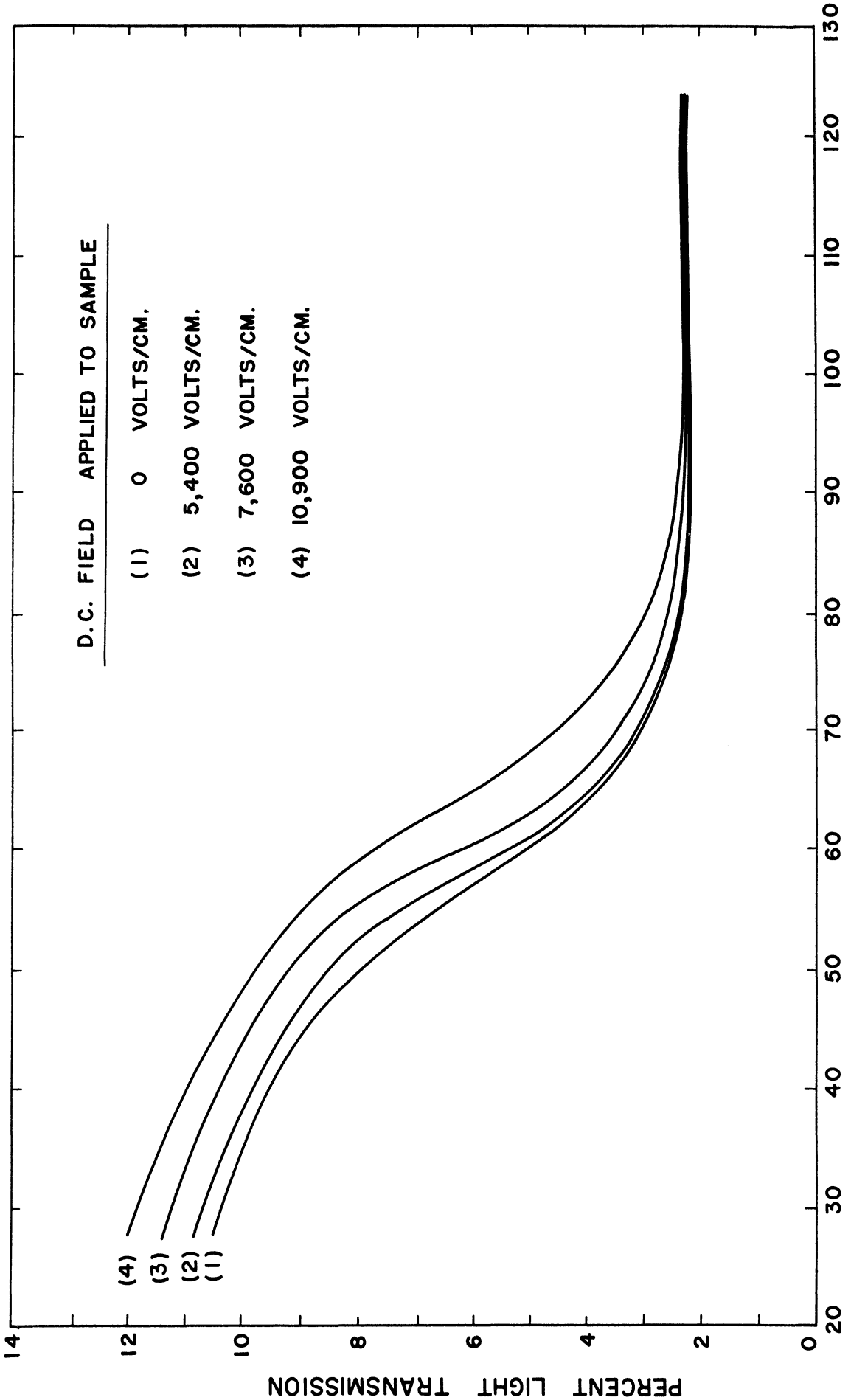


Figure 5.4. Percent Light Transmission vs. Temperature of Ceramic Sample 2, with Voltage as a Parameter.

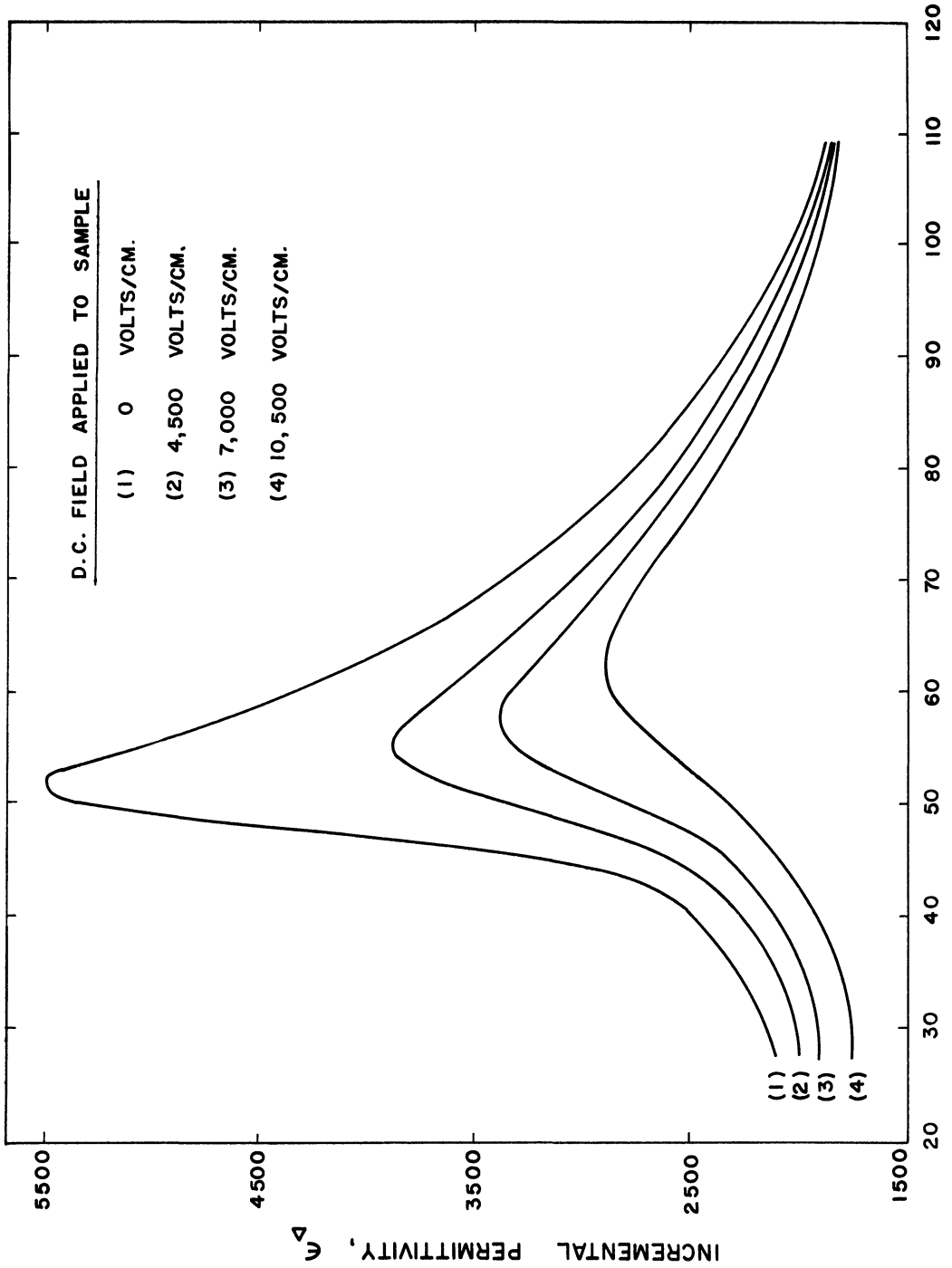


Figure 5.5. Incremental Permittivity vs. Temperature of Ceramic Sample 3, with Voltage as a Parameter.

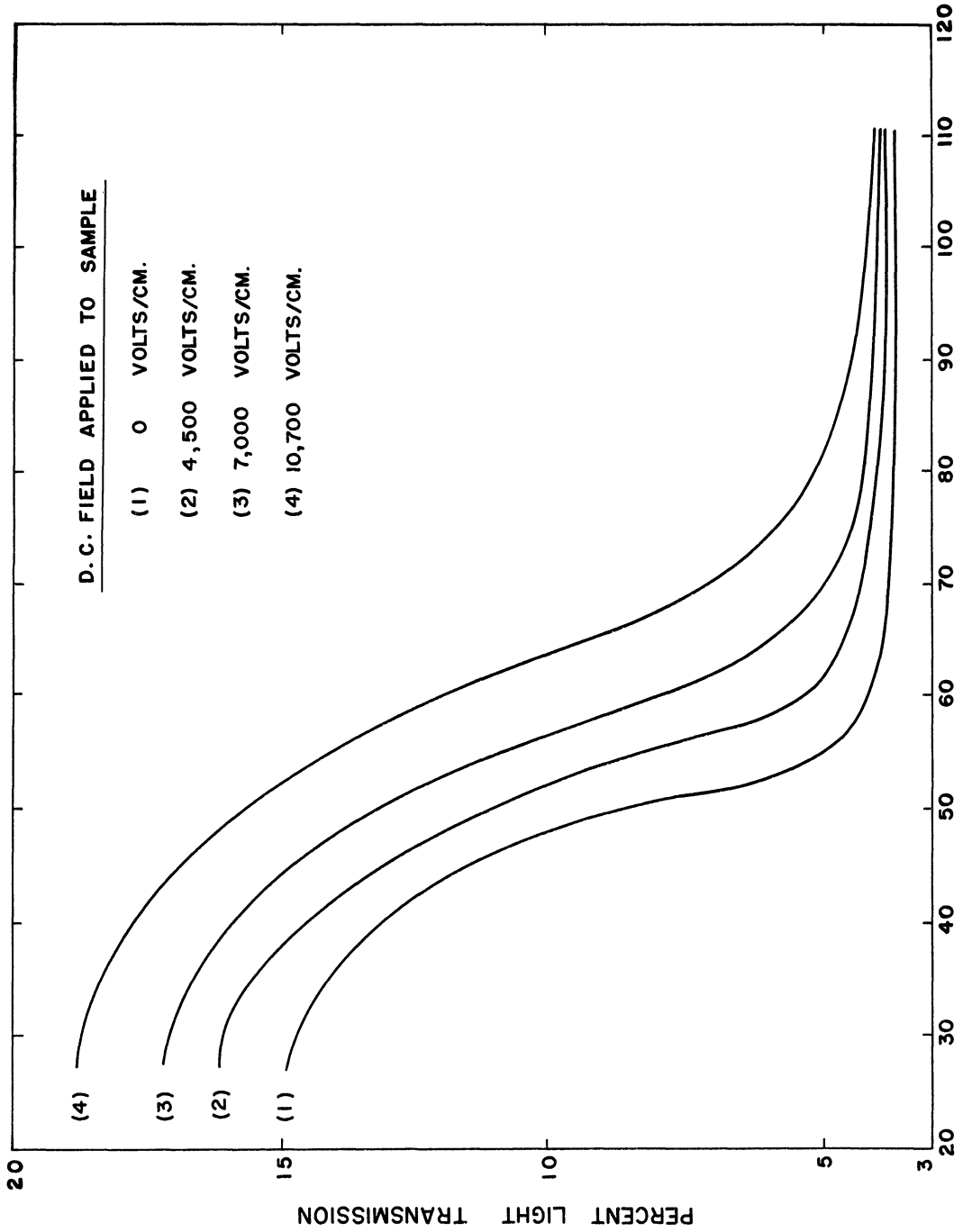


Figure 5.6. Percent Light Transmission vs. Temperature of Ceramic Sample 3, with Voltage as a Parameter.

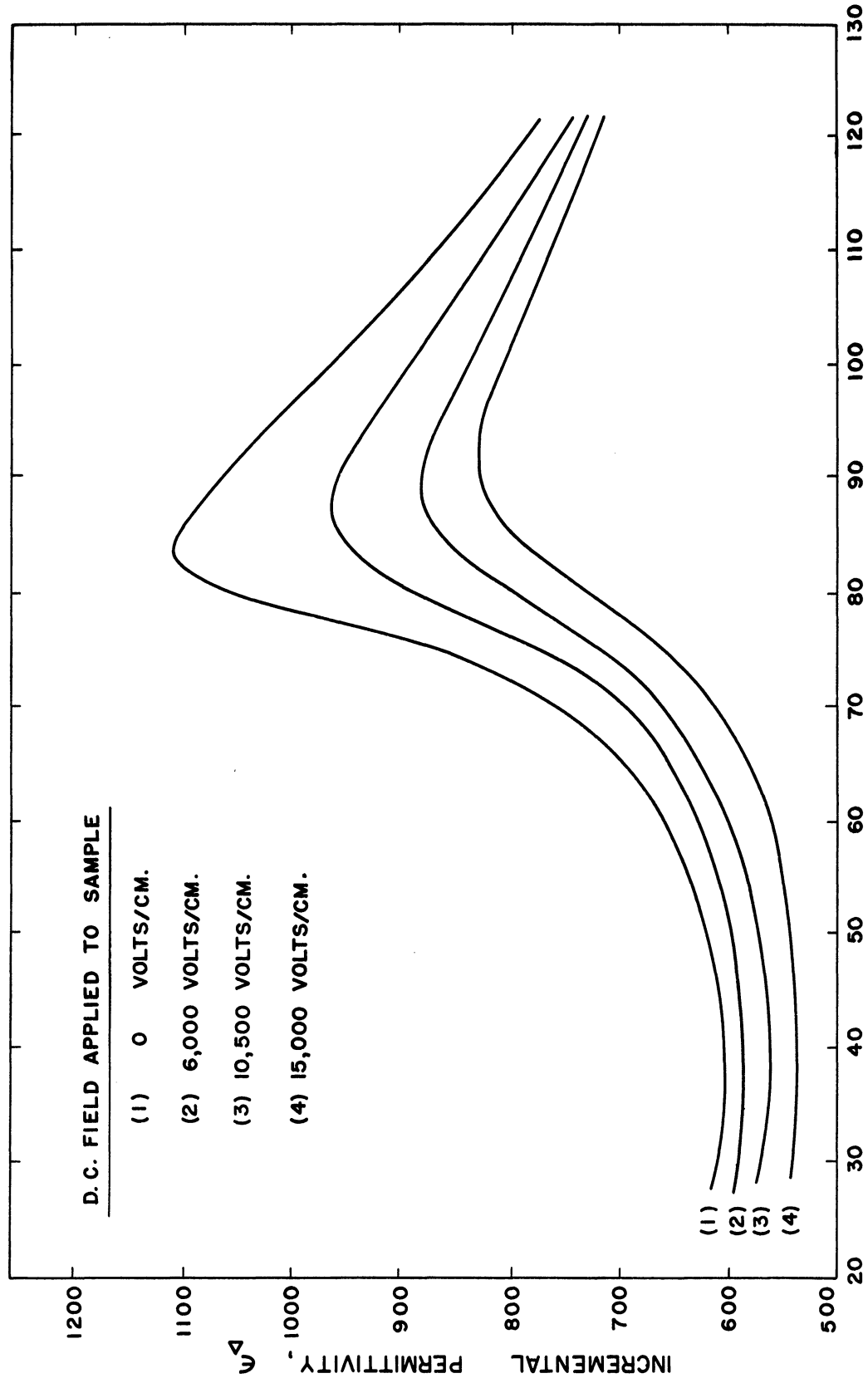


Figure 5.7. Incremental Permittivity vs. Temperature of Ceramic Sample 4, with Voltage as a Parameter.

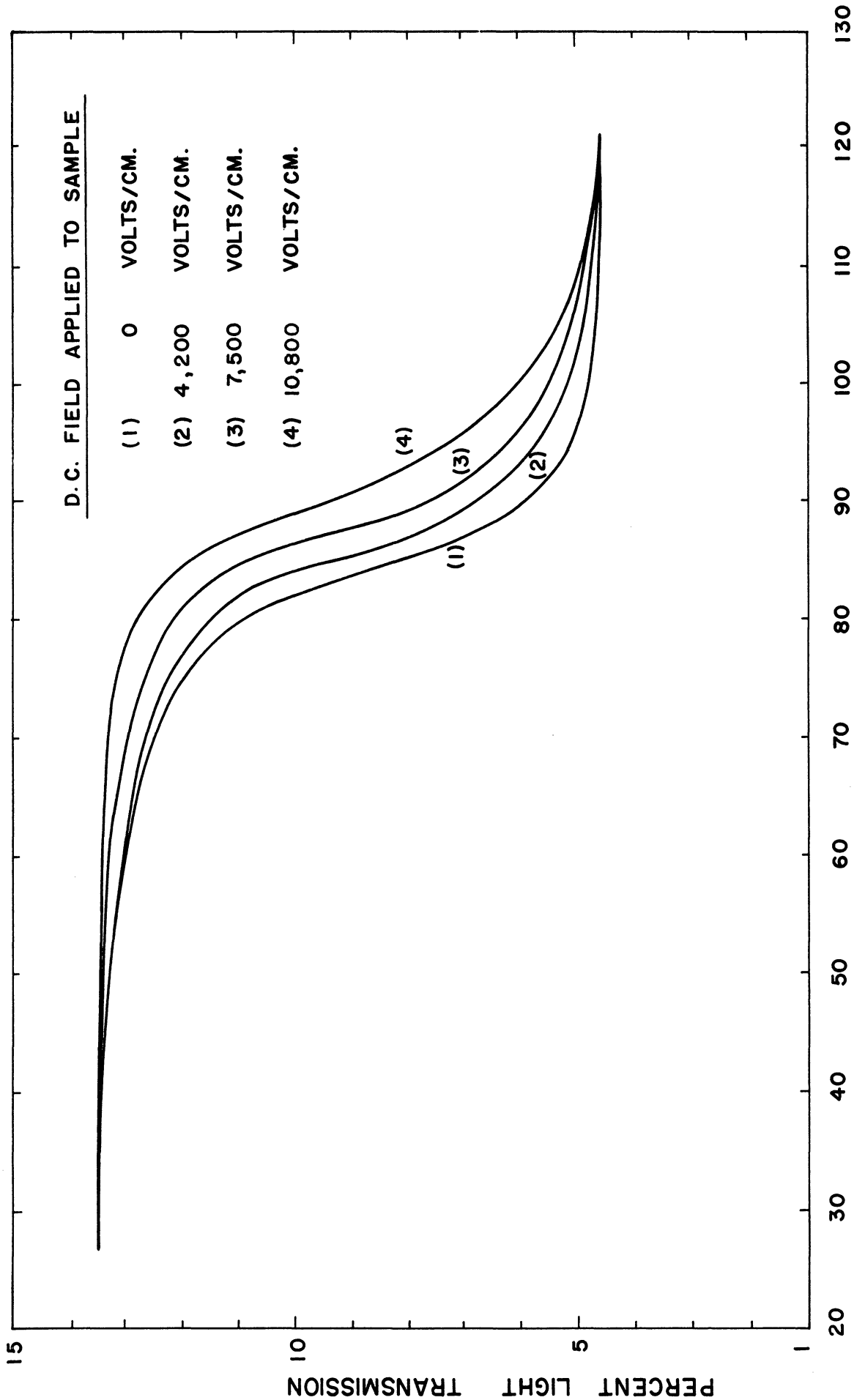


Figure 5.8. Percent Light Transmission vs. Temperature of Ceramic Sample 4, with Voltage as a Parameter.

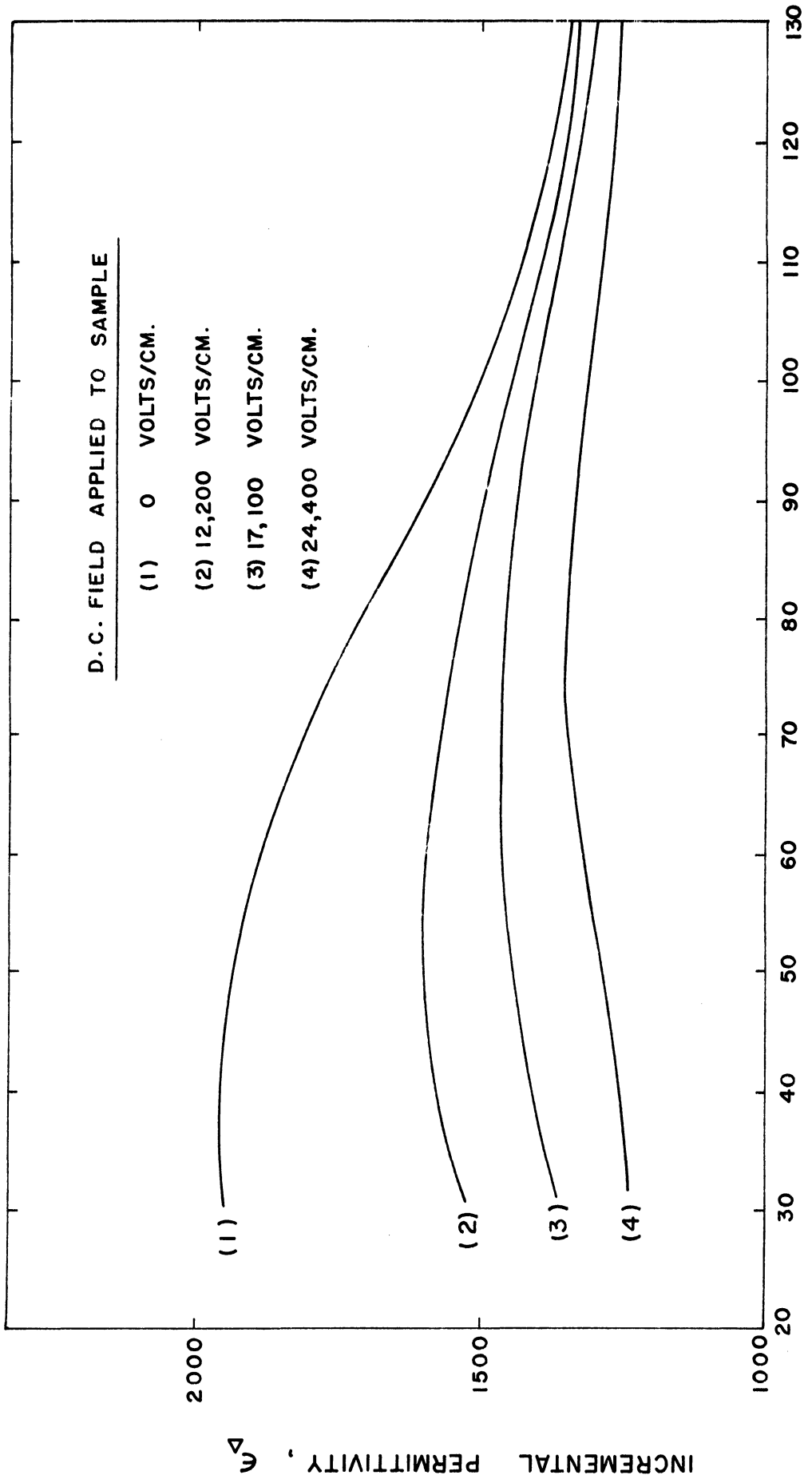


Figure 5.9. Incremental Permittivity vs. Temperature of Ceramic Sample 5, with Voltage as a Parameter.

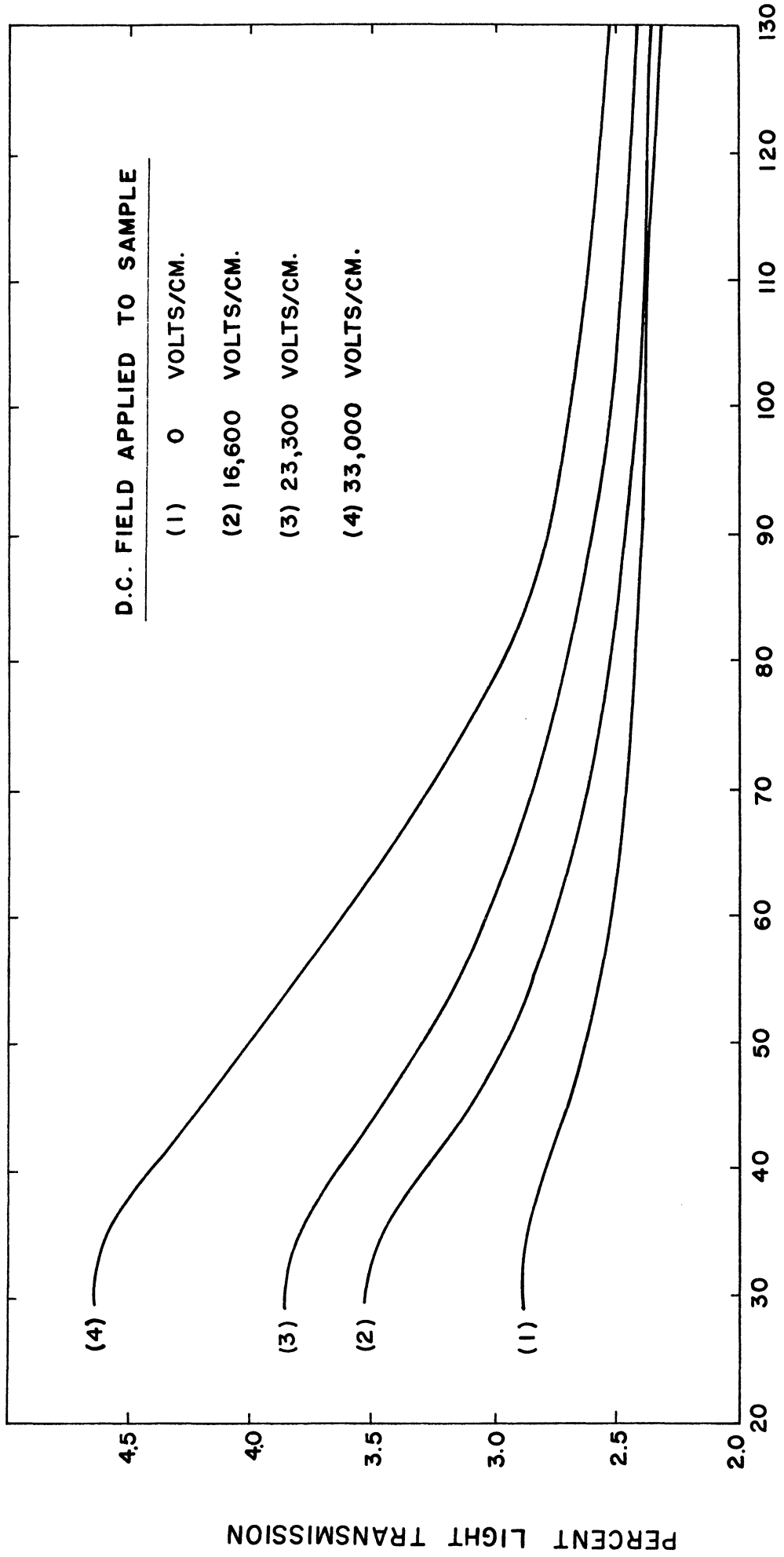


Figure 5.10. Percent Light Transmission vs. Temperature of Ceramic Sample 5, with Voltage as a Parameter.

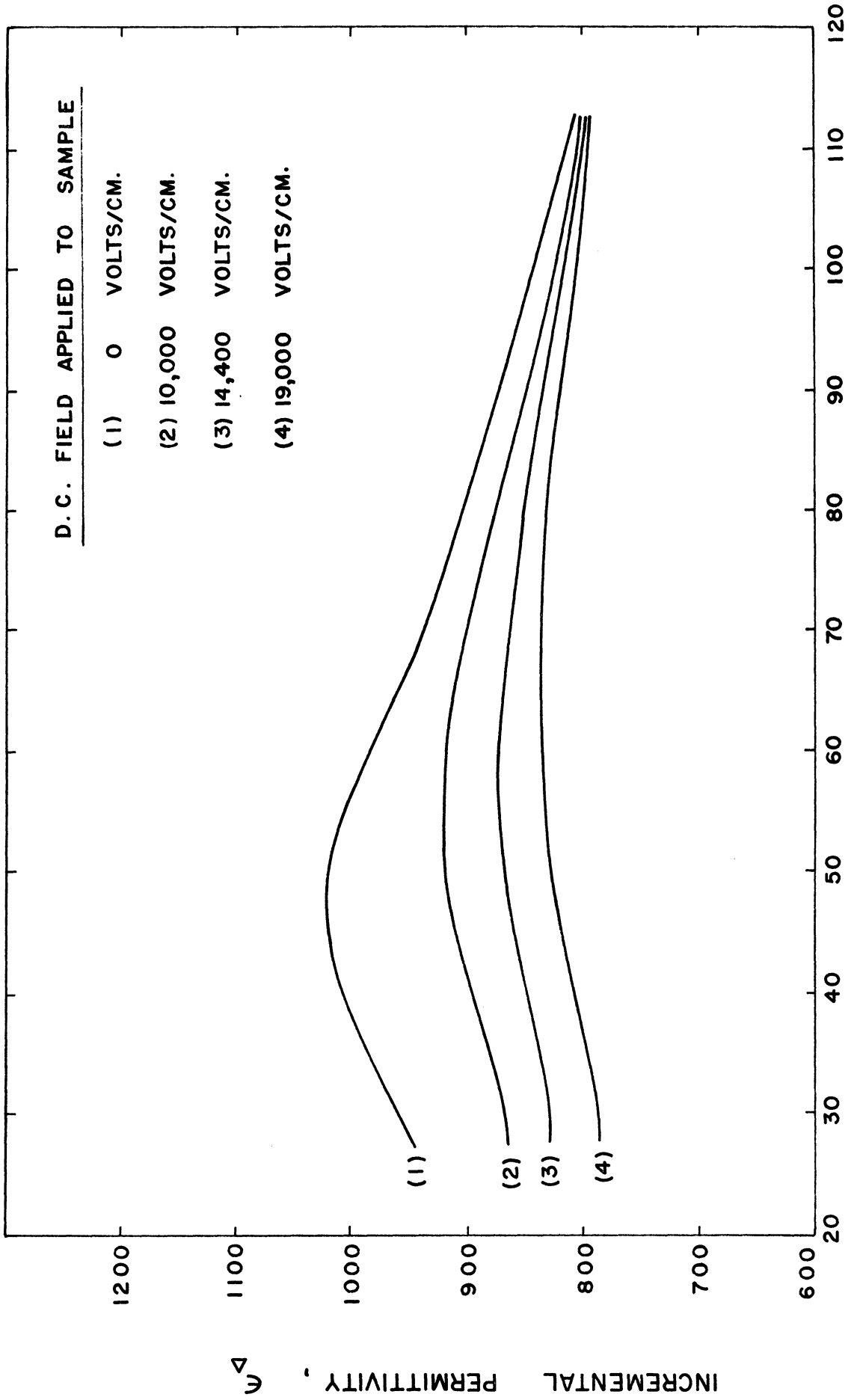


Figure 5.11. Incremental Permittivity vs. Temperature of Ceramic Sample 6, with Voltage as a Parameter.

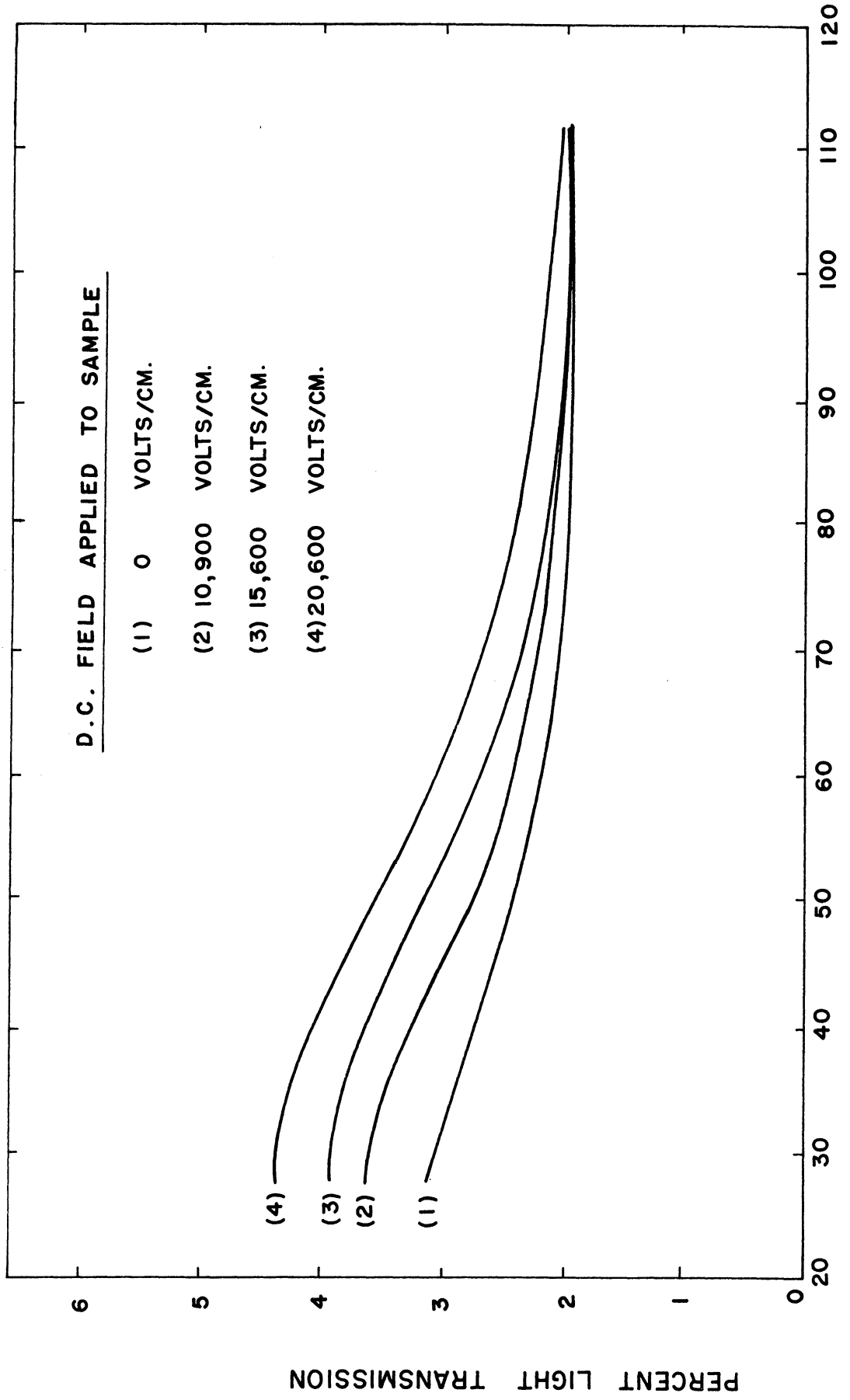


Figure 5.12. Polarization as a Function of Temperature, with and without a Biasing Field.

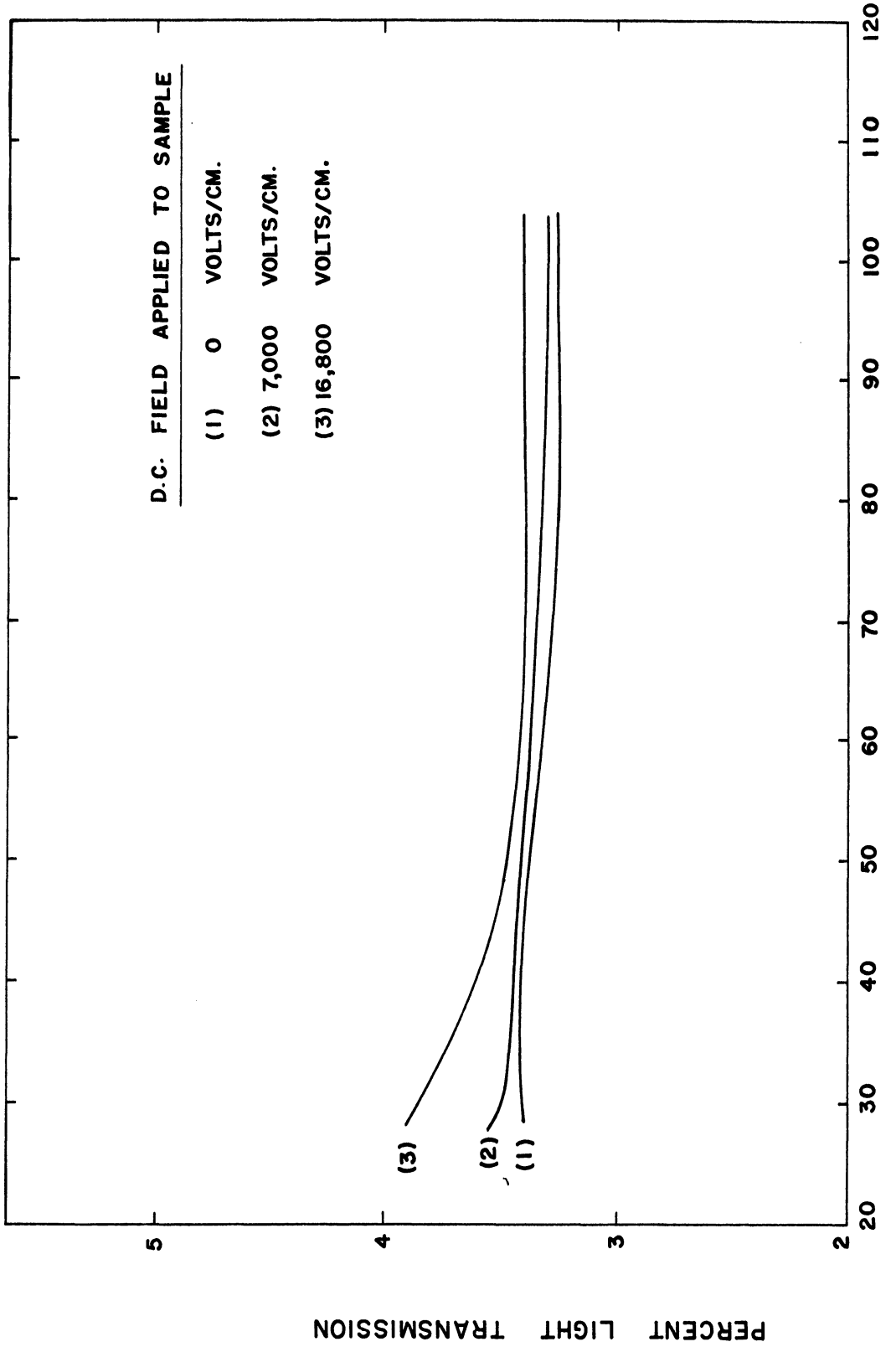


Figure 5.13. Percent Light Transmission vs. Temperature of Ceramic Sample 7, with Voltage as a Parameter.

following reasons:

1. Although a temperature hysteresis is observed in the samples, the effect is relatively small. Depending on the composition, it ranges from 0 - 3° between heating and cooling cycles.
2. The peak incremental permittivity in all samples is somewhat larger during the cooling cycle than the heating cycle, regardless of whether a field is applied to the sample or not. Condensing the heating and cooling curves into a single curve therefore does not change the relative dielectric behavior of the samples with respect to each other.
3. The light transmission data do not show any consistent hysteresis effect. The differences in the heating and cooling curves lie within the range of the estimated experimental error. The percent light transmission data is therefore presented as the best curve drawn between the points of measurement.

Appendix A shows tables of the point by point capacitance and percent light transmission measurements taken on the ceramic samples. Appendix C contains a sample calculation which illustrates the method by which the data were reduced.

2. Analysis of Curves

From the permittivity versus temperature curves with voltage as a parameter it can be seen that an applied DC field has the effect of:

1) reducing the value of the peak incremental permittivity, and

2) shifting the peak incremental permittivity to higher temperatures.

The effect of the field on the percent light transmission of the ceramics, the large grained samples in particular, is

1) a considerable increase in anisotropy, especially in the region of the tetragonal to cubic transition,

2) a shift of the curve of percent light transmission toward higher temperatures.

The samples measured can be divided into two categories: one containing ceramics with large grains, the other containing fine-grained material. Thin sections of the first category in which the grain size varies from 50 - 150μ are composed of a monolayer of grains. Thin sections of the second category made from the fine grained material with grain sizes ranging from about 3 to 15μ, consist of several layers of grains. Both groups show a similar trend in the dielectric and optical behavior with temperature and field. However, the light transmitted by the fine-grained samples is substantially reduced due to the large amount of scattering that takes place in the fine-grained complex.

Sample 1 (see Figures 5.1 and 5.2), Sample 2 (see Figures 5.3 and 5.4), Sample 3 (see Figures 5.5 and 5.6), and Sample 4 (see Figures 5.7 and 5.8) belong to the first large-grained category. Sample 5, a commercial barium-strontium titanate ceramic (see Figures 5.9 and 5.10), Sample 6 (see figures 5.11 and 5.12), and Sample 7 (see Figure 5.13) represent the fine-grained category. For a listing of the chemical composition of the samples see Table 4.1.

a. Large Grained Ceramics

Figures 5.1 - 5.8 represent the capacitance and percent light transmission data taken on four large-grained ceramic samples. It is seen in Figures 5.1, 5.3, 5.5 and 5.7, that large fields applied to the samples markedly reduce their peak permittivities. The permittivity and percent light transmission curves also experience a shift to higher temperatures with increasing fields.

Two mechanisms have been proposed in the literature to account for the field produced, non-linear dielectric behavior in perovskite-type ferroelectrics, such as solid solutions of barium-strontium titanate (see Section II-C and Section III-G. They will be briefly discussed here as

1) the mechanism of domain alignment, and

2) the mechanism of induced ferroelectricity.

According to the mechanism of domain alignment, the polar vectors in domains of ferroelectric ceramic grains tend to orient themselves in the direction of an applied field. In this respect, the ceramic is thought to behave similar to a single crystal of barium titanate. A twinned barium titanate crystal, for example, can be ideally transformed into one of uniform polarization by applying sufficiently large fields.[68,69] As a result of the proposed "alignment" of the polar vectors in the field direction, a pronounced decrease in the permittivity of the ceramic can be expected throughout the tetragonal, ferroelectric region. This follows from the dielectric anisotropy of the material. The permittivity along the c-axis of a single crystal of barium titanate permittivity $\epsilon_c \approx 200$, and and the permittivity along the a-axis $\epsilon_a \approx 4000$.

The second model attributes the lowering of the ceramic peak permittivity to a field induced ferroelectric state in the paraelectric grains in the ceramic. The domains in the ferroelectric grains are considered relatively static. 90° domain alignment does not occur according to this theory, although the existence of 180° domain alignment, i.e., a 180° reversal of the polar vector in the domains is recognized. 180° domain switching has been actually observed in ceramics by DeVries and Burke.[112] However, a 180° reversal of the polar vectors in the ceramic does not change the permittivity of the ferroelectric. 180° domain alignment alone therefore does not explain the observed field non-linearity in the ceramic.

According to the second mechanism, the Curie temperatures of the grains composing the ceramic are distributed about the peak permittivity temperature in a Gaussian distribution, the exact shape of which is determined by the history of the material. The grains do not all have the identical transition temperature; their transitions occur over a temperature range. Within this range, both ferroelectric and paraelectric grains can be found side by side, and a large external field produces a ferroelectric state in the paraelectric grains. The polar vector formed in the grains is considered to lie in the direction of the applied field. It can be shown that the total imcremental permittivity of the ceramic drops as a result of the applied field in this temperature region. The model also predicts the observed shift in the peak permittivity temperature with field. This shift has a parallel in the increase in the tetragonal to cubic transition temperature of a single crystal of barium titanate as a result of a large external field.[78]

In the following the dielectric and optical results obtained on the large-grained samples are examined in detail with respect to any evidence of either domain alignment or an induced ferroelectric state in the ceramic grains.

In order to compare the four different ceramic compositions, a reference point, namely the peak incremental permittivity temperature of each composition, is chosen. Criteria are set up at temperature intervals both below and above the peak incremental permittivity temperature. These aim at distinguishing between the possible effects of domain alignment and/or induced ferroelectricity on the behavior of the ceramics. They are compared with the actually observed changes in the incremental permittivity and percent light transmission data that has been brought about by an applied field. The temperature points at which the ceramics are examined in detail are:

1) 50°C below the peak incremental permittivity temperature
2) 25°C below the peak incremental permittivity temperature
3) 6°C above the peak incremental permittivity temperature
4) 25°C above the peak incremental permittivity temperature
5) 50°C above the peak incremental permittivity temperature

1. 50°C Below the Peak Incremental Permittivity Temperature

At 50°C below the peak incremental permittivity temperature, it may be safely assumed that almost all grains are ferroelectric. It has been estimated that at least half of the crystallites composing the large-grained samples have transitions that occur within $\pm$ 15°C of the peak incremental permittivity temperature of the ceramic.

If the domains tend to reorient themselves in the direction of the field as a result of 90° domain motion, a substantial increase in the percent light transmission of the thin section can be expected. The increase in the percent light transmission is the result of a rotation of the crystallites into a position of maximum anisotropy with respect to the crossed polars.* On the other hand, if the domains are sufficiently clamped so that 90° domain alignment with the accompanying mechanical strains cannot occur, then the effect of the field would be very small.

2. 25°C Below the Peak Incremental Permittivity Temperature

The ceramic compositions here are largely ferroelectric. However, as a result of the distribution of transition temperatures of the individual crystallites, there may be a smaller number of grains that are paraelectric.

For the case of domain orientation, the same arguments as above hold. For the case of induced ferroelectricity, a small overall decrease in the incremental permittivity and increase in the percent light transmission of the ceramic can be expected, due to the effect of the field on the paraelectric grains.

3. 6°C Above the Peak Incremental Permittivity Temperature

Slightly beyond the peak incremental permittivity temperature, the greater part of grains composing the ceramic are in the cubic state.

If 90° domain orientation occurs with field, it is restricted to a small, ferroelectric fraction of the grains. As a result, the capacitance of the sample is expected to decrease and the percent light transmission is expected to increase by a small amount. On the other hand, if

* The direction of the applied DC field is at about 45° with respect to the privileged directions of the polars.

ferroelectricity is induced in the paraelectric grains, it will be seen as optical anisotropy in the formerly cubic grains. This will result in a large increase in the percent of light transmitted by the thin section as compared to the zero field case. The overall incremental permittivity of the sample is generally expected to decrease with strong applied fields.

The above anticipated results from the mechanisms of both domain alignment and induced ferroelectricity differ from each other mainly in a matter of degree. It may therefore be difficult to interpret the data in terms of either one or the other postulate. In the latter part of this section some microscopic observations on individual grains are described, which provide a useful aid to the analysis of the incremental permittivity and light transmission curves.

4. 25°C Above the Peak Incremental Permittivity Temperature

The ceramic is composed mostly of cubic grains at this temperature.

The process of domain alignment can hardly take place. In terms of induced ferroelectricity, the effect of the field is also moderate, since ferroelectricity can no longer be induced in a large number of grains. (The range within which a ferroelectric state can be induced in a single crystal of barium titanate is derived from the thermodynamic relationships of the system (see Figure 6.12).

5. 50°C Above the Peak Incremental Permittivity Temperature

At this temperature, almost all grains are isotropic. A strong field is expected to produce little change in the optical and dielectric properties of the dielectric.

In the following paragraphs the dielectric and optical data obtained from the large-grained samples are analyzed, particularly with respect to the criteria established for distinguishing between the processes of domain alignment and an induced ferroelectric state in the ceramic grains.

The curves of the incremental permittivity versus temperature and DC field are shown in Figures 5.1, 5.3, 5.5 and 5.7. There is a relatively small decrease in the incremental permittivity with field at 50°C (Figure 5.7), and at 25°C (Figures 5.1, 5.3, 5.5 and 5.7) below the peak incremental permittivity temperature. The change at 6°C (Figures 5.1, 5.3, 5.5 and 5.7) above the peak incremental permittivity temperature is very large. Changes at 25°C and 50°C above the peak incremental permittivity temperature are respectively small and very small (Figure 5.1, 5.3, 5.5 and 5.7). From these observations it can be concluded that the incremental permittivity data taken on the large-grained ceramic compositions approximates the requirements proposed for the mechanism of induced ferroelectricity. The data show little evidence of any large field produced changes in the strictly ferroelectric region of the incremental permittivity curves. Such a result would be expected from the mechanism of domain alignment. At no point are the changes in the incremental permittivity very large except at the permittivity peak.

In Table 5.1, the percent increase in light transmission is listed for thin sections of the large-grained ceramic at several temperatures. In general, the greatest change in light transmission with field occurs slightly above the peak permittivity temperature, in which case the samples are

TABLE 5.1

INCREASE IN PERCENT LIGHT TRANSMISSION IN LARGE-GRAINED MIXED TITANATE COMPOSITIONS PRODUCED BY STRONG DC FIELDS

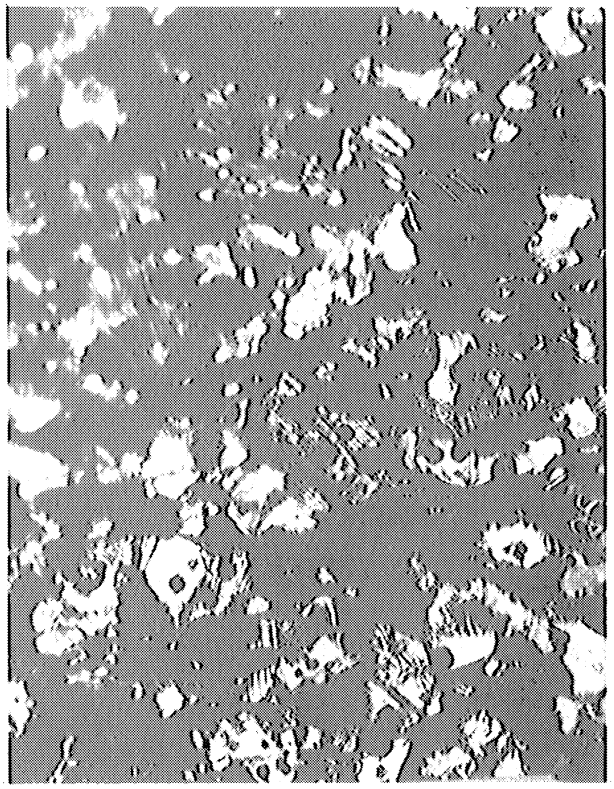
Sample	Maximum Permittivity Temperature, °C	Applied Max. DC Field, Volts/cm	Sample Thickness, Microns	Increase in the Absolute % Light Transmission Produced by the Field, Given at Temperatures on Either Side of the Peak ϵ_Δ Temperature*				
				-50°	-25°	+ 6°	+ 25°	+ 50°
1	49	17,000	40	---	2.9	6.6	3.5	1.2
2	51	10,900	35	---	2.0	3.6	.8	.1
3	52	10,700	35	---	3.8	8.6	2.2	.5
4	83	10,800	30	0	.4	3.5	.4	-

* The temperature of the peak incremental permittivity of each sample is taken as its reference temperature (0°). The negative temperatures indicate the ferroelectric side of the % light transmission curves. The positive temperatures indicate the paraelectric side. See figures 5.2, 5.4, 5.6, 5.8.

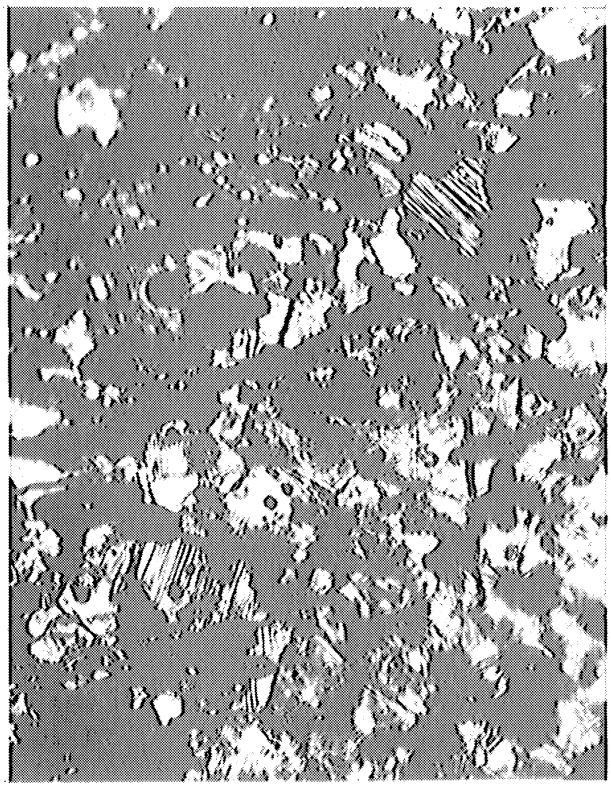
largely optically isotropic. This is seen very well in the light transmission curves (see Figures 5.2, 5.4, 5.6 and 5.8). The increase in light intensity with field in the ferroelectric region of the compositions is distinctly noticeable, except for Sample 4, in which the effect is small. In this connection it was observed that strong fields have little effect on the birefringence of a pure barium titanate ceramic at room temperature (barium titanate has a tetragonal to cubic transition at 120°C). Changes were noted only when barium titanate was heated to about 90°C. Sample 4, which has a peak incremental permittivity temperature at 83°C, is similar to barium titanate in that a field produces few optical changes at temperatures well below the peak incremental permittivity temperature (Figure 5.8).

In the region of the tetragonal to cubic transition the effect of the field on the percent light transmission is large. The optical data indicate the existence of an essentially isotropic ceramic at 6°C above the peak incremental permittivity temperature. After applying to a strong field, however, the percent light transmission approaches that of the ceramic in the ferroelectric region. Photographs taken on Sample 3 (Figure 5.14) show the field effect on the ceramic at room temperature and at 55°C. At the lower temperature (Figures 5.14a, 5.15b) the ceramic is ferroelectric, at the higher (Figures 5.14c, 5.14d) it is at its peak incremental permitivity temperature. The field induced optical anistropy makes the sample appear as bright at 55°C as it had been at room temperature.

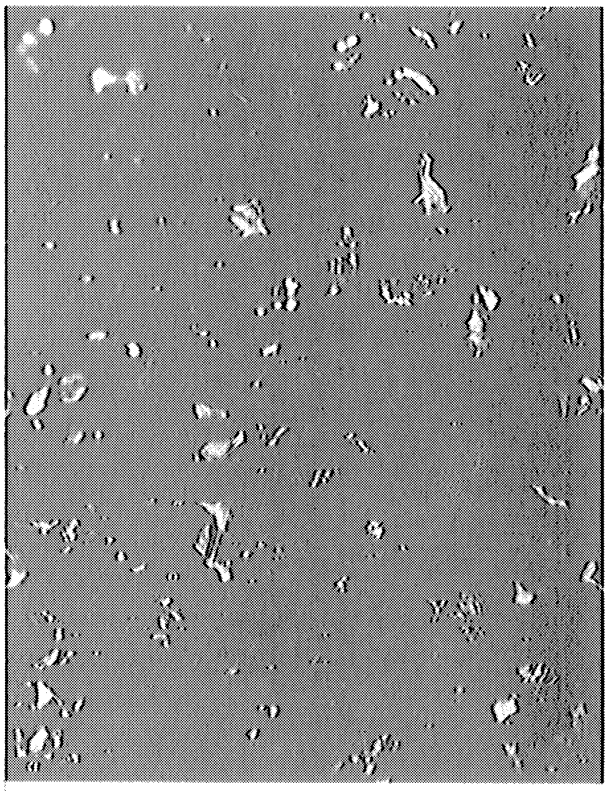
At temperatures considerably above that of the peak permittivity, the field effect is very small.



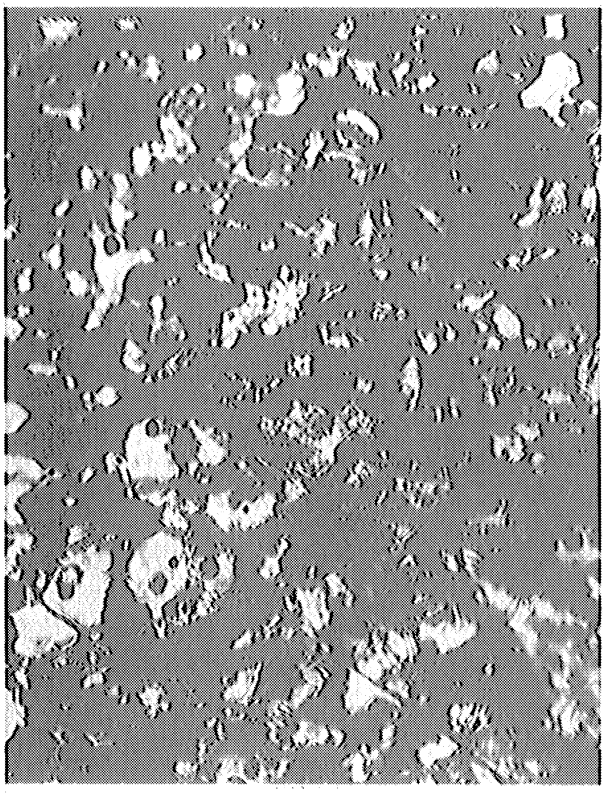
a) 25°C, zero applied field



b) 25°C, 12000 volts/cm



c) 55°C, zero applied field



d) 55°C, 12000 volts/cm

Figure 5.14. Effect of a Strong DC Field on the Optical Anisotropy of a Ferroelectric Ceramic, Sample 3. Peak incremental permittivity at 55°C, sample between crossed polars. (Mag. ≃ 335X)

At 25°C below the peak incremental permittivity temperature, a small, distinct field produced increase in intensity transmitted by the ceramic leads one to believe that the anisotropy of the ferroelectric grains is affected by strong fields.

The influence of a field on the optical behavior of individual grains is discussed in the latter part of this section.

b. Fine-Grained Samples

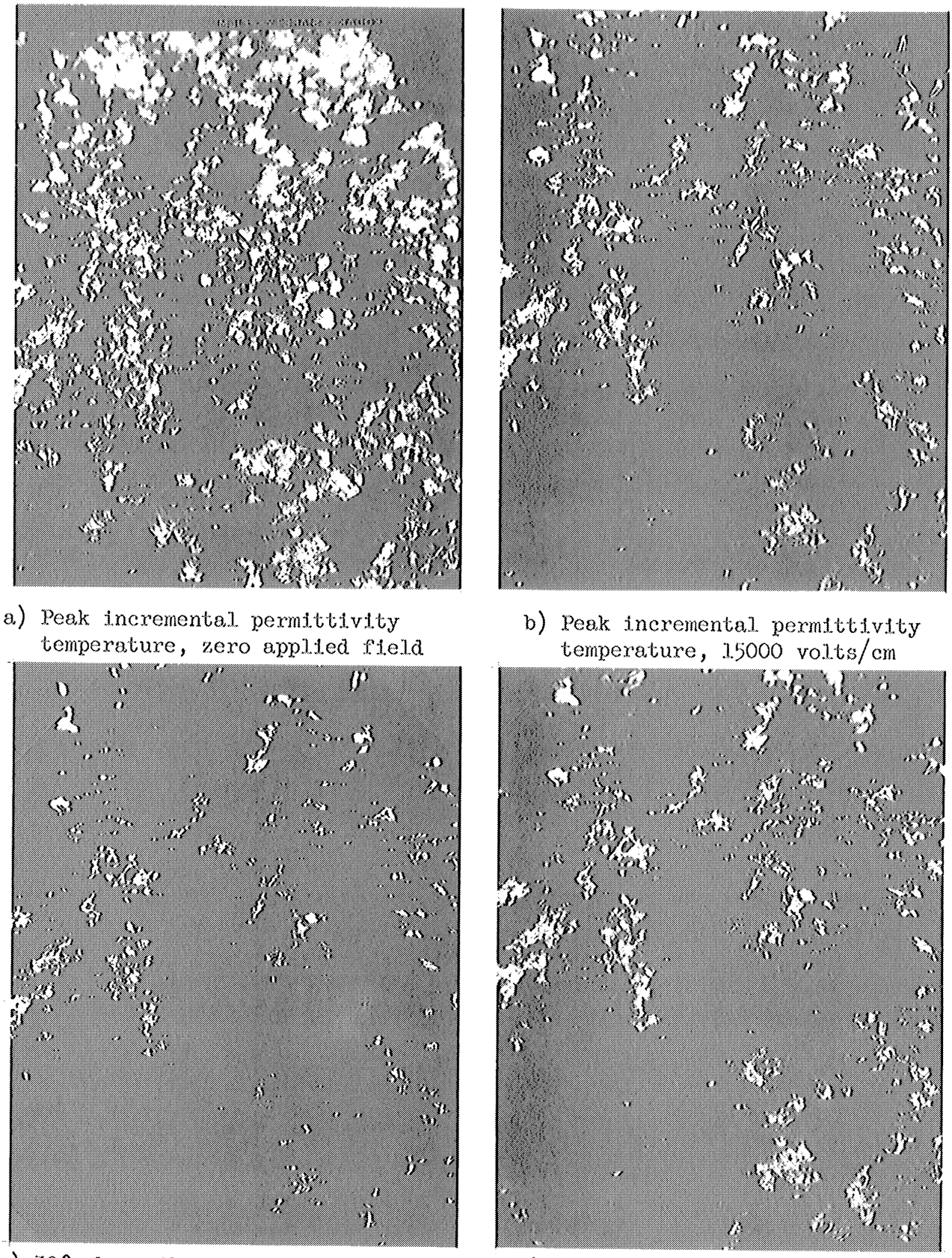
The fine-grained Samples 5 and 6 (Figures 5.9 and 5.11) are characterized by very broad incremental permittivity peaks and a fine-grained structure. Incremental permittivity data for Sample 7 are lacking. Accurate capacitance measurements could not be made on Sample 7, since the only sample available was a thin section, not a wedge. Sample 7 is nevertheless included in the data because it represents one of the few fine-grained ferroelectric ceramics prepared at the Electro-Materials Laboratory, Electrical Engineering Department, The University of Michigan. In many ways it resembles the commercial ceramic Sample 5.

The dielectric data of the fine-grained ceramics show the typical lowering of the incremental permittivity with field and a discernible shifting of the peak permittivity to higher temperatures. However, the percent-transmission data at best only give a small indication of the actual optical behavior of the ceramic, since the light traversing several layers of the ferroelectric is absorbed and scattered in the material. This explains the very low percent transmission values measured.

No evidence of domain structure can be observed in the individual grains in the ferroelectric region. In Sample 6 which "peaks" around

48°C, entire anisotropic patches covering large areas of the sample can be seen (Figure 5.15a). These patches are greatly enlarged when a field is applied (Figure 5.15b). As the thin section is heated, the number of patches gradually decreases, but the sample never extinguishes completely. (It appears that a strain-induced anisotropy exists in the fine-grained ceramics which is independent of temperature.) When a strong DC field is applied to Sample 6 at 78°C, 30°C above its peak incremental permittivity temperature, the microscope field becomes brighter, although not to the same degree as at the peak incremental permittivity temperature. At about 110°C the field induced anisotropy can no longer be detected. The strain anisotropy, however, still persists. Samples 5 and 7 behave in a similar manner.

In an x-ray and electron diffraction study on barium titanate, composed of colloidal particles, Anliker, Brugger and Kaenzig[117] have found that the ferroelectric to cubic phase is increasingly spread out over a wider temperature range as the particle size decreases. They report that the spontaneous strain, which is normally observed in the tetragonal phase, does not vanish completely even at several hundred degrees above the Curie point of the microscopic crystal. They attribute the anomalous effect to a highly strained surface layer of about 100 Å. The spontaneous tetragonal strain in this layer is independent of temperature and larger than the spontaneous strain in the interior of the small particle. Fatuzzo and Merz[118] have recently investigated the surfaces of single crystals, and have found a thin, electrically biased and mechanically strained layer which has a much smaller permittivity than the bulk



a) Peak incremental permittivity temperature, zero applied field

b) Peak incremental permittivity temperature, 15000 volts/cm

c) 30° above the peak incremental permittivity temperature, zero applied field

d) 30° above the peak incremental permittivity temperature, 15000 volts/cm

Figure 5.15. Effect of a Strong DC Field on the Optical Anisotropy of a Fine-Grained Ceramic, Sample 6. Sample between crossed polars. (Mag. ≃ 335X)

of the crystal. I. I. Ivanchik[119] mentions that ferroelectricity disappears completely if the thickness of a particle grain is less than 200 Å.

This seems to contradict the findings of Anliker et al.[117] who report the persistence of the Curie point in fine-grained particles upto very high temperatures. The high spontaneous strain at the surface of the small particles gives rise to their anomalous ferroelectric behavior. It is possible that the discrepancy arises from a difference in terminology. Ivanchik may not have chosen to describe the observed anomalous dielectric behavior as "ferroelectricity."

The fine-grained, mixed titanate materials investigated here are composed of grains 3 - 15μ in diameter. They consist of considerably larger particles than would be considered colloidal. However, the broad peak in the dielectric data and the observed strain anisotropy seem to suggest that surface effects are responsible for their anomalous ferroelectric behavior.

B. Observations

In the search for some indication of domain alignment and/or induced ferroelectricity in the compositions investigated, many field produced phenomena were observed in individual grains which could not be isolated by the integrated light measurements of the photocell. They are discussed in some detail below. The effects are classified as short term and long term.

1. Short Term Effects

Optical changes in ferroelectric thin sections which are produced by a short exposure to an external DC field and disappear when the field is removed are considered short term effects.

As mentioned previously, the effect of a strong DC field on the optical behavior of a ferroelectric titanate thin section at temperatures substantially below that of the peak incremental permittivity appears to be negligible. The room temperature observations on ceramic barium titanate and Sample 4 which "peak" at 120°C and 83°C respectively show no distinct changes in birefringence or in crystallographic orientation with field. However, in the temperature range approximately 25° below the peak incremental permittivity, a number of field induced effects are observed in the large grained compositions:

1) The field noticeably increases the interference colors in some grains. In Sample 1, 40μ in thickness, the field changes a first order yellow into a first order red-blue. (This corresponds to a change of birefringence of .010 to .015 with field.) Similarly, in Sample 3, 35μ thick, a first order yellow changes to a second order blue-green with field. (The corresponding increase in birefringence is almost .010.)

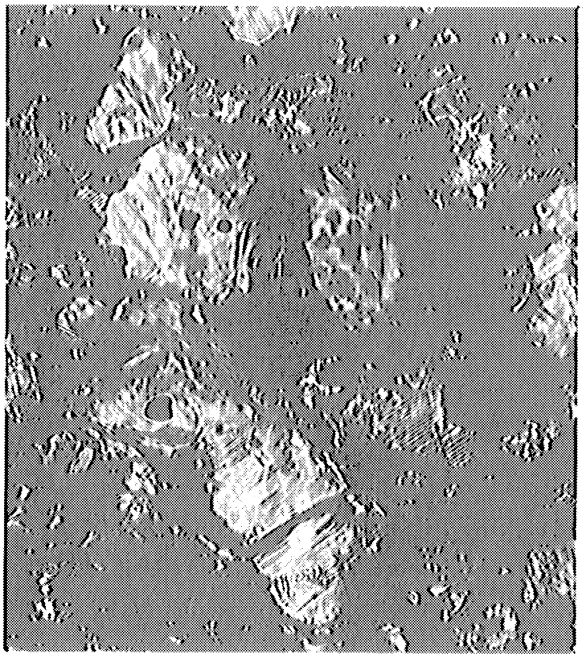
2) Twinning striations tend to disappear when the sample is heated close to its peak incremental permittivity temperature. These striations are due to 90° domains or twinning across the (101) plane. On heating, the parallel twin lines gradually become less well defined, and then disappear completely. Often the area which the striations have occupied at low temperatures appears to be of uniform color when heated. The color is usually a first order white or yellow.

Then, when a high DC field is applied to the sample, the twinning striations may reappear in their original direction and number. When heating the biased ceramic further, close to its transition temperatures, the field produced striations disappear. They are similarly replaced by areas of uniform interference color.

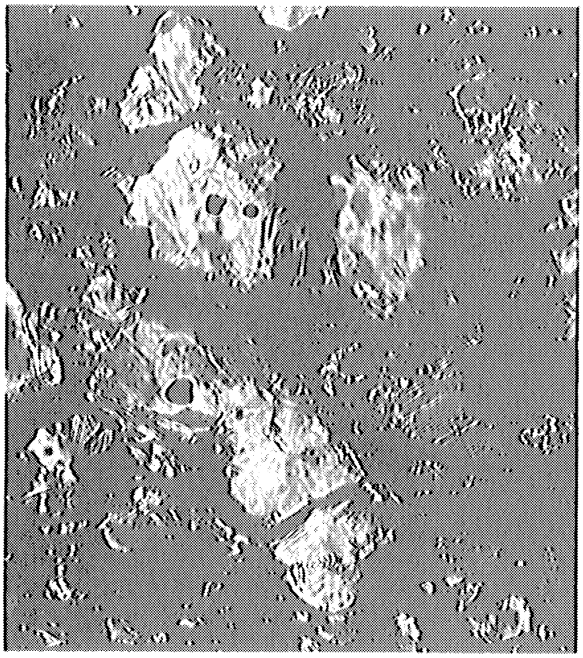
The reverse effect, an actual disappearing of twin lines with field, is very rarely observed. In Figures 5.16a and 5.16e, grain 1, the twinning striations are faint lines which do not all extend across the grain. As seen in Figure 5.16b, they disappear completely with the applied field. In the neighboring grain, Figures 5.16a and 5.16e, grain 2, where the striations are at 90° to the former, the field seems to lengthen the twinning lamellae.

3) Although the field tends to increase the overall light transmitted by a sample, some isolated grains become dark when a field is applied.

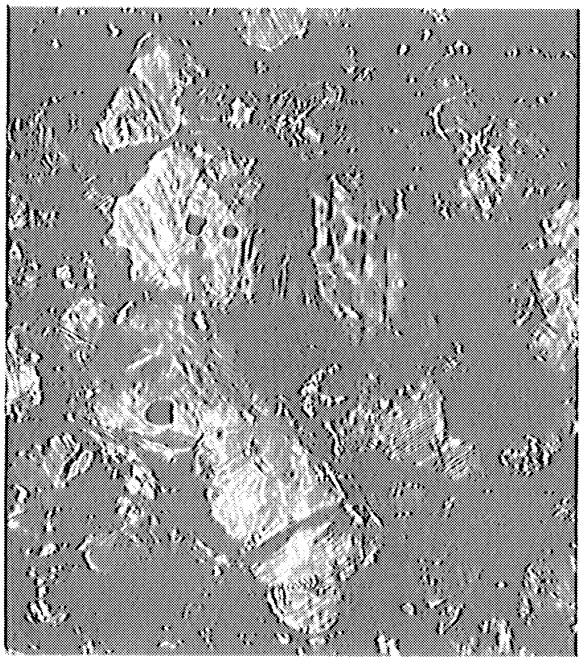
4) In some instances the "brightening" of a grain is not instantaneous, but seems to saturate over a time period that is noticeable by eye. The period is about .3 to 1 second. Also, a movement of dark, irregular lines within a grain has been frequently observed. Field induced effects of this latter type are very difficult to analyze since they are not reproducible. A detailed discussion of the above effects follows.



a) Before poling. Room temperature, no field applied



b) Before poling. Room temperature, field applied

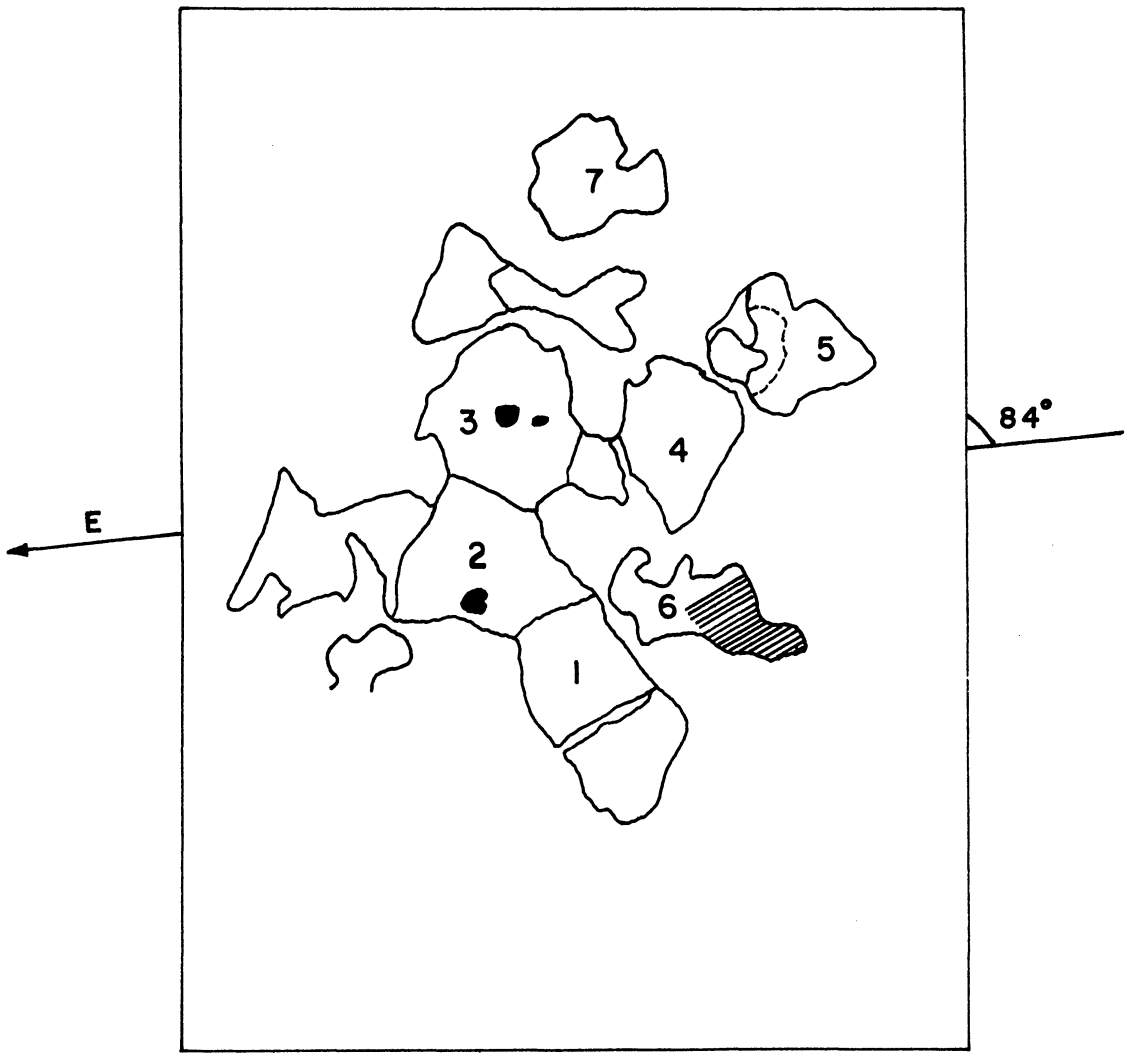


c) After poling. Room temperature, no field applied



d) After poling. Room temperature, field applied

Figure 5.16. Effect of Poling on the (101) Twinning Structure of a Ferroelectric Ceramic, Sample 1. Sample between parallel polars. (Mag.≃ 320X)



e) Outline of grains in photographs 5.16 a, b, c, and d.

Figure 5.16. (Continued)

a. Discussion of Observed Phenomena

The optical observation on ferroelectric, ceramic thin sections seems to indicate that their optical anisotropy is both a function of temperature and of an external DC field.

Unfortunately, no experimental data has yet been published on the optical properties of good barium-strontium titanate crystals, containing more than 10% strontium titanate. It is therefore necessary to rely on the observations made on ceramic materials in the course of the present investigation. Because of the nature of the material, these observations can only be descriptive. Nevertheless, it is possible to make some general statements about the optical behavior of the mixed titanate ferroelectrics with respect to temperature and electric field.

(1) Birefringence as a Function of Temperature

The birefringence in mixed barium-strontium titanate compositions appears to be lower than in pure barium titanate (Figure 5.17). For barium titanate it increases from approximately .025 at 120°C, the tetragonal to cubic transition temperature, to .060 at 0°C.[84] (Meyerhofer[120] reports an increase from .040 to .075 for the same range.) The highest interference color observed on the ceramic Sample 4, at room temperature, is a first order green for a thin section 30μ thick. The highest interference color observed at 83°, in the region of the tetragonal to cubic phase transition, is a first order white. Hence the change in birefringence is about .022 for a 60° range. In Figure 5.17c the curve of Sample 4 has been shifted along the temperature axis so that its transition temperature at 83°C coincides with the transition temperature of pure $BaTiO_3$.

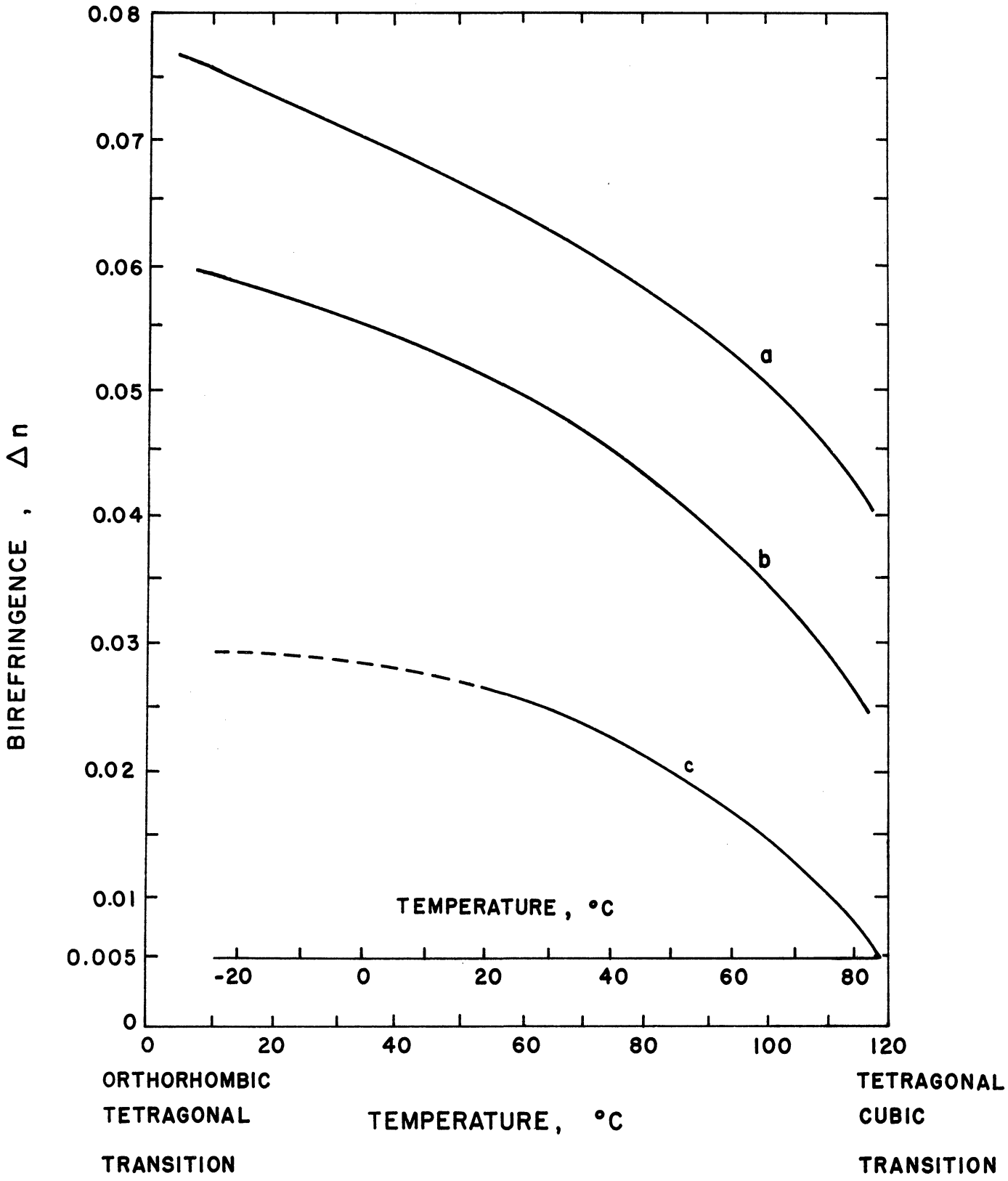


Figure 5.17. Variation of Birefringence with Temperature in Tetragonal Barium Titanate and $(Ba,Sr)TiO_3$ Ceramic.

(2) Birefringence as a Function of DC Field

Observations on ceramic barium titanate and Sample 4 indicate that the field has very little effect on the birefringence at temperatures substantially below the transition temperature; but within a range of about 20°C to 25°C of the peak incremental permittivity temperature, the field increases the optical anisotropy of the ceramic grains. At this point it should be mentioned that the electric field across the sample was placed at 30 to 45° with respect to the analyzer and polarizer. Any changes in the ceramic which the field might produce would in this way be readily observable.

The increase in anisotropy results in a general brightening of the entire thin section. Closer examination of the anisotropic effect seems to indicate that this is partially due to an induced anisotropy in a few paraelectric areas. It is also due to an increase in birefringence in some ferroelectric grains, when a strong DC field (of about 11,000 volts/cm for Sample 4), is applied to the ceramic. Higher interference colors appear with field than are observed at zero bias. In an aggregate of randomly oriented grains which show a first order grey, white, yellow and red at zero field, a second order blue can be detected when a field is applied. The higher order colors are not due to a more favorable orientation of the polar axes in the field direction, since they represent a birefringence which is larger than that of the highest interfence color found among the ceramic grains at zero field.

The estimated change in Δn of .005 with field corresponds to a change of temperature of about 14°C (see Figure 5.17c).

(3) The Effect of a Field on the Twinning Lamellae

Some areas which show twinning lamellae become areas of uniform interference colors at a temperature close to that of the transition. When a strong DC field is applied to the sample, the lamellae reappear. As Little[69] has pointed out, large mechanical as well as electrical stresses exist at 90° domain boundaries. This is the result of twinning along the face diagonal of a pseudocubic, tetragonal crystal. The resulting mechanical distortion explains why a 90° domain wall is readily visible in transmitted light.

Close to the transition temperature, a barium-strontium titanate ferroelectric very nearly approaches the cubic structure. The stresses are greatly reduced and the twin lamellae fade away. The twinned area then appears as a uniform region of first order white. It is possible that a strong field applied in a favorable direction will greatly stress one axis and thereby restore the anisotropy and mechanical distortion which led to the original 90° twin formation. In addition, field-induced twinning seems to be very temperature sensitive. A heating of only 2 to 3°C will again change the area into one of uniform polarization.

(4) Increase of Light Intensity with Time

In some samples, the initial field-induced change in anisotropy seems to increase with time. After several seconds, the observed transmitted light intensity saturates.

An interpretation here is difficult. Perhaps the initial stressing of the optical axis is followed by a small degree of orientation in the field direction.

On the other hand, the observed phenomena may be somehow or other associated with space-charge effects. For example, it is well known from classical electrodynamics that in a dielectric medium the space charge will diffuse according to

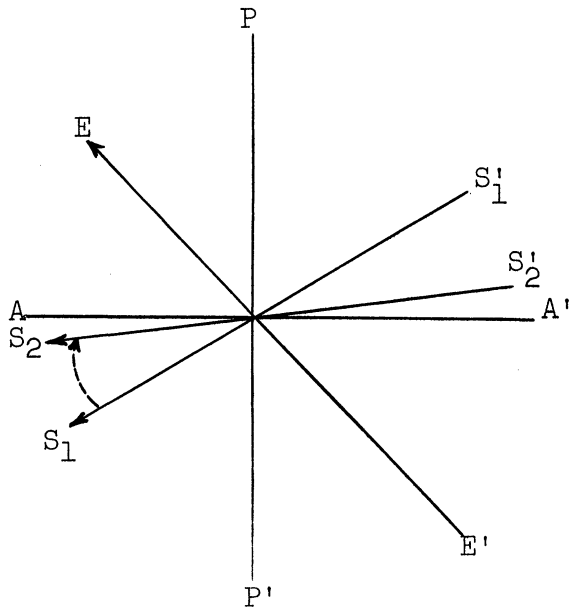
$$\rho = \rho_o e^{-\frac{\sigma t}{\epsilon}}$$

where ρ is the space charge density, ρ_o the initial density, σ the conductivity, ϵ the permittivity ($\epsilon = \epsilon_r \epsilon_o$, with ϵ_r the relative permittivity and ϵ_o the permittivity of a vacuum). In $BaTiO_3$, σ is of the order of $10^{-8}(\text{ohm}\cdot\text{m})^{-1}$ and $\epsilon_r \simeq 10^3$ and $\epsilon_o \simeq 10^{-11} \frac{\text{farads}}{\text{m.}}$, so that $\frac{\epsilon}{\sigma}$ (the time-constant for space-charge effects) becomes $\frac{10^3 \times 10^{-11}}{10^{-8}} \simeq 1$ sec. This is of the same order as the observed transient effects.

In order to examine this and other possibilities a more extensive study of these materials would have to be conducted.

(5) Domain Rotation

Domain rotation is difficult to detect. An increase in intensity with field may be either due to a rotation of the optic axis into the field direction (assuming that the field direction lies at about 45° to the privileged directions of the polars), or due to a field produced increase in the birefringence of the ceramic grain (Section V-B-2). On the other hand, a darkening of a grain with field, at constant temperature, seems to indicate that the field has rotated the optic axis to coincide more nearly with the privileged directions of the polars (Figure 5.18a).



PP' = privileged direction of polarizer
AA' = privileged direction of analyzer
EE' = direction of DC field
S_1S_1' = polar axis of domain at zero field
S_2S_2' = polar axis of domain with field

Figure 5.18a. Schematic: Rotation of the Polar Axis in a Ferroelectric Domain Produced by an Applied Field.

Merz[68] was able to show the existence of anti-parallel 180° walls by applying a strong field perpendicular to the direction of the spontaneous polarization (Figure 5.18b). The small rotation of the optic axes into the field direction produced a strain anisotropy at the domain boundaries which made 180° domains visible.

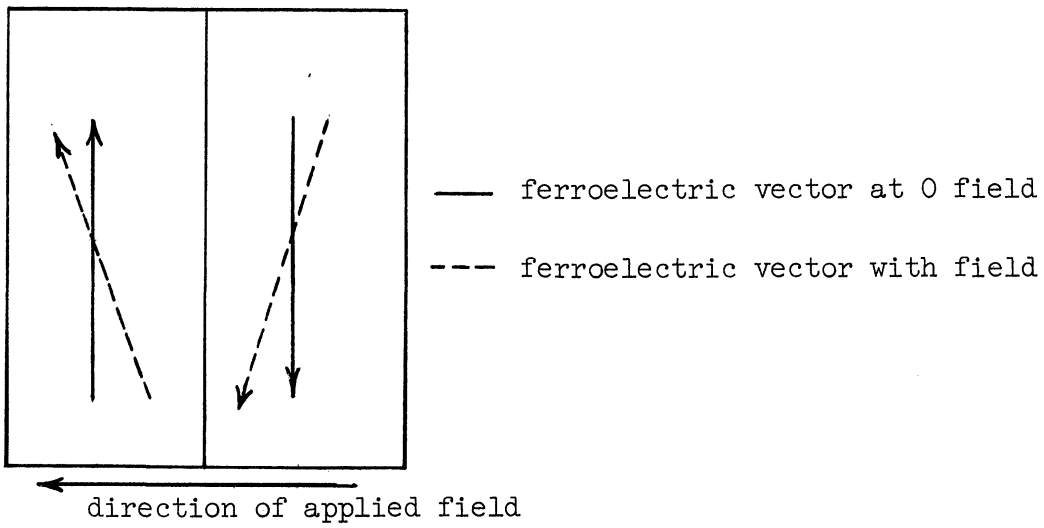


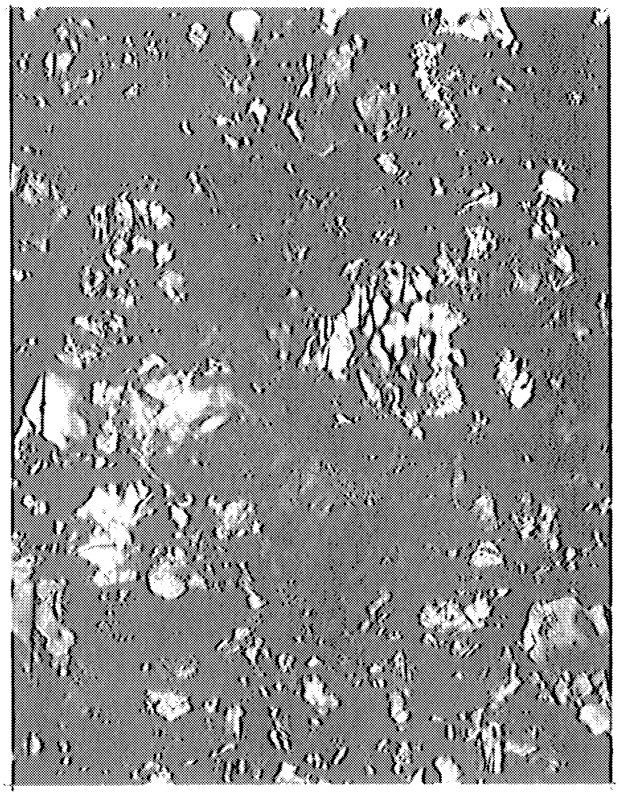
Figure 5.18b. Field Produced Rotation of the Polar Axes in Anti-parallel Domains.

It is felt, from observations on the ceramic grains, that the isolated occurrences of "domain rotation" are not the result of a field produced nucleation and growth of domains. They seem to arise from a small field-produced distortion of the optic axes, similar to the one produced in Merz's experiment.(68) This is illustrated in Figure 5.19, grain 5. An area is shown which appears relatively bright on zero field, but is dark at 18,000 volts/cm. The grain has been almost stressed into an extinction position by the field.

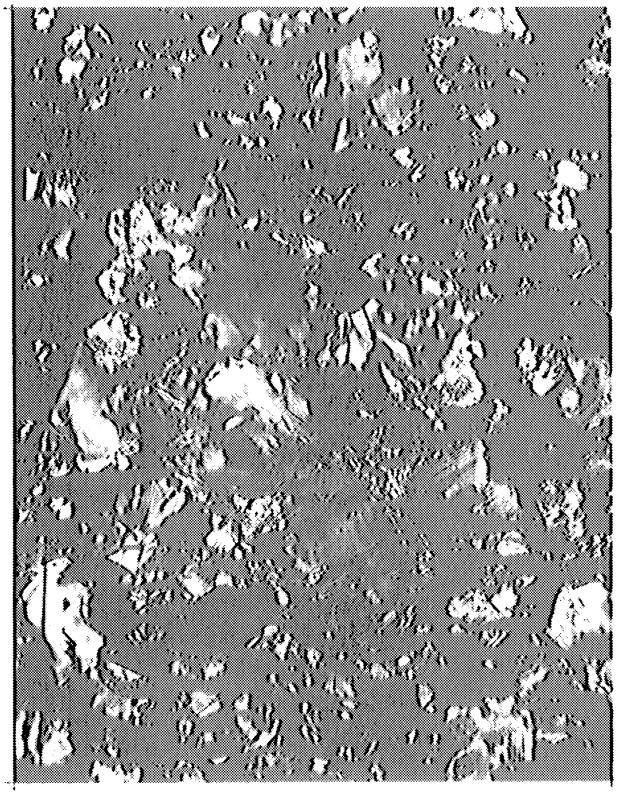
In Sample 2 and Sample 4, areas become light as well as dark when a field is applied. These samples are highly twinned and also have pronounced "domain movement." Rotation was not readily detected on any other compositions.

(6) "Domain Motion"

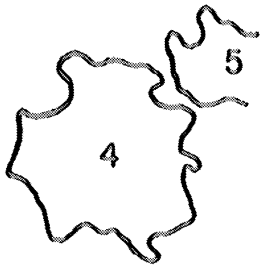
The movement observed in mixed titanate ceramics, again near the transition temperature, is confined to black, irregular lines which are sometimes distributed over the grains (Figure 5.19 grain 4). The lines do not necessarily adhere to grain boundaries. They have been observed only in a few compositions and seem to be affected by humidity, frequency of exposure to the field, and proximity to the electrodes. Under the influence of a DC field, they rearrange themselves into new patterns within a second or less. Sometimes they delineate bright areas which either increase or shrink as the field is switched on and off. This type of "motion" has constituted one of the most perplexing problems in the present study, mainly because of the total lack of reproducibility. It



a) 35°C, zero applied field



b) 35°C, 18000 volts/cm



c) Grain 4 - Light grain with irregular dark lines, located approximately in center of photographs

Grain 5 - Position as indicated in sketch, upper right hand corner of grain 4.

Figure 5.19. Extinction of an Anisotropic Area in a Ferroelectric Grain of Sample 1, Upon Applying a Strong DC Field. Sample between crossed polars. (Mag. ≃ 320X)

is now felt, that space charges are responsible for the movement. Space charges build up at the electrodes and in the interior of the ferroelectric when DC fields are used. The charge accumulation is especially serious near the Curie point. It depends largely on the type of electrical contact made to the crystal. Meyerhofer[120] has found that crystals with tin oxide electrodes have less space charges than those with evaporated metal electrodes. A permanent space charge layer in the cubic state has been described by Chynoweth.[121] He reports that a cubic barium titanate single crystal carries a small degree of surface polarization, although its spontaneous polarization is zero. At times the space charge is even large enough to induce birefringence in a cubic crystal.

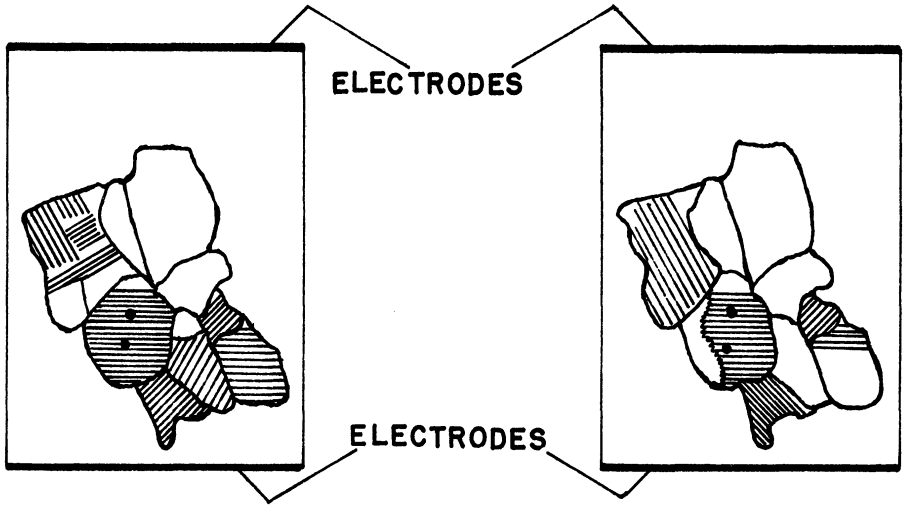
2. Long Term Effects

Optical and structural changes which are produced in a ferroelectric by the prolonged exposure to an external DC field, and which remain after the field is removed are described as long term, or "poling" effects.

Sample 1 provides a good example of the poling effect. A series of photographs were taken of the composition between parallel and crossed-polars, at different temperatures, and different applied electric fields. Repeated heating and cooling of a ceramic through its peak incremental permittivity temperature does not essentially change the original domain patterns. In some ways these patterns conform to an existing structural mold. Perhaps domains in single crystals nucleate at impurities and imperfections, and they are produced by the stresses existing at these

imperfections. Ceramic crystallites are, in addition, geometrically confined by their grain boundaries. The photographs of Figure 5.16 Sample 1, show that the repeated exposure of the ceramic to a field has produced some permanent changes, although the wedge was heated 20°C beyond its peak incremental permittivity temperature in the process. The areas in which poling can be detected are primarily in grains 1 and 2. Parallel twin lines are faintly visible. The grains are about to become isotropic, given another five degrees of heating. Twinning in grain 2 is perpendicular to the twinning in grain 1. When the field is applied, twinning completely disappears in grain 1 and is enhanced in grain 2. After exposing the sample intermittently to the field for a total of about 30 minutes, photographs Figure 5.16c were taken. Now grain 1 hardly shows any twin lamellae at zero field and the ones in grain 2 seem more pronounced. Grain 1 in photographs b and c have become almost identical. A high applied DC field does not alter the picture substantially, except that it increases the lines in grain 2, Figure 5.16d. No visible poling has occurred in grain 6. In grain 7, all twin lines seem to have been poled in one direction.

Another example of poling is illustrated in the sketches drawn from Sample 1 before and after a 20 minute exposure to a field of 17,000 volts/cm at room temperature (Figure 5.20). Aside from changes in direction of the twin lamellae, an increase in the interference colors of the grains was observed. These, unfortunately, cannot be recognized from the black and white photographs of Figure 5.16. Poling on other samples has not been observed to this extent. Sample 4 in particular seems insensitive to the field in its ferroelectric state. The reason for the variation in behavior of the different samples is not known.



(a) 0 - FIELD

INTERFERENCE COLORS
YELLOW, WHITE,
GREY.

(b) 17,000 VOLTS/CM. FOR 20 MINUTES

INTERFERENCE COLORS
GREEN, RED, YELLOW,
WHITE, GREY.

Figure 5.20. Poling in Sample 1. Thickness 40μ.

VI. CALCULATION OF THE LIGHT INTENSITIES TRANSMITTED BY (Ba, Sr) TITANATE CERAMIC THIN SECTIONS

Several aspects of the percent light transmission versus temperature data taken on the ceramic barium-strontium titanate thin sectionsare examined more closely in this section on calculations.

First, the following basic question is posed: Given a ferroelectric barium-strontium titanate thin section, what percentage of the incident light can be theoretically expected to emerge from the analyzer if the section is placed between crossed polars? The ceramic section is considered to consist of a single layer of randomly oriented crystallites, all of which are in the ferroelectric, anisotropic phase, and have the same value of maximum birefrigence.

Secondly, the percentage of light transmission versus temperature of a barium-strontium titanate thin section is calculated from theoretical considerations. It seems a reasonable assumption that the transition temperatures of a large aggregate of crystallites composing some barium-strontium titanate composition should be distributed about the peak permittivity temperature of the ceramic in a Gaussian distribution. The distribution of transition temperatures results from the compositional inhomogeneities in the ceramic as well as from internal strains in the material which affect the Curie temperature of the crystallites.

The percent of light transmitted by a thin section of a barium-strontium titanate ceramic through crossed polars is closely related to the number of anisotropic, ferroelectric grains in the thin section. The number of ferroelectric grains existing at some temperature, T , may be

derived by integrating over the distribution curve of transition temperatures from the lower limit up to the desired temperature (Figure 6.6). When the integration is performed for all temperatures, one obtains a relationship of the percentage of anisotropic grains in the ceramic with respect to temperature. It will be subsequently shown that such a curve is of the form $(1-erf)$, where erf is the error function (Figure 6.7).

The shape of the experimental percent light transmission curves, as shown in Figures 5.2, 5.4, 5.6, 5.8, 5.10, 5.12, 5.13, closely seem to resemble the function $(1-erf)$. In order to make an exact comparison of the predicted and experimental percent light transmission data, theoretical light transmission curves have been calculated for four large grained samples, samples 1-4. The shift of the transmission curves with field, as predicted theoretically and determined experimentally have been compared in Figures 6.8, 6.9, 6.10, 6.11. The agreement between the theoretical and experimental curves for both samples is good.

The calculations in this section fall under the following three headings:

A. Fraction of light transmitted by a (Ba, Sr) TiO_3 ceramic thin section at some temperature, T, in the ferroelectric region.

B. Change with temperature in the relative amount of light transmitted by a barium-strontium titanate thin section.

C. Change with temperature and applied DC field in the relative amount of light transmitted by a barium-strontium titanate thin section.

D. Comparison of the relative theoretical and experimental light transmission curves.

The temperature range of interest and the one considered here lies between 20°C and 140°C. This range includes the tetragonal-ferroelectric to cubic-paraelectric transition only. None of the ferroelectric transitions which occur at lower temperatures (for barium titanate, the orthorhombic to tetragonal occurs at about 0°C, and the rhombohedral to orthorhombic at -80°C) have been taken into account here.

The calculations are based on a rough physical model which does not fully describe the structural complexities in the actual ceramic. However, the model is a starting point for an analysis of the optial anisotropy which exists in these ceramics, and should provide at least a prediction of their qualitative behavior.

A. Fraction of Light Transmitted by a (Ba, Sr) TiO_3 Ceramic Thin Section at Some Temperature, T, in the Ferroelectric Region

The intensity of an emerging ray passing through a crystal section between polars has been given by Johannsen[122] as

$$I = I_o[\cos^2\varphi - \sin 2(\theta-\varphi)\sin 2\theta \sin^2(\frac{\pi(n_2-n_1)m}{\lambda})] \quad \text{(see Figure 6.1)} \quad (6.1)$$

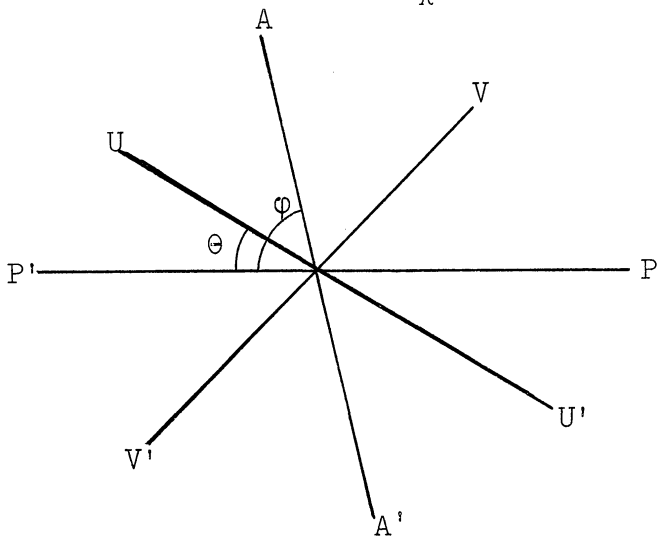


Figure 6.1. Orientation of the Privileged Directions of a Crystal in the Optical Field of a Polarizing Microscope.

AA', PP' are the privileged directions of the analyzer and polarizer,

UU', VV' are the privileged directions of the crystal examined,

φ is the angle between the privileged direction of the analyzer and polarizer, and

θ is the acute angle between the privileged direction of the polarizer and one of the crystal directions.

In Equation (6.1) I represents the intensity of the emerging light, and I_o the intensity of the incident light. n_2 and n_1 are the indices of the crystal for the privileged directions U and V, m is the thickness of the crystal, and λ the wave length in air of the incident light.

When the polars are crossed, $\varphi = 90°$. Then Equation (6.1) reduces to

$$I = I_o \sin^2 2\theta \sin^2\left(\frac{\pi(n_2-n_1)m}{\lambda}\right). \qquad (6.2)$$

The relative intensity R of a monochromatic ray passing through a crystal thus becomes

$$R \equiv \frac{I}{I_o} = \sin^2 2\theta \cdot \sin^2\left(\frac{\pi\Delta nm}{\lambda}\right). \qquad (6.3)$$

In order to estimate roughly the relative light intensity that is transmitted by a monolayer of randomly oriented grains, a simple physical model is substituted for the more complex ceramic thin section. The thin section is replaced by an "equivalent" crystallite with a maximum birefringence of $\epsilon-\omega$ (n_c-n_a) of about -.015, as experimentally determined from a large grained thin section, illustrated in Figure 5.17. The "equivalent" crystallite lies at some angle θ with respect to the polars, which ideally

transmits a percentage of light equivalent to the amount which is transmitted by a multitude of randomly oriented crystallites. For purposes of calculation, the light passing through the "equivalent" crystallite is arbitrarily chosen to be composed of wavelengths between 5200 Å and 6200 Å only. This band approximately represents the range of maximum sensitivity of the photocell. It corresponds roughly to the area under the relative sensitivity curve of the photocell bounded by 4800 Å to 6400 Å (Figure 6.4).

The relative transmitted light intensity is correlated with the thickness of the equivalent crystallite. Intensities for a crystal varying from 20 to 60 μ have been calculated. The results are given in Table 6.1.

1. Calculation of θ

θ represents the acute angle of one of the privileged directions of the "equivalent" crystallite with respect to the privileged direction of the polarizer (see Figure 6.1). When $\theta = 0$ or 90°, the privileged directions of the tetragonal crystal coincide with the privileged directions of the polarizer and analyzer, and the crystal is at extinction. When $\theta = 45°$, a maximum of light is transmitted by the anisotropic crystal. To find an average value for the transmitted light intensity for the entire collection of randomly oriented anisotropic grains in the thin section, the relative transmitted light intensity is averaged over all angles θ from 0° to 90°. From Equation (6.3), the relative transmitted light intensity

$$R = \frac{I}{I_o} = \sin^2 2\theta \sin^2\left(\frac{\pi \Delta nm}{\lambda}\right).$$

Then the average relative transmitted light intensity R_1 of the equivalent

crystallite, as a function of birefringence Δn , crystal thickness m , and wave length λ of the incident light is represented by

$$R_1(\Delta n,m,\lambda) = \sin^2(\frac{\pi\Delta nm}{\lambda}) \frac{\int_0^{\pi/2} \sin 2\theta d\theta}{\int_0^{\pi/2} d\theta} . \qquad (6.4)$$

Equation (6.4) can be reduced to

$$R(\Delta n,m,\lambda) = \sin^2(\frac{\pi\Delta nm}{\lambda}) \frac{\frac{1}{2}[\frac{1}{2}(2\theta) - \frac{1}{4}\sin 4\theta]_0^{\pi/2}}{\pi/2}$$

$$= \frac{1}{2}\sin^2\frac{\pi\Delta nm}{\lambda} . \qquad (6.5)$$

From Equation (6.5) it is seen that the relative intensity of the equivalent crystallite R_1 can be represented by a sine squared function of x , where $x = \frac{\pi\Delta n}{\lambda}$, the phase difference angle. This is shown in Figure 6.2. It is interesting to note that the maximum value of the function is 0.5. This means that in a randomly oriented aggregate of anisotropic crystals the distribution of the crystallites alone limits the emerging light intensity to one-half of the incident light intensity. This is true for the most favorable values of birefringence, crystal thickness, and wavelengths of transmitted light.

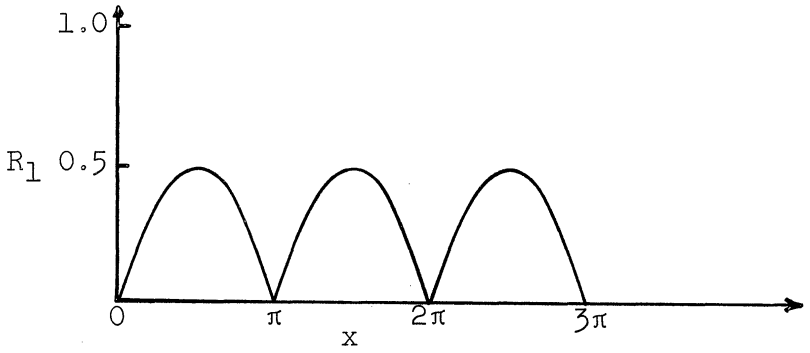


Figure 6.2. Relative Intensity R_1 of the Equivalent Crystallite with Respect to x , the Phase Difference Angle (see Equation 6.5).

2. Calculation of the Birefringence of the Equivalent Crystallite

As previously described, the "equivalent" crystallite is substituted for the actual grains that compose a ferroelectric thin section in order to facilitate the calculations of optical light transmission.

From experimental observations, the maximum birefringence of a barium-strontium titanate grain is known to be .015 at about 20° below the peak incremental permittivity temperature (Figure 5.17). The birefringence of the equivalent crystallite is obtained by estimating the average of all observed values of birefringence in the randomly oriented crystallites of the ferroelectric thin section. The birefringence of the "equivalent" crystallite can also be obtained by averaging over all values of birefringence in the uniaxial indicatrix, having $\omega - \epsilon$ or $n_a - n_c = .015$.

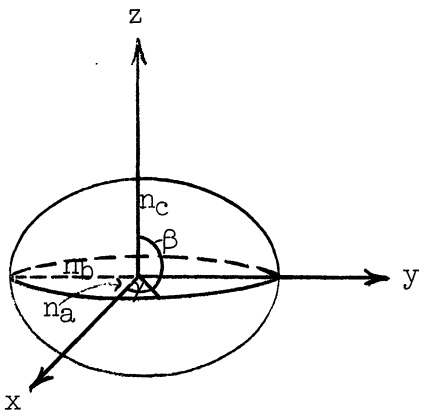


Figure 6.3. Ellipsoid of Revolution.

The equation of an ellipsoid of revolution or of a biaxial indicatrix is given in polar form, by

$$\frac{n^2 \cos^2\gamma \cos^2\beta}{n_a^2} + \frac{n^2 \sin^2\gamma \cos^2\beta}{n_b^2} + \frac{n^2 \sin^2\beta}{n_c^2} = 1 \qquad (6.6)$$

where n_a, n_b, and n_c are the principal indices of the indicatrix, and n is some index which is related to n_a, n_b, and n_c by the angles γ and β, (see Figure 6.3). For $n_a = n_b \neq n_c$, as is the case for the uniaxial inditrix, the equation condenses to

$$n(\gamma, \beta) = \left(\frac{\cos^2\beta}{n_a^2} + \frac{\sin^2\beta}{n_a^2} \right)^{-1/2} , \tag{6.7}$$

$$= \frac{n_c}{(1-k^2\cos^2\beta)^{1/2}} \tag{6.8}$$

where

$$k^2 = 1 - \frac{n_c^2}{n_a^2} .$$

If the birefringence

$$\Delta n = n_a - n ,$$

then

$$\Delta n = n_a - \frac{n_c}{(1-k^2\cos^2\beta)^{1/2}} . \tag{6.9}$$

By averaging over all values of n of the indicatrix from $\beta = 0$ to $\beta = \pi/2$, the average index $n_{av.}$ and hence the average birefringence $\Delta n_{av.}$ can be obtained.

$$\Delta n_{av.} = n_a - \frac{\int_{\beta=0}^{\pi/2} \frac{n_c d\beta}{(1-k^2\cos^2\beta)^{1/2}}}{\int_{\beta=0}^{\pi/2} d\beta} \tag{6.10}$$

This is graphically represented in Figure 6.5, which shows the birefringence Δn as a function of the angle β. By dividing the area under the curve by β, an average $\Delta n_{av.}$ of .00757 is obtained. The value used for $\omega = n_a$ is 2.4 and for $\epsilon = n_c$ is 2.385.

3. Calculation of the Relative Intensity for All Wave Lengths from 5200Å to 6200Å

As mentioned previously, the photocell employed in measuring the light intensity is essentially sensitive in the yellow portion of the spectrum. Hence, a constant amplitude band between 5200Å and 6200Å has been chosen to approximate the range of maximum sensitivity in the spectral intensity curve of the photocell (Figure 6.4).

The relative intensity is given by (cf. Equation (6.5))

$$R(\Delta n,m,\lambda) = \frac{1}{2}\sin^2\left(\frac{\pi\Delta nm}{\lambda}\right) .$$

Let

$$\lambda = \frac{c}{f} ,$$

where c is the velocity of light and f the frequency. Then

$$R(\Delta n,m,f) = \frac{1}{2}\sin^2\left(\frac{\pi\Delta nmf}{c}\right) . \qquad (6.11)$$

Averaging between $f_1 = \frac{c}{\lambda_1}$ and $f_2 = \frac{c}{\lambda_2}$ where $\lambda_1 = 6200Å$ and $\lambda_2 = 5200Å$, we get

$$R(\Delta n,m) = \frac{\frac{1}{2}\int_{f_1}^{f_2} \sin^2\left(\frac{\pi\Delta nm}{c}\right) f\,df}{\int_{f_1}^{f_2} df} \qquad (6.12)$$

Let

$$A \equiv \frac{\pi\Delta nm}{c} ,$$

and

$$Af = x,$$

$$dx = Adf.$$

Then (6.12) can be written as

$$R(\Delta n,m) = \frac{\frac{1}{2}\int_{Af_1}^{Af_2} \frac{1}{A}\sin^2 Af \, d(Af)}{\int_{f_1}^{f_2} df} \qquad (6.13)$$

$$= \frac{1}{4} - \frac{(\sin 2Af_2 - \sin 2Af_1)}{8A(f_2-f_1)} \quad . \qquad (6.14)$$

Equation (6.14) represents the relative light-intensity transmitted by the equivalent crystallite, for wavelengths between 5200Å and 6200Å. Some numerical values for the transmitted intensity can be obtained by assuming the previously calculated value of an average birefringence $\Delta n_{av.} = .00757$, and thicknesses varying from 20μ to 60μ. The results of these calculations are listed in Table 6.1.

4. Discussion of the Calculated Relative Transmitted Intensities

The object of the above calculations is to obtain an estimate of the transmitted light intensity that emerges from a thin section of a typical ferroelectric $(Ba,Sr)TiO_3$ composition when the latter is placed between crossed polars. The model used is a rough one. Absorption losses have not been considered, nor has the effect of light scattering and multiple reflections on the emerging intensity been taken into account. These undoubtedly take place in the ceramic thin section, but are difficult to determine with any degree of accuracy.

Two factors which emerge from the calculations seem to be worth noting here:

TABLE 6.1

RELATIVE LIGHT INTENSITY $\bar{R}$ (BETWEEN 5200Å AND 6200Å) TRANSMITTED BY A $(Ba,Sr)TiO_3$ CRYSTALLITE UNDER CROSSED POLARS.

RELATIVE INTENSITY $\bar{R}$ VS THICKNESS OF SAMPLE

$$\bar{R}\ (\Delta n, m) = \frac{1}{4} - \frac{(\sin 2Af_2 - \sin 2Af_1)}{8A(f_2 - f_1)}$$

Sample Thickness, m (in microns)	$2Af_2 = \frac{2\pi\Delta nm}{\lambda_2}$	$2Af_1 = \frac{2\pi\Delta nm}{\lambda_1}$	$\sin 2Af_2$	$\sin 2Af_1$	$\sin 2Af_2 - \sin 2Af_1$	$8A(f_2-f_1)$	$\frac{\sin 2Af_2 - \sin 2Af_1}{8A(f_2-f_1)}$	$\bar{R}(\Delta n, m)$
20	.584π	.488π	.966	.998	-.032	1.18	-.027	.277
25	.730π	.610π	.755	.940	-.185	1.47	-.126	.376
30	.876π	.732π	.345	.743	-.368	1.77	-.208	.458
35	1.020π	.854π	-.070	.438	-.508	2.06	-.247	.497
40	1.165π	.976π	-.515	.070	-.585	2.36	-.248	.498
45	1.314π	1.098π	-.834	-.301	-.533	2.65	-.201	.451
50	1.460π	1.220π	-.993	-.636	-.357	2.95	-.121	.371
55	1.606π	1.342π	-.946	-.883	-.063	3.24	-.019	.269
60	1.752π	1.464π	-.707	-.994	+.287	3.54	.081	.169

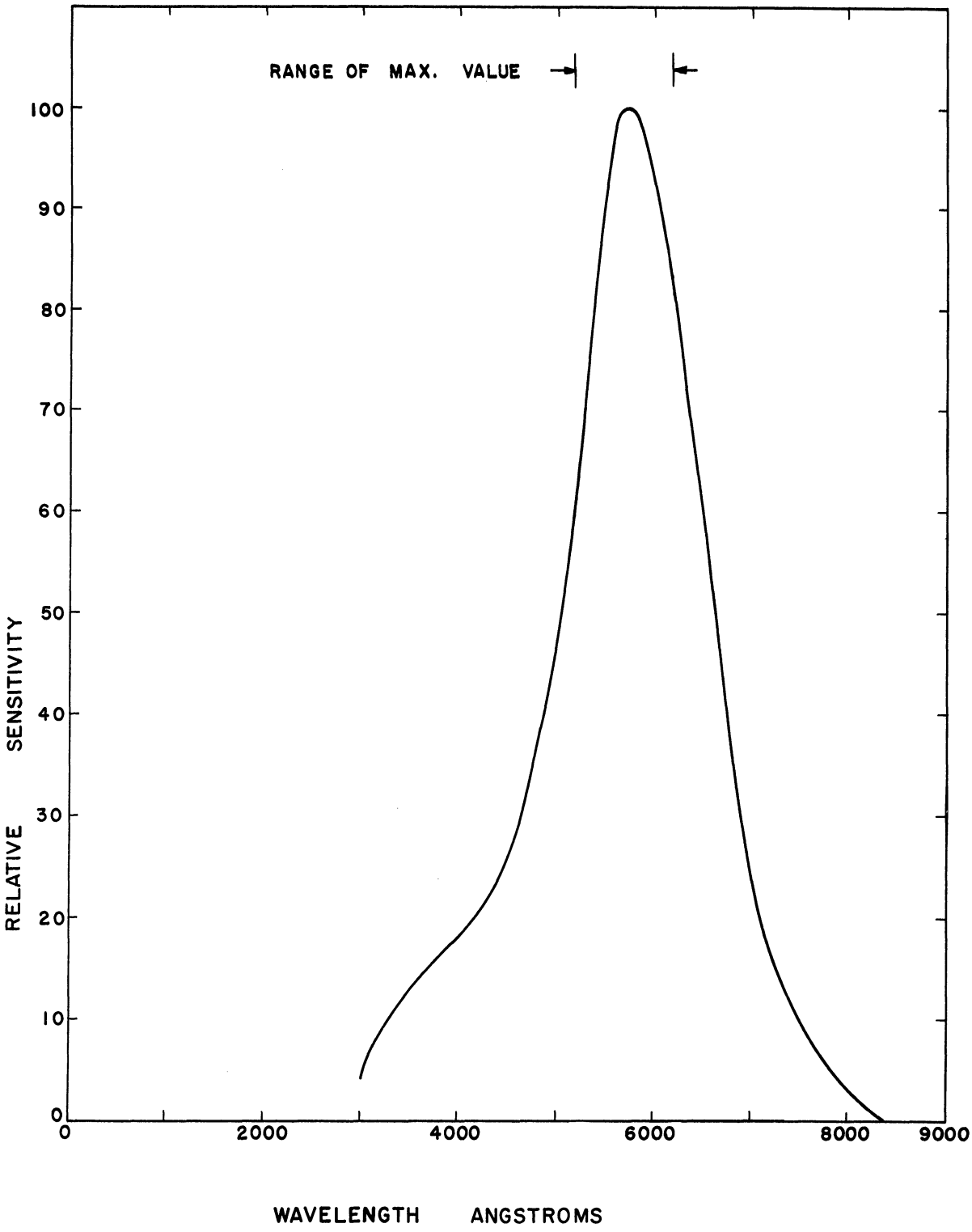


Figure 6.4. Spectral Sensitivity Curve of RCA Photocell 6957.

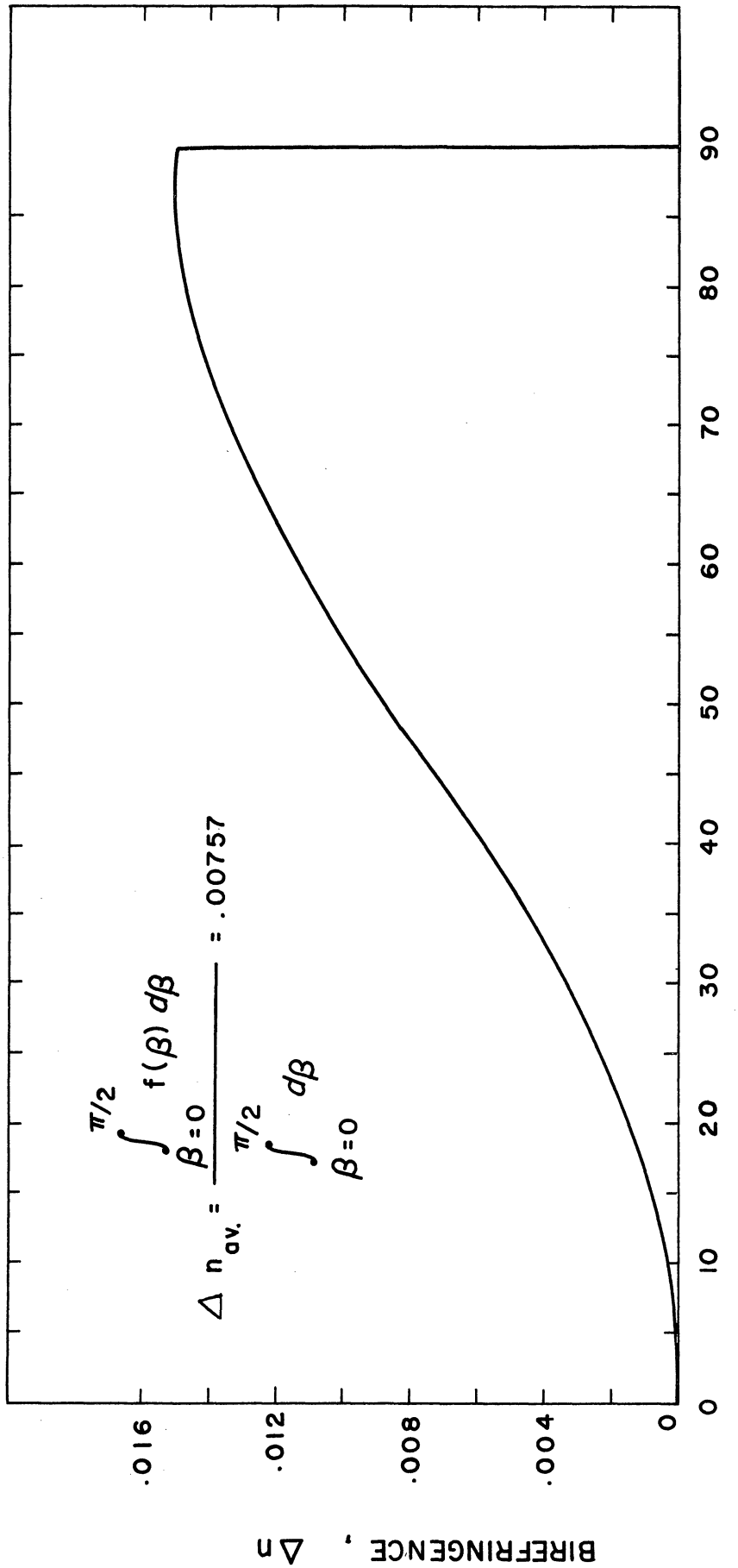


Figure 6.5. Birefringence Δn of a Barium-Strontium Titanate Crystal as a Function of Angle β.

First, Equation (6.5) and Figure 6.2 show that the light intensity transmitted by a two dimensional aggregate of randomly oriented anisotropic grains, between crossed polars, can at most be one-half of the incident intensity. The treatment neglects reflection and absorption losses in the ceramic which would further reduce this value.

Secondly, Table 6.1 illustrates the dependency of the relative transmitted intensity on the sample thickness for the specified wavelengths and average birefringence used in Equation (6.14). Between thicknesses of 30 to 45μ, the calculated relative light intensity varies between 45 to almost 50%. Hence thin sections of 30 to 45μ will transmit an optimum amount of light.

The four large-grained ceramics used for light intensity measurements are 30 to 40μ thick. Their relative transmitted intensities vary between 12 and 22%.

B. Change with Temperature in the Relative Amount of Light Transmitted by a Barium-Strontium Titanate Thin Section

Since the upper ferroelectric to paraelectric Curie transition in an unstressed barium-strontium titanate single crystal represents a phase transition from the tetragonal to the cubic state, the existence or the lack of an optical anisotropy in such a crystal becomes a means of determining the phase of the crystal.

Similarly, for a ceramic, the optical anisotropy of a barium-strontium titanate thin-section can give an indication of the crystallographic state of the ceramic, if the following factors are taken into account:

1) In a thin-section prepared from a commercial mixed titanate ceramic, the transition from a totally ferroelectric to totally paraelectric state does not take place at some definite temperature, as is the case for a single crystal. Instead, the transition in the ceramic occurs over a temperature range, owing to the variations in Curie temperatures of the grains composing the ceramic. (These small variations in transition temperature are essentially caused by compositional inhomogeneities [123] in the material. A complete reaction of the compositional end members of "mixed" barium-strontium titanate can be promoted by prolonged sintering at higher temperatures. However, materials thus reacted are generally too brittle and show too sharp a peak in permittivity to be of commercial value).

2) It seems a reasonable assumption that the Curie temperatures of the ceramic grains are distributed with temperature in the form of a Gaussian curve, with the maximum occurrences (Curie transitions) at the peak incremental permittivity temperature, see Figure 6.6. The area under the curve represents the total number of tetragonal to cubic transitions and therefore the total number of grains in the ceramic material.

3) The optical anisotropy in a ferroelectric ceramic thin-section can be empirically correlated with its tetragonal phase by measuring the intensity transmitted by the section between crossed polars. The observed intensity is the result of the light transmitted by the randomly oriented ferroelectric, tetragonal grains in the thin-section. When such intensity

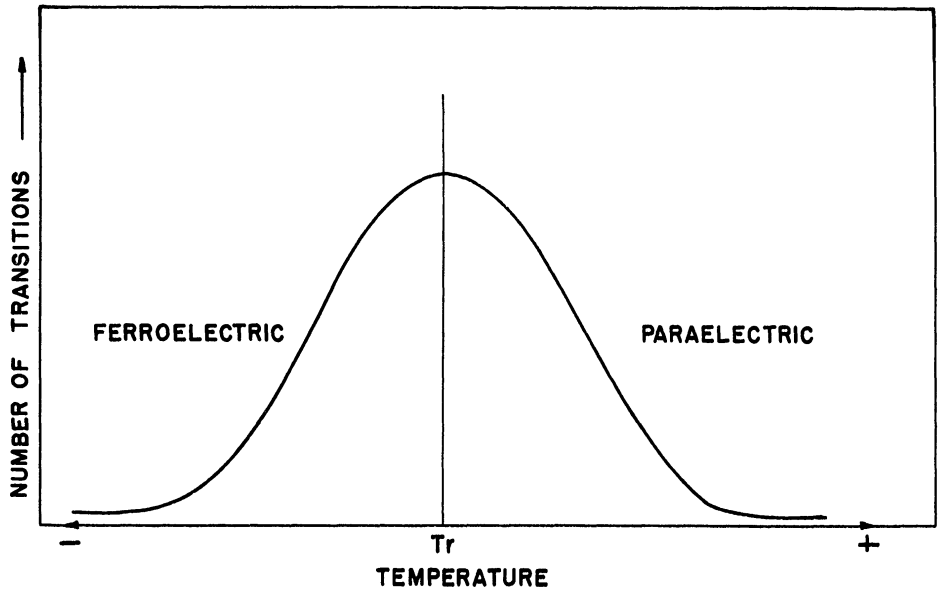


Figure 6.6. Assumed Distribution of the Tetragonal to Cubic Phase Transitions of the Ceramic Grains About the Peak Incremental Permittivity Temperature Tr of the Ceramic.

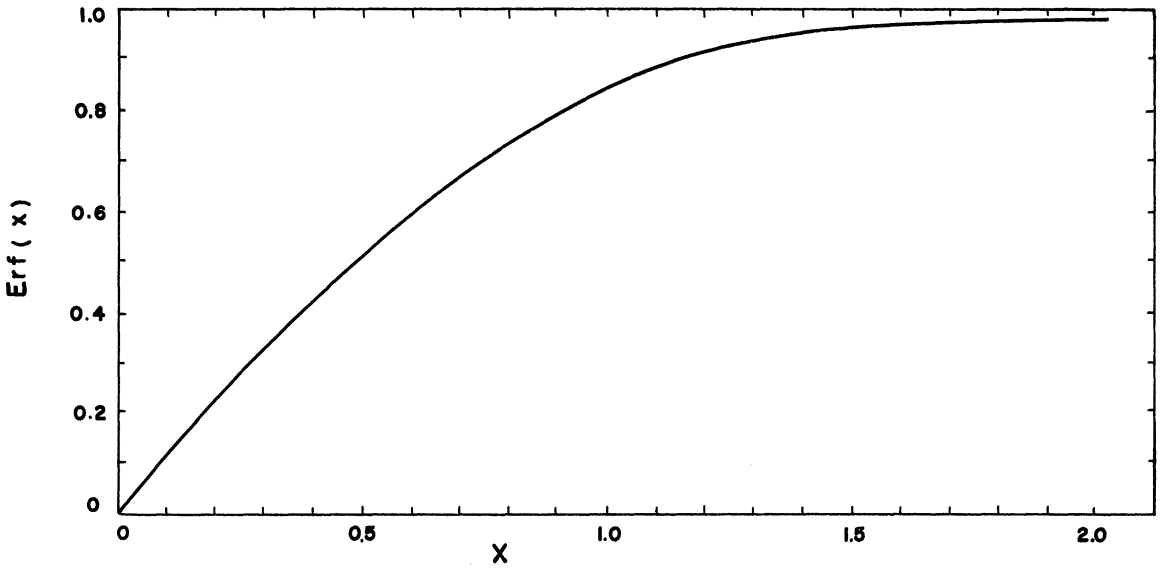


Figure 6.7. The Error Function $\text{erf}(x) = \frac{2}{\sqrt{\pi}} e^{-x^2}$.

measurements are taken on a barium-strontium titanate thin-section over a temperature range which includes the peak incremental permittivity temperature, the transmitted intensity shows the following behavior: It changes from some relatively high value of light intensity for the ferroelectric phase to almost complete extinction in the paraelectric phase. The relative transmitted light intensity of the thin-section can be directly related to that fraction of grains of the ceramic which are ferroelectric and tetragonal at any given temperature. At temperatures close to that of the peak incremental permittivity, the relative light intensity will experience its most significant changes. This follows from the substantial number of transitions which take place in the cermic at the peak incremental permittivity temperature, as seen in the schematic in Figure 6.6. It will be subsequently shown that the curve of the relative transmitted light intensity with temperature is of the form of (1-erf), where erf is the error function (Figure 6.7).

Consider a $(Ba,Sr)TiO_3$ ceramic composed of numerous grains.* The ceramic has a peak incremental permittivity at some temperature T_r. Let the probability of one grain changing phase from ferroelectric to paraelectric within the temperature range of dT be given by

$$dP(T) = P_o \, e^{-\left(\frac{T-T_r}{\alpha}\right)^2} dT \qquad (6.15)$$

* The assumption is made that it is valid to consider the phase transition temperatures of the ceramic grains to follow a normal distribution.

P is the probability, P_o is a constant, T is the temperature variable, T_r is the temperature of the peak incremental permittivity for a particular composition, and α is a variance parameter which will determine how broad the distribution will be. Now let the total number of grains in a ceramic be N. Let dn/dT be the number of grains transforming (i.e. changing phase) in a range dT such that

$$\int_0^\infty \left(\frac{dn}{dT}\right) dT = N \tag{6.16}$$

Let dn/dT be proportional to dP/dT as a reasonable assumption. Then

$$\frac{dn}{dT} = n_o e^{-\left(\frac{T-T_r}{\alpha}\right)^2}, \tag{6.17}$$

and

$$N = \int_0^\infty n_o e^{-\left(\frac{T-T_r}{\alpha}\right)} dT. \tag{6.18}$$

Thus the total number of grains in the ceramic are described as the number which change phase between the temperature limits of 0°K to ∞. It is assumed here for purposes of calculation that no other phases except the tetragonal and the cubic exist within this range.

To calculate the value of n_o, let

$$n_o = \frac{N}{\int_0^\infty e^{-\left(\frac{T-T_r}{\alpha}\right)^2} dT}. \tag{6.19}$$

Compute

$$\int_0^\infty e^{-\left(\frac{T-T_r}{\alpha}\right)^2} dT. \tag{6.20}$$

By substituting $x = \frac{T-T_r}{\alpha}$ into Equation (6.20), we get

$$\alpha \int_{\frac{-T_r}{\alpha}}^{\infty} e^{-x^2}\, dx \,. \tag{6.21}$$

From the tables of integrals it is known that

$$\int_0^{\infty} e^{-x^2}\, dx = \frac{\sqrt{\pi}}{2} \tag{6.22}$$

Equation (6.21) can be also written as

$$\alpha \int_{\frac{-T_r}{\alpha}}^{0} e^{-x^2}\, dx + \alpha \int_0^{\infty} e^{-x^2}\, dx \,, \tag{6.23}$$

$$\alpha \int_{\frac{-T_r}{\alpha}}^{0} e^{-x^2}\, dx + \alpha \frac{\sqrt{\pi}}{2} \,. \tag{6.24}$$

T_r for one of the measured mixed titanate ceramics is about 330°K, α is about 15. The lower limit of integration in Equation (6.24) is therefore about -22. According to the tables of error functions[124] the error integral,

$$\begin{aligned} \text{erf} = \frac{2}{\sqrt{\pi}} \int_{-x}^{0} e^{-x^2}\, dx &= -\frac{2}{\sqrt{\pi}} \int_0^{-x} e^{-x^2}\, dx \\ &= \frac{2}{\sqrt{\pi}} \int_0^{x} e^{-x^2}\, dx \,, \end{aligned} \tag{6.25}$$

reaches 99.9% of its full value for $x = -2.4$. At $x = -22$, the error integral can be considered to be unity (Figure 6.7). Hence, by extending

$-x$ to $-\infty$ in Equation (6.25), the value of the error integral essentially remains the same. Likewise, the following approximations can be made for Equation (6.24):

$$\alpha \int_{\frac{-T_r}{\alpha}}^{0} e^{-x^2}\, dx + \alpha \frac{\sqrt{\pi}}{2} \approx \alpha \int_{-\infty}^{0} e^{-x^2}\, dx + \alpha \frac{\sqrt{\pi}}{\alpha} \simeq \alpha\sqrt{\pi} \qquad (6.26)$$

Equation (6.19) therefore becomes

$$n_o \simeq \frac{N}{\alpha\sqrt{\pi}} \qquad (6.27)$$

Thus, Equation (6.18), which represents the total number of grains that change phase from tetragonal to isotropic within the temperature interval from 0 to ∞ can be alternately written as

$$N = \frac{N}{\alpha\sqrt{\pi}} \int_{0}^{\infty} e^{-\left(\frac{T-T_r}{\alpha}\right)^2} dT \,. \qquad (6.28)$$

As previously indicated, the intensity of the light transmitted by a ferroelectric thin section between crossed polars can be assumed to be proportional to the number of anisotropic or tetragonal grains in the ceramic. The limits of integration in Equation (6.28) can be modified to give the function

$$f(T) = \frac{N}{\alpha\sqrt{\pi}} \int_{0}^{T} e^{-\left(\frac{T-T_r}{\alpha}\right)^2} dT \qquad (6.29)$$

This expression represents the number of isotropic grains in the material at some temperature T, i.e., the number of grains that have changed phase between 0°K to T°K. The remaining anisotropic grains in the ceramic at T are therefore described by

$$N - f(T) = N\left[1 - \frac{1}{2\sqrt{n}} \int_0^T e^{-\left(\frac{T-T_r}{\alpha}\right)^2} dT\right] . \qquad (6.30)$$

If the assumptions made in the present calculation are valid, there should be a direct relationship between the number of anisotropic grains in the ceramic, as a function of temperature, and the optical behavior of the experimental light transmission curves.

Equation (6.30) can be evaluated in the following manner. Let the fraction of anisotropic grains in the ceramic be given by

$$g(T) = 1 - \frac{f(T)}{N} = 1 - \frac{1}{\alpha\sqrt{\pi}} \int_0^T e^{-\left(\frac{T-T_r}{\alpha}\right)^2} dT . \qquad (6.31)$$

Substitute $x \equiv \frac{T-T_r}{\alpha}$ into Equation (6.31). Then

$$g(T) = 1 - \frac{1}{\sqrt{\pi}} \int_{\frac{-T_r}{\alpha}}^{\frac{T-T_r}{\alpha}} e^{-x^2} dx . \qquad (6.32)$$

Equation (6.32) can also be written as

$$g(T) = 1 - \frac{1}{\sqrt{\pi}} \int_{\frac{-T_r}{\alpha}}^{0} e^{-x^2} dx + \int_0^{\frac{T-T_r}{\alpha}} e^{-x^2} dx . \qquad (6.33)$$

The integral $\frac{2}{\sqrt{\pi}} \int_{\frac{-T_r}{\alpha}}^{0} e^{-x^2} dx$ for $-\frac{T_r}{\alpha} < -2.7$ is approximately unity (Figure 6.7). $-\frac{T_r}{\alpha}$ for the measured barium-strontium titanate thin sections is about -22. Equation (6.33) therefore becomes

$$g(T) = 1 - \frac{1}{2}\left[1 + \frac{2}{\sqrt{\pi}} \int_0^{\frac{T-T_r}{\alpha}} e^{-x^2}\, dx\right], \qquad (6.34)$$

$$= .5 + \frac{1}{\sqrt{\pi}} \int_0^{\frac{T-T_r}{\alpha}} e^{-x^2}\, dx\,. \qquad (6.35)$$

The integral $\frac{2}{\sqrt{\pi}} \int_0^{\frac{T-T_r}{\alpha}} e^{-x^2}\, dx$ can be directly evaluated from the tables of integrals. As the temperature T ranges from 293°K to 393°K, with T_c being about 330°K and $\alpha \cong 15$, the integral goes from -1 to 1, and the function g(T) from 1 to 0. Hence g(T) describes the ceramic as being composed of exclusively anisotropic crystallites at the low end of the temperature scale and of exclusively isotropic crystallites at the high end.

g(T) has been calculated for four large-grained thin sections, both for conditions of zero field, and for large biasing fields. The computed curves have been rescaled to allow comparison with the experimental percent light transmission data. Results are shown in Figures 6.8, 6.9, 6.10, and 6.11.

C. Change with Temperature and Applied DC Field in the Relative Amount of Light Transmitted by a Barium-Strontium Titanate Thin Section

Several investigators[78, 79, 100] have reported a shift in the Curie temperature of single crystal barium titanate under the influence of a field. The Curie temperature is shifted to higher values when the field is applied either parallel or perpendicular to the polar axis of the crystal. Measurements made by Merz[78] at temperatures above the Curie point of "good" $BaTiO_3$ single crystals show that he was able to induce a ferroelectric state in the crystals on alternate cycles of a strong

60-cycle field. It has been also noted experimentally that a strong field causes a shift in the peak incremental permittivity temperatures of ceramic barium titanate and barium-strontium titanate ferroelectrics. (Figures 2.4 and 2.5)

According to Merz, [78] the Curie temperature shift ΔT of a crystal which is subjected to an electric field E can be expressed to the first approximaltion by the formula

$$\Delta T = C \times |E| \quad . \tag{6.36}$$

ΔT represents the increase in the Curie temperature of the biased crystal in °C , E is the field applied in volts/cm, and C is to a first approximation a constant = 1.43×10^{-3} °C cm/volt. By adapting Equation (6.36) to the case of ceramics, the "new" peak incremental permittivity temperature, T_r^* , of the crystallites composing an electrically biased ceramic thin section, can be expressed by

$$T_r^* = T_r + \gamma |E| \quad . \tag{6.37}$$

T_r is the peak incremental permittivity of the ceramic at zero electric field, γ is a constant expressed in °C cm/volts, and E is the applied field in volts/cm. By using T_r^* for T_r and $x' = \frac{T-T_r^*}{\alpha}$ in Equation (6.33), we obtain an expression for the anisotropy in a mixed titanate ceramic thin section as a function of temperature and electric field.

$$g(T)^* = 1 - \frac{1}{\sqrt{\pi}} \left[\int_{\frac{-T_r^*}{\alpha}}^{0} e^{-x'^2} dx' + \int_{0}^{\frac{T-T_r^*}{\alpha}} e^{-x'^2} dx' \right] \tag{6.38}$$

Again, Equation (6.38) can be simplified to

$$g(T)^* = 1 - \frac{1}{2}\left[1 + \frac{2}{\sqrt{\pi}} \int_0^{\frac{T-T_r^*}{\alpha}} e^{-x'^2}\, dx'\right] \tag{6.39}$$

$$= .5 + \frac{1}{\sqrt{\pi}} \int_0^{\frac{T-T_r^*}{\alpha}} e^{-x'^2}\, dx' \,. \tag{6.40}$$

Since the peak incremental permittivity temperature T_r^* of a biased ceramic is greater than the temperature T_r in the unbiased state, the function $g(T)^*$ will be located at higher values along the temperature axis than $g(T)$. This is shown in Figures 6.8, 6.9, 6.10, 6.11.

D. Comparison of the Relative Theoretical and Experimental Light Transmission Curves

A meaningful evaluation of the percent light transmission vs temperature curves for a mixed titanate thin section using (6.35) and (6.40) depends on the correct choice of the constants T_r , T_r^* and α . Since good single crystal data on solid solutions of barium-strontium titanates are lacking, it is not possible to evaluate the Curie temperature and the shift in Curie temperature of these compositions directly. The constants T_r , T_r^* , as well as the variance or dispersion parameter of the ceramic distribution α , have therefore been obtained from available experimental as well as theoretical[62] data on ceramic compositions.

1. Consideration of T_r, the Peak Incremental Permittivity Temperature of the Ceramic at Zero Field

It is known[64] that a linear relationship exists between the peak incremental permittivity temperature of barium-strontium titanate ceramics and their composition. For pure barium titanate, the transition

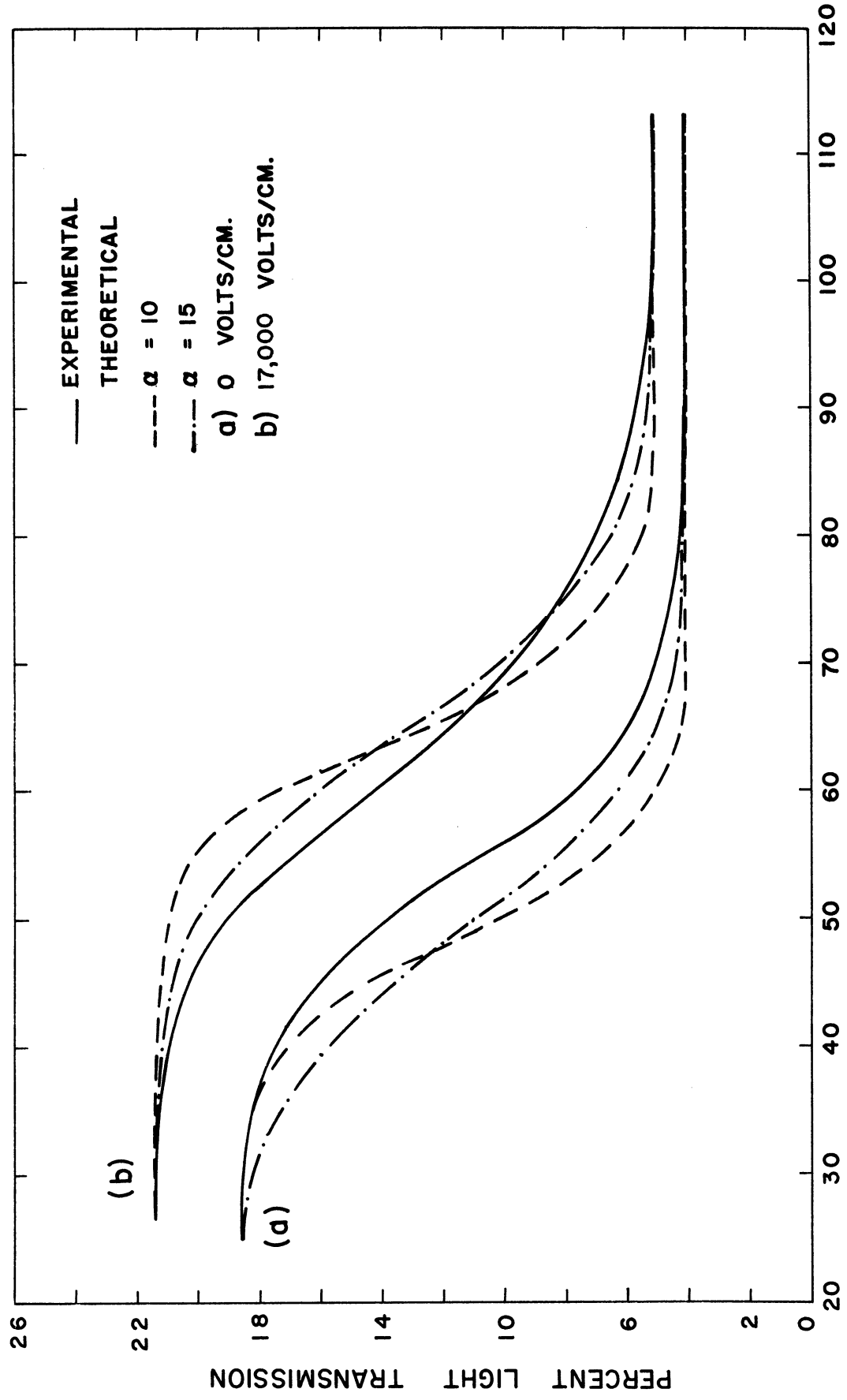


Figure 6.8. Comparison of Theoretical and Experimental Percent Light Transmission Curves for a Ceramic Thin Section, Sample 1.

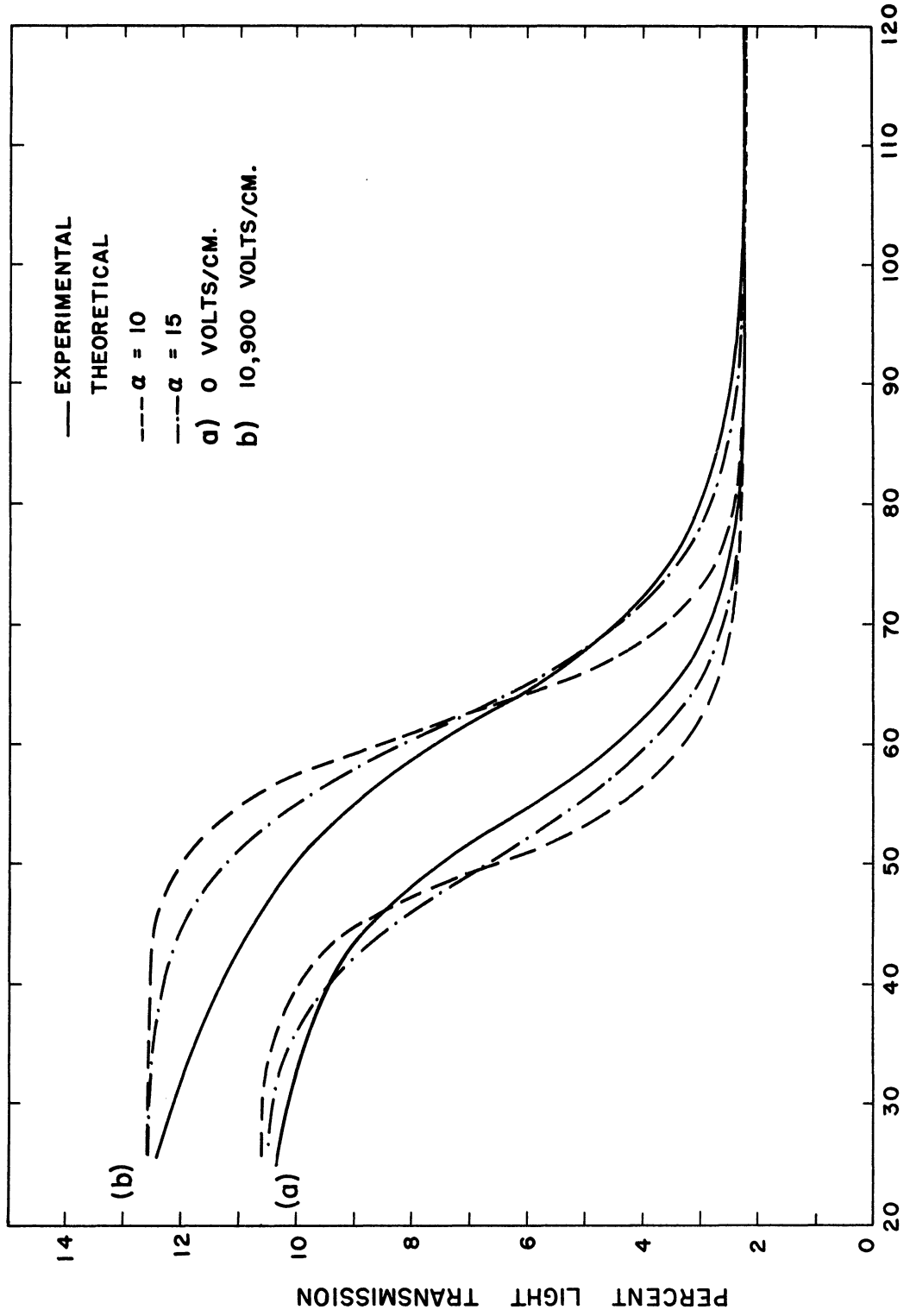


Figure 6.9. Comparison of Theoretical and Experimental Percent Light Transmission Curves for a Ceramic Thin Section, Sample 2.

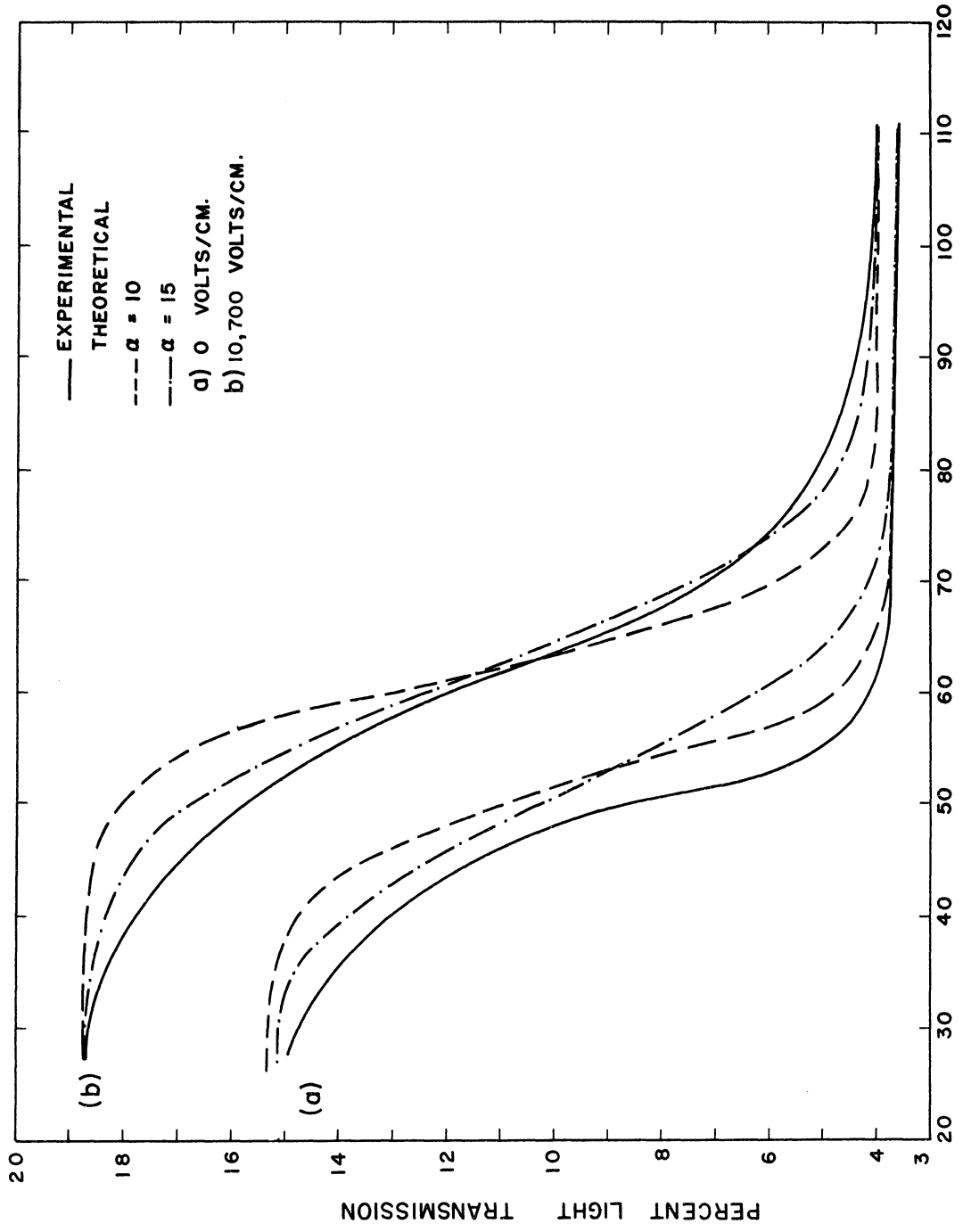


Figure 6.10. Comparison of Theoretical and Experimental Percent Light Transmission Curves for a Ceramic Thin Section, Sample 3.

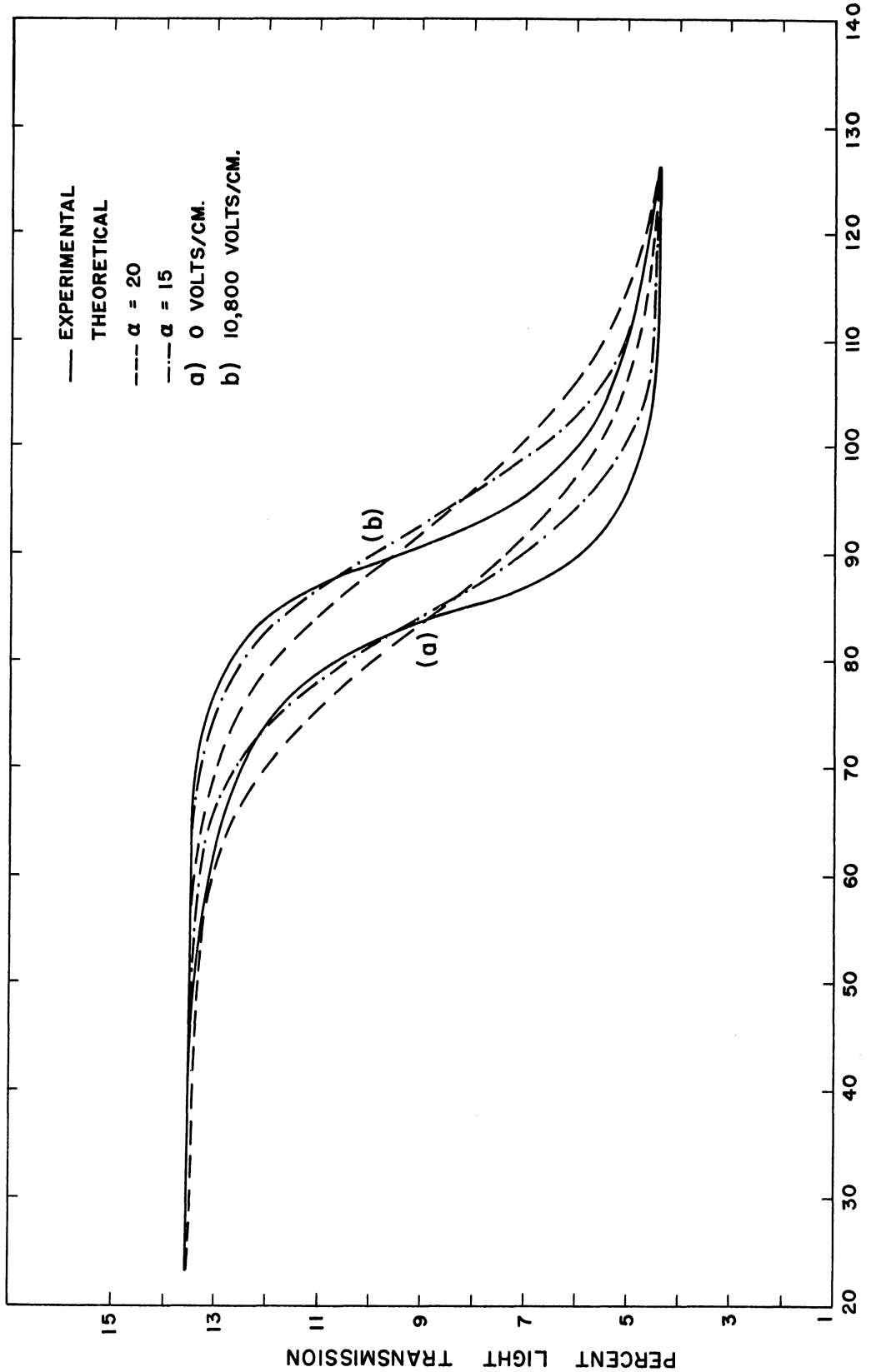


Figure 6.11. Comparison of Theoretical and Experimental Percent Light Transmission Curves for a Ceramic Thin Section, Sample 4.

occurs at about 120°C and decreases linearly with additions of strontium to absolute zero for pure strontium titanate. It should therefore be possible to determine the peak incremental permittivity of such a ceramic if its composition were known. Unfortunately, the peak permittivity temperatures of the mixed titanates are influenced not only by their composition, but by the completeness of the stoichiometric reaction, and by factors like impurities and internal strains. In general, the harder the ceramics are fired, the higher their peak incremental permittivity temperature. (Pure barium titanate ceramics prepared at the Electromagnetic Materials Laboratory of the University of Michigan, Department of Electrical Engineering, have shown peaks in incremental permittivity varying from 120°C to 140°C. In every instance, the material was commercially acceptable, i.e., it was not "underfired". The method of preparation of the "green body" was essentially the same, the firing cycles, however, varied somewhat in length.) Hence the linear relationship between the transition temperature and composition in mixed barium-strontium titanates can at best only be a guide. An important factor influencing the peak incremental permittivity temperatures of two of the four samples measured here are the small amounts of fluxing agents added to two compositions. (Table 4.1). The particular metal oxides added to the compositions tend to increase grain growth; they also increase the peak incremental permittivity temperature by about 20°C over the predicted temperature for the "pure" mixed titanate.

For these reasons, T_r has been taken directly from the experimental zero field permittivity vs temperature data. T_r is defined as the peak incremental permittivity temperature of a particular barium-strontium

titanate ceramic with a specific history of preparation. It is also that temperature at which the largest number of crystallites change phase with in the ceramic.

2. Consideration of T_r^*, the Peak Incremental Permittivity Temperature of a Ceramic Under the Influence of an Electric Field

The shift in the peak incremental permittivity temperature with field is obtained in the following manner: the value γ in the Equation $T_r^* = T_r + \gamma E$ is determined from the incremental permittivity vs temperature data of a specific mixed titanate sample. Knowing the value γ and the electric field across the thin section end of the sample, the shift in the peak permittivity temperature at the thin section end can be evaluated. Several γ's are listed in Table 6.2. The values of γ are lower than for single crystal barium titanate which has been reported as 1.2°cm/Kv by Kaenzig and Maikoff,[79] 1.4°cm/Kv by Merz,[78] and 1.6°cm/Kv by Kawabe[100].*

When a certain critical temperature is exceeded, a ferroelectric phase can no longer be induced in a single crystal, regardless of the applied field strength. Below the critical temperature, the polarization of the single crystal experiences a sudden increase as the crystal goes from paraelectric to ferroelectric. Above the critical temperature, the polarization changes continuously with increasing field (see Figure 6.12b).

---

* It should be pointed out that strictly speaking, γ is not a constant. γ, the shift in the transition temperature with field decreases with increasing fields. Since the values of γ on $(Ba,Sr)TiO_3$ ceramics were determined at high fields, they are necessarily somewhat lower than the average γ for the entire "inducable" temperature range.

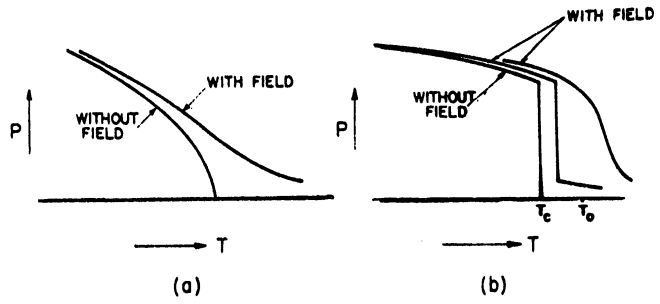


Figure 6.12. Polarization as a Function of Temperature, With and Without a Biasing Field.
(a) Near a Second Order Transition.
(b) Near a First Order Transition (After Devonshire)[125].

From Merz's[78] double hysteresis loop experiments on barium titanate it can be calculated that the critical temperature is about 12°C above the Curie temperature of the unbiased single crystal. Kawabe reports observing a field produced shift in the transition temperature of about 15°C.

In mixed barium-strontium titanate ceramics it is difficult to determine the maximum field produced shift in the Curie temperatures of the grains composing the ceramic because of their distribution over a temperature range. Based on single crystal data of barium titanate, the maximum obtainable shift is assumed to be about 15°C for the ceramic materials. $T_r^* - T_r$ for the relative light intensity curves of sample 1 is therefore taken to be 15°C rather than the calculated 19°C.

3. Discussions of α, the Variance Parameter of the Ceramic Distribution

The value for α in the expression of the theoretical light intensity is obtained by fitting the experimental permittivity vs temperature

curves to theoretical curves with known values of α. It has been shown by Diamond[62] that the zero field incremental permittivity of a barium-strontium titanate ceramic at some temperature can be evaluated from the expression

$$\overline{\epsilon(T)} = \frac{\int_0^\infty \epsilon(T,T_c)\, e^{-\left(\frac{T_c-T_r}{\alpha}\right)^2} dT_c}{\int_0^\infty e^{-\left(\frac{T_c-T_r}{\alpha}\right)^2} dT_c} \qquad (6.41)$$

where

$$\epsilon(T,T_c) = \begin{cases} \epsilon_{av.} & \text{for } T \leq T_c \\ \frac{4\pi C}{T-T_o} & \text{for } T > T_c \end{cases} . \qquad (6.42)$$

$\overline{\epsilon(T)}$ is the average permittivity at temperature T of the randomly distributed barium-strontium titanate crystallites that compose the ceramic. In this model, the Curie temperatures T_c of the crystallites form a Gaussian distribution about some chosen temperature, T_r, which is primarily dependent on the composition of the mixed titanate. Furthermore, $\epsilon(T,T_c)$, the incremental permittivity of the individual crystallite, assumes a similar dielectric behavior as observed on a barium titanate single crystal. At temperatures below the Curie temperature T_c, the permittivity takes on a value $\epsilon_{av.}$ obtained by averaging over the ellipsoid associated with the permittivity tensor of the individual crystallite. (The lower temperature ferroelectric transitions have not been considered in this treatment.) At temperatures higher than T_c, the incremental permittivity of the crystallite follows the Curie Weiss law, $\epsilon = \frac{4\pi C}{T-T_o}$, where C is the Curie constant and T_o for $BaTiO_3$ is about 10°C lower than T_c. Based on Equation (6.41),

Diamond computed the incremental permittivity vs temperature characteristics of some typical barium-strontium titanate compositions for different values of α. The curves in Figure 6.13 represent α's of 10, 15, 20, and 50. $T_r = 300°K$, $T_c = T_o + 10$[78] and the Curie constant $C = 1.4 \times 10^4$.[78] When the experimental permittivity curves of samples 1, 2, 3, and 4 (Figures 5.1, 5.3, 5.5, 5.7) are compared with the theoretical curves shown in Figure 6.13 several differences immediately become apparent:

First, the incremental permittivities of Samples 1-4 are considerably lower than the theoretical values. The theoretical model represents an ideal ceramic, in which the permittivities of the ceramic crystallites are equivalent to that of single crystals. High values of permittivity are obtained in a sufficiently large, well sintered and dense piece of ceramic. The samples used for the present percent light transmission experiments, however, are less than 1 cm long and .1 cm wide, with thicknesses ranging from about .1cm at one end to 40μ at the other. The initial low porosity of the material was increased during the grinding and polishing process. Some tearing-out of the material could not be avoided and the holes introduced were not completely removed by subsequent polishing. This fact may in part explain the low measured capacitances of the samples.*

Secondly, when the experimental permittivity curves are superimposed on the theoretical curves of Figure 6.13 by adjusting the experimental

---

* Even small amounts of porosity would be very effective in reducing the permittivity if the basic material was a high permittivity ceramic (cf. Lichtenecker's Formula[126]: $\ell n \epsilon_T = x_1 \ell n \epsilon_1 + x_2 \ell n \epsilon_2 + \ldots$) .

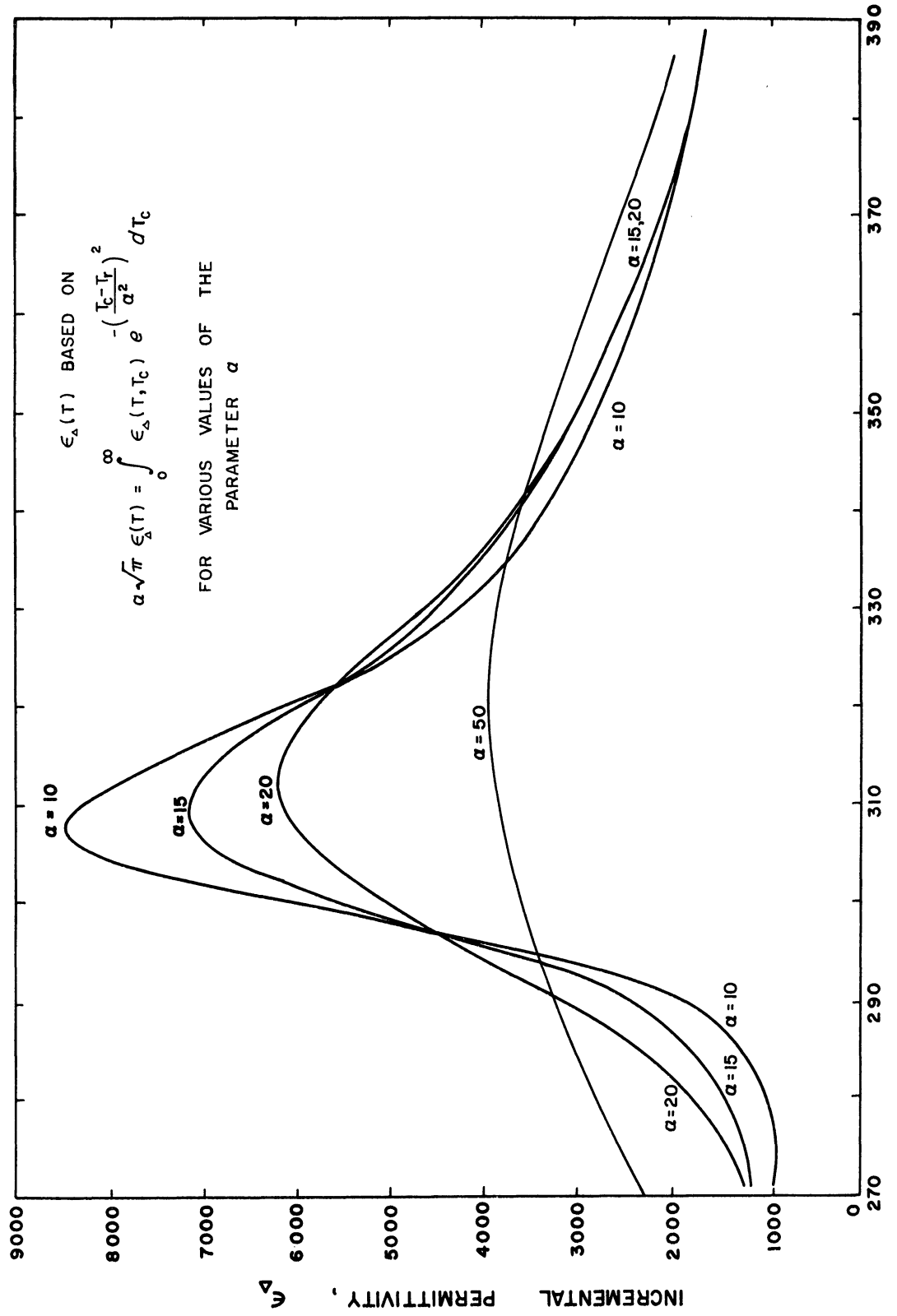


Figure 6.13. Theoretical Incremental Permittivity vs. Temperature Curves for Various Values of the Parameters α.

permittivity value and temperature of the peak incremental permittivity to fit that of the theoretical curve, a distortion in the experimental curves on both sides of the peak becomes visible (Figures 6.14 - 6.17). It is felt that the misfit results from the diffifulty encountered in determining small capacitances (about 30μμf) with the instrumentation used. Although precautions were taken to account for stray capacitances (see Section IV), it is possible that some systematic errors have been introduced during the measurement of the samples.

Figures 6.14, 6.16, 6.17 show that the incremental permittivity vs temperature curves of 3 samples closely resemble the theoretical curves for which α is 10 and 15. In Figure 6.15 the experimental curves resemble the theoretical ones for which $\alpha = 15$ and 20 . These values for α have been used to plot the theoretical vs experimental percent light transmission curves (Figures 6.8-6.11).

4. Comparison of the Experimental and Theoretical Transmitted Light Intensity Curves

Figures 6.8 to 6.11 represent the experimental light transmission vs temperature measurements taken on four large grained $(Ba,Sr)TiO_3$ ceramics, and their respective theoretical transmission curves, based on Equation (6.35) and (6.40). The two sets of curves shown in each figure illustrate the optical behavior of the ceramic at zero field and at the strongest field employed during the experiment. Fields higher than the latter caused sparking at the sample electrodes and breakdown of the ceramic.

A comparison of the theoretical and experimental curves shows that both have a relatively flat portion at the lower side of the temperature scale, followed by a sharp drop in the percent light transmission over

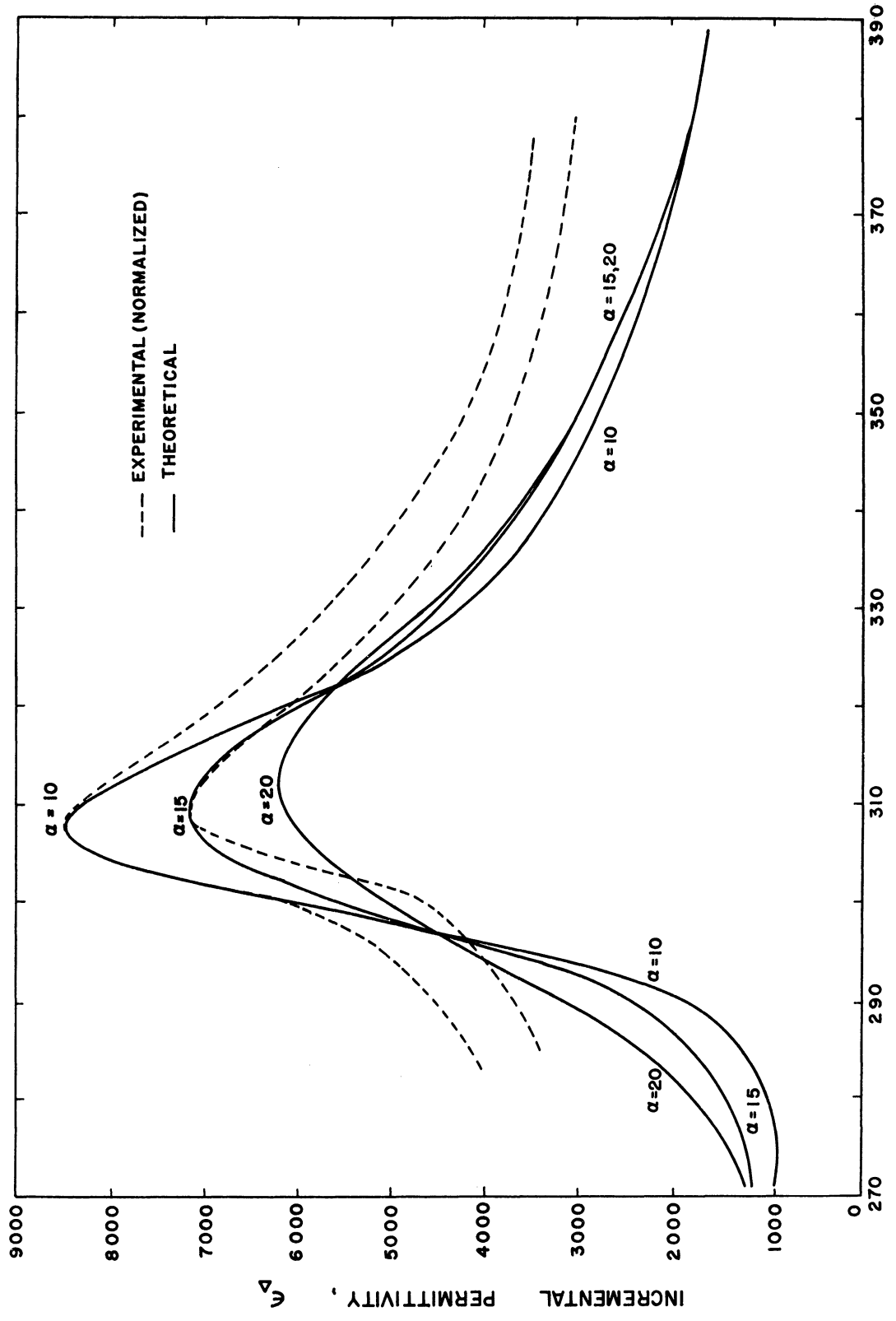


Figure 6.14. Comparison of Theoretical and Normalized Experimental Incremental Permittivity vs. Temperature Curves for Sample 1.

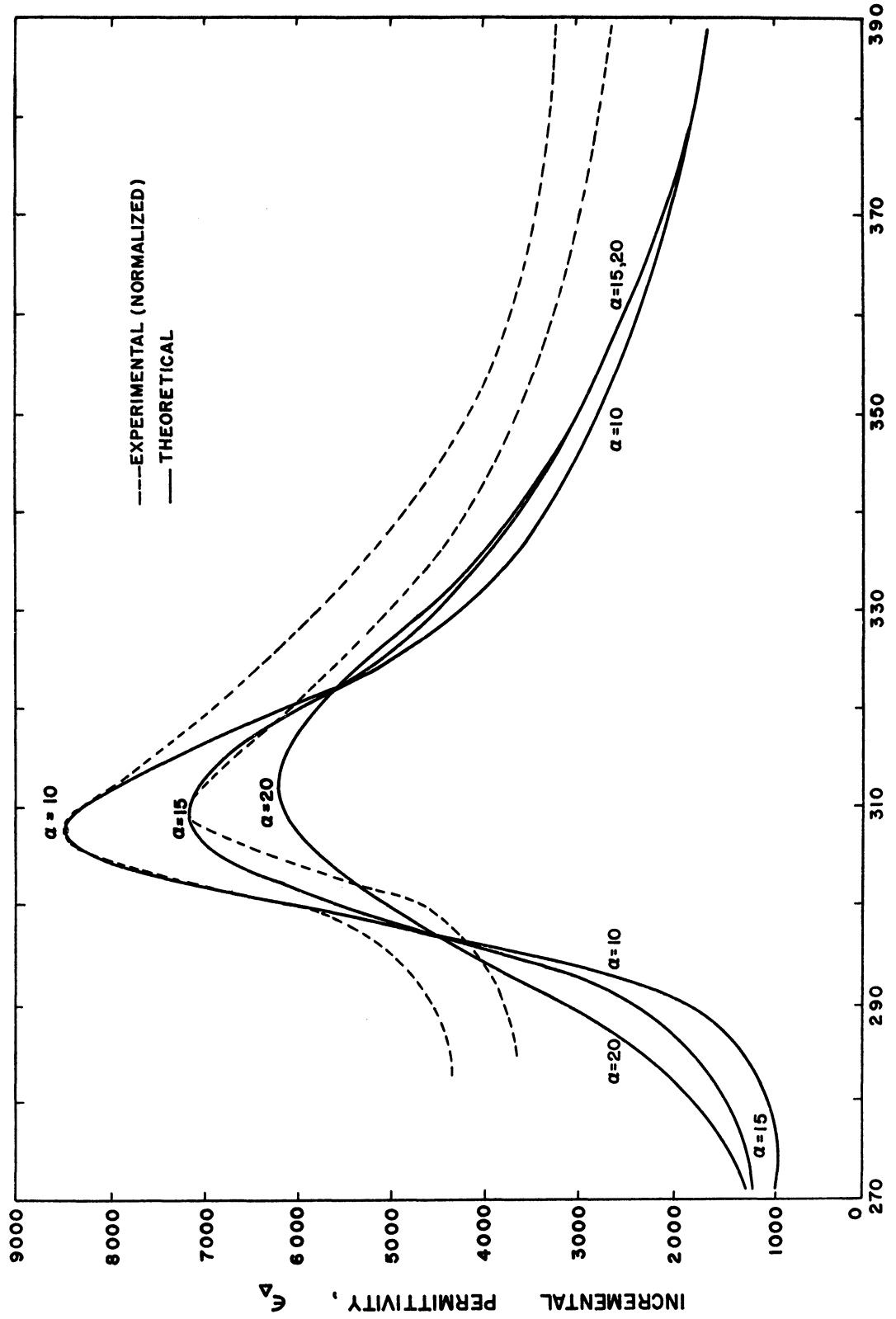


Figure 6.15. Comparison of Theoretical and Normalized Experimental Incremental Permittivity vs. Temperature Curves for Sample 2.

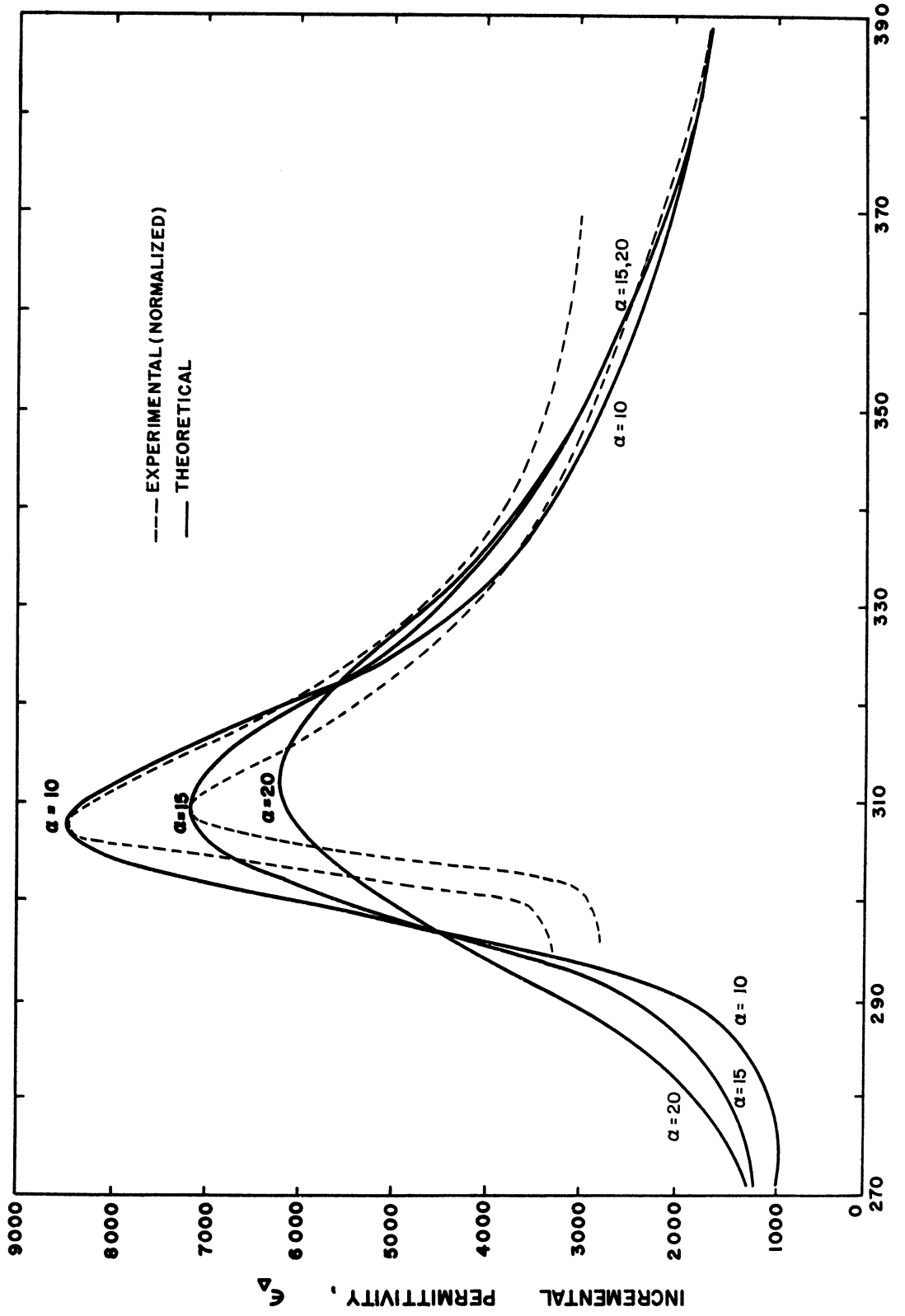


Figure 6.16. Comparison of Theoretical and Normalized Experimental Incremental Permittivity vs. Temperature Curves for Sample 3.

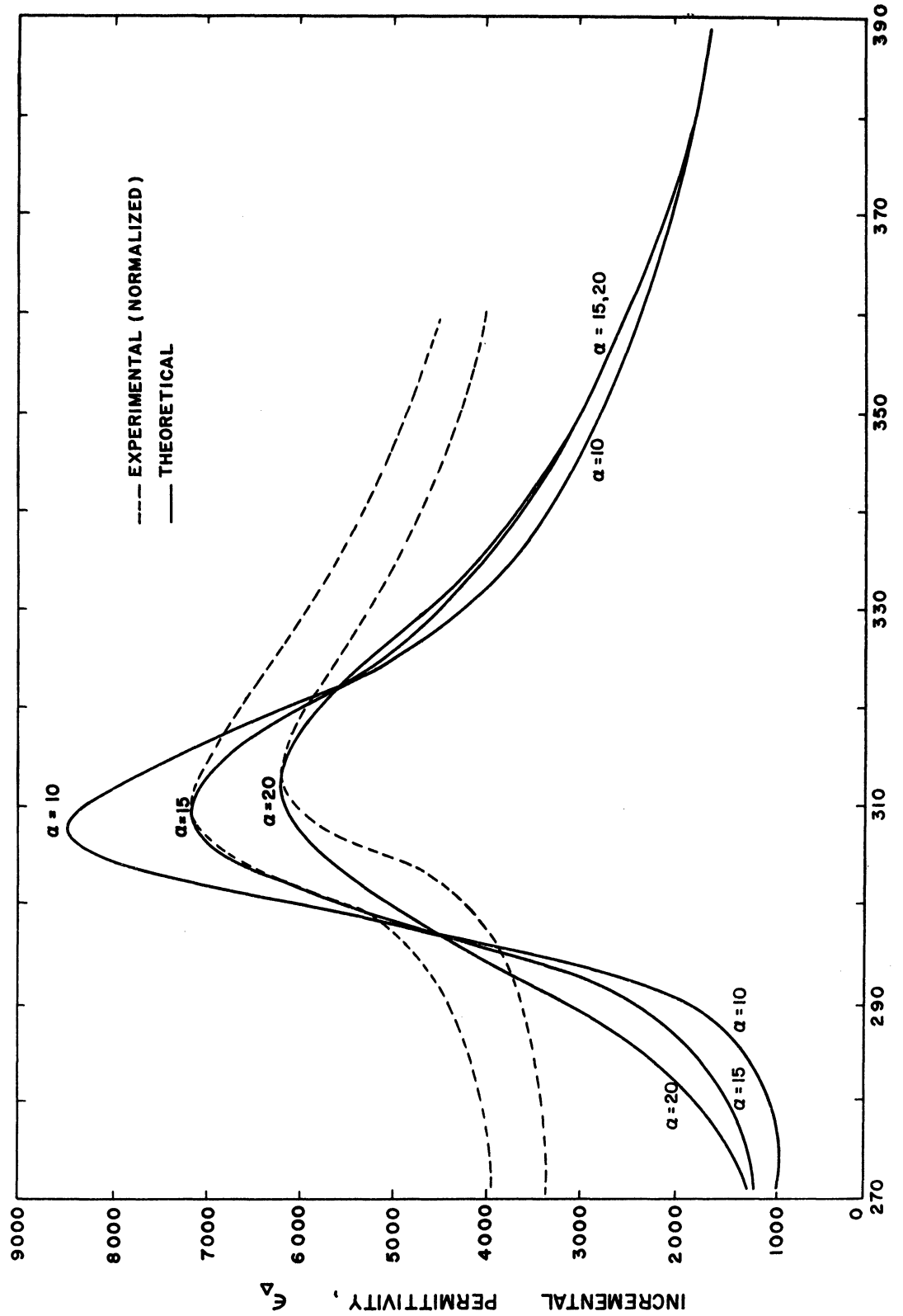


Figure 6.17. Comparison of Theoretical and Normalized Experimental Incremental Permittivity vs. Temperature Curves for Sample 4.

a narrow temperature range. At high temperatures, the slope of the curve is again relatively small. The steep portion of the curve describes the temperature range at which most ferroelectric to paraelectric transitions in the ceramic occur.

The fit between the theoretical and experimental curves is not necessarily good in every instance. As indicated earlier, the accuracy with which Equations (6.34) and (6.39) can predict the ratio of anisotropic to isotropic grains at any given temperature depends on the choice of the constants T_r , T_r^* and α for any given sample. Above all, the model on which the calculations are based must be basically valid. The model rests on two assumptions:

1) Each crystallite in the ceramic, which is considered the smallest ferroelectric unit with a distinct polar vector, has a tetragonal to cubic transition at which the optical anisotropy drops from some constant, high average value of birefringence to a constant low value. The biasing field simply shifts the transition to higher temperatures. This is seen from Equation (6.37) where $T_r^* = T_r + \gamma E$.

2) The transition temperature of the individual crystallites are numerically distributed about some temperature T_r in a Gaussian distribution. The exact position and shape of the distribution is determined by the constants T or T_r^* and α as expressed in Equations (6.35) and (6.40).

The validity of the first assumption can be partly tested against the optical transmission measurements performed by Kawabe on a single crystal of barium titanate.[100] Figure 6.18 shows that at zero applied field the

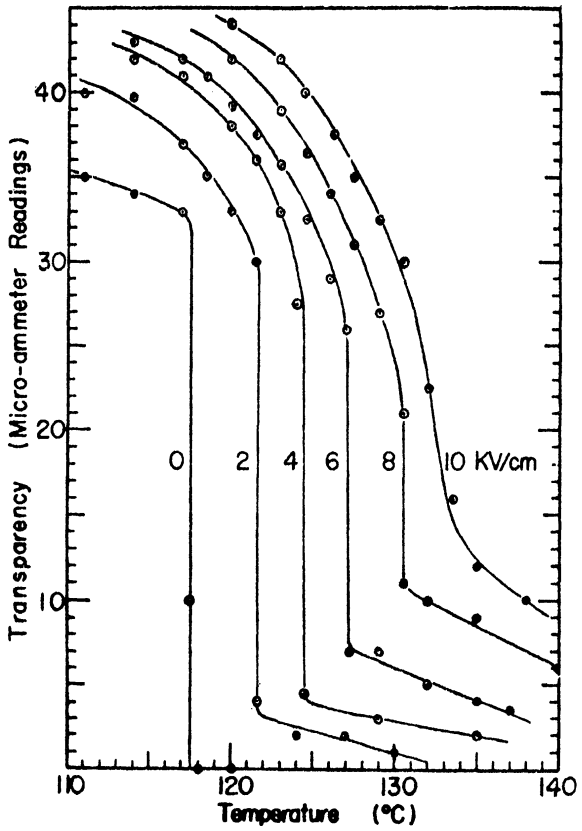


Figure 6.18. Temperature Dependence of the Optical Transmission of Barium Titanate with Various Applied Fields Near 120°C.

crystal goes from anisotropic to completely isotropic at the transition temperature. Below the transition temperature, there is a gradual increase in transparency with temperature. This follows from the known increase in birefringence upon cooling the crystal from its cubic-tetragonal to tetragonal-orthorhombic transition (see Figure 5.17). When increasing fields are applied to the single crystal, the transition temperature not only shifts to higher temperatures (Figure 6.18) but the difference in transparency between the induced ferroelectric and paraelectric states becomes increasingly smaller. At sufficiently high temperatures a ferroelectric phase can no longer be induced by the field. Thus, in addition to a simple temperature dependence as observed for the birefringence of the crystal at zero field, the transparency of the biased crystal depends on the field in that it

1) shifts the transition temperature, and

2) produces a temperature dependent strain anisotropy in both the paraelectric and ferroelectric states.

The present theoretical model of a ceramic does not take the temperature dependence of the optical anisotropy into account. A strain anisotropy of constant value is indirectly introduced in both paraelectric and ferroelectric states by fitting the error curve within the end points of the experimentally determined transmission curves. These end points represent the maxima and minima of the percent light transmission curves. In general, they are somewhat higher for the biased ceramic (Figures 6.8 to 6.11, curves b) than for the unbiased ceramic (Figures 6.8 to 6.11, curves a). The decrease of the percent light transmission with temperature, whether it be in the predominantly ferroelectric region, in the transition region,

or in the predominantly paraelectric region, merely follows from the distribution of transition temperatures of the crystallites composing the ceramic. As calculated, the decrease in intensity is not due to a temperature dependence of the anisotropy or of the field produced strain anisotropy.

This simplification of the model explains the relatively sharp corners observed in the theoretical curves in Figures 6.8 to 6.11, especially for the transmission curves with field. If the temperature dependence of the anisotropy were incorporated into the theoretical calculations, a more accurate description of the relative transmitted light intensity would undoubtedly result. Such a refinement, however, is beyond the intent of the present study.

The accuracy with which the constant T_r , T_r^* and α can be determined is limited by the uncertainties in the experimental data. T_r is obtained from the peak incremental permittivity vs temperature curves (Table 4.1 and Figures 5.1, 5.3, 5.5, 5.7). It represents the average of the peak permittivity temperatures of the heating and cooling curves taken on four ceramic samples. T_r is therefore easily subject to an error of $\pm$ 1 - 2°C.

The accuracy of $T_r^* = T_r + \gamma E$, the peak incremental permittivity temperature produced by a field, depends on T_r and γE . As stated above, T_r can vary by $\pm$ 1 - 2°C, γ is obtained from the observed maximum shift of the incremental permittivity peak with field (Table 6.2). For the average crystallite with a Curie temperature at T_r , the determination of γ from the ceramic permittivity curves is difficult because one cannot establish the limiting temperatures and fields up to which a transition to the ferroelectric state can be induced. The ceramic is not exclusively composed of

TABLE 6.2

SHIFT IN THE PEAK INCREMENTAL PERMITTIVITY TEMPERATURE WITH FIELD FROM Tr TO Tr*, USED IN THE EVALUATION OF THE THEORETICAL PERCENT LIGHT TRANSIMSSION CURVES (FIG. 6.7-6.10)

From ϵ_Δ vs T Data:			Calculated γ °/Kv/cm	Max. Field Applied to Thin Section, Kv/cm	Shift from Tr to Tr* for the % Light Transmission Curves, in °C	
Sample	Max. Applied Field Kv/cm	Observed Shift of Peak Permittivity Temperature, °C			Calculated Shift, °C	Value Actually Used, °C
1	14.2	15	1.06	17.0	18.0	15
2	13.2	14	1.06	10.9	11.6	12
3	10.5	10	.95	10.7	10.2	10
4	15.0	10	.666	10.8	7.2	7

crystallites with Curie temperatures T_r , but of crystallites having a distribution of Curie temperatures. When, for example, a crystallite with transition temperature T_r has reached its maximum field-produced shift in the peak permittivity temperature, crystallites with Curie temperatures lower than T_r are already in a permanently paraelectric state, whereas those with Curie temperatures above T_r can still be subjected to an induced ferroelectric state. The temperature range in which some degree of ferroelectricity can be induced in a ceramic is therefore wider than in a single crystal. Furthermore, at high biasing fields, the "peaks" of the permittivity vs temperature curves are considerably reduced. The choice of the peak incremental permittivity temperature is consequently subject to greater error than for low fields. Hence values of T_r^* as listed in Table 6.3 are approximate, with estimated errors up to $\pm$ 4°C. Based on observations on single crystals of barium titanate the maximum shift of the peak incremental permittivity with field has been limited to 15°C.

The choice of a variance parameter from the incremental permittivity vs temperature curves becomes very difficult when the measured curves are adapted for comparison to the theoretical curves (see Figures 6.14-6.18). The figures show the experimental curves with the two values of α which most closely resemble the theoretical ones. These two parameters largely determine the shape of the theoretical light transmission curves as seen in Figures 6.8-6.11.

When one considers that the evaluation of the theoretical relative transmission curves is subject to the many errors described above, the resemblance between the theoretical and experimental curves must be considered

TABLE 6.3

CONSTANTS USED TO EVALUATE THE THEORETICAL PERCENT LIGHT TRANSMISSION CURVES, BASED ON EQUATIONS (6.35) AND (6.40)

Sample	α	Tr	Tr*
1	10, 15	49	64
2	10, 15	51	63
3	10, 15	52	62
4	15, 20	84	91

α = variance parameter of the ceramic distribution, °C

Tr = peak incremental permittivity temperature, at 0 field, °C

Tr* = peak incremental permittivity temperature, at maximum applied field, °C

a good one. In most cases, a better coincidence of the curves can be achieved by shifting the theoretical T_r by one or two degrees, and/or by adjusting γ within the limits of the possible error. Such a refinement, however, was regarded as neither necessary nor desirable in the present analysis. In general, the theoretical curves with $\alpha = 15$ for Sample 1 (Figure 6.8), $\alpha = 15$ for Sample 2 (Figure 6.9), $\alpha = 10$ for Sample 3 (Figure 6.10), and $\alpha = 15$ for Sample 4 (Figure 6.11), follow the experimental curves quite well. A better fit of the curves representing the biased sample, notably for samples 2 and 3 (Figures 6.9 and 6.10), would result after including the temperature dependence of the strain anisotropy in the calculations.

Nevertheless, as represented, the data of the theoretical relative light transmission basically reflects the trend of the optical light transmission of a barium-strontium titanate thin section as a function of temperature and field. It can be therefore concluded that the assumptions made in the analysis of the relative transmitted intensity are essentially valid.

VI CONCLUSIONS

The objective of the optical study of ceramic barium-strontium titanate thin-sections has been to correlate optical and electrical properties by direct observation of the ferroelectric to paraelectric phase transition. The effect of a strong electric field on the optical behavior of the ceramic grains at the transition temperature has been given particular consideration. The predominant question throughout this investigation has been: Are the observed changes with field of the incremental permittivity of the ceramics in the region of the ferroelectric to paraelectric transition mainly due to a reorientation of the ferroelectric polar vectors in the direction of the field? Or are they a result of an induced ferroelectric state?

The data indicate that the field induced decrease in the incremental permittivity peak, as observed in Figures 5.1, 5.3, 5.5 and 5.7, mainly results from an induced ferroelectric state in the paraelectric grains. There exists a marked increase in the percent light transmission curves (Figures 6.7 - 6.11) and the photographs (Figure 5.14) taken on the large-grained (50 to 150μ) ceramics. These changes in transmission are largest at a temperature somewhat beyond the peak incremental permittivity temperature of the ceramic. The unbiased ceramic is mostly paraelectric at that temperature. The incremental permittivity of a ferroelectric grain (near the transition temperature) is smaller than the permittivity of a paraelectric grain (near the Curie temperature), when measured either parallel or perpendicular to the polar axis. Therefore, the existence of an induced ferroelectric state in many grains in the

ceramic will necessarily lower its total incremental permittivity. In addition, the direction of the induced polar vector - which is also the direction of the induced uniaxial optic axis - lies in the direction of the applied field. In this position, it represents the lowest possible incremental permittivity value when measured along the field direction (Figure 2.5).

The optical data taken on three fine-grained (5 to 15μ) samples show a trend similar to that of the large grained samples, although the transmitted intensities are lower. Thin sections of about 30 to 40μ prepared from these materials actually represent a three dimensional aggregate of grains. A larger percentage of the light that enters the thin section is scattered at the numerous grain boundaries of the small grained material than in the large grained material. This accounts for the low percentage in transmitted intensities seen in the optical data of the fine grained materials (Figures 5.10, 5.12 and 5.13). Contrary to the case of large grained ceramics, no domains can be distinguished in the fine-grained samples at magnifications of 500X to 700X. Hence no analysis of domain movement can be made here. An anisotropy that exists well beyond the peak incremental permittivity temperature has been observed in the fine-grained ceramics. This anisotropy is found in the cubic phase of the ceramic, and in the electrically unbiased state. It indicates the existence of some very highly strained areas in the ceramics. Such areas have been observed in microcrystalline ceramics (grain size = 1μ) and have been attributed to strains at the grain boundaries.[117]

The model of induced ferroelectricity assumes that the ceramic ferroelectric crystallites are "frozen in," that is, no field produced 90° domain formation is considered possible although a field may produce a reversal of the polarization vector. 180° domain switching does not affect the incremental permittivity because of the symmetry of the polarization axis for 180° reversals. Neither can 180° domain switching be ordinarily observed by optical means, since it does not involve any change in the orientation of the optical indicatrix. 90° domain alignment, however, would significantly change the incremental permittivity of the ceramic. This follows from the large dielectric antisotropy which exists in a barium-strontium titanate single crystal. 90° domains are readily visible under crossed polars as a series of lamellae, separated by sharp lines which have been called 90° domain walls.

The optical observations on the large-grained ceramic thin sections show a frequent occurrence of 90° twinning in the ferroelectric grains. However, no field produced changes have been observed in the position of the twinning striations which could be interpreted as 90° wall motion. The changes are essentially restricted to the temperature region bordering the peak incremental permittivity temperature. The effect of the field gradually becomes less pronounced as the ferroelectric is increasingly cooled below or heated above the peak incremental permittivity temperature. It therefore appears that the observed small increase in anisotropy in the ferroelectric region* of the ceramic cannot

* The ferroelectric region of the ceramic is broadly defined as that temperature range for which the majority of the ceramic grains are ferroelectric. It therefore includes all temperatures below T_r and above the temperature of the orthorhombic-tetragonal transition. Although the orthorhombic phase is also ferroelectric, the observations made here are restricted only to the tetragonal, ferroelectric phase.

be explained by an alignment of polar vectors in the field direction. Another explanation is given below:

1) The increase in the optical anisotropy with field arises in part from a certain percentage of grains in the ceramic whose Curie temperatures lie below the mean (peak) incremental permittivity temperature, T_r . When the ceramic is heated, these grains will become isotropic at lower temperatures than the rest of the material. Hence, they will also be susceptible to an induced anisotropy at temperatures below T_r . In this manner, they contribute to the field produced increase in anisotropy of the "ferroelectric" ceramic.

2) The increased anisotropy in the ferroelectric grains is also based on the temperature dependence of their birefrigence. Observations on the grains in the thin sections have shown that the birefringence of the ferroelectric grains increases with decreasing temperatures (Figure 5.17). In addition, the field produces a strain anisotropy in both ferroelectric and paraelectric grains. This is clearly seen in the transmittency data of a single crystal of barium titanate (Figure 6.18).

Optically it is not possible to distinguish between variations in anisotropy produced either by a change in temperature, or by a field, in the form of induced ferroelectricity and strain anisotropy. Detailed observations seem to indicate, however, that these three factors - in

different degrees of importance - essentially account for the observed changes in the transmitted intensities of mixed titanate ceramic thin sections.

A mathematical model has been proposed to describe the relative light intensity transmitted by a ceramic thin section as a function of temperature and electric field. The ceramic is considered to consist of a very large number of crystallites whose transition temperatures are spread in a normal distribution over a temperature range centered about T_r . The transmitted light intensity is taken to be proportional to the number of ferroelectric or induced ferroelectric grains in the ceramic. No allowance has been made for the temperature dependence of the birefringence or the field-produced strain anisotropy. Even though the model is a simple one, the calculated curves (Figures 6.8 to 6.11) show a good resemblance to the experimental data within the limits of error introduced during the evaluation of the theoretical curves.

It can therefore be concluded that, in a mixed barium-strontium titanate ceramic, the field-produced changes in anisotropy in the peak incremental permittivity region are primarily due to an induced ferroelectric state in the paraelectric grains. In comparison, the effect of the field on the ferroelectric grains is small. 90° domain motion does not satisfactorily explain the observed dielectric non-linearity with field since the 90° reorientation requires a relatively long exposure to a biasing field (20 minutes and up). The lowering of the incremental permittivity, however, follows almost immediately after

the application of the field to the ceramic. The fact that an anisotropic state is also instantaneously induced by a field in the paraelectric grains at the tetragonal to cubic transition region indicates that this mechanism is chiefly responsible for the dielectric non-linearity in mixed barium-strontium titanate ceramics.

APPENDIX A

TABLES A-1 - A-6 CAPACITANCE AND PERCENT LIGHT TRANSMISSION DATA AS A FUNCTION OF TEMPERATURE AND APPLIED DC FIELDS, FOR 6 CERAMIC BARIUM-STRONTIUM TITANATE SAMPLES

TABLE A-7 PERCENT LIGHT TRANSMISSION DATA AS A FUNCTION OF TEMPERATURE AND APPLIED DC FIELDS, FOR CERAMIC BARIUM-STRONTIUM TITANATE SAMPLE 7

TABLE A-8 VOLTAGES APPLIED TO CERAMIC WEDGES AND DIMENSIONS OF WEDGES

ABBREVIATIONS USED IN THE RECORDING OF THE DATA

mv = millivolt reading of an iron-constantan temperature thermocouple.

$T, {}^{o}C$ = temperature at which the capacitance and photocell current data was taken.

c_x, c_y = capacitance* readings on the Q-meter

c_o = capacitance* of the sample, as measured on the Q-meter at 1600 Kc. $c_o = c_x - c_y$.

c_s = actual capacitance* of the sample as computed from Equation (3).

C_h = capacitance* of the sample holder.

ϵ = incremental permittivity of the sample { for definition see Sec. II, p.12 / for calculation see Appendix C, p.165

μa = photocell current measuring the percent of light transmitted by a ceramic thin section.

L = percentage of the incident light transmitted by a thin section between crossed polars.

Superscripts and Subscripts:

1 = data taken at zero biasing field

2, 3, 4 = data taken with samples exposed to increasing DC fields, (see Table A-8).

*See Section IV, p. 44.

TABLE A-1

Sample 1

mv	T, °C	σ_y^1	σ_o^1	σ_s^1	ϵ_1	μa_1	L_1	σ_y^2	σ_o^2	σ_s^2	ϵ_2	μa_2	L_2
1.38	26.6	54.6	38.4	33.6	1500	21.0	18.6	55.8	37.2	32.4	1445	21.6	19.5
1.60	30.8	53.8	39.2	37.0	1650	20.9	18.2	54.3	37.7	33.4	1490	21.6	19.5
1.80	34.6	53.1	39.9	38.8	1730	20.6	17.8	54.7	38.3	35.0	1560	21.3	18.8
1.90	36.5	52.5	40.5	40.4	1800	20.25	17.4	54.5	38.5	35.4	1580	21.4	19.0
2.00	38.4	51.8	41.2	42.2	1880	20.25	17.4	54.0	39.0	36.6	1630	21.6	19.5
2.10	40.4	50.6	42.4	45.1	2020	20.00	17.0	53.7	39.3	37.3	1670	21.5	19.3
2.20	42.5	49.4	43.6	48.6	2170	19.70	16.6	53.3	39.7	38.3	1710	21.25	18.8
2.30	44.0	46.8	46.2	54.1	2420	19.40	16.2	52.2	40.8	41.0	1830	21.20	18.62
2.40	46.0	44.2	48.8	63.9	2850	19.10	15.5	51.0	42.0	44.2	1970	20.75	18.50
2.50	48.0	43.0	50.0	67.9	3030	18.60	14.8	49.5	43.5	48.2	2150	20.30	17.4
2.60	50.0	43.3	49.7	66.8	2980	18.00	14.1	48.5	44.5	50.8	2270	20.10	17.0
2.70	52.1	43.6	49.4	65.8	2940	16.80	12.6	47.7	45.3	53.2	2370	19.20	15.9
2.80	54.1	44.3	48.7	63.6	2840	15.70	11.5	47.7	45.3	53.2	2370	18.35	14.6
2.90	55.6	45.0	48.0	61.3	2740	14.20	9.8	47.8	45.2	52.3	2360	17.20	13.2
3.00	57.4	45.8	47.2	58.7	2620	13.10	8.9	48.0	45.0	52.3	2330	16.20	12.0
3.20	61.2	46.8	46.2	55.8	2490	11.00	6.9	48.7	44.3	50.3	2250	13.70	9.33
3.40	64.9	47.9	45.1	52.7	2350	9.60	5.7	49.2	43.8	49.0	2180	11.80	7.59
3.60	68.7	49.3	43.7	48.7	2170	8.65	5.1	50.4	42.6	45.7	2040	10.10	6.17
3.80	72.3	50.5	52.5	45.5	2030	8.20	4.8	51.1	41.9	43.9	1960	9.15	5.50
4.00	76.2	51.3	41.7	43.3	1930	7.80	4.6	52.9	40.1	40.7	1810	8.60	5.13
4.30	82.1	52.8	40.2	41.0	1830	7.60	4.3	53.3	39.7	38.2	1710	8.10	4.8
4.60	87.2	53.1	38.9	36.3	1640	7.50	4.3	54.5	38.5	35.4	1580	7.80	4.6
5.00	94.8	55.3	37.7	33.6	1500	7.30	4.1	55.6	37.4	32.7	1460	7.60	4.47
5.50	104.0	57.0	36.0	29.7	1350	7.30	4.1	57.1	35.9	30.0	1340	7.50	4.3
6.00	113.0	58.0	35.0	27.3	1230	7.30	4.2	58.1	34.9	27.3	1220	7.40	4.3
6.50	122.1	58.8	34.2	25.9	1155	7.25	4.2	59.0	34.0	25.4	1130	7.30	4.2
6.20	116.7	58.3	34.7	26.8	1190	7.20	4.2	58.5	34.5	26.5	1180	7.20	4.2
5.80	110.5	57.5	35.5	28.6	1275	7.20	4.2	57.6	35.4	28.4	1260	7.20	4.2
5.30	100.4	56.2	36.8	31.4	1400	7.20	4.3	56.2	26.8	31.4	1400	7.20	4.4
4.80	91.0	54.5	38.5	35.4	1580	7.10	4.3	54.7	38.3	35.0	1560	7.25	4.6
4.40	83.6	52.7	40.3	39.9	1780	7.20	4.4	53.3	39.7	38.2	1700	7.40	4.7
4.10	78.0	51.4	41.6	43.1	1930	7.30	4.5	52.0	41.0	41.0	1850	7.80	5.0
3.90	74.2	50.3	42.7	46.0	2050	7.60	4.8	51.2	42.8	46.3	2065	8.30	5.4
3.70	70.5	49.2	43.8	49.0	2180	7.80	4.9	50.1	42.9	46.5	2075	8.80	5.7
3.50	66.8	47.9	45.1	52.7	2350	8.30	5.4	49.5	43.5	48.2	2150	9.70	6.5
3.30	63.1	46.5	46.5	56.7	2530	9.25	6.2	48.5	44.5	50.8	2270	11.00	7.6
3.10	59.2	45.0	48.0	61.3	2740	10.60	7.2	47.7	45.3	53.2	2470	13.00	9.6
2.90	55.6	43.4	49.6	66.5	2970	13.00	9.6	47.2	45.8	54.6	2440	15.00	11.8
2.70	52.1	42.2	50.8	70.6	3150	15.40	12.2	47.3	45.7	54.3	2420	16.90	13.8
2.60	50.0	41.7	51.3	72.4	3230	16.6	13.5	48.0	45.0	52.3	2430	17.90	15.1
2.50	48.0	41.5	51.5	73.1	3260	17.6	14.8	49.0	44.0	49.6	2210	18.50	16.2
2.40	46.0	42.4	50.6	69.8	3110	18.1	15.5	50.1	42.9	46.5	2070	18.90	16.6
2.30	44.0	45.1	47.9	60.8	2710	18.5	16.0	52.1	40.9	41.2	1835	19.30	17.2
2.20	42.5	48.2	44.8	51.8	2310	18.9	16.6	52.8	40.2	39.5	1760	19.60	17.8
2.10	40.4	50.0	43.0	46.7	2080	19.2	17.0	53.3	39.7	38.3	1710	19.75	18.2
2.00	38.4	51.1	41.9	43.7	1950	19.4	17.4	53.8	39.2	37.1	1660	20.10	18.6
1.90	36.5	52.0	41.0	41.4	1840	19.6	17.8	54.2	38.8	36.1	1610	20.30	18.8
1.70	32.7	53.0	40.0	39.0	1740	20.0	18.2	54.8	38.2	34.6	1570	20.60	19.2
1.50	28.8	53.6	39.4	37.5	1670	20.2	18.6	57.2	35.8	29.3	1310	20.60	19.2

C_x = 93.0 C_h = 23.8 ϵ = 44.6 C_s

mv	T, °C	σ_y^3	σ_o^3	σ_s^3	ϵ_3	μa_3	L_3	σ_y^4	σ_o^4	σ_s^4	ϵ_4	μa_4	L_4
1.38	26.6	56.8	36.2	30.1	1340	22.3	20.6	58.3	34.7	26.8	1190	23.2	22.2
1.60	30.8	56.3	36.7	31.2	1400	22.25	20.6	58.1	34.9	27.3	1215	23.4	22.4
1.80	34.6	56.1	36.9	31.7	1410	22.1	20.2	57.8	35.2	27.9	1245	23.3	22.4
1.90	36.5	55.8	37.2	32.4	1440	22.75	20.6	57.9	25.1	27.8	1240	23.3	22.4
2.00	38.4	55.6	37.4	32.8	1460	22.5	20.9	57.5	35.5	28.6	1275	23.4	22.4
2.10	40.4	55.4	37.6	33.3	1470	22.45	20.9	57.4	35.6	28.8	1280	23.3	22.4
2.20	42.5	54.9	38.1	34.5	1530	22.3	20.6	57.3	35.7	29.4	1320	23.1	21.9
2.30	44.0	54.2	38.8	36.1	1610	21.9	20.0	57.0	36.0	28.9	1290	22.8	21.4
2.40	46.0	53.5	39.5	37.9	1690	21.6	19.5	56.6	36.4	30.5	1360	22.5	20.9
2.50	48.0	52.7	40.3	39.7	1770	21.2	18.6	56.1	36.9	31.7	1430	22.1	20.4
2.60	50.0	51.5	41.5	42.7	1900	20;8	18.2	55.5	37.5	33.1	1475	21.8	20.0
2.70	52.1	50.8	42.2	44.7	1990	20.2	17.4	55.0	38.0	34.2	1520	21.3	18.6
2.80	54.1	50.5	42.5	45.5	2030	19.6	16.2	54.5	38.5	35.4	1580	20.8	18.2
2.90	55.6	50.5	42.5	45.5	2030	18.4	14.6	54.2	38.8	36.1	1610	20.2	17.4
3.00	57.4	50.5	42.5	45.5	2030	17.5	13.5	54.0	39.0	36.7	1635	19.3	15.9
3.20	61.2	50.3	42.7	45.6	2040	15.5	11.2	53.7	39.3	37.3	1660	17.7	13.4
3.40	64.9	50.8	52.2	44.6	1990	13.7	9.3	53.7	39.3	37.3	1660	16.25	12.0
3.60	68.7	51.5	41.5	42.7	1910	11.6	7.4	53.8	39.2	37.1	1650	14.30	10.0
3.80	72.3	52.1	40.9	41.2	1830	10.4	6.45	53.1	39.9	38.8	1730	12.80	8.5
4.00	76.2	52.8	40.2	39.6	1760	9.7	5.9	54.5	38.5	35.4	1580	11.90	7.7
4.30	82.1	54.1	38.9	36.4	1640	8.8	5.3	55.3	37.7	33.5	1495	10.70	7.8
4.60	87.2	54.8	38.2	34.6	1540	8.3	4.9	55.9	37.1	32.1	1430	9.90	6.17
5.00	94.8	45.0	37.0	31.9	1420	8.0	4.7	56.8	36.2	30.1	1340	9.30	5.6
5.50	104.0	57.4	35.6	28.8	1280	7.75	4.5	57.8	35.2	27.9	1240	8.70	5.0
6.00	113.0	58.4	34.6	26.7	1190	7.60	4.4	58.6	34.4	26.2	1170	8.25	4.8
6.50	122.1	59.2	33.8	24.9	1110	7.50	4.4	59.4	33.6	24.6	1100	7.90	4.9
6.20	116.7	58.6	34.4	26.2	1170	7.40	4.3	59.0	34.0	25.4	1130	7.85	4.9
5.80	110.5	57.9	35.1	27.7	1230	7.30	4.2	58.3	34.7	26.8	1195	8.00	5.1
5.30	100.4	56.6	36.4	30.5	1360	7.50	4.8	57.2	35.8	29.3	1310	8.50	5.6
4.80	91.0	55.1	37.9	34.0	1520	7.70	4.9	55.8	37.2	32.4	1450	9.20	6.0
4.40	83.6	53.8	39.2	37.1	1650	8.10	5.2	54.9	38.1	34.5	1540	10.00	6.8
4.10	78.0	52.7	40.3	39.7	1770	8.70	5.6	54.2	38.8	36.3	1620	11.20	7.8
3.90	74.2	52.1	40.9	41.2	1830	9.40	6.3	53.9	39.1	36.8	1640	12.00	8.5
3.70	70.5	51.3	41.7	43.3	1930	10.20	7.0	53.5	39.5	37.8	1680	12.90	9.3
3.50	66.8	50.8	42.2	44.6	1990	11.30	8.0	53.5	39.5	37.8	1680	14.20	10.7
3.30	63.1	50.3	42.7	45.8	2040	12.90	9.3	53.5	39.5	37.8	1680	15.60	12.3
3.10	59.2	50.1	42.9	46.5	2070	14.70	11.2	53.2	39.8	38.6	1720	17.00	14.1
2.90	55.6	49.9	43.1	47.1	2100	16.50	13.5	54.2	38.8	36.1	1610	18.30	15.9
2.70	52.1	50.5	42.5	45.5	2030	17.90	15.1	54.8	38.2	34.5	1535	19.25	17.0
2.60	50.0	51.3	41.7	43.3	1930	18.60	16.2	55.5	37.5	33.1	1475	19.80	18.2
2.50	48.0	52.5	40.5	40.3	1800	19.1	17.0	56.2	36.8	32.5	1450	20.10	18.6
2.40	46.0	53.2	39.8	38.5	1720	19.4	17.4	56.5	36.5	30.8	1370	20.3	19.1
2.30	44.0	54.3	38.7	35.7	1590	19.8	18.2	57.1	35.9	29.4	1330	20.6	19.3
2.20	42.5	54.8	38.2	34.7	1550	20.0	18.2	57.2	35.8	29.8	1300	20.7	19.5
2.10	40.4	55.1	37.9	33.9	1510	20.2	18.6	57.5	35.5	28.6	1275	20.8	19.5
2.00	38.4	55.3	37.7	33.4	1490	20.4	19.0	57.6	35.4	28.4	1265	21.0	20.0
1.90	36.5	55.7	37.3	32.6	1450	20.6	19.0	57.8	35.5	28.6	1280	21.25	20.4
1.70	32.7	56.0	37.0	31.9	1420	20.8	19.0	57.9	35.1	29.1	1300	21.40	20.6
1.50	28.8	56.3	36.7	31.2	1390	20.9	19.5	58.2	34.8	27.1	1210	21.40	20.6

C_x = 93.0 C_h = 23.8 ϵ = 44.6 C_s

TABLE A-2

Sample 2

mv	T,°C	C_y^1	C_o^1	C_s^1	ϵ_1	μa_1	I_1	C_y^2	C_o^2	C_s^2	ϵ_2	μa_2	I_2
1.42	27.4	55.2	37.8	33.9	2500	23.2	11.22	56.0	37.0	32.5	2160	23.4	11.4
1.60	30.8	54.8	38.2	34.8	2310	22.8	10.96	55.7	37.3	32.7	2170	23.8	11.2
1.80	34.6	54.2	38.8	35.9	2390	22.3	10.30	55.3	37.7	33.7	2240	22.6	10.7
2.00	38.4	53.0	40.0	37.1	2600	21.9	10.00	54.2	38.8	36.4	2420	22.2	10.4
2.20	42.5	51.5	41.5	42.8	2850	21.4	9.60	53.2	39.8	38.7	2570	21.6	9.8
2.30	44.0	49.6	43.4	48.1	3190	21.2	9.40	52.7	40.3	39.9	2650	21.6	9.8
2.40	46.0	47.4	45.6	54.1	3600	21.0	9.33	51.8	41.2	42.1	2800	21.4	9.7
2.50	48.0	95.1	47.9	59.7	3970	20.5	8.91	50.1	42.9	46.8	3110	21.1	9.5
2.60	50.0	43.9	49.1	65.1	4330	19.7	8.32	48.2	44.8	52.2	3470	20.3	8.8
2.74	52.5	44.0	49.0	65.8	4380	18.8	7.76	47.7	46.3	56.5	3750	19.6	8.3
2.78	53.7	44.2	48.8	64.1	4260	18.3	7.41	47.5	45.5	54.0	3590	19.2	8.0
2.90	55.6	44.7	48.3	62.5	4160	17.3	6.76	47.5	45.5	54.0	3590	18.2	7.3
3.00	57.4	45.5	47.5	59.8	3970	16.2	5.75	47.5	45.5	54.0	3590	17.2	6.6
3.10	59.2	46.0	47.0	58.4	3880	15.0	5.30	48.0	45.0	52.6	3500	15.8	5.7
3.20	61.2	46.4	46.6	57.3	3810	14.1	4.90	48.0	45.0	52.6	3430	14.8	5.2
3.40	64.9	47.8	45.2	53.1	3530	12.0	3.84	48.9	44.1	51.4	3415	12.6	4.1
3.60	68.7	49.1	43.9	49.4	3280	10.8	3.31	49.9	43.1	47.1	3130	11.2	3.4
3.80	72.3	50.1	42.9	46.8	3110	9.9	2.95	50.8	42.2	44.8	2980	10.1	3.0
4.00	76.2	51.0	42.0	44.3	2940	9.4	2.75	51.6	41.4	42.8	2850	9.4	2.7
4.20	80.0	52.2	40.8	41.3	2740	8.7	2.51	52.5	40.5	40.6	2770	8.8	2.5
4.42	84.0	53.1	39.9	38.9	2580	8.4	2.34	53.3	39.7	38.4	2555	8.5	2.4
4.60	87.2	53.7	39.3	36.9	2450	8.3	2.34	54.0	39.0	36.7	2440	8.3	2.4
4.80	91.0	54.7	38.2	35.2	2340	8.1	2.29	55.0	38.0	34.4	2290	8.2	2.3
5.00	94.8	55.5	37.5	33.2	2210	8.0	2.29	55.7	37.3	32.9	2190	8.1	2.3
5.30	100.4	56.3	36.7	31.4	2090	7.9	2.24	54.5	36.5	31.0	2060	7.9	2.2
5.60	106.0	57.2	35.8	29.4	1950	7.8	2.19	57.4	35.6	29.0	1930	7.8	2.2
6.10	114.9	57.9	35.1	27.9	1850	7.8	2.19	58.0	35.0	27.7	1845	7.8	2.2
6.50	122.1	58.8	34.2	26.3	1760	7.8	2.19	58.8	35.0	27.7	1845	7.8	2.2
5.70	108.3	57.1	35.9	29.7	1970	7.8	2.19	57.2	35.8	29.4	1955	7.8	2.2
5.40	102.2	56.1	36.9	31.9	2120	7.8	2.19	56.3	36.7	31.4	2090	7.8	2.2
5.10	96.7	55.4	37.6	33.4	2220	7.9	2.24	55.6	37.4	33.0	2190	7.9	2.2
4.90	92.9	55.0	38.0	34.5	2290	8.0	2.29	55.0	38.0	34.4	2290	8.0	2.3
4.70	89.2	54.2	38.8	36.3	2410	8.0	2.29	54.3	38.7	36.0	2400	8.1	2.3
4.50	85.4	53.3	39.7	39.5	2620	8.1	2.29	53.5	39.5	39.0	2590	8.2	2.3
4.30	82.1	52.3	40.7	41.0	2720	8.3	2.34	52.7	40.3	40.0	2660	8.4	2.4
4.10	78.0	51.4	41.6	43.3	2880	8.5	2.49	51.9	41.1	42.5	2830	8.6	2.45
3.90	74.2	50.2	42.8	46.4	3080	8.9	2.57	50.8	42.2	44.8	2980	9.1	2.70
3.70	70.5	49.2	43.8	49.2	3270	9.4	2.88	50.0	43.0	47.0	3130	9.8	2.90
3.50	66.8	47.8	45.2	53.1	3530	10.5	3.16	49.0	44.0	44.7	3300	10.8	3.30
3.20	61.2	45.6	47.4	59.7	3960	13.2	4.36	47.7	45.3	53.3	3540	13.5	4.50
3.10	59.2	45.1	47.9	61.2	4060	13.9	4.68	47.0	46.0	55.4	3680	14.7	5.1
3.00	57.4	44.5	48.5	63.1	4190	15.0	5.37	46.9	46.1	55.7	3700	16.0	5.8
2.90	55.6	44.0	49.0	64.7	4300	15.8	5.75	46.8	46.2	55.8	3715	16.7	6.3
2.80	54.1	43.3	49.7	66.9	4440	16.8	6.46	46.7	47.3	59.3	3940	17.8	7.0
2.70	52.1	42.7	50.3	68.9	4580	17.7	6.91	46.9	46.1	55.7	3700	18.6	7.6
2.60	50.0	42.5	50.5	69.7	4630	18.6	7.59	47.9	45.1	52.8	3510	19.5	8.2
2.50	48.0	43.1	49.9	67.6	4490	19.4	8.13	49.5	43.5	48.4	3220	20.2	8.8
2.40	46.0	45.0	48.0	61.7	4100	20.0	8.51	51.3	41.7	43.7	2910	20.6	9.0
2.30	44.0	48.1	44.9	52.2	3470	20.4	8.91	52.4	40.6	40.6	2700	20.9	9.3
2.20	42.5	50.7	42.3	45.3	3010	20.7	9.12	53.3	39.7	38.6	2570	21.3	9.6
1.94	36.9	53.1	39.9	38.9	2580	21.5	9.77	54.4	38.6	35.9	2390	21.8	10.0
1.80	34.6	53.6	39.4	37.7	2500	21.7	10.00	54.8	38.2	34.8	2320	22.1	10.3
1.60	30.8	53.3	38.7	36.0	2390	22.0	10.00	55.5	37.5	33.4	2220	22.3	10.5

C_x = 93.0 C_h = 23.6 ϵ = 66.5 C_s

mv	T,°C	C_y^3	C_o^3	C_s^3	ϵ_3	μa_3	I_3	C_y^4	C_o^4	C_s^4	ϵ_4	μa_4	I_4
1.42	27.4	57.1	35.9	29.7	1975	23.7	11.7	58.7	34.3	26.0	1760	24.2	12.3
1.60	30.8	56.9	36.1	30.2	2010	23.5	11.5	58.4	34.6	26.9	1790	24.0	12.0
1.80	34.6	54.4	36.6	31.1	2070	22.9	11.0	58.3	34.7	27.1	1805	23.5	11.5
2.00	38.4	55.9	37.1	32.3	2150	22.5	10.6	57.8	35.2	28.1	1870	23.1	11.0
2.20	42.5	55.2	37.8	33.9	2250	22.0	10.2	57.5	35.5	28.6	1900	22.7	10.7
2.30	44.0	54.9	38.1	34.7	2310	22.2	10.4	57.1	35.9	29.7	1975	22.6	10.6
2.40	46.0	54.1	38.9	36.5	2430	21.8	10.0	57.0	360	29.9	1990	22.6	10.6
2.50	48.0	53.2	39.8	38.8	2580	21.5	9.8	56.5	36.5	30.9	2055	22.2	10.2
2.60	50.0	52.1	40.9	41.5	2760	20.9	9.3	55.7	37.3	32.7	2175	21.8	10.0
2.74	52.5	51.2	41.8	43.8	2895	20.2	8.9	55.2	37.8	33.9	2250	21.4	9.8
2.78	53.7	51.0	42.0	44.3	2945	20.0	8.6	55.1	37.9	34.2	2280	21.1	9.55
2.90	55.6	50.8	42.2	44.7	2970	19.0	7.8	54.6	38.4	35.3	2350	20.4	8.91
3.00	57.4	50.5	42.5	45.4	3020	18.2	7.3	54.3	38.7	36.2	2410	19.7	8.32
3.10	59.2	50.3	42.7	46.0	3060	16.8	6.4	54.0	39.0	36.8	2450	18.6	7.59
3.20	61.2	50.5	42.5	45.5	3030	15.8	5.7	54.0	39.0	36.8	2450	18.0	7.24
3.40	64.9	50.8	42.2	44.7	2970	13.3	4.4	53.6	39.4	37.7	2510	16.2	6.03
3.60	68.7	51.4	41.6	43.8	2910	11.8	3.7	53.9	39.1	37.0	2460	13.8	4.68
3.80	72.3	52.0	41.0	41.6	2770	10.5	3.2	54.0	39.0	36.6	2435	12.2	3.89
4.00	76.2	52.7	40.3	39.9	2650	9.6	2.8	54.4	38.6	35.7	2370	10.9	3.35
4.20	80.0	53.2	39.8	38.8	2580	9.0	2.6	54.6	38.4	33.5	2230	10.0	3.02
4.42	84.0	54.0	39.0	36.8	2450	8.6	2.45	55.2	37.8	33.9	2250	9.3	2.69
4.60	87.2	54.6	38.4	35.3	2350	8.4	2.4	55.7	37.3	32.7	2170	8.9	2.57
4.80	91.0	55.3	37.7	33.7	2240	8.2	2.3	56.3	36.7	31.4	2090	8.6	2.46
5.00	94.8	56.0	37.0	32.1	2140	8.1	2.3	56.7	36.3	30.5	2030	8.4	2.40
5.30	100.4	56.9	36.1	30.2	2010	7.9	2.2	57.6	35.4	28.5	1895	8.2	2.34
5.60	106.0	57.7	35.3	28.4	1890	7.8	2.2	58.1	34.9	27.4	1850	8.1	2.29
6.10	114.9	58.3	34.7	26.9	1790	7.8	2.2	58.7	34.3	26.1	1770	7.9	2.24
6.50	122.1	59.1	33.9	25.2	1675	7.8	2.2	59.4	33.6	24.7	1640	7.8	2.19
5.70	108.3	57.3	35.7	29.0	1930	7.8	2.2	57.7	35.3	28.4	1890	8.1	2.29
5.40	102.2	56.5	36.5	29.6	1970	7.8	2.2	57.1	35.9	29.7	1975	8.2	2.29
5.10	96.7	55.8	37.2	32.5	2160	7.9	2.2	56.5	36.5	31.0	2060	8.2	2.34
4.90	92.9	55.4	37.6	33.4	2220	8.0	2.3	56.2	36.8	31.7	2110	8.5	2.51
4.70	89.2	54.6	38.4	35.3	2350	8.2	2.3	55.7	37.3	32.6	2170	8.7	2.51
4.50	85.4	54.0	39.0	36.8	2450	8.2	2.3	55.1	37.9	34.1	2270	9.0	2.60
4.30	82.1	53.4	39.6	38.1	2540	8.5	2.4	54.6	38.4	35.3	2350	9.7	2.88
4.10	78.0	52.7	40.3	39.9	2650	8.8	2.6	54.3	38.7	36.1	2400	10.4	3.16
3.90	74.2	51.8	41.2	42.1	2800	9.4	2.8	53.9	39.1	36.8	2450	11.8	3.72
3.70	70.5	51.4	41.6	43.2	2870	10.3	3.1	53.8	39.2	37.2	2470	13.3	4.40
3.50	66.8	50.7	42.3	45.0	2990	11.8	3.7	53.5	39.5	37.9	2520	15.4	5.50
3.20	61.2	50.1	42.9	46.8	3110	14.7	5.1	53.7	39.3	37.5	2495	18.5	7.59
3.10	59.2	50.0	43.0	47.0	3130	16.2	6.0	54.0	39.0	37.2	2470	19.5	8.13
3.00	57.4	50.1	42.9	46.8	3110	17.2	6.6	54.2	38.2	36.3	2410	19.9	8.51
2.90	55.6	50.1	42.9	46.3	3110	18.0	7.2	54.5	38.5	35.5	2360	20.7	9.12
2.80	54.1	50.5	42.5	45.5	3030	18.9	7.8	54.9	38.1	34.5	2300	21.3	9.55
2.70	52.1	50.9	42.1	44.5	4960	19.6	8.3	55.3	37.7	33.6	2240	21.6	9.78
2.60	50.0	52.2	40.8	41.3	2750	20.3	8.8	56.2	36.8	31.7	2170	22.3	10.23
2.50	48.0	53.1	39.9	38.9	2590	20.9	9.3	56.7	36.3	30.5	2030	23.3	10.23
2.40	46.0	54.1	38.9	36.6	2430	21.4	9.7	57.2	35.8	29.4	1960	23.0	10.96
2.30	44.0	54.8	38.2	34.8	2310	21.6	9.9	57.5	35.5	28.7	1910	23.0	10.96
2.20	42.5	55.4	37.6	33.6	2230	22.0	10.0	57.8	35.2	28.1	1870	23.4	11.30
1.94	36.9	56.3	36.7	31.4	2080	22.3	10.5	58.3	34.7	27.0	1795	23.5	11.50
1.80	34.6	56.4	36.6	31.1	2070	22.5	10.7	58.3	34.7	27.0	1795	23.6	11.50
1.60	30.8	56.7	36.3	30.5	2030	22.6	10.7	58.6	34.4	26.3	1750	23.6	11.50

C_x = 93.0 C_h = 23.6 ϵ = 66.5 C_s

TABLE A-3

Sample 3

mv	T,°C	C_y^1	C_o^1	C_s^1	ϵ_1	μa_1	L_1	C_y^2	C_o^2	C_s^2	ϵ_2	μa_2	L_2
1.40	27.0	60.7	32.3	22.3	2107	20.5	15.0	61.1	31.9	21.5	2032	21.5	16.5
1.60	30.8	60.3	32.7	23.1	2183	20.2	14.8	60.8	32.2	22.1	2088	21.5	16.5
1.80	34.6	59.8	33.2	24.1	2277	19.8	14.2	60.5	32.5	22.7	2145	21.0	15.8
2.00	38.4	59.0	34.0	25.8	2438	18.1	12.2	60.0	33.0	23.6	2230	20.3	14.8
2.20	42.5	58.0	35.0	28.0	2646	18.3	12.4	59.5	33.5	24.8	2344	20.0	14.5
2.40	46.0	54.9	38.1	34.9	3298	17.0	11.0	57.5	35.5	29.1	2750	18.5	12.6
2.50	48.0	50.0	43.0	47.3	4470	16.2	10.2	56.0	37.0	32.4	3062	18.0	12.2
2.60	50.0	47.1	45.9	54.6	5160	14.3	8.2	53.6	39.4	38.0	3591	17.1	11.0
2.70	52.1	46.6	46.4	56.8	5368	12.7	7.0	53.1	39.9	39.3	3714	16.3	10.2
2.80	54.1	47.6	45.4	53.9	5094	10.4	5.2	52.6	40.4	40.4	3818	14.6	8.6
2.90	55.6	48.0	45.0	52.8	4990	9.5	4.8	52.5	40.5	40.7	3846	13.7	7.8
3.00	57.4	49.6	43.4	48.3	4564	8.7	4.2	53.0	40.0	39.5	3733	12.0	6.4
3.10	59.2	50.1	42.9	46.8	4423	8.2	4.0	53.4	39.6	38.5	3638	10.6	5.5
3.20	61.2	50.7	41.3	42.7	4035	8.0	3.9	53.7	39.3	37.8	3572	10.1	5.2
3.40	64.9	53.7	39.3	37.8	3572	7.7	3.7	54.8	38.2	35.1	3317	9.0	4.4
3.60	68.7	54.2	38.8	36.6	3459	7.6	3.6	55.7	37.3	33.0	3119	8.4	4.1
3.80	72.3	55.3	37.7	34.0	3213	7.6	3.6	55.6	36.4	31.1	2939	8.1	4.0
4.00	76.2	56.6	36.4	31.0	2930	7.6	3.6	57.7	35.3	28.6	2703	8.0	3.9
4.30	82.1	57.9	35.1	28.2	2665	7.6	3.6	58.6	34.4	26.7	2523	6,7	3.8
4.60	87.2	59.2	33.8	25.4	2400	7.6	3.6	59.7	33.3	24.4	2306	7.7	3.7
5.00	94.8	60.0	33.0	23.7	2240	7.6	3.6	60.4	32.6	23.9	2259	7.7	3.7
5.50	104.0	61.3	31.7	21.1	1994	7.6	3.6	61.5	31.5	20.8	1966	7.7	3.7
5.80	110.5	61.8	31.2	20.1	1899	7.6	3.6	62.1	30.9	19.6	1852	7.7	3.7
5.30	100.4	60.9	32.1	21.9	2070	7.6	3.6	61.2	31.8	21.4	2022	7.7	4.0
4.80	91.0	59.4	33.6	25.0	2363	7.6	3.6	59.8	33.2	24.1	2277	7.8	4.1
4.40	83.6	58.0	35.0	28.0	2646	7.6	4.0	58.7	34.3	26.4	2495	7.9	4.2
4.10	78.0	56.8	36.2	30.5	2882	7.6	4.0	57.5	35.5	29.1	2750	8.0	4.2
3.90	74.2	55.6	37.4	38.3	3147	7.6	4.0	56.5	36.5	31.2	2948	8.1	4.3
3.70	70.5	54.7	38.3	35.3	3336	7.6	4.0	56.1	36.9	32.1	3033	8.3	4.4
3.50	66.8	54.0	39.0	37.1	3506	7.6	4.0	55.0	38.0	34.6	3270	8.7	4.7
3.30	63.1	50.9	42.1	44.7	4224	7.7	4.0	53.7	39.3	37.8	3572	9.6	5.2
3.10	59.2	49.6	43.4	48.3	4564	8.0	4.2	53.2	39.8	38.9	3676	10.8	6.0
3.00	57.4	48.4	44.6	51.6	4876	8.3	4.4	52.9	40.1	39.7	3752	11.9	6.8
2.90	55.6	47.5	45.5	54.2	5122	8.8	4.7	52.3	40.7	41.2	3893	13.2	7.8
2.80	54.1	46.6	46.4	56.9	5377	9.6	5.2	51.6	41.4	43.0	4064	13.2	7.8
2.70	52.1	45.8	47.2	59.3	5604	11.7	6.6	53.0	40.0	39.5	3733	15.8	10.1
2.60	50.1	46.3	46.7	57.7	5427	13.7	8.2	54.1	38.9	36.8	3478	16.9	11.4
2.50	48.0	48.9	44.1	50.3	4753	15.5	9.8	56.5	36.5	31.3	2958	17.8	12.4
2.30	44.0	57.9	35.1	28.2	2665	17.0	11.4	58.9	34.1	26.0	2457	18.6	13.2
2.10	40.4	58.6	34.4	26.7	2523	18.0	12.5	59.9	33.1	24.0	2268	19.4	14.1
1.90	36.5	59.6	33.4	24.6	2325	18.7	13.4	60.8	32.2	22.1	2088	20.0	14.4
1.70	32.7	60.3	32.7	23.1	2183	19.4	14.2	61.0	32.0	21.8	2060	20.3	15.2
1.50	28.8	60.7	32.3	22.4	2117	19.8	14.6	61.3	31.7	25.1	1994	20.6	15.6

C_x = 93.0 C_h = 23.4 ϵ = 94.5 C_s

mv	T,°C	C_y^3	C_o^3	C_s^3	ϵ_3	μa_3	L_3	C_y^4	C_o^4	C_s^4	ϵ_4	μa_4	L_4
1.40	27.0	61.7	31.3	20.3	1918	22,3	17.6	62.2	30.8	19.4	1833	23,1	19.0
1.60	30.8	61.5	31.5	20.7	1956	22.2	17.5	62.2	30.8	19.4	1833	23.2	19.0
1.80	34.6	61.1	31.9	21.5	2032	21.8	17.0	61.9	31.1	19.9	1880	23.0	19.0
2.00	38.4	60.8	32.2	22.1	2088	21.3	16.2	61.6	31.4	20.5	1937	22.5	18.0
2.20	42.5	60.1	32.9	23.5	2221	20.6	15.2	61.2	31.8	21.4	2022	22.0	17.2
2.40	46.0	59.0	34.0	25.8	2438	19.8	14.2	60.5	32.5	22.8	2155	21.2	16.0
2.50	48.0	58.1	34.9	27.7	2618	19.4	13.8	60.0	33.0	23.7	2240	21.0	15.8
2.60	50.0	56.2	36.8	31.9	3015	18.6	12.8	58.8	34.2	26.2	2476	20.5	15.0
2.70	52.1	55.7	37.3	33.1	3128	18.2	12.4	58.5	34.5	26.9	2542	20.3	14.8
2.80	54.1	54.9	38.1	34.9	3298	17.2	10.2	57.8	35.2	28.4	2684	19.6	14.0
2.90	55.6	54.7	38.3	35.4	3345	16.5	10.4	57.5	35.3	28.6	2703	19.3	13.6
3.00	57.4	54.8	38.2	35.1	3317	15.0	9.0	57.2	35.8	29.7	2807	18.4	12.5
3.10	59.2	55.1	37.9	34.5	3260	13.6	7.7	57.2	35.8	29.7	2807	17.3	11.6
3.20	61.2	55.1	37.9	34.5	3260	17.7	7.0	57.3	36.7	31.7	2996	16.6	10.6
3.40	64.9	55.8	37.2	32.8	3100	10.8	5.6	57.5	36.5	31.3	2958	14.7	9.7
3.60	68.7	56.7	36.3	30.9	2920	9.7	4.9	57.9	36.1	30.4	2873	13.1	7.3
3.80	72.3	57.4	35.6	29.2	2759	9.0	4.4	58.4	34.6	27.1	2561	11.7	6.2
4.00	76.2	58.2	34.8	27.5	2599	8.5	4.2	58.9	34.1	26.0	2457	10.4	5.4
4.30	82.1	59.1	33.9	25.6	2419	8.2	4.0	59.7	33.3	24.3	2296	9.4	4.6
4.60	87.2	60.0	33.0	23.7	2240	8.2	3.9	60.4	32.6	22.9	2164	8.8	4.3
5.00	94.8	60.7	32.3	22.3	2107	7.9	3.8	61.0	32.0	21.8	2060	8.5	4.2
5.50	104.0	61.8	31.2	20.1	1899	7.85	3.8	62.0	31.0	19.7	1862	8.2	3.9
5.80	110.5	62.1	30.9	19.6	1852	7.8	4.0	62.4	30.6	19.0	1796	8.2	4.0
5.30	100.4	61.4	31.6	20.9	1975	7.9	4.1	61.6	31.4	20.6	1947	8.3	4.2
4.80	91.0	60.1	31.9	21.5	2032	8.0	4.2	60.4	32.6	22.9	2164	8.9	4.7
4.40	83.6	59.1	33.9	25.6	2419	8.3	4.4	59.6	33.4	24.6	2325	9.5	5.1
4.10	78.0	58.0	35.0	27.9	2637	8.6	4.6	58.8	34.2	26.2	2476	10.6	5.8
3.90	74.2	57.2	35.8	29.7	2807	9.1	4.9	58.3	34.7	27.3	2580	11.8	6.7
3.70	70.5	56.9	36.1	30.4	2873	9.4	5.1	58.1	34.9	27.7	2618	12.6	7.3
3.50	66.8	56.0	37.0	32.3	3052	10.4	5.7	57.5	35.5	29.0	2741	14.3	8.8
3.30	63.1	55.2	37.8	34.3	3241	12.2	7.0	57.3	35.7	29.5	2788	16.4	10.8
3.10	59.2	54.3	38.7	36.3	3430	13.9	8.4	57.3	35.7	29.5	2788	17.8	12.4
3.00	57.4	54.7	38.3	38.3	3336	15.2	9.6	57.5	35.5	29.1	2750	18.6	13.2
2.90	55.6	54.6	38.4	35.6	3364	16.2	10.5	57.6	34.4	27.2	2570	19.2	14.0
2.80	54.1	55.0	38.0	34.7	3279	17.0	11.4	58.0	35.0	27.9	(2637)	19.7	14.5
2.70	52.1	55.7	37.3	33.0	3185	18.0	12.6	58.8	34.2	26.2	2476	20.3	15.2
2.60	50.1	56.9	36.1	30.3	2863	18.6	13.2	59.3	33.7	25.2	2381	20.7	15.8
2.50	48.0	58.5	34.5	26.9	2542	19.2	13.8	60.5	32.5	22.7	2145	31.0	16.2
2.30	44.0	60.2	32.8	23.4	2211	19.8	14.6	61.4	31.6	20.9	1975	21.3	16.6
2.10	40.4	60.7	32.3	22.3	2107	20.3	15.2	61.9	31.1	19.9	1881	21.6	16.6
1.90	36.5	61.4	31.6	20.9	1975	20.7	15.8	62.1	30.9	19.6	1852	22.0	17.6
1.70	32.7	61.7	31.3	20.3	1918	21.0	16.2	62.5	30.5	18.2	1720	22.2	18.0
1.50	28.8	61.8	31.2	20.1	1899	21.3	16.6	62.5	30.5	18.2	1720	22.3	18.1

C_x = 93.0 C_h = 23.4 ϵ = 94.5 C_s

TABLE A-4

Sample 4

mv	T, °C	σ_y^1	σ_o^1	σ_s^1	ϵ_1	μa_1	I_1	σ_y^2	σ_o^2	σ_s^2	ϵ_2	μa_2	I_2
1.40	27.0	55.3	37.7	33.7	634	19.2	13.9	55.6	37.4	33.0	620	19.2	13.8
1.65	31.8	55.6	37.4	33.0	621	19.2	13.9	56.0	37.0	32.1	602	19.1	13.8
1.90	36.5	55.9	37.1	32.3	608	19.2	13.9	56.2	36.8	31.6	594	19.2	13.8
2.20	42.5	55.8	37.2	32.5	612	19.0	13.8	56.2	36.8	31.6	594	19.0	13.6
2.50	48.0	55.7	37.3	32.8	617	18.9	13.6	56.2	36.8	31.6	594	18.9	13.5
2.80	54.1	55.2	37.8	33.9	637	18.8	13.4	56.0	37.0	32.2	605	18.8	13.4
3.10	59.2	54.9	38.1	34.6	650	18.6	13.0	55.6	37.4	33.0	620	18.6	13.0
3.40	64.9	54.3	38.7	36.0	677	18.6	13.0	55.1	37.9	34.2	642	18.6	13.0
3.60	68.7	53.3	39.7	38.4	722	18.4	12.8	54.7	38.3	35.1	660	18.5	13.0
3.80	72.3	52.5	40.5	40.3	758	18.2	12.6	53.9	39.1	37.0	695	18.3	12.7
3.90	74.2	51.1	41.9	44.0	828	18.1	12.4	53.2	39.8	38.6	725	18.2	12.6
4.00	76.2	49.6	43.4	48.0	902	17.9	12.2	52.2	40.8	41.2	775	18.1	12.4
4.10	78.0	48.0	45.0	52.5	986	17.6	11.8	51.2	41.8	43.8	824	17.9	12.2
4.20	80.0	46.3	46.8	55.3	990	17.2	11.4	50.8	42.2	44.7	840	17.6	11.8
4.30	82.1	46.4	46.6	57.1	1074	16.6	10.6	49.7	43.3	47.8	900	17.2	11.0
4.40	83.6	46.1	46.9	58.1	1092	15.7	9.8	49.1	43.9	49.4	930	16.4	10.2
4.50	85.4	46.3	46.7	57.4	1080	14.4	8.4	48.9	44.1	50.0	940	15.3	9.4
4.60	87.2	46.3	46.7	57.4	1080	13.5	7.6	49.0	44.0	49.6	932	14.5	8.4
4.80	91.0	47.1	45.9	55.1	1036	10.3	5.4	49.1	43.9	49.5	930	12.1	6.5
5.00	94.8	47.6	45.4	53.6	1010	10.4	5.4	49.7	43.3	47.8	900	10.9	5.8
5.30	100.4	49.0	44.0	49.6	931	9.5	4.8	50.4	42.6	46.0	865	9.8	5.0
5.60	106.0	49.7	43.3	47.8	900	9.4	4.7	50.8	42.2	44.8	842	9.7	5.0
6.00	113.0	50.9	42.1	44.6	838	9.3	4.7	51.9	41.1	42.0	790	9.4	4.7
6.50	122.1	52.3	40.7	40.8	768	9.3	4.7	53.0	40.0	39.2	738	9.3	4.6
6.30	118.5	51.7	41.3	42.4	798	9.2	4.6	52.5	40.5	40.3	758	9.25	4.5
5.80	110.5	50.3	42.7	46.2	868	9.4	4.7	51.1	41.9	44.1	830	9.50	4.8
5.50	104.0	49.2	43.8	49.2	924	9.4	4.7	50.2	42.8	47.3	890	9.50	4.8
5.20	98.5	48.2	44.8	51.9	976	9.7	4.9	49.5	43.5	48.5	912	10.00	5.1
4.90	92.9	46.8	46.2	55.9	1050	10.5	5.4	48.7	44.3	50.5	950	11.2	6.0
4.70	89.2	46.0	47.0	58.4	1100	11.3	6.0	48.1	44.9	52.1	980	12.2	6.6
4.50	854	45.7	47.3	59.3	1120	12.8	7.0	48.2	44.8	52.0	976	14.0	8.1
4.40	83.6	45.6	47.4	59.6	1120	14.2	8.3	48.2	44.8	52.0	976	15.3	9.4
4.30	82.1	45.6	47.4	59.6	1120	15.0	9.0	48.4	44.6	51.3	965	17.1	11.2
4.20	80.0	46.1	46.9	58.1	1091	16.1	10.2	48.8	44.2	50.1	941	16.8	11.0
4.10	78.0	46.2	46.8	57.7	1084	16.7	10.8	49.5	43.5	48.5	912	17.2	11.4
4.00	76.2	47.2	45.8	54.8	1030	17.2	11.4	50.6	42.4	45.3	850	17.5	11.8
3.90	74.2	49.6	43.4	48.0	903	17.6	11.9	52.2	40.8	41.2	774	17.6	11.8
3.70	70.5	52.3	40.7	41.0	770	17.8	12.1	53.5	39.5	38.0	714	18.0	12.3
3.50	66.8	53.4	39.6	38.2	718	18.0	12.4	54.3	38.7	36.1	678	18.1	12.4
3.20	61.2	54.2	38.8	36.3	683	18.2	12.6	55.2	37.8	33.9	638	18.2	12.6
2.90	55.6	55.1	37.9	34.2	643	18.4	12.9	55.7	37.3	32.8	616	18.4	12.9
2.60	50.0	55.5	37.5	33.2	624	18.5	13.0	56.2	36.8	31.7	596	18.5	13.0
2.30	44.0	55.9	37.1	32.4	608	18.5	13.0	56.3	36.7	31.5	593	18.5	13.0
2.00	38.4	56.2	26.8	31.6	594	18.5	13.0	56.6	36.4	30.8	579	18.5	13.0
1.70	32.7	56.3	36.7	31.5	592	18.5	13.0	56.6	36.4	30.8	579	18.5	13.0
1.40	27.0	56.[illegible]	37.0	32.1	603	18.5	13.0	56.5	36.5	30.9	581	18.6	13.0

C_x = 93.0 C_h = 23.6 ϵ = 18.8 C_s

mv	T, °C	σ_y^3	σ_o^3	σ_s^3	ϵ_3	μa_3	I_3	σ_y^4	σ_o^4	σ_s^4	ϵ_4	μa_4	I_4
1.40	27.0	56.2	36.8	31.6	594	19.2	13.8	56.8	36.2	30.2	568	19.2	14.0
1.65	31.8	56.6	36.4	30.7	578	19.1	13.8	57.2	35.8	29.4	553	19.1-2	14.0
1.90	36.5	56.9	36.1	30.1	573	19.2	13.8	57.5	35.5	28.8	542	19.25	14.0
2.20	42.5	56.8	36.2	31.2	586	19.1	13.8	57.5	35.5	28.8	542	19.25	14.0
2.50	48.0	56.9	36.1	30.1	566	19.0	13.6	57.4	35.6	29.0	545	19.2	14.0
2.80	54.1	56.7	36.3	30.5	573	19.0	13.6	57.3	35.7	29.2	549	19.2	14.0
3.10	59.2	56.7	36.3	30.5	573	18.9	13.5	57.1	35.9	29.7	558	19.1	13.8
3.40	64.9	56.0	37.0	32.2	605	18.9	13.5	56.7	36.3	30.5	572	19.0	13.6
3.60	68.7	55.7	37.3	32.8	616	18.8	13.4	56.3	36.7	31.5	592	19.0	13.6
3.80	72.3	55.0	38.0	34.3	645	18.6	13.0	55.9	37.1	32.4	610	19.0	13.6
3.90	74.2	54.4	38.6	35.8	673	18.5	13.0	55.5	37.5	33.2	628	18.9	13.6
4.00	76.2	53.8	39.2	35.8	673	18.4	12.9	54.8	38.2	34.9	656	18.9	13.6
4.10	78.0	53.1	39.9	38.9	732	18.3	12.7	54.3	38.7	36.0	678	18.9	13.6
4.20	80.0	52.2	40.8	41.2	775	18.2	12.6	53.9	39.1	37.0	695	18.7	13.4
4.30	82.1	51.4	41.6	43.3	815	17.8	12.1	53.9	39.1	37.0	695	18.5	13.0
4.40	83.6	51.1	41.9	44.0	827	17.3	11.5	52.4	40.6	40.7	765	18.2	12.6
4.50	85.4	50.8	42.2	44.7	840	16.5	9.4	52.2	40.8	41.2	775	17.7	12.0
4.60	87.2	50.5	42.5	45.6	856	14.8	8.8	51.8	41.2	42.2	793	17.2	11.4
4.80	91.0	50.4	42.6	45.8	861	13.4	7.6	51.6	41.4	42.6	800	15.0	9.0
5.00	94.8	50.8	42.2	44.8	844	11.9	6.4	51.8	41.2	42.2	795	13.4	7.6
5.30	100.4	51.3	41.7	43.5	818	10.3	5.4	51.9	41.1	42.0	790	11.2	5.9
5.60	106.0	51.7	41.3	42.4	797	10.0	5.1	52.3	40.7	40.8	768	10.4	5.4
6.00	113.0	52.4	40.6	40.7	766	9.4	4.7	52.9	40.1	39.2	736	9.6	4.8
6.50	122.1	53.2	39.8	38.7	727	9.3	4.6	53.5	39.5	38.0	715	9.2	4.6
6.30	118.5	52.7	40.3	40.0	752	9.2	4.4	53.1	39.9	39.6	745	9.2	4.6
5.80	110.5	51.8	41.2	42.2	794	9.5	4.8	53.2	39.8	39.5	743	9.7	4.9
5.50	104.0	51.0	42.0	44.2	830	9.7	5.0	51.9	41.1	41.9	787	10.2	5.2
5.20	98.5	50.2	42.8	46.4	872	10.5	5.5	51.2	41.8	43.8	824	11.4	6.0
4.90	92.9	49.8	43.2	47.5	883	12.2	6.6	50.7	42.3	45.1	848	13.5	7.6
4.70	89.2	49.5	43.5	48.3	910	13.5	7.8	50.9	42.1	44.6	838	15.2	9.2
4.50	85.4	49.7	43.3	47.8	900	15.4	9.4	51.1	41.9	44.1	828	16.8	11.2
4.40	83.6	50.0	43.0	47.1	885	16.5	10.6	51.5	41.5	43.1	810	17.4	11.6
4.30	82.1	50.1	42.9	46.7	878	17.0	11.1	51.8	41.2	42.1	790	17.7	12.0
4.20	80.0	50.9	42.1	44.6	838	17.5	11.8	52.1	40.9	41.5	780	18.0	12.3
4.10	78.0	51.3	41.7	43.6	820	17.6	11.8	52.5	40.5	40.4	760	18.1	12.4
4.00	76.2	52.1	40.4	41.6	782	17.9	12.2	53.5	39.5	37.9	713	18.2	12.6
3.90	74.2	53.7	39.3	37.5	705	18.0	12.3	54.5	38.5	35.7	671	18.3	12.7
3.70	70.5	54.5	38.5	35.6	670	18.1	12.4	55.5	37.5	33.2	624	18.4	12.8
3.50	66.8	55.3	37.7	33.7	634	18.3	12.7	56.1	36.9	31.9	600	18.5	13.0
3.20	61.2	55.9	37.1	32.3	607	18.3	12.7	56.6	36.4	30.8	579	18.5	13.0
2.90	55.6	56.4	36.6	31.2	586	18.4	12.9	57.1	35.9	29.6	556	18.6	13.2
2.60	50.0	57.1	35.9	29.6	556	18.6	13.0	57.4	35.6	29.0	545	18.6	13.2
2.30	44.0	57.0	36.0	29.9	562	18.5	13.0	57.6	35.4	28.6	538	18.6	13.2
2.00	38.4	57.2	35.8	29.5	554	18.5	13.0	57.8	35.2	28.2	530	18.6	13.2
1.70	32.7	57.1	35.9	29.6	557	18.6	13.0	57.8	35.2	28.2	530	18.8	13.2
1.40	27.0	57.0	36.0	29.9	562	18.6	13.0	57.6	35.4	28.5	536	18.6	13.2

C_x = 93.0 C_h = 23.6 ϵ = 18.8 C_s

TABLE A-5

Sample 5

mv	T,°C	C_y^1	C_o^1	C_s^1	ϵ_1	μa_1	L_1	C_y^2	C_o^2	C_s^2	ϵ_2	μa_2	L_2
1.60	30.8	62.9	30.1	17.7	1930	13.7	2.80	65.0	28.0	13.9	1520	15.3	3.3
1.80	34.6	52.9	30.1	17.7	1930	13.8	2.85	64.9	28.1	14.0	1525	15.5	3.3
2.00	38.4	62.8	30.2	17.9	1950	13.6	2.75	64.8	28.2	14.4	1570	15.3	3.3
2.50	48.0	63.0	30.0	17.5	1960	13.1	2.65	64.6	28.4	14.6	1590	14.5	3.0
3.00	57.4	63.1	29.9	17.4	1945	12.7	2.55	64.6	28.4	14.6	1590	13.8	2.8
3.50	66.8	62.5	29.5	16.7	1840	12.6	2.50	64.7	28.3	14.4	1570	13.7	2.8
4.00	76.2	62.7	29.3	16.2	1770	12.3	2.45	64.8	28.2	14.2	1550	12.9	2.6
4.50	85.4	64.2	28.8	15.3	1670	12.1	2.40	65.0	28.0	13.9	1520	12.6	2.5
5.00	94.8	64.8	28.2	14.4	1570	12.2	2.40	65.2	27.8	13.5	1470	12.5	2.5
5.50	104.0	65.0	28.0	13.9	1520	12.1	2.40	65.5	27.5	13.0	1415	12.3	2.45
6.00	113.0	65.4	27.6	13.1	1430	12.1	2.40	65.2	27.4	12.9	1410	12.2	2.4
6.50	122.1	65.9	27.1	12.4	1350	12.1	2.40	65.9	27.1	12.3	1340	12.2	2.4
7.00	131.5	66.0	27.0	12.1	1320	12.2	2.40	66.0	27.0	12.0	1310	12.3	2.45
6.80	128.0	65.9	27.1	12.4	1350	12.25	2.45	66.0	27.0	12.0	1310	12.3	2.45
6.30	118.5	65.6	27.4	12.8	1395	12.25	2.45	65.8	27.2	12.4	1350	12.4	2.45
5.80	110.5	65.4	27.6	18.1	1430	12.3	2.45	65.5	27.5	13.0	1415	12.5	2.5
5.30	100.4	65.0	28.0	13.9	1520	12.3	2.45	65.3	27.7	13.4	1460	12.5	2.5
4.80	91.0	64.6	28.4	14.6	1590	12.4	2.45	65.0	28.0	13.9	1490	12.6	2.5
4.30	82.1	64.1	28.9	15.6	1700	12.4	2.45	64.9	28.1	14.0	1525	12.8	2.6
3.80	72.3	63.8	29.2	16.1	1760	12.6	2.50	64.7	28.3	14.4	1570	13.1	2.7
3.30	63.1	63.4	29.6	16.8	1830	12.7	2.50	64.7	28.3	14.4	1570	13.5	2.8
2.80	54.1	63.1	29.9	17.4	1890	13.0	2.60	64.6	28.4	14.6	1590	13.9	2.8
2.50	48.0	63.0	30.0	17.5	1920	13.2	2.65	64.5	28.5	14.7	1600	14.6	3.1
2.30	44.0	62.9	30.1	17.8	1940	13.4	2.70	64.6	28.4	14.6	1590	14.9	3.2
2.10	40.4	62.8	30.2	17.9	1950	13.7	2.81	64.8	28.2	14.2	1550	15.2	3.25
1.90	36.5	62.8	30.2	17.9	1950	14.0	2.90	64.8	28.2	14.2	1550	16.0	3.5
1.73	33.3	62.8	30.2	17.9	1950	14.2	2.95	64.8	28.2	14.2	1550	16.4	3.6
1.53	29.4	62.8	30.2	17.9	1950	14.3	3.00	64.9	28.1	14.0	1525	16.5	3.7

C_x = 93.0 C_h = 23.7 ϵ = 109 C_s

mv	T,°C	C_y^3	C_o^3	C_s^3	ϵ_3	μa_3	L_3	C_y^4	C_o^4	C_s^4	ϵ_4	μa_4	L_4
1.60	30.8	65.8	27.2	12.4	1350	16.7	3.7	66.5	26.5	11.3	1230	18.7	4.5
1.80	34.6	65.7	27.3	12.6	1370	16.8	3.8	66.4	26.6	11.4	1240	18.7	4.5
2.00	38.4	65.6	27.4	12.8	1390	16.7	3.7	66.4	26.6	11.4	1240	18.6	4.45
2.50	48.0	65.4	27.6	13.1	1430	15.8	3.4	66.2	26.8	11.8	1285	17.6	4.05
3.00	57.4	65.4	27.6	13.1	1430	15.0	3.2	66.0	27.0	12.1	1320	16.6	3.70
3.50	66.8	65.3	27.7	13.2	1440	14.7	3.1	65.9	27.1	12.3	1340	16.2	3.6
4.00	76.2	65.2	27.8	13.5	1470	13.7	2.8	65.9	27.1	12.3	1340	14.8	3.06
4.50	85.4	65.3	27.7	13.2	1440	13.0	2.6	65.9	27.1	12.3	1340	13.4	2.75
5.00	94.8	65.5	27.5	13.0	1415	12.8	2.6	66.0	27.0	12.1	1320	13.6	2.80
5.50	104.0	65.6	27.4	12.8	1395	12.6	2.5	66.1	26.9	11.9	1290	13.2	2.70
6.00	113.0	65.9	27.1	12.3	1340	12.4	2.5	66.2	26.8	11.8	1280	12.8	2.60
6.50	122.1	66.0	27.0	12.1	1320	12.4	2.45	66.2	26.8	11.8	1280	12.8	2.60
7.00	131.5	66.1	26.9	11.9	1300	12.4	2.45	66.4	26.6	11.4	1240	12.7	2.55
6.80	128.0	66.1	26.9	11.9	1300	12.5	2.5	66.3	26.7	11.5	1250	12.8	2.60
6.30	118.5	65.9	27.1	12.3	1340	12.6	2.5	66.2	26.8	11.8	1285	12.9	2.60
5.80	110.5	65.8	27.2	12.4	1350	12.7	2.55	66.1	26.9	11.9	1300	13.2	2.70
5.30	100.4	65.6	27.4	12.8	1410	12.7	2.55	66.0	27.0	12.1	1320	13.3	2.70
4.80	91.0	65.5	27.5	13.0	1420	12.8	2.6	66.0	27.0	12.1	1320	13.6	2.80
4.30	82.1	65.4	27.6	13.1	1430	13.2	2.7	65.9	27.1	12.3	1340	14.1	2.90
3.80	72.3	65.3	27.7	13.4	1460	13.6	2.8	65.9	27.1	12.3	1340	14.7	3.10
3.30	63.1	65.3	27.7	13.4	1460	14.3	3.0	66.0	27.0	12.1	1320	15.7	3.40
2.80	54.1	65.4	27.6	13.1	1430	14.9	3.15	66.2	26.8	11.8	1285	16.6	3.70
2.50	48.0	65.3	27.7	13.4	1460	15.6	3.4	66.2	26.8	11.8	1285	17.2	3.90
2.30	44.0	65.5	27.5	13.0	1420	16.2	3.6	66.3	26.7	11.5	1250	17.8	4.15
2.10	40.4	65.5	27.5	13.0	1420	16.6	3.7	66.3	26.7	11.5	1250	18.2	4.30
1.90	36.5	65.6	27.4	12.8	1395	17.3	3.9	66.4	26.6	11.4	1240	19.1	4.65
1.73	33.3	65.6	27.4	12.8	1395	17.8	4.1	66.4	26.6	11.4	1240	19.5	4.80
1.53	29.4	65.7	27.3	12.6	1370	17.8	4.1	66.4	26.6	11.4	1240	19.5	4.80

C_x = 93.0 C_h = 23.7 ϵ = 109 C_s

TABLE A-6

Sample 6

mv	T,°C	C_y^1	C_o^1	C_s^1	ϵ_1	μa_1	L_1	C_y^2	C_o^2	C_s^2	ϵ_2	μa_2	L_2
1.40	27.0	62.3	30.7	189	945	13.8	3.01	63.0	30.0	176	880	14.8	3.35
1.60	30.8	62.2	30.8	192	960	13.5	2.95	63.0	30.0	176	880	14.8	3.35
1.80	34.6	62.0	31.0	196	980	13.2	2.80	62.9	30.1	178	890	14.7	3.35
2.00	38.4	61.8	31.2	199	995	12.7	2.75	62.8	30.2	181	905	14.2	3.20
2.10	40.4	61.0	31.3	201	1005								
2.20	42.5	61.7	31.3	201	1005	12.2	2.60	62.8	30.2	181	905	13.3	2.95
2.40	46.0	61.6	31.4	204	1020	11.7	2.50	62.7	30.3	182	910	13.1	2.85
2.50	48.0	61.6	31.4	204	1020								
2.60	50.0	61.6	31.4	204	1020	11.4	2.40	62.7	30.3	18.2	910	12.7	2.75
2.80	54.1	61.6	31.4	204	1020	10.9	2.30	62.5	30.5	186	930	12.2	2.65
3.00	57.4	61.8	31.2	199	995	10.6	2.40	62.6	30.4	184	920	11.6	2.45
3.20	61.2	61.9	31.1	198	990	10.4	2.15	62.7	30.3	182	910	11.2	2.35
3.40	64.9	62.2	30.8	192	960	10.2	2.10	62.8	30.2	181	905	10.8	2.25
3.80	72.3	62.4	30.6	186	930	9.8	2.00	62.8	30.2	181	905	10.3	2.15
4.20	80.0	62.7	30.3	182	910	9.8	2.00	63.0	30.0	176	880	10.0	2.05
4.60	87.2	63.0	30.0	176	880	9.7	2.00	63.3	29.7	172	860	9.8	2.00
5.00	94.8	63.2	29.8	172	860	9.7	2.00	63.4	29.6	169	845	9.8	2.00
5.50	104.0	63.5	29.5	168	840	9.5	1.95	63.7	29.3	164	820	9.6	1.95
6.00	113.0	63.8	29.2	161	805	9.5	1.95	63.9	29.1	161	805	9.5	1.95
5.30	100.4	63.4	29.6	169	845	9.5	1.95	63.6	29.4	165	825	9.5	1.95
4.80	91.0	63.1	29.9	174	870	9.5	2.00	63.4	29.6	169	845	9.6	2.05
4.30	82.1	62.8	30.2	181	905	9.5	2.00	63.2	29.8	174	870	9.7	2.10
4.00	76.2	62.6	30.4	183	915	9.7	2.10	63.0	30.0	176	880	10.0	2.15
3.70	70.5	62.4	30.6	186	930	9.8	2.10	62.9	30.1	178	890	10.3	2.25
3.40	64.9	62.2	30.8	192	960	10.0	2.15	62.7	30.3	182	910	10.7	2.35
3.10	59.2	62.0	31.0	196	980	10.2	2.20	62.7	30.3	182	910	11.2	2.50
2.90	55.6	61.8	31.2	199	995	10.4	2.30	62.6	30.4	184	920	11.7	2.65
2.70	52.1	61.6	31.4	204	1020	10.7	2.35	62.7	30.3	182	910	12.2	2.75
2.50	48.0	61.6	31.4	204	1020	11.2	2.50	62.8	30.2	181	905	12.7	2.85
2.30	44.0	61.6	31.4	204	1020	11.5	2.55	62.9	30.1	178	890	13.4	3.10
2.10	40.4	61.7	31.3	201	1005	12.1	2.75	63.0	30.0	176	880	14.0	3.30
1.90	36.5	62.0	31.0	196	980	12.6	2.85	63.1	29.9	174	870	14.6	3.50
1.70	32.7	62.0	31.0	196	980	13.1	3.05	63.1	29.9	174	870	15.25	3.70
1.50	28.8	62.2	30.8	192	960	13.5	3.15	63.3	29.7	171	855	15.7	3.85

C_x = 93.0 C_h = 23.6 ϵ = 50 C

mv	T,°C	C_y^3	C_o^3	C_s^3	ϵ_3	μa_3	L_3	C_y^4	C_o^4	C_s^4	ϵ_4	μa_4	L_4
1.40	27.0	63.5	29.5	166	830	16.1	3.80	63.9	29.1	159	795	17.0	4.10
1.60	30.8	63.4	29.6	169	845	16.0	3.75	63.8	29.2	162	810	17.1	4.20
1.80	34.6	63.4	29.6	169	845	15.7	3.55	63.8	29.2	162	810	16.7	4.00
2.00	38.4	63.4	29.6	169	845	15.2	3.50	63.7	29.3	163	815	16.2	3.80
2.10	40.4												
2.20	42.5	63.2	29.8	173	865	14.8	3.38	63.6	29.4	165	825	15.8	3.70
2.40	46.0	63.1	29.9	174	870	14.1	3.15	63.5	29.5	166	830	15.3	3.55
2.50	48.0												
2.60	50.0	63.0	30.0	176	880	13.8	3.05	63.5	29.5	166	830	14.9	3.40
2.80	54.1	63.1	29.9	174	870	13.4	2.95	63.4	29.6	169	845	14.5	3.30
3.00	57.4	63.1	29.9	174	870	12.7	2.75	63.5	29.5	166	830	13.8	3.10
3.20	61.2	63.1	29.9	174	870	12.2	2.65	63.5	29.5	166	830	13.4	2.95
3.40	64.9	63.1	29.9	174	870	11.8	2.55	63.5	29.5	166	830	12.9	2.80
3.80	72.3	63.2	29.8	173	865	11.0	2.30	63.5	29.5	166	830	11.9	2.55
4.20	80.0	63.4	29.6	169	845	10.6	2.40	63.5	29.5	166	830	10.4	2.40
4.60	87.2	63.5	29.5	166	830	10.2	2.10	63.7	29.3	163	815	10.7	2.25
5.00	94.8	63.6	29.4	165	825	10.0	2.10	63.7	29.3	163	815	10.4	2.15
5.50	104.0	63.8	29.2	162	810	9.7	2.10	63.9	29.1	159	795	10.0	2.05
6.00	113.0	64.0	29.0	158	790	9.6		64.0	29.0	158	790	9.7	2.00
5.30	100.4	63.7	29.3	164	820	9.7	2.10	63.8	29.2	162	810	10.1	2.10
4.80	91.0	63.5	29.5	166	830	9.9	2.15	63.6	29.4	165	825	10.5	2.25
4.30	82.1	63.3	29.7	172	860	10.2	2.20	63.6	29.4	165	825	11.0	2.40
4.00	76.2	63.3	29.7	172	860	10.7	2.35	63.5	29.5	166	830	11.7	2.60
3.70	70.5	63.2	29.8	173	865	11.1	2.45	63.5	29.5	166	830	12.4	2.70
3.40	64.9	63.2	29.8	173	865	11.8	2.65	63.5	29.5	166	830	13.1	3.05
3.10	59.2	63.1	29.9	174	870	12.5	2.85	63.5	29.5	166	830	13.9	3.25
2.90	55.6	63.2	29.8	173	865	13.1	3.05	63.5	29.5	166	830	14.4	3.55
2.70	52.1	63.2	29.8	173	865	13.6	3.20	63.7	29.3	163	815	15.0	3.65
2.50	48.0	63.2	29.8	173	865	14.2	3.35	63.7	29.3	163	815	15.5	3.80
2.30	44.0	63.4	29.6	169	845	14.8	3.55	63.8	29.2	162	810	16.2	4.00
2.10	40.4	63.5	29.5	166	830	15.3	3.72	64.0	29.0	158	790	16.7	4.20
1.90	36.5	63.6	29.4	165	825	15.8	3.90					17.3	4.40
1.70	32.7	63.6	29.4	165	825	15.5	3.80	64.1	28.9	157	785	17.5	4.50
1.50	28.8	63.7	29.3	164	820	16.7	4.20	64.2	28.8	154	770	17.8	4.60

C_x = 93.0 C_h = 23.6 ϵ = 50 C

TABLE A-7

Sample 7

mv	T, °C	μa_1	L_1	μa_2	L_2	μa_3	L_3
1.48	28.4	19.1	3.40	19.5	3.55	20.0	3.70
1.60	30.8	19.1	3.40	19.4	3.50	20.5	3.85
1.80	34.6	19.1	3.40	19.3	3.45	22.0	3.70
2.00	38.4	19.0	3.40	19.2	3.45	19.9	3.65
2.20	42.5	18.9	3.35	19.2	3.45	19.6	3.60
2.40	46.0	18.8	3.35	19.1	3.40	19.4	3.50
2.60	50.0	18.75	3.30	19.0	3.40	19.3	3.45
2.80	54.1	18.8	3.35	19.0	3.40	19.3	3.45
3.00	57.4	18.8	3.35	19.0	3.40	19.25	3.45
3.50	66.8	18.8	3.35	19.0	3.40	19.2	3.45
4.00	76.2	18.5	3.25	18.8	3.35	19.0	3.40
4.50	85.4	18.5	3.25	18.8	3.35	19.0	3.40
5.00	94.8	18.5	3.25	18.7	3.30	19.0	3.40
5.50	104.0	18.5	3.25	18.7	3.30	19.0	3.40
5.20	98.5						
4.70	89.2	18.5	3.25	18.7	3.30	19.0	3.40
4.30	82.1	18.6	3.25	18.7	3.30	19.1	3.40
3.80	72.3						
3.30	63.1	18.6	3.25	18.7	3.30	19.1	3.40
2.80	54.1	18.6	3.25	18.8	3.35	19.3	3.45
2.70	52.1						
2.50	48.0	18.75	3.30	18.9	3.35	19.5	3.55
2.30	44.0						
2.10	40.4	18.80	3.35	19.1	3.40	19.7	3.60
1.90	36.5						
1.70	32.7	19.1	3.40	19.4	3.50	20.2	3.75
1.50	28.8						

TABLE A-8

VOLTAGES APPLIED TO CERAMIC WEDGES AND DIMENSIONS* OF WEDGES

Sample (see Table 4.1 for compositions)	Length of Wedge (cm)	Average Width of Wedge (cm)	Width of Wedge at Thin Section End (cm)	Average Thickness of Wedge (cm)	Thickness at Thin Section End (cm)	DC Voltages Applied to Sample (Volts)	Field Applied to Wedge (Volts/cm)	DC Field Applied to Thin Section (Volts/cm)
1	.97	.069	.058	.018	.004	390 600 980	5700 8700 14200	6900 9500 17000
2	.96	.076	.092	.016	.0035	500 700 1000	6600 9200 13200	5400 7600 10900
3	.90	.072	.071	.010	.0035	320 500 760	4500 7000 10500	4500 7000 10700
4	.83	.037	.052	.036	.003	220 390 560	6000 10500 15000	4200 7500 10800
5	.61	.041	.030	.007	.003	500 700 1000	12200 17100 24400	16600 23300 33000
6	.670	.050	.046	.017	.004	500 720 950	10000 14400 19000	10900 15600 20600
7	-	-	.057	-	-	400 960	- -	7000 16800

* Dimensions measured with an eye piece micrometer.

APPENDIX B

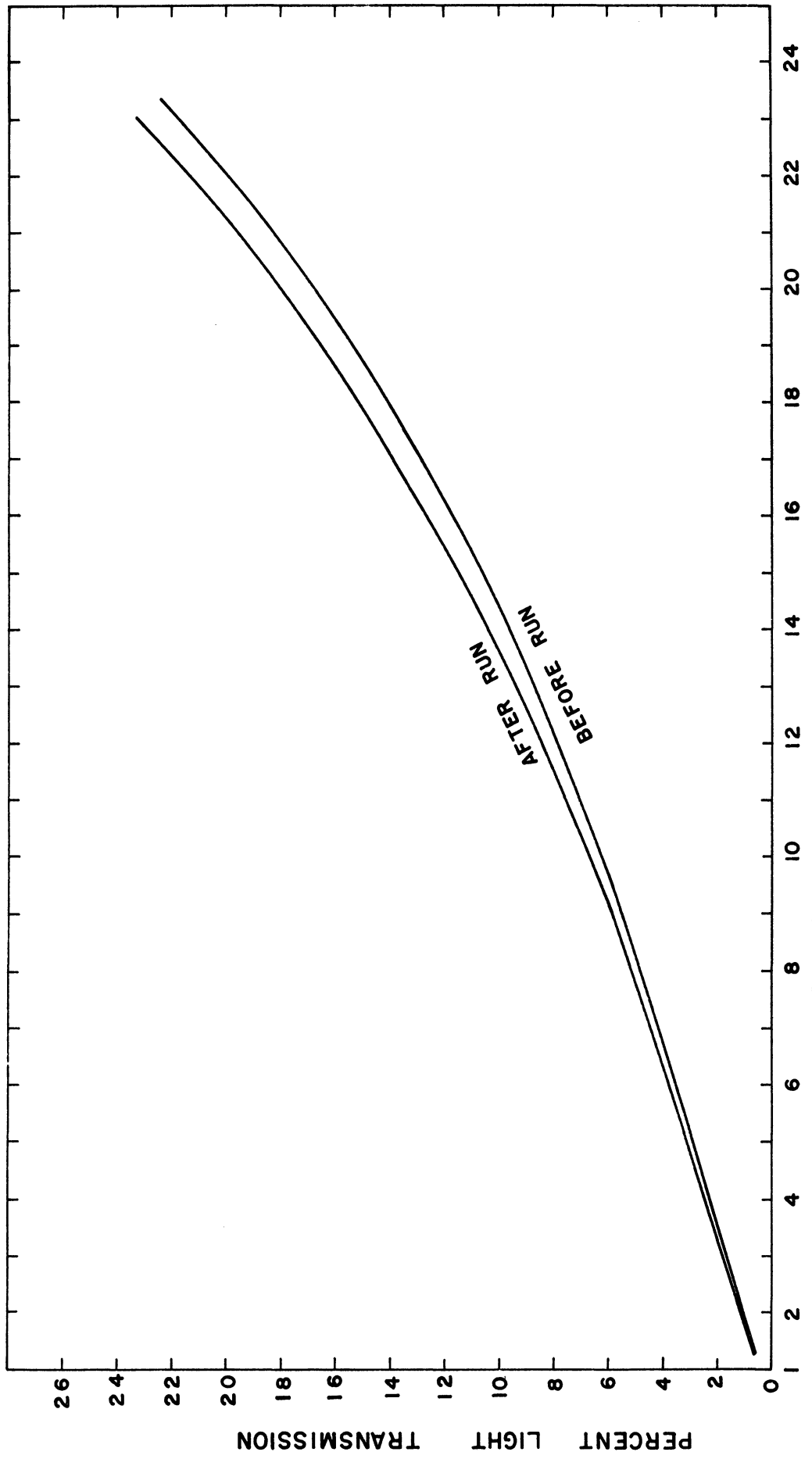


Figure B-1. Calibration Curve for the Percent Light Transmission Measurements of Ceramic Sample 1. Photocell Current vs. Percent Light Transmitted by a Calibrated Diffuse Density Filter.

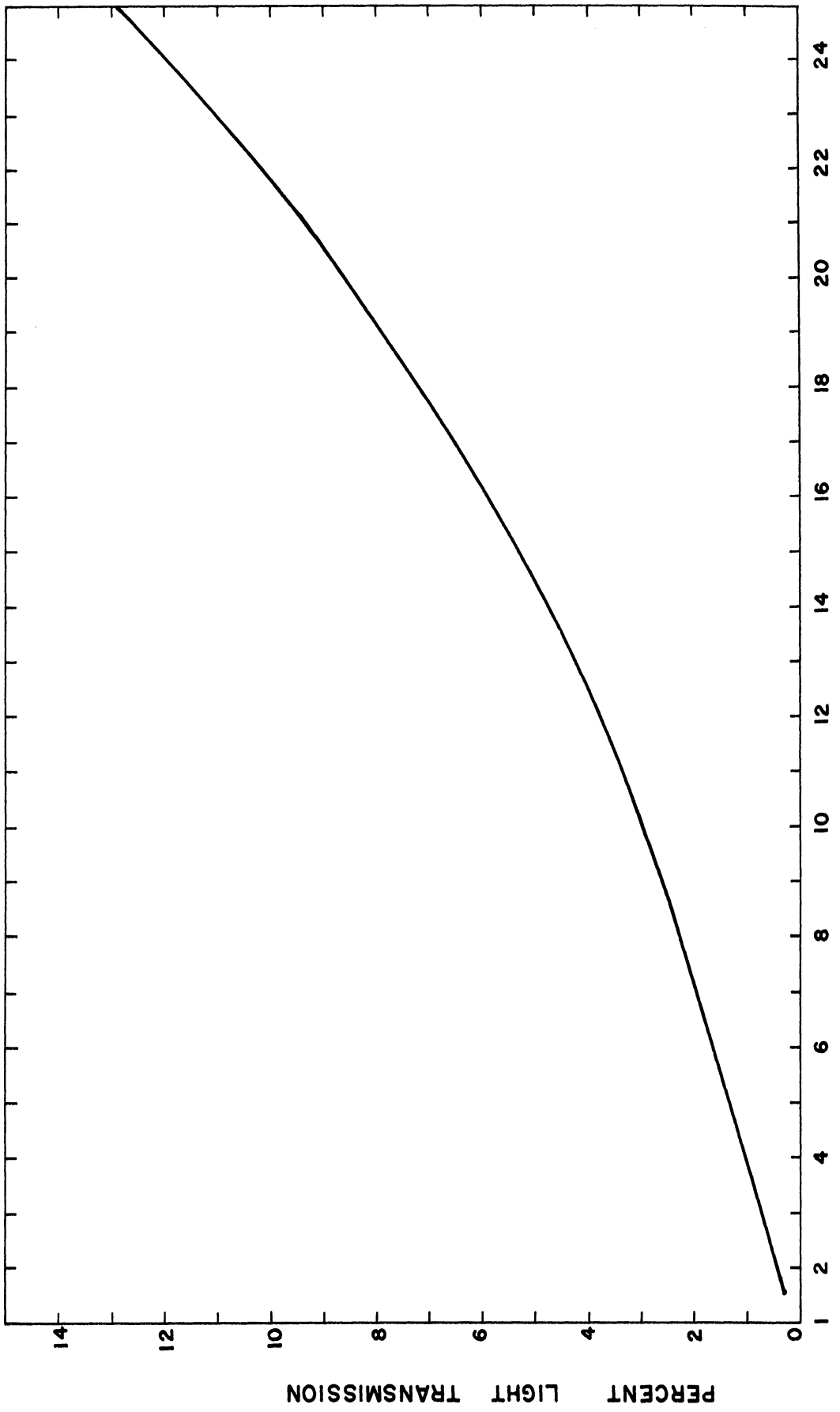


Figure B-2. Calibration Curve for the Percent Light Transmission Measurements of Ceramic Sample 2. Photocell Current vs. Percent Light Transmitted by a Calibrated Diffuse Density Filter.

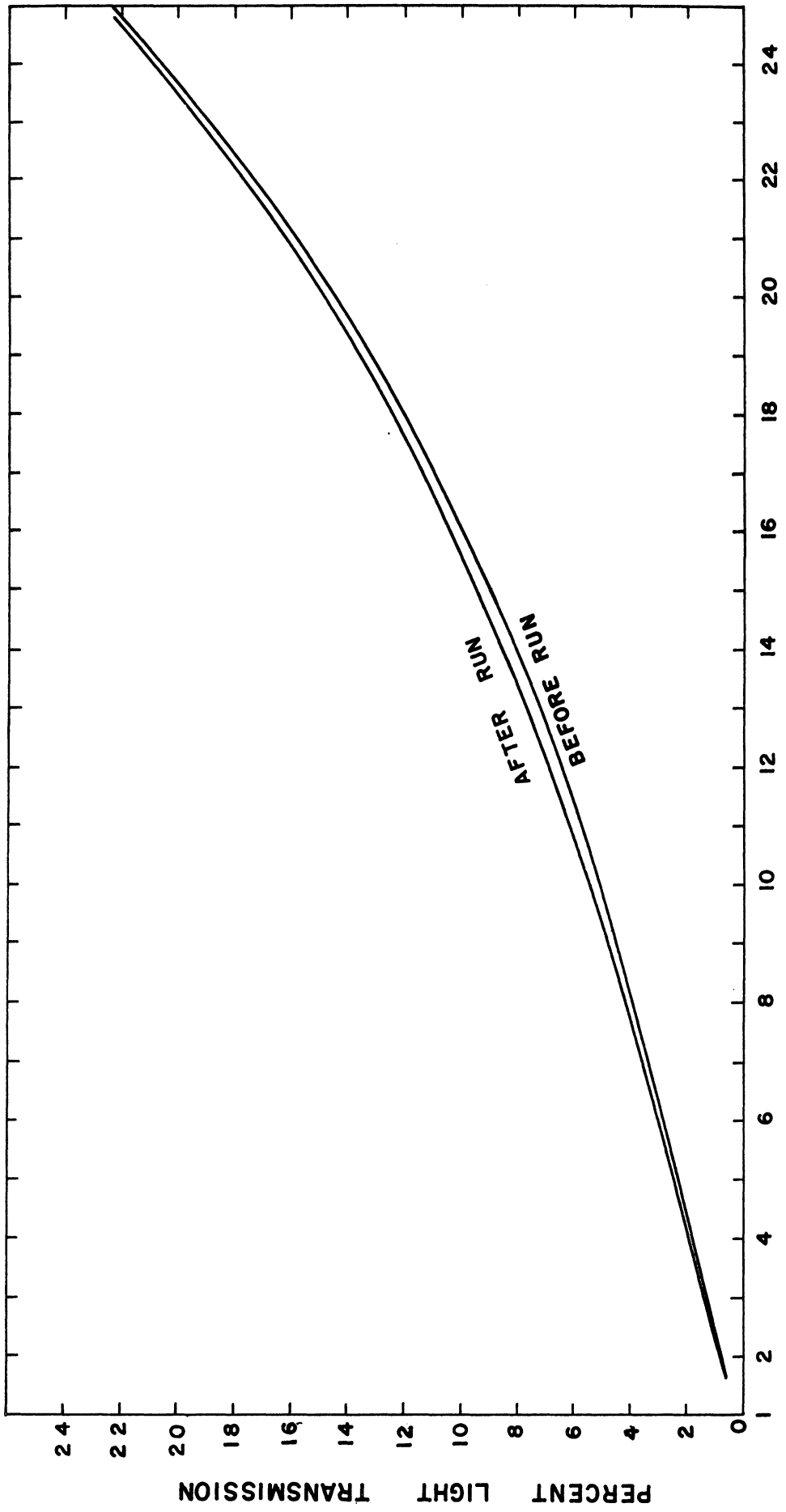


Figure B-3. Calibration Curve for the Percent Light Transmission Measurements of Ceramic Sample 3. Photocell Current vs. Percent Light Transmitted by a Calibrated Diffuse Density Filter.

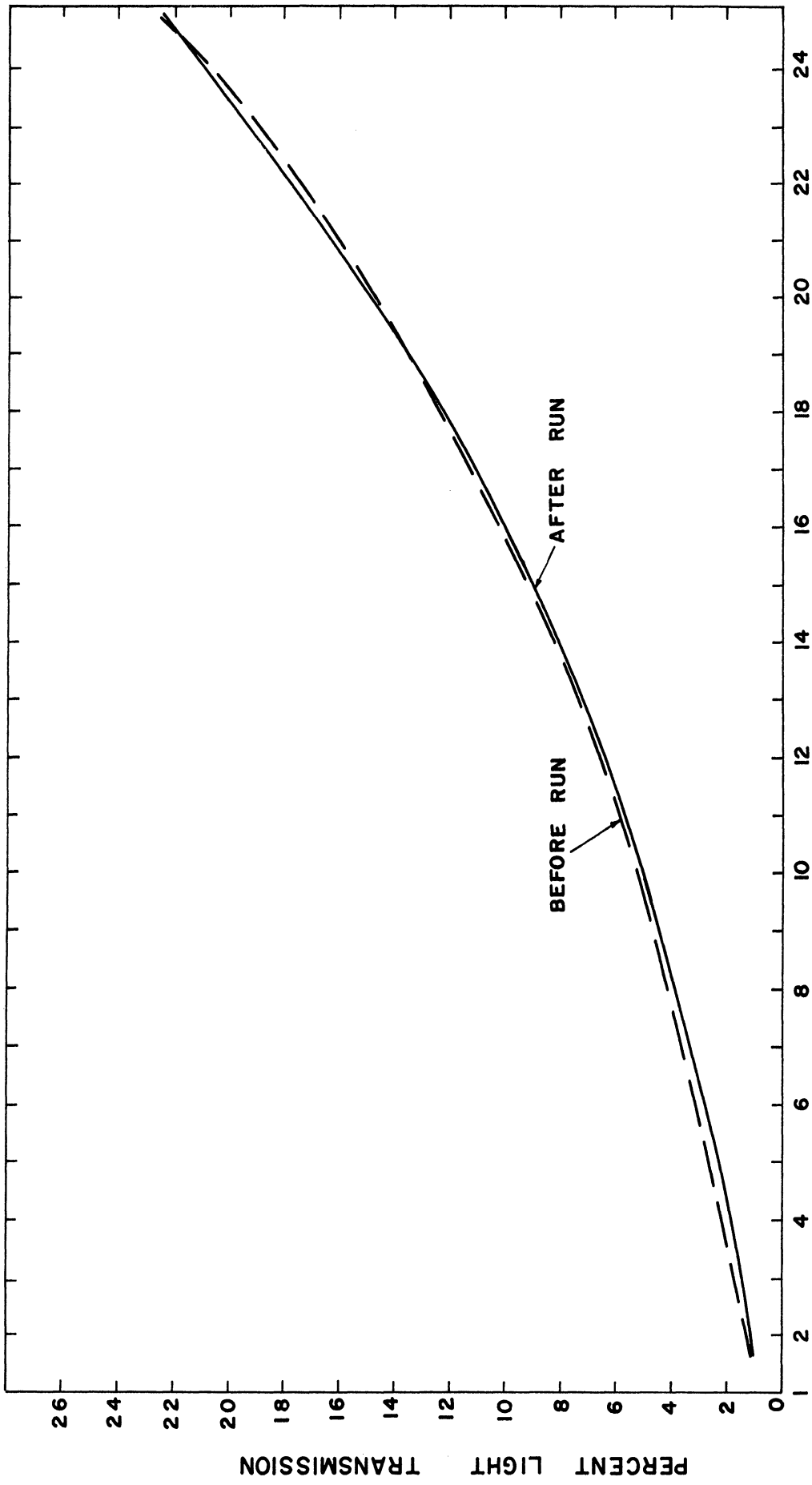


Figure B-4. Calibration Curve for the Percent Light Transmission Measurements of Ceramic Sample 4. Photocell Current vs. Percent Light Transmitted by a Calibrated Diffuse Density Filter.

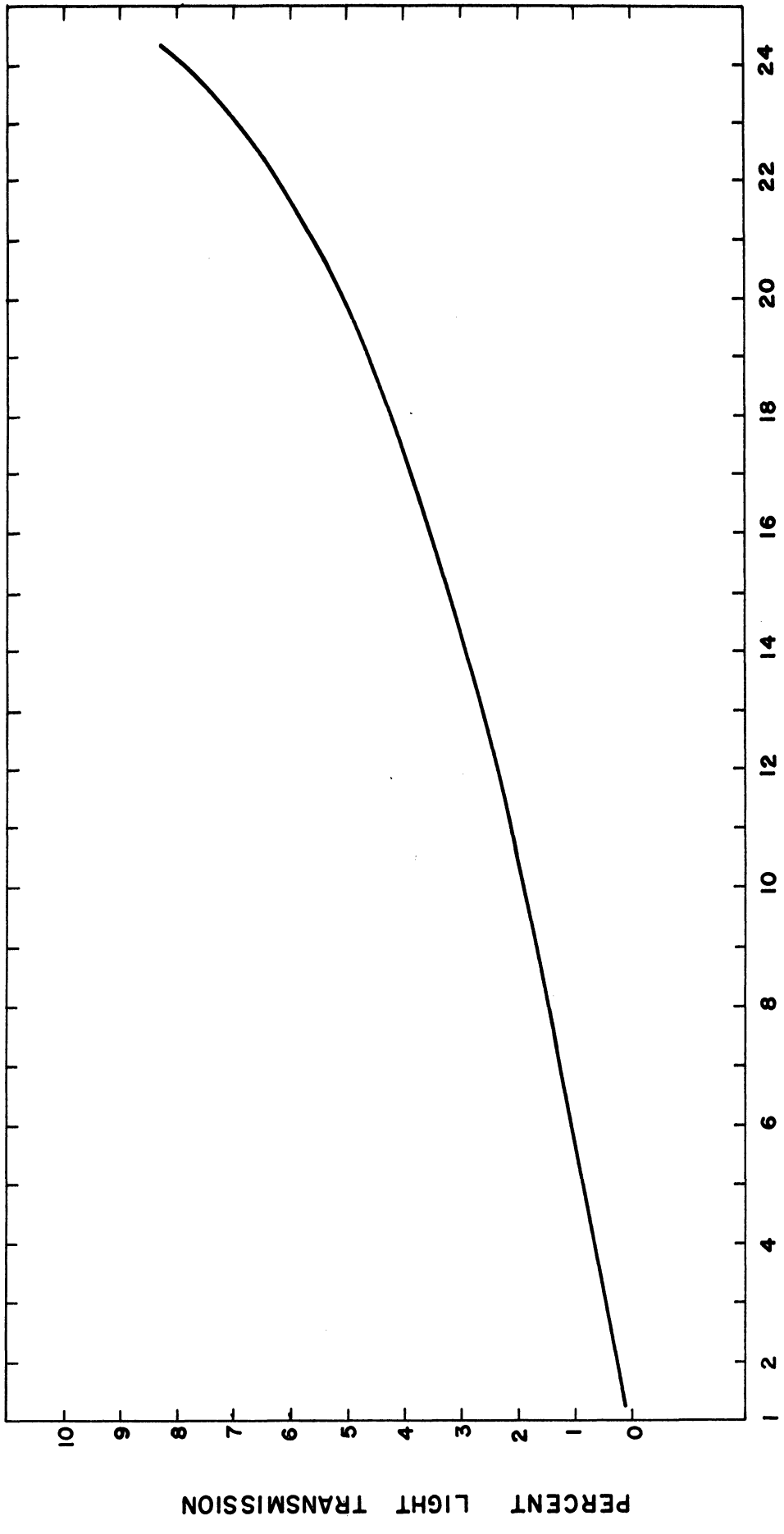


Figure B-5. Calibration Curve for the Percent Light Transmission Measurements of Ceramic Sample 5. Photocell Current vs. Percent Light Transmitted by a Calibrated Diffuse Density Filter.

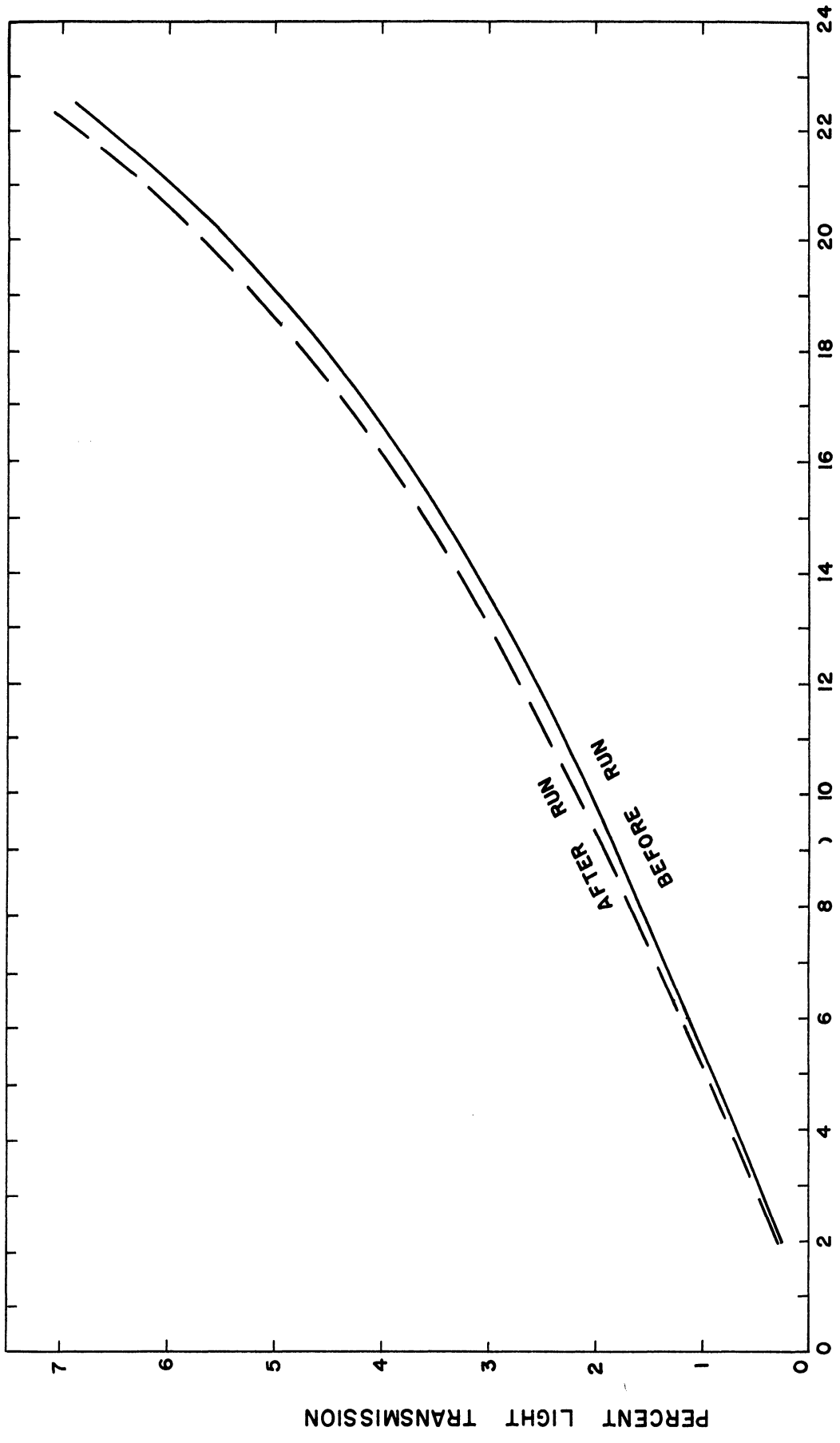


Figure B-6. Calibration Curve for the Percent Light Transmission Measurements of Ceramic Sample 6. Photocell Current vs. Percent Light Transmitted by a Calibrated Diffuse Density Filter.

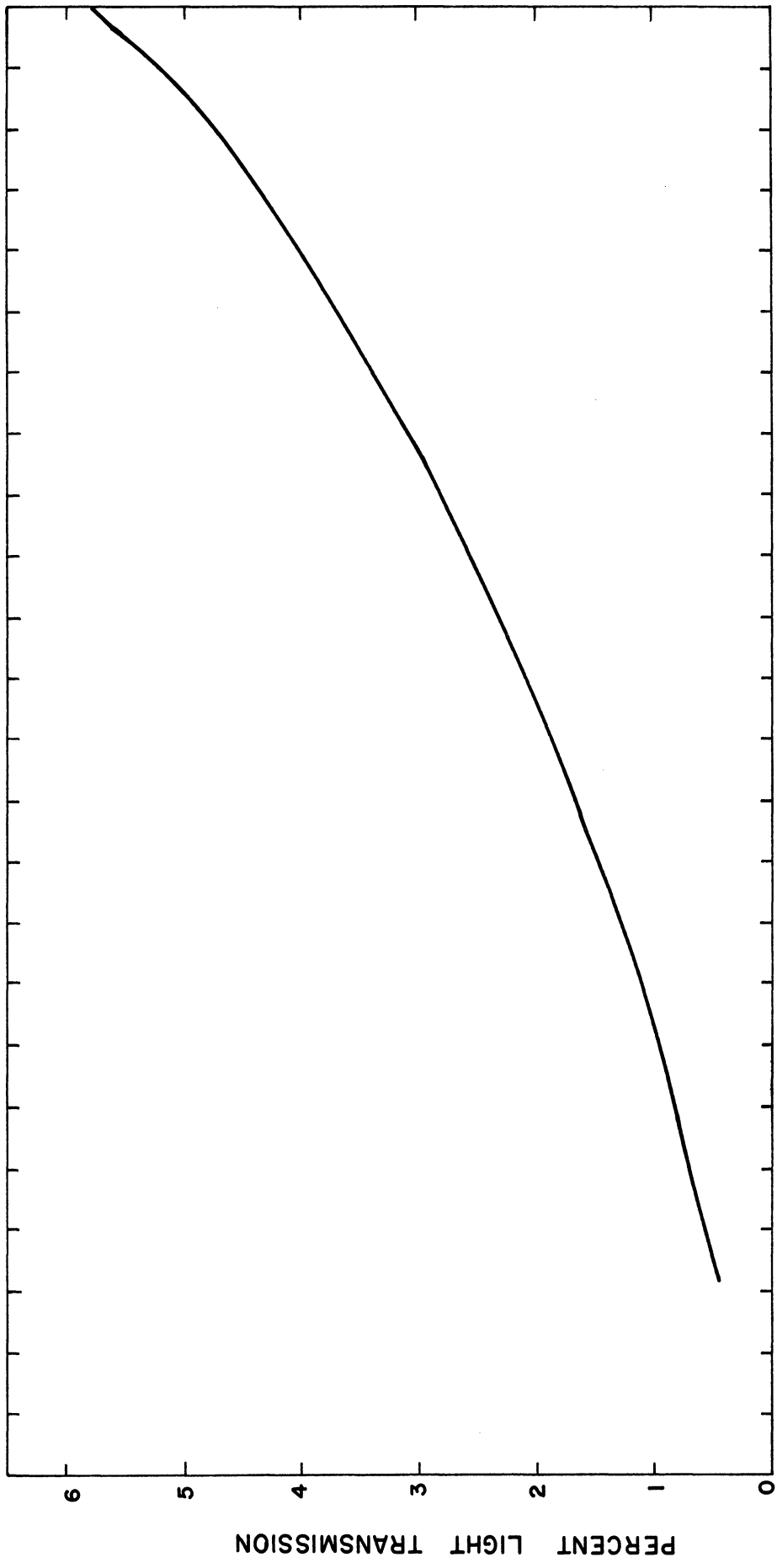


Figure B-7. Calibration Curve for the Percent Light Transmission Measurements of Ceramic Sample 7. Photocell Current vs. Percent Light Transmitted by a Calibrated Diffuse Density Filter.

APPENDIX C

SAMPLE CALCULATION AND CALCULATION OF ERRORS

The data presented in the preceding section on the incremental permittivity of the barium-strontium titanate compositions is subject to two types of errors; systematic errors, which are inherent in the measuring equipment, and random errors, which are introduced by the observer.

The capacitance data which were taken on a Bontoon Q-meter, are accurate to within ± 2% for the conditions of measurement.* A ± 1.5% error is due to the limitations of the instrument itself. Another ± 1% error is introduced during the course of the measurements by the observer. The compounded errors of instrument and observer are therefore somewhat less than ± 2% for each capacitance measurements.

In measuring the dimensions of the ceramic sample, a calibrated Bausch and Lomb mechanical microscope stage, an eye-piece micrometer, and a micrometer slide were used. The scales of these measuring devices were judged to be accurate. Certainly any deviations in their dimensions from the absolute length were insignificant in comparison with the accidental errors introduced during the measuring of the sample dimensions. Because of the small irregularities in the geometry of the wedges, an error of ± .02cm is estimated for the length of the wedges, and an error of ± .01cm is estimated for each measurement of the width and thickness (at the thick end) of the wedges.

A. Sample Calculation of the Incremental Permittivity of a Wedge of Ceramic Barium-Strontium Titanate.

It is shown in Section IV, that the capacitance of a ceramic sample can be calculated from the capacitance data by the following

* The samples all had a capacitance below 100μμf and were measured at 1600 KC.

equation:

$$C_S = \frac{C_o(C_{ST} + C_H) - C_{ST}C_H}{C_{ST} - C_o} , \qquad (C\text{-}1)$$

where C_o is the capacitance of the sample as measured on the Q-meter,

C_{ST} is the standard capacitance of the circuit,

C_H is the capacitance of the sampler holder,

C_S is the actual capacitance of the sample (see Figure 4.4, p.43).

The capacitance data of Sample 3, at zero field and 27°C (see data on Sample 3, Appendix A), is given as:

$C_o = 32.3 \mu\mu f$,

$C_{ST} = 110.0 \mu\mu f$,

$C_H = 23.4 \mu\mu f$.

Therefore

$$C_S = \frac{32.3(110 + 23.4) - (110)(23.4)}{110 - 32.3} \ \mu\mu f,$$

$$= 22.3 .$$

The incremental permittivity is defined as

$$\epsilon_\Delta = \frac{C_S \times t}{A \times .0885} \qquad (C\text{-}2)$$

where ϵ_Δ is incremental the permittivity of a sample,

t is the distance between the electrodes,

A is the area occupied by one electroded surface,

C_S is the capacitance of the sample.

A schematic of a wedge-shaped ceramic sample is shown in Figure 4.1, page 40.

For Sample 3 the dimensions are as follows:

Length of wedge = .90 cm,

Width of wedge = .072 cm,

Average thickness of wedge = .0095 cm.

Hence the incremental permittivity of Sample 3 at 27°C and zero bias is:

$$\epsilon_\Delta = \frac{22.3 \times .072}{.90 \times .0095 \times .0885} ,$$

$$= 2120 .$$

B. Calculation of Probable Errors in the Permittivity of a Ceramic Barium-Strontium Titanate Wedge.

The general formula for the calculation of errors states that if

$$\bar{R} = f(\bar{r}_1, \bar{r}_2), \qquad (C\text{-}3)$$

the probable error in $\bar{R}$, $E_{\bar{R}}$, can be written as

$$E_{\bar{R}} = \left[\left(\frac{\partial \bar{R}}{\partial \bar{r}_1}\right)^2 E_{\bar{r}_1}{}^2 + \left(\frac{\partial \bar{R}}{\partial \bar{r}_2}\right)^2 E_{\bar{r}_2}{}^2 \right]^{1/2} \qquad (C\text{-}4)$$

where $E_{\bar{r}_1}$ is the error in $\bar{r}_1$, and $E_{\bar{r}_2}$ is the error in $\bar{r}_2$.

The errors associated with the calculated incremental permittivity of Sample 3 at 27°C and zero bias are due to

1) Measurements of capacitance which are each subject to an error of $\pm$ 2%.

2) Measurements of the sample dimensions which are subject to errors varying between $\pm$ .01 and $\pm$ .02cm.

The data for Sample 3, including probable errors, are given below.

Capacitance data: $C_o = 93.0 \pm 2.0 - 60.7 \pm 1.2 = 32.3 \pm 2.3 \mu\mu f.$

$C_{ST} = 110.0 \pm 2.2 \mu\mu f.$

$C_H = 23.4 \pm 0.5 \mu\mu f.$

Dimensions: $A = (.095 \pm .01)(.9 \pm .02)\ cm^2.$

$t = .072 \pm .017\ cm.$

1. Probable Error in Sample Capacitance, E_{C_S}

$$C_{sample} = \frac{C_o\,(C_{ST} + C_H) - C_{ST}C_H}{C_{ST} - C_o} \quad . \tag{C-1}$$

Let $C_o\,(C_{ST} + C_H) - C_{ST}C_H = C_A$,

$C_{ST}C_H = C_B$,

$C_{ST} - C_o = C_C$.

Then

$$C_{sample} = \frac{C_A - C_B}{C_C} \quad .$$

a. Error in C_A, E_{C_A}

Equation (C-4) is used to solve for E_{C_A}.

Let $C_A = f[C_o, (C_{ST} + C_H)]$

Then $E_{C_A} = [(\frac{\partial C_A}{\partial C_o})^2 E_{C_o}^{\ 2} + (\frac{\partial C_A}{\partial (C_{ST}+C_H)})^2 E_{(C_{ST}+C_H)}^{\ 2}]^{1/2}$

$C_A = C_o\,(C_{ST} + C_H)$

$= 32.3 \pm 2.3\ (110.0 \pm 2.2 + 23.4 \pm .05)\mu\mu f^2$

$= 32.3 \pm 2.3\ (133.4 \pm 2.3)\mu\mu f^2$

$= 4309 \pm E_{C_A}\ \mu\mu f^2$

$$E_{C_A} = [(133.4)^2\ (2.3)^2 + (32.3)^2\ (2.3)^2]^{1/2}$$

$$= 316 \mu\mu f^2 .$$

Therefore

$$C_A = 4309 \pm 316 \mu\mu f^2$$

b. Error in C_B, E_{C_B}

$$C_B = C_{ST} C_H ,$$

$$= (110.0 \pm 2.2)(23.4 \pm 0.5)\ \mu\mu f^2,$$

$$= 2574 \pm E_{C_B}\ \mu\mu f^2.$$

According to Equation (C-4),

if $C_B = f(C_{ST}, C_H)$,

then $$E_{C_B} = [(\frac{\partial C_B}{\partial C_{ST}})^2 E_{C_{ST}}{}^2 + (\frac{\partial C_B}{\partial C_H})^2 E_{C_H}{}^2]^{1/2} ,$$

$$= [(110.0)^2\ (0.5)^2 + (23.4)^2\ (2.2)^2]^{1/2}\ \mu\mu f^2 ,$$

$$= 75 \mu\mu f^2 .$$

Therefore $C_B = 2574 \pm 75 \mu\mu f^2$.

c. Error in C_C , E_{C_C}

$$C_C = C_{ST} - C_o ,$$

$$= (110.0 \pm 2.2) - (32.3 \pm 2.3) \mu\mu f ,$$

$$= 77.7 \pm 3.2 \mu\mu f .$$

d. Probable Error in C_S , E_{C_S}

$$C_S = \frac{C_A - C_B}{C_C}$$

$$= \frac{(4309 \pm 316)-(2574 \pm 75)}{77.7 \pm 3.2} \ \mu\mu f \ ,$$

$$= \frac{1735 \pm 325}{77.7 \pm 3.2} \ \mu\mu f \ ,$$

$$= 22.33 \pm E_{C_S} \ .$$

According to Equation (C-4) ,

If $C_S = f[(C_A-C_B), C_C]$

then $E_{C_S} = [(\frac{\partial C_S}{\partial(C_A-C_B)})^2 E_{(C_A-C_B)}^2 + (\frac{\partial C_S}{\partial C_C})^2 E_{C_S}^2]^{1/2}$,

$$= [(\frac{1}{77.7})^2 (325)^2 + (-\frac{1735}{77.7^2})^2 3.2^2]^{1/2} \ ,$$

$$= 4.28 \ .$$

Therefore $C_S = 22.3 \pm 4.3$.

f. Probable Error in the Incremental Permittivity of the Sample, E_{ϵ_Δ}

The incremental permittivity has been defined in the early part of this appendix as

$$\epsilon_\Delta = \frac{C_S \times t}{A \times .0885} \ . \qquad \text{(C-2)}$$

Inserting the capacitance of the sample C_S in Equation (C-2) and the dimensions of thickness (t) and the area (A) of the sample, the incremental permittivity of the sample is given by

$$\epsilon_\Delta = \frac{(22.3 \pm 4.3)(.072 \pm .017)}{(.095 \pm .01)(.9 \pm .02) \times .0885} \ ,$$

$$= 2120 \pm E_{\epsilon_\Delta} \ .$$

2. Probable Error in ϵ_Δ , $E_{\epsilon\Delta}$,

where $\epsilon_\Delta = \frac{C \times t}{A \times .0885}$. (C-2)

Probable error in numerator, E_N

If numerator $N = f(C,t)$

Then $E_N = [(\frac{\partial N}{\partial C})^2 E_C^2 + (\frac{\partial N}{\partial t})^2 E_t^2]^{1/2}$,

$= [(22.3)^2(.0017)^2 + (.0072)^2(4.3)^2]^{1/2}$,

$= .003$.

Probable error in denominator, E_D

If denomenator $D = f(\ell,w)$ where ℓ = length, and w = width,

then $E_D = [(\frac{\partial N}{\partial \ell})^2 E_\ell^2 + (\frac{\partial N}{\partial w})^2 E_w^2]^{1/2} \times .0885$

$= [(.095)^2(.01)^2 + (.9)^2(.02)^2]^{1/2} \times .0885$

$= .0016$.

Probable error in ϵ_Δ , $E_{\epsilon\Delta}$

If $\epsilon_\Delta = f(N,D)$,

then $E_{\epsilon\Delta} = [(\frac{\partial \epsilon_\Delta}{\partial N})^2 E_N^2 + (\frac{\partial \epsilon_\Delta}{\partial D})^2 E_D^2]^{1/2}$,

$= [(\frac{1}{.00756})^2(.003)^2 + (\frac{1.61}{.00756^2})^2(.0016)^2]^{1/2}$,

$= 44$.

$\therefore$ ϵ_Δ for Sample 3 = 2120 ± 44 .

APPENDIX D

PREPARATION OF $(Ba,Sr)TiO_3$ CERAMICS

The mixed titanate ceramics, with the exception of Sample 5, a commercial ceramic, were all prepared at the Electromagnetic Materials Laboratory, Electrical Engineering Department, University of Michigan.

Stoichiometric proportions of a high purity grade $BaTiO_3$ and $SrTiO_3$, sometimes with small additions of metal oxide fluxing agents (see Table 4.1), are combined in a porcelain ball mill to which water and a binder such as methyl cellulose or the commercial "Hyform" preparation is added. The powders are ball-milled with porcelain balls for one hour. The slurry is then drained into pans and oven-dried at about 80°C. After drying, the soft cake is granulated and passed through a 20 mesh screen. The powder is pressed into a thin rectangle at about 5000 lb. per sq. in. The slabs are placed on a platinum sheet, dusted with some of the prepared powder, and fired in a Globar furnace. The temperature of the furnace is increased at a rate of 250°C/hr to 1350°C, and is held at that temperature for two hours. The furnace is then allowed to cool naturally.

This procedure produces dense ceramics which can be easily ground into wedges (see Section IV).

BIBLIOGRAPHY

1. Wainer, E. and Salomon, A. N., Titanium Alloy Mfg. Co., Elec. Rept. No. 8, (1942), Elec. Rept. No. 9, 10, (1943).

2. von Hippel, A., Breckenridge, R. G., Chesley, F. G., and Tisza, Laszlo, "High Dielectric Constant Ceramics," Ind. Eng. Chem., 8, No. 11, (1946), 1097.

3. Bunting, E. N., Shelton, G. R., and Creamer, A. S., "Properties of Barium-Strontium Titanate Dielectrics," J. Am. Ceram. Soc., 30, (1947), 114.

4. Wul, B., and Goldman, I.M., C. R. Acad. Sci. U.R.S.S., 46, (1945), 139.

5. Ibid, 49, (1945), 177.

6. Blattner, H., Matthias, B. T., Merz, W., and Scherrer, P., "Investigation of Barium Titanate Single Crystals," Experientia, 3, (1947), 148.

7. Remeika, J. P., "A Method for Growing Barium Titanate Single Crystals," J. Amer. Chem. Soc., 76, (1954), 940.

8. Valasek, J., "Piezoelectric and Allied Phenomena in Rochelle Salt," Phys. Rev., 17, (1921), 475.

9. Busch, G. and Scherrer, P., "Eine neue seignette-elekstrische Substanz," Naturwissenschaften, 23, (1935), 737.

10. Devonshire, A. F., "Theory of Ferroelectrics," Advances in Phys., 3, No. 10, 1954.

11. Mason, W. P., and Matthias, B. T., "Theoretical Model for Explaining the Ferroelectric Effect in Barium Titanate," Phys. Rev., 74, (1948), 1622.

12. Slater, J. C., "The Lorentz Correction in Barium Titanate," Phys. Rev., 78, (1950), 748.

13. Jaynes, E. T., "Displacement of Oxygen in $BaTiO_3$," Phys. Rev., 79, (1950), 1008.

14. Megaw, H. D., "Origin of Ferroelectricity in Barium Titanate and Other Perovskite-Type Crystals," Acta Cryst., 5, (1952), 739.

15. Triebwasser, S., "Free Energy, Internal Fields, and Ionic Polarizibilities in $BaTiO_3$," J. Phys. Chem. Solids, 3, (1957), 53.

16. Cochran, W., "Crystal Stability and the Theory of Ferroelectricity," Advances in Phys., 9, (Oct. 1960), 387.

17. Nakamura, T., "Kinematic Theory of Ferroelectric Domain Growth," J. Phys. Soc. Japan, 15, No. 8, (Aug. 1960), 1379.

18. Sommerhalder, H., "Free Energy of 180° Domain Walls and Surfaces in the Body-Centered Cubic Dipole Lattice," Helv. Phys. Acta, 33, Nos. 6-7, (1960), 617.

19. Abe, R., "Theoretical Study on the Properties of Coercive Field of $BaTiO_3$ Single Crystal," J. Phys. Soc. Japan, 15, No. 5, (May 1961), 795.

20. Kinase, Wataru, "Theory of the Dielectric Constants of Barium Titanate," J. Phys. Soc. Japan, 17, No. 1, (1962), 70.

21. Baldwin, W. J., "Factors Affecting Ceramic and Electrical Properties of High-Dielectric Constant Titanates," Ceram. Age, 53, No. 4, (1949), 188.

22. Graf, E. G., "Effect of Impurities on Dielectric Properties of Barium Titanate," Ceram. Age, 58, No. 6, (1951), 16.

23. Coffeen, W. W., "Effect of Minor Constituents in High Dielectric Constant Titanate Capacitors," Trans. Am. Inst. Elec. Engrs. (Part I, Communications and Electronics), 72, (1953), 704.

24. Oshry, H. I., "Stabilized High-Permittivity Barium Titanate," Proc. Electronic Components Symposium, Am. Inst. Elec. Engrs., (1954), 63.

25. Marks, G. W., and Monson, L. A., "Effect of Certain Group IV Oxides on the Dielectric Constant and Dissipation Factor of Barium Titanate," Ind. Eng. Chem., 47, No. 8, (1955), 1611.

26. Sakudo, Tunetaro, "Effect of Iron Group Ions on Dielectric Properties of $BaTiO_3$ Ceramics," J. Phys. Soc. Japan, 12, No. 9, (1957), 1050.

27. Schofield, D., and Brown, R. F., "Improved Barium Titanate Compositions," J. Acoust. Soc. Am., 29, (1957), 394.

28. Plessner, K. W., and West, R., "The Effect of Small Additions of Magnesia on Some High Permittivity Ceramics Based on Barium Titanate," J. Electronics and Control, First Series, 4, No. 1, January 1958.

29. Baxter, P., Hellicar, N. J., and Lewis, B., "Effect of Additives of Limited Solid Solubility on the Ferroelectric Properties of Barium Titanate Ceramics," J. Am. Ceram. Soc., 42, (1959), 465.

30. Coursey, P. R., and Brand, K. G., "Dielectric Constants of Some Titanates," Nature, 157, (1946), 287.

31. Shelton, G. R., Bunting, E. N., Creamer, A. S., "Development and Properties of Some Ceramic Dielectrics," Proc. Natl. Electronics Conf., 4, (1948), 24.

32. Durst, G., Grotenhuis, M., Barkow, A. G., "Solid Solubility Study of Barium, Strontium and Calcium Titanates," J. Am. Ceram. Soc., 33, (1950), 133.

33. Coffeen, W. W., "Dielectric Bidies in the Quaternary System $BaTiO_3$- $BaSnO_3$- $SrSnO_3$- $CaSnO_3$," J. Am. Ceram. Soc., 36, No. 7, (1953), 215.

34. McQuarrie, M., and Behnke, F. W., "Structural and Dielectric Studies in the System $(Ba,Ca)(TiZr)O_3$," J. Am. Ceram, Soc., 37, No. 11, (1954), 539.

35. McQuarrie, M. C., "Barium Titanate and Other Ceramic Ferroelectrics: III, Related Materials," Am. Ceram. Soc. Bull., 34, (1955), 256.

36. McQuarrie, M. C., "IV, Solid Solutions of Ferroelectrics," Am. Ceram. Soc. Bull., 34, (1955), 295.

37. McQuarrie, M. C., "Structural Behavior in the System $(Ba,Ca,Sr)TiO_3$ and Its Relation to Certain Dielectric Characteristics," J. Am. Ceram. Soc., 38, (1955), 444.

38. DeVries, R. C., and Roy, R., "Phase Equilibria in the System $BaTiO_3$- $CaTiO_3$," J. Amer. Ceram. Soc., 38, (1955), 142.

39. Egerton, L., Dillon, Dolores M., "Piezoelectric and Dielectric Properties of Ceramics in the System Potassium-Sodium Niobate," J. Am. Ceram. Soc., 42, (1959), 438.

40. Subbarao, E. C. and Shirane, G., "Dielectric and Structural Studies in the Systems $Ba(Ti,Nb)O_3$ and $Ba(Ti,Ta)O_3$," J. Am. Ceramic Soc., 42, (1959), 279.

41. Ikeda, T., "Studies on the $(Ba\text{-}Pb)(Ti\text{-}Zr)O_3$ Systems," J. Phys. Soc. Japan, 14, No. 2, (1959), 168.

42. Kulscar, F., "Electromechanical Properties of Lead Titanate Zirconate Ceramics with Lead Partially Replaced by Calcium or Strontium," J. Am. Ceram. Soc., 42, (1959), 49.

43. Kulscar, F., "Electromechanical Properties of Lead Titanate Zirconate Ceramics Modified with Certain Three- or Five-Valent Additions," J. Am. Ceram. Soc., 42, (1959), 343.

44. Kwestroo, W. and Paping, H. A. M., "The Systems BaO-SrO-TiO_2, BaO-CaO-TiO_2, and SrO-CaO-TiO_2," J. Am. Ceram. Soc., 42, (1959), 292.

45. Nelson, K. E., and Cook, R. L., "Ceramic and Dielectric Properties of Lead Metaniobate Electrical Ceramics," J. Am. Ceram. Soc., 42, (1959) 138.

46. Smoleski, G. A., Isupov, V. A., and Agranovskaya, A. L., "New Ferroelectrics of Complex Composition of the Type $A_2^{+2}(B_1^{+3}B_{11}^{+5})O_6$ Sov. Physics, Solid State, 1, No. 1, (1959), 150.

47. McQuarrie, M. C., and Buessem, W. R., "Aging Effect in Barium Titanate," Am. Ceram. Soc. Bull., 34, (1955), 402.

48. Plessner, K. W. "Ageing of the Dielectric Properties of Barium Titanate Ceramics," Proc. Phys. Soc. (London), 69, (1956), 1261.

49. Sawaguchi, E. and Charters, M. L., "Aging and the Double Hysteresis Loop of $Pb_xCa_{1-x}TiO_3$ Ceramics," J. Am. Ceram. Soc., 42, (1959), 157.

50. Baldwin, W. J., and Hathaway, A. J., "Control Testing of Dielectric Titanates and Some Anomalies Noted," Ceram. Age., 58, No. 2, (1951), 25.

51. Callahan, R. M., and Murray, J. F., "Preparation of Reproducible Barium Titanate," Am. Ceram. Soc. Bull., 33, No. 5, (1954), 131.

52. Egerton, L. and Koonce, S. E., "Effect of Firing Cycles on the Structure and Some Dielectric and Piezoelectric Properties of Barium Titanate Ceramics," J. Am. Ceram. Soc., 38, No. 11, (1955), 412.

53. Gray, A. L., and Herbert, J. M., "Preparation of Barium Titanate Ceramics," Acustica, 6, (1956), 229.

54. Brajer, E. J., "Effect of Some Ceramic Techniques on the Piezoelectric Properties of Barium Titanate," Am. Ceram. Soc. Bull., 36, No. 9, (1957), 333.

55. Nelson, K. E., and Cook, R. L., "Effect of Contamination Introduced During Wet Milling on the Electrical Properties of Barium Titanate," Am. Ceram. Soc. Bull., 38, (1959), 499.

56. Donley, H. L., "Barium Titanate and Barium Strontium Titanate Resonators," RCA Rev., 9, (1948), 218.

57. Mason, W. P., Wick, R. F., "Ferroelectrics and the Dielectric Amplifier," Proceedings of IRE, 42, (1954), 1606.

58. Shelton, G. R., and Marzullo, S., "Dielectrics for Ceramic Components," Rept. No. 3, National Bureau of Standards Rept. 3294, (May 1, 1954).

59. Jonker, C. H., "Capacitor Materials with High Permittivity," Philips Tech. Rev., 17, No. 5, (1955), 129.

60. Schofield, D., and Brown, R. F., "Barium Titanate Compositions for Transducer Applications," Canad. J. Phys., 35, (1957), 594.

61. Marutake, Masakazu, "A Calculation of Physical Constants of Ceramic Barium Titanate," J. Phys. Soc. Japan, 11, No. 8, (1956), 807.

62. Diamond, H., "Variation of Permittivity with Electric Field in Perovskite-Like Ferroelectrics," J. Appl. Phys., 32, No. 5, (May, 1961), 909.

63. Megaw, H. D., Ferroelectricity in Crystals, Methuen and Co. Ltd., London, 1957.

64. Rushman, D. F., Strivens, M. A., "Permittivity of Polycrystals of the Perovskite Type," Trans. Faraday Soc., 42A, (1946), 231.

65. Jackson, W., and Reddish, W., "High Permittivity Crystalline Aggregates," Nature, 156, (1945), 717.

66. Sawyer, C. B., and Tower, C. H., "Rochelle Salt as a Dielectric," Phys. Rev., 35, (1930), 269.

67. Merz, W. J., "Domain Properties in Barium Titanate," Phys. Rev., 88, (1952), 421.

68. Merz, W. J., "Domain Formation and Domain Wall Motions in Ferroelectric Barium Titanate Single Crystals," Phys. Rev., 95, (1954), 690.

69. Little, E. A., The Dynamic Behavior of Domain Walls in Barium Titanate, Tech. Report 87, Laboratory for Insulation Research, Massachusetts Institute of Technology, October, 1954.

70. Merz, W. J., "The Electric and Optical Behavior of Barium Titanate Single-Domain Crystals," Phys. Rev., 76, (1949), 1221.

71. von Hippel, A., "Ferroelectricity, Domain Structure, and Phase Transitions of Barium Titanate," Rev. Mod. Phys., 22, (1950), 221.

72. McQuarrie, M. C., "Role of Domain Processes in Polycrystalline Barium Titanate," J. Am. Ceram. Soc., 39, No. 2, (1956), 54.

73. Butler, T. W., University of Michigan Department of Electrical Engineering, E. D. G. Quart. Prop. Rept. 1 (August 1959), 37.

74. Merz, W. J., "The Effect of Hydrostatic Pressure on the Curie Point of Barium Titanate Single Crystals," Phys. Rev., 78, (1950), 52.

75. Shirane, G., and Sato, K., "Effects of Mechanical Pressures on the Dielectric Properties of Polycrystalline Barium-Strontium Titanate," J. Phys. Soc. Japan, 6, (1951), 20.

76. Shirane, Gen, and Takeda, Akitsu, "Volume Change in Transitions in $BaTiO_3$ Ceramic," J. Phys. Soc. Japan, 6, (1951), 128.

77. Cook, W. R., Jr., Berlincourt, D. A., and Scholz, F. J., "Thermal Expansion and Pyroelectricity in Lead Titanate Zirconate and Barium Titanate," J. Appl. Phys., 34, No. 5, (1963).

78. Merz, W. J., "Double Hysteresis Loop of $BaTiO_3$ at the Curie Point," Phys. Rev., 91, No. 3, (1953), 513.

79. Kaenzig, W., and Maikoff, N., "Ist die seignette-elektrische 120°C - Umwandlung von Bariumtitanat erster order zweiter Art?," Helv. Phys. Acta, 24, (1951), 343.

80. Burbank, R. D., and Evans, H. T., Jr., "The Crystal Structure of Hexagonal $BaTiO_3$," Acta Cryst., 1, (1948), 330.

81. Rase, D. E. and Roy, R., "Phase Equilibria in the System $BaO-TiO_2$," J. Am. Ceram. Soc., 38, (March 1955), 102-113.

82. Megaw, H. D., "Crystal Structure of $BaTiO_3$," Nature, 155, (1945), 484.

83. Rhodes, R. G., "Structure of $BaTiO_3$ at Low Temperatures," Acta Cryst., 2, (1949), 417.

84. Kay, H. F., and Vousden, P., "Symmetry Changes in Barium Titanate at Low Temperatures and Their Relation to Its Ferroelectric Properties," Phil. Mag. Series 7, 40, (1949), 1019.

85. Buerger, M., Phase Transformations in Solids, Wiley and Sons, New York, (1951).

86. Busch, G., Flury, H., and Merz, W., "Elektrische Leitfaehigheit und Brechungsindex des Bariumtitanats," Helv. Phys. Acta, 21, (1948), 212.

87. Cross, L. E., Nicolson, M. M., Zlotnicki, B., and Whiddington, R., "Dispersion of the Birefringence in Barium Titanate," Nature, 165, (1950), 440.

88. Forsbergh, P. W., Jr., "Domain Structures and Phase Transitions in Barium Titanate," Phys. Rev., 76, No. 8, (October 1949), 1187.

89. Blattner, H., Kaenzig, W., Merz, W., and Sutter, H., "Domain Structure of Barium Titanate Crystals," Helv. Phys. Acta, 21, (1948), 207.

90. Matthias, B., and von Hippel, A., "Domain Structure and Dielectric Response of Barium Titanate Single Crystals," Phys. Rev., 73, (1948), 1378.

91. Kay, H. F., "Preparation and Properties of Crystals of Barium Titanate," Acta Cryst., 1, (1948), 229.

92. Hooton, J. A. and Merz, W. J., "Etch Patterns and Ferroelectric Domains in Barium Titanate Single Crystals," Phys. Rev., 98, (1955), 400.

93. Campbell, D. S., and Stirland, D. J., "A Modified Replica Technique and Its Application to the Examination of Etched Single Crystals of Barium Titanate," Brit. J. Appl. Phys., 7, (1956), 62.

94. Miller, R. C. and Savage, A., "Direct Observation of Antiparallel Domains During Polarization Reversal in Single Crystal Barium Titanate," Phys. Rev. Letters, 2, (April 1959), 294.

95. Spivak, G. V., Igras, E., and Zheludev, I. S., "An Electron-Microscope Study of Ferroelectric Domain Structure," Soviet Phys. Doklady, 3, No. 5, (1958), 943.

96. Bhide, V. G. and Bapat, N. J., "Interferometric Study of Domain Structure in Barium Titanate," Physica (Netherlands), 27, No. 6, (June, 1961), 531.

97. Kaenzig, W., "Ferroelectrics and Antiferroelectrics," Solid State Physics, 4, Academic Press Inc., New York, (1957), 102.

98. Cross, L. E., Phil. Mag. Series 7, 44, (1953), 1161.

99. Drougard, M. E. and Young, D. R., "Dielectric Constant Behavior of Single-Domain, Single Crystals of Barium Titanate in the Vicinity of the Curie Point," Phys. Rev., 95, (1954), 1152.

100. Kawabe, K., "Optical Studies on the Effect of Electric Fields on the Transition of Barium Titanate," J. Phys. Soc. Japan, 14, (1959), 1755.

101. Husimi, K. and Kataoka, K., "Pulse Width Dependence of the Switching Velocity in Barium Titanate Crystal," J. Appl. Phys., 30, (March 1959), 323.

102. Husmini, K., "180° Domain Wall Motions in $BaTiO_3$ Crystal," J. Phys. Soc. Japan, 5, No. 4, (April 1960), 731.

103. Nakamura, T., "Kinematic Theory of Ferroelectric Domain Growth," J. Phys. Soc. Japan, 15, No. 8, (Aug. 1960), 1379.

104. Abe, R., "Theoretical Treatment of the Movement of 180° Domains in a $BaTiO_3$ Single Crystal," J. Phys. Soc. Japan, 14, No. 5, (1959), 633.

105. Miller, R. C., "Some Experiments on the Motion of 180° Domain Walls in Barium Titanate," Phys. Rev., 112, (1958), 413.

106. Burfoot, J. C., "Wall Velocity in Ferroelectrics," Proc. Phys. Soc., 75, Part 2, (Feb. 1960), 314.

107. Miller, R. C., and Savage, A., "Motion of 180° Domain Walls Under the Application of a Train of Voltage Pulses," J. Appl. Phys., 32, No. 4, (1961), 714.

108. Ruediger, O., "Uebermikroskopischer Nachweis der Elementar-bereichsstruktar bei vielkristallinem Barium Titanat," Naturwissenschaften, 42, (1955), 644.

109. Cook, W. R., "Domain Twinning in Barium Titanate Ceramics," J. Am. Soc., 39, No. 1, (1956), 17.

110. Kulscar, Frank, "A Microstructure Study of Barium Titanate Ceramics," J. Am. Ceram. Soc., 39, (1956), 13.

111. Kontoleon, D. and Tomlinson, J., "Micro-Examination of Barium Titanate," Metal Progr., 69, (1956), 98.

112. DeVries, R. C., and Burke, J. E., "Microstructure of Barium Titanate Ceramics," J. Am. Ceram. Soc., 40, (1957), 200.

113. de Boer, J., "Domain Structure in Ceramic Barium Titanate," Chem. Weekblad, 54, (1958), 137.

114. Pearson, G. L., and Feldman, W. L., "Powder Pattern Techniques for Delineating Ferroelectric Structures," J. Phys. Chem. Solids, 9, (January 1959), 28; Bull. Am. Phys. Soc., 3, (1958), 366.

115. Tennery, V. J., and Anderson, F. R., "Examination of the Surface and Domain Structure in Ceramic Barium Titanate," J. Appl. Phys., 29, No. 8, (1958), 755.

116. Andres, E. H., and Richardson, J. H., "New Cement for Preparation of Ceramic Thin Sections," J. Am. Ceram. Soc., 43, No. 5, (1960).

117. Anliker, M., Brugger, H. R., und Kaenzig, W., "Das Verhalten von kolloidalen Seignetteelektrika III, Bariumtitanat $BaTiO_3$," Helv. Phys. Acta, 27, (1954), 99.

118. Fatuzzo, E., and Merz, W. J., "Surface Layer in $BaTiO_3$ Single Crystals," J. Appl. Phys., 32, No. 9, (Sept. 1961), 1685-7.

119. Ivanchik, I. I., "Macroscopic Theory of Ferroelectrics," Sov. Phys. Solid State, 3, No. 12, (December 1961).

120. Meyerhofer, D., Transition to the Ferroelectric State in Barium Titanate, Laboratory for Insulation Research, Mass. Institute of Technology, Technical Report 121, Oct. 1957.

121. Chynoweth, A. G., "Effect of Space Charge Fields on Polarization Reversal and the Generation of Barkhausen Pulses in Barium Titanate," J. Appl. Phys., 30, (March 1959), 280.

122. Johannsen, Albert, Manual of Petrographic Methods, New York, McGraw-Hill Book Company, Inc., 1914.

123. Nomura, Shoichiro, "Solid State Reaction Between Barium Titanate and Strontium Titanate," J. Phys. Soc. Japan, 11, No. 9, (Sept. 1956), 924.

124. Jahnke, E., and Emde, F., Tables of Functions, Dover Publications, New York, 1945.

125. Devonshire, A. F., "Theory of Ferroelectricity," Phil. Mag., Supplement, 3, (April 1954), 85.

126. Lichtenecker, K., "Die Dielektrizitaetskonstante natuerlicher und kuenstlicher Mischkoerper," Phys. Z., 27, (1926), 115.

UNIVERSITY OF MICHIGAN
3 9015 03695 6095